

Use of ionic crosslinking for Pressure-Sensitive Adhesives

Dissertation zur Erlangung des Grades der Doktorin
der Naturwissenschaften
der Naturwissenschaftlich-Technischen Fakultäten
der Universität des Saarlandes
von

Justine Tavera

2019

Under the supervision of:

Prof. Dr. Aránzazu Del Campo
Leibniz Institute for New Materials
& University of Saarland

Dr. Matthias Gerst
BASF SE, Polymers for Adhesives

Use of ionic crosslinking for Pressure-Sensitive Adhesives

Dissertation zur Erlangung des Grades der Doktorin der Naturwissenschaften
der Naturwissenschaftlich-Technischen Fakultäten der Universität des
Saarlandes

von
Justine Marie Tavera

Saarbrücken 2019

Under the supervision of:

Prof. Dr. Aránzazu Del Campo – Leibniz Institute for New Materials
& University of Saarland
Dr. Matthias Gerst – BASF SE, Polymers for Adhesives

Tag des Kolloquiums:
19.11.2019

Dekan:
Prof. Dr. G. Kickelbick

Berichterstatter/in:
Prof. Dr. A. del Campo
Prof. Dr.-Ing. M. Gallei

Vorsitz:
Prof. Dr. D. Scheschkewitz

Akad. Mitarbeiter:
Dr. R. Hensel



This project has received funding from the European Union's Horizon 2020 research and innovation programme under the Marie Skłodowska-Curie grant agreement No 642861.



UNIVERSITÄT
DES
SAARLANDES

 **BASF**
We create chemistry

Summary

Pressure Sensitive Adhesives (PSA) need to integrate viscous and elastic properties to ensure tackiness and resistance to strain in the application. The use of physical interactions as crosslink points has been proposed as a molecular design strategy to solve these apparently contradictory requirements. In this context, this PhD Thesis proposes synthesis routes to obtain PSA formulations with physical crosslinks based on oppositely charged moieties. The derived materials present improved adhesion performance based on stress dissipation by the remodeling of the ionic bonds during deformation.

In a first approach, the emulsion polymerization of n-butylacrylate (n-BA) and styrene with ionic comonomers methacrylic acid and 2-(Methacryloyloxy)ethyl trimethylammonium chloride (MAETAC) was studied. The hydrophilicity of the cationic monomer led to homopolymerization in the water phase and hindered the formulation of adhesive mixtures. In a second alternative, the synthesis of acrylate-based polyampholytes was attempted by polymerization of n-BA, Methyl methacrylate, MAETAC and 2-hydroxyethyl methacrylate ester phosphoric acid using isopropanol as solvent. Adhesive formulations with tunable adhesion performance depending on the content, the stoichiometry and the nature of ionic monomers were obtained. Finally, secondary water-borne dispersions were developed from these copolymers in order to avoid the presence of organic solvent in the final product. The polymer networks showed high adhesion-cohesion balance and compete with commercialized products.

Zusammenfassung

Haftklebstoffe müssen Viskosität und Elastizität in die gleiche Formulierung integrieren, um Klebrigkeit und Beständigkeit gegen Dehnung in den Anwendungen zu gewährleisten. Die Verwendung physikalischer Wechselwirkungen als Vernetzungspunkte wurde als molekulare Entwurfsstrategie vorgeschlagen, um diese widersprüchlichen Anforderungen zu lösen. In diesem Zusammenhang schlägt diese Doktorarbeit vor, Synthesewege zu finden, um Haftklebmassen Formulierungen mit physikalischen Vernetzungen auf der Basis von entgegengesetzt geladenen Einheiten zu erhalten. Die abgeleiteten Materialien weisen verbessertes Adhäsionsverhalten auf, das auf dem Spannungsabbau durch das Umordnen der Ionenbindungen während der Verformung beruhen.

Zunächst wurde die Emulsionspolymerisation von n-Butylacrylat (n-BA) und Styrol mit ionische Comonomere Methacrylsäure und 2-(Methacryloyloxy)ethyltrimethylammoniumchlorid (MAETAC) untersucht. Durch hohe Hydrophilie, neigte das kationische Monomer allerdings zu einer Homopolymerisation und führte nicht zur gewünschten ionischen Vernetzung und verbesserten Klebstoffeigenschaften. Daraufhin wurden Polyampholyte auf Acrylatbasis durch die Polymerisation von n-BA, Methylmethacrylat, MAETAC und Phosphorsäure 2-hydroxyethyl Methacrylester in Isopropanol hergestellt. Das Adhäsionsverhalten der Polymere konnte durch Änderung des Gehalts, der Stöchiometrie und der Art der ionischen Monomere eingestellt werden. Schließlich wurden aus diesen Copolymeren sekundäre Dispersionen auf Wasserbasis entwickelt, um die Anwesenheit von organischem Lösungsmittel im Endprodukt zu vermeiden. Es wurde ein gutes Adhäsions-Kohäsions Verhältnis gefunden, sogar konkurrenzfähig zu bestehenden kommerziellen Produkten.

Acknowledgments

First of all, I would like to express my sincere gratitude to my supervisors, Prof. Aránzazu Del Campo for accompanying me and advising me throughout this thesis, for giving so much time and patience; and Dr. Matthias Gerst for the support, the discussions, valuable guidance and supervision during these 3 years at BASF.

Thanks to the Polymers for Adhesives Group leaders: Drs. Matthias Gerst, Paul Birnbrich, Ulrike Licht, Tina Mark, Annika Spies and Gemma Sanders, for listening to my group presentations and giving advices.

Thanks to Dr. Helmut Winterling for hosting me and the BioSmartTrainee Project in the RAD Department. Thanks to Stefanie Cuzik, Mia Hammann and Martina Bonnard for their kind help.

Vielen Dank für RAD/OK und RAD/OG lab teams: Miriam Müller, Anja Hubert, Udo Spuhler, Alexander Gies, Sven Burgey and Jürgen Siroky for their help in the labs. Special thanks for Andreas Schwarz and Stephan Möbius who have trained me and helped in the lab but also on theoretical issues.

Many thanks to Dr. Rainer Schulze for helping me writing the patents. Thank you to all the colleagues from the development, material physics and analytics and especially Reinhard Erker, Christian Saffert, Isabelle Kronauer, Beate Prescha, Ralf Scheidhauer, Marcus Brinkrolf and Andreas Hopf.

Huge thanks also go to colleagues from other departments who helped me for hours, in sample or machine preparation, training me and letting me use the lab instruments: to Bernd Kümmerling für so viele Stunden mit dem AFM, Rainer Eherer und Olaf Waldhauser für application tests, Stefan Forster und Ute Grau für dem Zug-DehnungsTest, Christopher Ruder for the conductivity measurements.

Many thanks to Dr. Rui de Oliveira, Dr. Maik Nowak, Dr. Meik Ranft, Dr. Ute Heinemeyer, Dr. Stephanie Tomcin, Dr. Bastian Staal, Dr. Paul Achatz, Dr. Thomas Weiss, Dr. Ingolf Hennig for answering my questions.

I would also like to address warm thanks to the whole BioSmart Trainee network, for their great collaboration, the great organization of all events and the great atmosphere. My thanks also go especially to Sandra Martinka for organizing everything so well and Alla Synytska for supervising the whole project.

Also thanks a lot to Prof. Marleen Kamperman and the whole Soft Matter lab in Wageningen for hosting me. Thanks to Ilse, Aljosha and Ivan for the good times during the secondment and training schools.

Un grand merci à Prof. Costantino Creton d'avoir répondu à toutes mes questions et de m'avoir permis de passer du temps au SIMM de l'ESPCI Paris, et merci à tout le laboratoire pour l'accueil. Merci à Artem, Gabo, Helen, Valentine, Jingwen, Paul et tous les autres pour leur aide et accueil. Merci beaucoup à Cécile, Antoine et Cyprien pour la bonne ambiance du bureau et surtout le soutien mutuel.

Huge thanks to the BioSmart Trainee students, PhDs graduates and Doctors to be, awesome people and great scientists: Maria, Vaishali, Aurélie, Mehdi, Francisco, Ugo, Marco, Dimitris, Victor and Maceij, for the amazing atmosphere and time we had every time. Special thanks to Marco, Mehdi and Francisco for hosting me in their labs.

Danke Jeevana für deine Freundlichkeit and Unterstützung immer. Ich bin so froh, dass wir uns kennen gelernt haben.

Danke Isabel für die Lunch, die Abendessen, deine Freundlichkeit und deine gute Laune.

Tausend Danke an Ulrike. Ich danke dir für ein tolles Deutsch Training, deine Freundlichkeit und Hilfe. Ich bin dankbar, dass der Zufall unsere Wege gekreuzt hat. Ich hatte großes Glück, du als Lehrerin zu haben.

Mille mercis à Alix, Martin, Cyprien, Ulysse, Jordan, Thomas, Thomas casquette, Eugénie, Anne-Laure, Yanis, Rossi, pour les soirées, les BBQ et les bières.

Merci beaucoup à Maxime mon ami et ancien collègue, de m'avoir fourni le monomère sans lequel rien de cela ne serait écrit...

Grand merci à Frédéric pour son aide, ses corrections, et pour m'avoir écoutée me plaindre ; aussi à Antoine, pour les cafés, l'optimisme et les encouragements.

Many thanks to Gemma for being a great officemate and colleague/friend, sharing snacks and chocolate always!

Thanks a lot, to all my friends (and their partners) who made my life during the PhD special, easier and always encouraged me: Sil, Samane, Gordana, Natalia, Amrith, Madhura and Dominic. Thanks to Sil, Gordana and Massimo for being present, supportive and sharing the experience of PhDs at BASF. Special thanks to Samane for being a patient consultant on my thesis during the last months.

Merci mille fois à toute ma famille et mes amis pour leur soutien. Merci à mes sœurs et mes beaux-frères pour leur soutien, aussi à Marcel et Lucien de m'avoir remonté le moral sans vraiment le savoir.

Merci à mes parents de m'avoir permis de poursuivre des études et aussi de m'avoir soutenu lors de mes déménagements à travers le monde.

Et surtout merci à Thomas de m'avoir toujours soutenue et de m'avoir supportée à distance pendant cette longue période !

Table of contents

Summary	4
Zusammenfassung	5
Acknowledgements.....	6
Table of contents	9
Abbreviations and acronyms	13
Chapter I. Adhesion & pressure-sensitive adhesives	19
I.1. Adhesives and adhesion	21
A. History of adhesives	21
B. How does glue stick.....	24
I.2. Pressure-sensitive adhesives	27
A. PSA in industry	27
B. Chemistry of PSA and their influence on polymer properties	29
C. New types of chemistries for PSA	31
D. Synthesis of PSAs.....	49
E. Testing adhesion of PSAs	55
F. Adhesion theory of PSAs	64
G. Mechanical properties and viscoelastic behaviour of PSAs	67

I.3. Thesis outline	71
I.4. References	73
Chapter II. Adhesive Polyampholyte Particles prepared by emulsion polymerization	83
II.1. Introduction	85
II.2. Results	87
A. Selection of surfactant.....	88
B. Selection of initiating system	90
C. Selection of cationic monomer	91
D. Effect of the ionic monomer ratio on emulsion stability	93
E. Effect of a chain transfer agent on the gel content.....	94
F. Effect of the amount of ionic comonomers and pH on the polymer structure and physical properties of the films	96
II.3. Discussion.....	120
II.4. Conclusion	125
II.5. References.....	126

Chapter III. Adhesive polyampholyte polymers prepared by solution polymerization 131

III.1. Introduction	133
III.2. Results & discussion.....	135
A. Variation of ionic crosslinking density of the polymers and the effects on the mechanical and adhesive properties of the resulting films.....	136
B. The role of stoichiometry between ionic groups on the mechanical and adhesive properties of polymer films	160
C. Effect of the nature of ionic groups on the mechanical and adhesive properties of the polymer films	171
D. Comparison of adhesive performance to commercialized products.....	186
E. Optimization of the molecular weight using a batch process.....	189
III.3. General conclusion.....	209
III.4. References	211

Chapter IV. Secondary dispersions: from dissolved to dispersed 215

IV.1. Introduction	217
IV.2. Results	220
A. Synthesis of polyampholytes	220
B. Preparation and characterization of secondary dispersions	221

C. Physico-chemical properties of the polymers and their dried films	225
D. Mechanical properties of the polymer films.....	227
E. Adhesive properties of the polymer films	235
IV.3. Discussion	242
IV.4. Conclusion	246
IV.5. References	247
Chapter V. General conclusions.....	251
Chapter VI. Appendixes	257
VI.1. Experimental part	264
A. Materials	264
B. Chapter II. Synthesis by emulsion polymerization	265
C. Chapter III. Synthesis by free radical solution polymerization	268
D. Chapter IV. Preparation of secondary dispersions	271
E. Characterization of the polymers and their films.....	273
VI.2. Additional graphs and data tables	280
A. Chapter II. Adhesive polyampholyte particles prepared by emulsion polymerization ..	280
B. Chapter III. Adhesive polyampholyte polymers prepared by solution polymerization..	297
C. Chapter IV. Secondary dispersions: from dissolved to dispersed	327

Abbreviations and acronyms

ϵ	Strain
ϵ_B	Strain/elongation at break
ϵ_{\max}	Strain/elongation at maximum stress
η_{flow}	Flowing viscosity
ω	Angular frequency
ω_{Bonding}	Angular frequency at bonding frequency
ω_c	Angular frequency at cross-over
$\omega_{\text{Debonding}}$	Angular frequency at debonding frequency
γ	Shear amplitude
σ_B	Stress at break
σ_{\max}	Maximal stress
σ_{peak}	Stress at peak
σ_{plateau}	Stress at plateau
σ_Y	Stress at yield
ν	Conformation factor
a_T	Horizontal shift factor
A	Adhesive failure
b_T	Vertical shift factor
AFM	Atomic Force Microscopy
ATR-IR	Attenuated total reflection infrared spectroscopy
AUC	Analytic Ultracentrifuge
CTA	Chain transfer agent

C_s	Chain transfer constant
D	Dispersed state
$D_{10\%}$	Average particle diameter for 10% of the population
$D_{50\%}$	Average particle diameter for 50% of the population
$D_{90\%}$	Average particle diameter for 90% of the population
DMAEMA	Dimethylaminoethyl methacrylate
DTMACl	Dodecyl trimethylammonium chloride
DMSO	Dimethylsulfoxide
DP	Degree of polymerization
DP_n	Number average degree of polymerization
DSC	Differential scanning calorimetry
E	Young's modulus
EDX	Energy dispersive X-ray spectroscopy
eq	Molar equivalent
EtOH	Ethanol
F	Filmic failure
$Fe_2(SO_4)_3$	Iron II trisulfate heptahydrate
F_{mean}	Mean peel force
G	Glassy failure
G'	Shear storage/Elastic modulus
G''	Shear loss modulus
G_c	Shear elastic modulus at cross-over
GC	Gas chromatography
Gel%	Gel content
HDC	Hydrodynamic chromatography

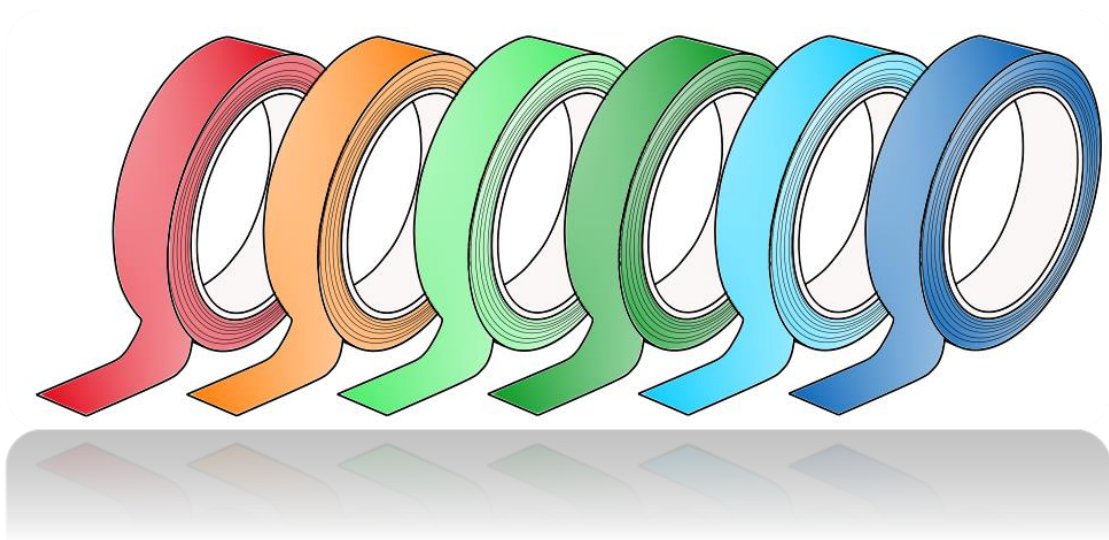
HFIP	Hexafluoroisopropanol
HPLC	High performance liquid chromatography
H ₂ O ₂	Hydrogen peroxide
ionicX	Ionic comonomers weight fraction
iPrOH	Isopropanol
IR	Infrared spectroscopy
K	Cohesive failure
KOH	Potassium hydroxide
M	Molar mass
MAA	Methacrylic acid
MAETAC	(2-(Methacryloyloxy)ethyl) trimethylammonium chloride solution
MAEEOAMS	(2-(2-(2-methylprop-2-enoyloxy)ethoxy)ethyl) trimethylammonium methylsulfate
MALLS	Multi-angle light scattering
MAMPTAC	3-(methacryloylamino)propyl trimethylammonium chloride
MAPTAMS	(3-(2-methylprop-2-enoyloxy)propyl)trimethylammonium methylsulfate
M _c	Molecular weight between crosslinks
M _e	Molecular weight between entanglements
MEK	Methyl ethyl ketone
MMA	Methyl methacrylate
M _n	Number average molecular weight
M _w	Weight average molecular weight
NaPS	Sodium persulfate

n-BA	n-butyl acrylate
NH ₃	Ammonia
NMR	Nuclear magnetic resonance spectroscopy
PDI	Polydispersity index
PE	Polyethylene
PET	Polyethylene terephthalate
Polystep®	Phosphoric acid 2-hydroxyethyl methacrylate ester
PP	Polypropylene
pphm	Party per hundred monomers
PSA	Pressure-sensitive adhesive
PUD	Polyurethane dispersions
PVC	Polyvinylchloride
RAFT	Reversible addition-fragmentation chain transfer
RI	Refractive index
r_i	Reactivity ratio
R_g	Radius of gyration
Rongalit C	Sodium formaldehyde sulfoxylate
S	Solution state
S+KOH	Solution with added KOH state
SEC	Size-exclusion chromatography
SPP	Single particle preparation
St	Styrene
T	Temperature
$t_{1/2}$	Half-life time
$\tan \delta$	Shear tan modulus

t-BHP	tert-butyl hydroperoxide
t-BPPVT	tert-Butyl peroxy-pivalate
t-BP2EH	tert-Butyl peroxy-2-ethylhexanoate
t_c	Contact time
t-DMK	Tert-dodecyl mercaptan
TEM	Transmission electron microscopy
T_g	Glass transition temperature
TTS	Time-temperature superposition
UV	Ultraviolet
v_{deb}	Debonding velocity
VOC	Volatile organic compound
W_{deb}	Work of debonding
Z	Zippy failure

I.

Adhesion & pressure-sensitive adhesives



I. Adhesion & pressure-sensitive adhesives.....	19
I.1. Adhesives and Adhesion.....	21
A. History of adhesives.....	21
B. How does glue stick.....	24
I.2. Pressure-Sensitive Adhesives.....	27
A. PSA in industry	27
B. Chemistry of PSA and their influence on polymer properties	29
C. New types of chemistries for PSAs	31
D. Synthesis of PSAs	49
E. Testing adhesion of PSAs	55
F. Adhesion theory of PSAs	64
G. Mechanical properties and viscoelastic behaviour of PSAs.....	67
I.3. Thesis outline	71
I.4. References	73

I.1. ADHESIVES AND ADHESION

A. History of adhesives

While adhesion might appear as a very common and trivial process nowadays, the use of adhesives during Prehistory was a proof of advanced cognitive state. The first evidence found of adhesives goes back to the Middle Stone Age approx. 200 000 years ago[1] (Middle Pleistocene). During that period, adhesives were formulated from plant resins and were used to assemble tools such as knives and arrows. Many studies refer to birch bark gums as adhesives for making of tools. The bark was distilled into pitch and then chewed to make it malleable. Recently, scientists were able to recover DNA from the adhesive gum[2, 3] and could propose a visual appearance and diet of the individuals living during the Mesolithic period in Scandinavia; making also adhesives important archeologic aid. In Ancient Egypt (~3000 BC), adhesives[4] were prepared from honey, starch and beeswax for constructions, paints and papyrus. Later on, latex from caoutchouc trees was imported in Europe during the conquest of America in the 16th century. It was then widely used in industries, allowing the invention of rubbers and development of many other products of our era.

Nowadays, adhesives are also widely used in direct consumer applications such as office or masking tapes; these last even became decorative items in the last 15 years. Silicon joints or hot glue guns for private use are also very common. From a Business to Business perspective, adhesives also find many applications in construction (e.g. binders in mortars, joints in plumbing, tapes for electrical wires...), in furniture, electronics, automotive, aviation, pharmaceuticals and the food industry[5]. Adhesives in automotive and aviation raise currently high interest because they lower weight and surface roughness when applied to external structures; thus, minimizing drag of air or water in comparison to mechanical binding (screws, etc...). They also enlarge bonding area and lower stress concentration for longer life-time of products.

Most of adhesives are not used as such but are the results of thorough research on syntheses and formulations. Additives such as wetting agents, tackifiers, starch or thickeners can be used to improve the different features of adhesive products. Surface treatments can also be realized to attain this goal; they can consist of changing the chemistry of the substrates (phosphate, chrome conversions...), their physical properties with plasma and corona or their topography with cleaning and abrasion.

The strong dependence of adhesion on surface interactions represents the major disadvantage of adhesive bonding. Surfaces might need intense, costly and time-consuming preparation to reach an acceptable performance. Adhesives must be formulated for each type of application, as the adhesion properties are surface specific. Adhesives are thus advanced technology and tailor-made solutions need to be found for each final application. Their ubiquity and versatility make them relevant materials throughout the centuries, yet current environmental challenges push the economy to a circular approach which encourages reuse, refurbishment, remanufacturing and recycling of various products. In many cases, adhesives are used to join two parts together without targeting a possible disassembly which might be an ambush to those circular processes. It thus appears the sustainability of products and their design need to be considered already upfront in their chemistry. The prospects for adhesives are therefore strongly related to recyclability; in cardboards and in laminated packaging or even labeling.

The future of adhesives should also be in the aerospace and aeronautic fields. Lighter, high performing adhesives which sustain extreme environmental conditions are always required; not only for costs saving but also for reducing oil consumption and pollution. Stimuli-responsive adhesives are also getting more and more interest for medical applications especially transdermal drug delivery. New methods for wound dressing (external or transdermal) aim for the procedures to be less invasive, improve the healing rate and the patient's recovery. Finally, conductive adhesives are becoming of high interests for electronics, solar panels and electrical batteries, and should become one of the biggest trends in the special purpose segment.

This thesis falls within the scope of finding high performance pressure-sensitive adhesives by using a new crosslinking chemistry, first for standard application like labels, tapes and packaging. Once sufficient knowledge will be gathered, the technology could be developed for specific purposes in different fields.

B. How does glue stick

In 2019, adhesion is still a phenomenon that stimulates many interrogations. Different adhesion mechanisms have been proposed in the last decades. The key theories are outlined in the following paragraphs[6-10]. Each individual mechanism is not necessarily universal but can contribute to some extent to the adhesive performance of a glue. Some illustration schemes are given in Figure 1.

- Mechanical interlocking[11]:

The mechanical interlocking refers to adhesion resulting from anchoring to a substrate by filling the empty cavities created by surface roughness. This adhesion mechanism is only effective if the surface is clean and that no impurity is filling the rough topography of the substrate. The rheological properties of the adhesive are important: the adhesive should have a Newtonian-type behavior to be able to flow in the small cavities and increase the contact area between the two adherents. However, adhesives are typically viscoelastic materials and do not act as Newtonian fluids. Plus, the theory doesn't provide an explanation for successful adhesion on smooth surfaces.

- Adhesion by diffusion[12]:

Diffusion theory suggests that the molecules of the adhesive and the substrate intermingle at the surface in the range of 1 to 100 nm so that no physical discontinuity is observed between them. For this mechanism to apply, both adherends should be composed of long polymer chains with high mobility and that the solubility between both materials is high. This theory is applicable for adhesion between soft surfaces, for elastomers and structural adhesives.

- Adhesion based on electrostatic interactions[13, 14]:

Electrostatic interactions apply to the cases where two surfaces with uneven electron distribution are brought into contact, electrons are exchanged to favor a lower energetical state; this results in the formation of an electrical double layer at the interface and strong interaction. Yet, it has been demonstrated that this phenomenon is not of high contribution[10] in the case of strong adhesion of soft polymers (as studied in this thesis).

- Adhesion by intermolecular forces[15]:

This theory suggests intermolecular forces are formed across the interface of the two adherends. Hydrogen, van der Waals, dipole-dipole and London dispersion interactions contribute and improve the bond between two adherends. The theory is applicable to a very wide range of materials, but all these types of interactions necessitate a very close contact between adherends when considering their scale of actions.

- Adhesion by wetting[16, 17]:

Wetting refers to the ability of a liquid or material to form an interfacial contact with a surface. Wetting theory therefore proposes that adhesion between the two adherends result from intimate continuous contact. However, such contact requires that the adhesive owns a lower surface tension (critical surface energy) than the substrate. Adhesion will be defective in the case of incomplete wetting (interfacial defects) and for low energy substrate (usually plastics like polyethylene, polypropylene...). For the latter case, surface treatments were developed to increase the surface energy and polarity and improve adhesion.

- Rheological theory for adhesion[18-21]:

Most previous theories report adhesion mostly as an interfacial phenomenon while it was recently suggested that adhesion is a property of the entire system adhesive-substrate-interface chemistry; and that the bulk properties of the adhesive play an important role. The rheological properties of an adhesive determine its capacity to flow under an applied stress. Yet, various stresses (compressive, shear...) are applied onto an adhesive system, which should thus be restrained to prevent fracture of the adhesive bond. It was demonstrated that pure adherence (interfacial chemistry) had a lower impact on the strength of this bond while the capacity for deformation (rheological properties) was determinant; further details will be given in I.2.F.

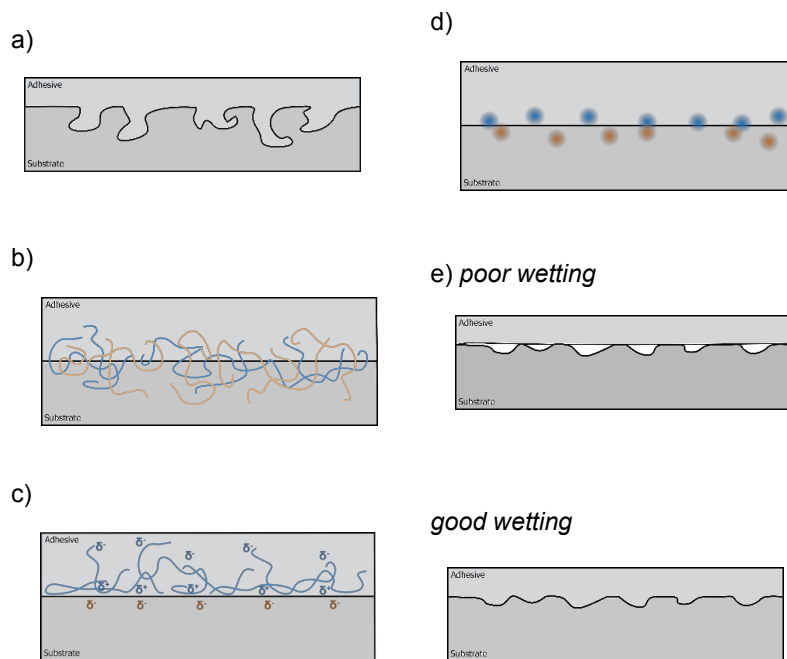


Figure 1. Schematic illustration of adhesion mechanisms: a) mechanical interlocking, b) diffusion, c) electrostatic interactions, d) chemical interactions and e) wetting

I.2. PRESSURE-SENSITIVE ADHESIVES

Pressure-sensitive adhesives (PSA) are a class of adhesives for which high adhesion should not require a pressure exceeding the one given by a finger or a hand. They are viscoelastic polymers and should readily form contact with the substrate (stickiness or tackiness feature) preferably within the application time and temperature. They are composed of an adhesive layer coated on a backing that can be made of various materials such as paper, polyethylene terephthalate (PET), polypropylene (PP), polyvinyl chloride (PVC), etc. They are widely used products and many studies have been aiming to understand their adhesion mechanism and link to their mechanical properties.

A. PSA in industry

Pressure-sensitive adhesives (PSA) are the largest end use for adhesives in the world before Packaging and Woodworking (market segments are displayed in Figure 2). They represented about 27% of the sales volume in 2014[22] and are still on top of the adhesive market in 2019. PSAs market segments include food & beverage, construction, electronics, automotive and healthcare. Growing demand of speciality tapes especially for automotive and healthcare, highly contribute to the PSAs global sales.

In Europe, the PSA market was worth around 840 million € in 2018 and is expected to worth around 860 million € this year 2019 (internal numbers). Italy is the first regional manufacturer of PSA in Western Europe but Germany has the largest market share (~23%)[22]. Globally, 49% of the market is led by the Asia pacific region, followed by North America and Europe[23, 24]. The world market was evaluated to 80 billion € (90 billion \$) in 2016, by 2024 it is projected to reach 135 billion € (150 billion \$) with an annual growth rate of 6.5%[25].

The price of PSA products is mostly influenced by the raw materials & production energy costs. And on the other hand, trending PSA products trends are becoming more environmentally friendly: water-based and with paper backing and suggest an opening on this market segment.

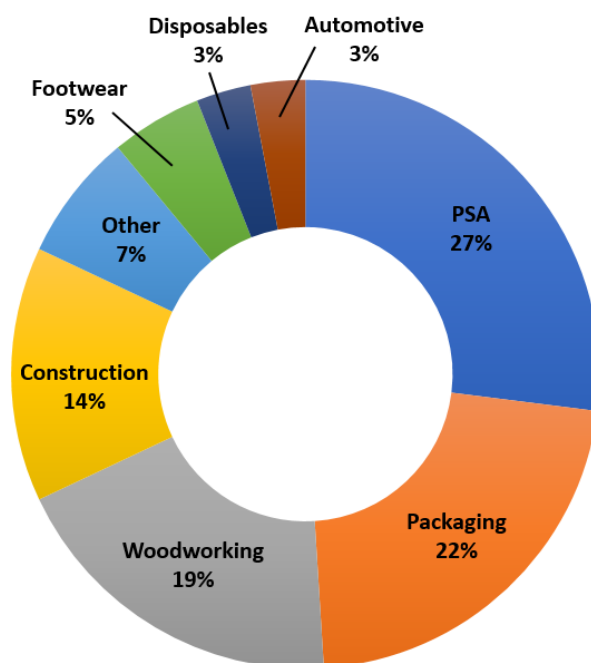


Figure 2. Market segments for adhesives

B. Chemistry of PSA and their influence on polymer properties

PSA can be prepared as hot-melts, solvent or water-borne polymers, by radical or anionic polymerizations. Various types of monomers are usually used: acrylates, acrylamides, isocyanates, acetates, vinyls and divinyls. Each monomer brings a certain functionality to the adhesive but functional monomers can be also added for preferable end-use features such as water-resistance, favoured stability or adhesion to specific substrate etc[26].

The mechanical properties of the adhesive films can be adjusted by the chemical design of the polymer. The main characteristics on which PSA can be tuned are the following: the molecular weight M_w and the molecular weight between entanglements M_e , the glass transition temperature (T_g), the crosslinking density d_c and the degree of chain branching. The molecular weight of the polymer plays a key role as it should be low enough for the chains to follow viscous flow but high enough so that the entanglements provide inner cohesion to the polymer. The M_w and its distribution can be tuned in different ways, the amount of initiator can be adjusted, different process techniques can be used, chain-transfer agents (CTA) can also be added to control the polydispersity[27]. The T_g corresponds to the temperature above which the polymer is amorphous, and the polymer chains answer only to reptation i.e. viscous flow. The latter is important to achieve good tack of a PSA, the qualitative tackiness corresponds to the ability of the PSA to quickly stick to a surface, i.e. quickly optimize contact area. The T_g of a PSA is adjusted with different combinations of monomers[27, 28].

The polymer chain architecture affects the mechanics and adhesion. Slight branching can slightly increase the stiffness of the polymer and provide inner-strength to the adhesive without losing much substrate binding. Chain branching can be induced deliberately in the prepolymer structure, though in most adhesive formulations, the presence of branched chains results from transfer reactions of the growing polymer chains.

The crosslinking density also has a strong influence on the viscoelasticity of the polymer and thus the adhesion properties. Usual crosslinks are covalent, they can be introduced during the polymerization with a crosslinking agent or after application, this is the case for UV crosslinkers in acrylic formulations[29]. These PSAs have the advantage that they can be applied in their non-crosslinked state, so viscous and still very tacky. The covalent crosslinks are then triggered by UV light and provide high cohesion to the system while the two adherends are already bonded. Non-permanent crosslinks are technologies being developed to improve adhesives performance (especially underwater or in wet environment) and will be discussed in the next paragraph I.2.C.

The challenge of PSA chemistry thus lies in the delicate balance between the linearity of polymer chains, required for good flowing and bond formation, and the rigidity of a polymer network, to provide mechanical resistance. Although both properties are antagonists, they are at the same time interconnected; adhesion is a measurement of both features at the same time. This limitation is actually also an advantage as it allows us to design PSA products for specific applications. However, in order to always obtain better performing PSAs, both properties need to be improved at the same time.

C. New types of chemistries for PSAs

The exploitation of reversible interactions (i.e. dynamic bonds that can break and reform) for mechanical reinforcement of crosslinked networks, has been investigated in different fields. Non covalent bonds for self-healing coatings[30-36] and medical hydrogels[37-39] and for drug delivery polymers[40-44] have been reported. Adhesives are no exception.

Current inspiration for new developments in adhesive design comes from materials designs in living organisms: animals[45-47], insects[48, 49] or even plants[50-53] have develop their own adhesives to survive within harsh environments, protect from predators or catch preys. One of the most studied organisms which can produce adhesives with outstanding performance underwater are mussels and sandcastle worms. The two adhesives are based on non-covalent interactions: ionic, hydrogen bonds and metal coordination. These interactions intervene in the setting mechanism and/or the interfacial interactions and/or the cohesive strength (crosslinking). They have inspired various work on new synthetic adhesives and PSAs and showed strong potential in stimuli-responsiveness, wet adhesion and tuning rheological/mechanical properties.

- i. Metal coordination and hydrogen bonding
 - The adhesive composition of mussel adhesive proteins

Mussels are marine animals that adhere to a variety of surfaces underwater. Anchoring of mussels occurs by secretion of mussel foot adhesive proteins (mfps), which interact with the surfaces of the rocks[54-58]. More than nine different proteins take part in the adhesion and coating of the mussel byssus, the most important ones were illustrated by Wei et al.[59] in Figure 3. The threads are made of the mussel foot protein mfp-1 which contain around 10-15 mol% of hydroxylated tyrosine residues into 3,4-dihydroxyphenyl-L-alanine (dopa). mfp-2, mfp-4 and mfp-6 proteins are the core of the byssal foot and insure the cohesion between the adhesive plaque and the byssal threads.

The cohesive strength of mussel adhesive relies on complexation between Fe^{3+} ions and catecholate groups (from dopa)[59]. Other reversible interactions like electrostatic interactions between phosphate and quaternary ammonium groups, cation- π interactions and hydrogen bonding contribute as well. Covalent bonds formed between dopa-quinone after oxidation of catechol also participate.

It was recognized that mfp-3 and mfp-5 are the proteins providing adhesion to the surfaces and are so called “adhesion primers”. They contain the highest amount of dopa which was thus recognized as the main provider of adhesion through surface interactions. Mfp-3 are mainly composed of 10-20 mol% of dopa and hydroxylated arginine (R) and Mfp-5 of phosphoserine plus 30 mol% of dopa residues.

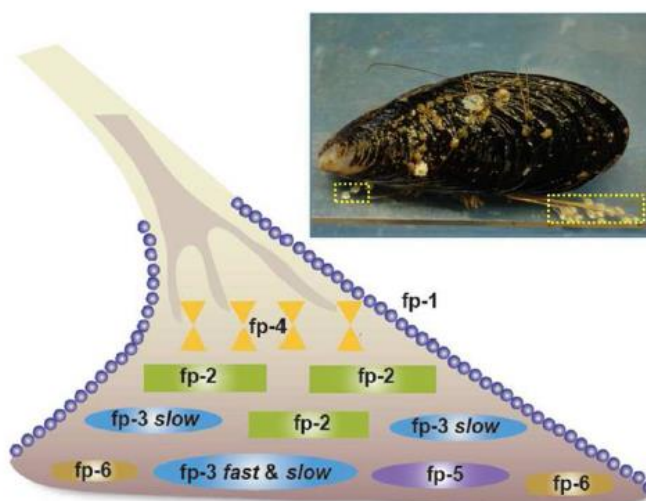


Figure 3. “Byssal plaque proteins of *Mytilus*. A mussel (*M. californianus*, inset) is shown attached to a polymer plate. One of its plaques (shown in dotted yellow box) is enlarged as a schematic drawing to illustrate the approximate distribution of known proteins.” Reprinted with permission from *Hydrophobic Enhancement of Dopa-Mediated Adhesion in a Mussel Foot Protein*, W. Wei et al., *Journal of the American Chemical Society*, 2013, 135, 1, 377-383[59], Copyright © 2012 American Chemical Society.

The adhesion of the three mussel foot proteins mfp-1, mfp-3 and mfp-5 was studied[60] with a surface force apparatus (SFA) and showed high dependence over the substrate nature and therefore interfacial properties. It was also shown that the contact time influenced adhesion as it followed the order of molecular flexibility $\text{mfp-3} > \text{mfp-5} > \text{mfp-1}$. But in general, the main adhesion promoter of the mussel foot is the bidentate hydrogen bonding between the byssus and the substrate. However, it can be suppressed in neutral and high pH conditions. Wei et al.[59] have studied the other mechanisms involved in adhesion in the mfp-3 when the hydrogen bonding is abolished (neutral pH).

Adhesion of mfp-3 slow to mica, the self-interactions of mfp-3 and the interactions of mfp-3 with other proteins were tested thanks to a SFA[59]. The trend of the adhesion of mfp-3 slow on mica decreasing with highering the pH was demonstrated. At pH 7.5, mfp-3 slow still showed significant adhesion, and suggested the dopa groups may be differentially prone to oxidation than in mfp-3 fast. Moreover, the adhesion of mfp-3 slow at pH 3, 5.5 and 7.5 was dependent of the contact time. For longer contact time, adhesion was much higher at pH 5.5 and 7.5 than at pH 3. The authors suggested that when the pH increases to 7.5, the dopa-mediated interactions are lowered, the pI of the protein is reached, and the proteins are almost neutralized. This results in a more packed structure of the proteins, favoring inter-residue H-bonding (dopa/dopa, dopa/other amino acid residue) and hydrophobic interactions.

- Dopa coordination and ionic bonding in bioinspired adhesives

Based on the dopa chemistry, several mussel-mimicking adhesives[61-66] and metal-coordination crosslinking for polymers[35, 61, 67-69] were proposed. By combining both ionic interactions and the chemistry of dopa, Kim, Hwang et al.[63] have disclosed the preparation of a very efficient adhesive sealant for urinary fistula. A “water-immiscible mussel protein-based bioadhesive” (WIMBA) was prepared by mixing the recombinant mussel adhesive protein (rMAP) fp-151 and hyaluronic acid (HA), as illustrated in Figure 4.

rMAP was prepared by *E. coli* expression hosting and the tyrosine residues were modified post-synthesis to dopa, by mushroom tyrosinase[63]. Overall, rMAP contained around 18 mol% of dopa residue. To form the coacervate adhesive (polyelectrolyte dense phase) by interpolymer electrostatic interactions, rMAP was mixed with HA with a weight ratio of 6:4 and pH>5.5. As in the mussel foot, curing and cross-linking of the adhesive was realized by dopa oxidation. To ensure fast curing, sodium periodate (NaIO₄) was added as catechol oxidant. Lap-shear tests were carried out underwater to measure the adhesive cohesive strength. Concentrations of 100mM of NaIO₄ and curing time above 6 h were necessary to obtain sufficient bulk cohesion of the adhesive.

Adhesion of the coacervate to aluminium was good ($G=0.88$ MPa) and was the highest to porcine skin (0.12 MPa) and rat bladder (0.14 MPa) in comparison to the 2-octyl cyanoacrylate and fibrin glue. The authors recognized that the dopa residues not only improved the adhesion to biological tissues through hydrogen bonding but also through covalent bonding with nucleophilic groups such as -NH₂, -SH, -OH and -COOH[63]. Finally, ex-vivo experiments showed that the developed WIMBA could seal punctured bladder and withstand intravesical pressure.

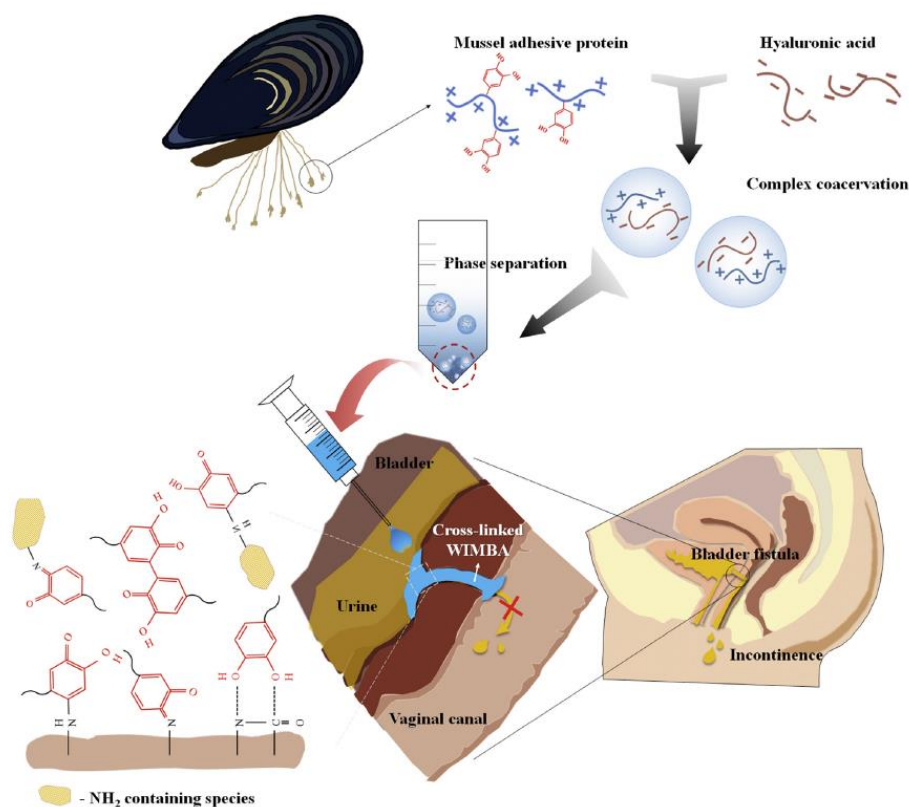


Figure 4. “Schematic representation of WIMBA, rMAP-based water-immiscible fluid bioadhesive, employed by the chemistries of dopa and complex coacervation for urinary fistula sealing.” Reprinted with permission from [63]. Copyright © 2015 Elsevier Ltd.

- Other metal-coordination bonds as reversible crosslinkers

The combination of metal-coordination and hydrogen bonding [70-72] has also been proposed to build metallocupramolecular polymers with interesting adhesive properties [73-79]. One example was obtained by introducing 2,6-bis(1'-methylbenzimidazolyl)-pyridine (Mebip) ligands in telechelic poly(ethylene-co-butylene) (PEB) and mixing with zinc (II) bistriflimide ($\text{Zn}(\text{NTf}_2)_2$) metal ions. The metallo polymer $[\text{Zn}_x(\text{Mebip-PEB-Mebip})(\text{NTf}_2)_{2x}]$ was compared with the same PEB modified with ureidopyrimidinone (Upy) motifs; which provide intermolecular hydrogen bonding for the final polymer (Upy-PEB-UPy) (illustration given in Figure 5[70]). Optimum coordination with the divalent zinc ion was obtained by mixing 0.8 mol of $\text{Zn}(\text{NTf}_2)_2$ and gave the polymer $[\text{Zn}_{0.8}(\text{Mebip-PEB-Mebip})(\text{NTf}_2)_{1.6}]$ [70].

Both metal-ligand and urea motifs acted as crosslinks for the rubbery PEB but at 25°C, $[\text{Zn}_{0.8}(\text{Mebip-PEB-Mebip})(\text{NTf}_2)_{1.6}]$ was much stiffer (higher tensile storage modulus) than Upy-PEB-UPy as the interactions are stronger. As the metal-ligands absorb UV light, it is transformed in heat and induce dissociation of the motif. Under exposure to UV light, the polymer can thus regain its flowing character. The reversible adhesion of $[\text{Zn}_{0.8}(\text{Mebip-PEB-Mebip})(\text{NTf}_2)_{1.6}]$ and Upy-PEB-UPy was thus measured by lap shear between quartz substrates. Bonding and debonding were enabled both by exposure to UV light and heat[70]. For $[\text{Zn}_{0.8}(\text{Mebip-PEB-Mebip})(\text{NTf}_2)_{1.6}]$, 2 min irradiation with 900 mW.cm^{-2} and 2 min at 200°C , were sufficient to obtain a shear strength $\sim 2 \text{ MPa}$. A UV-light absorber (Tinuvin 326) was added to Upy-PEB-UPy to make it UV-light sensitive. In this case, 2 min irradiation with 900 mW.cm^{-2} and 5 min at 80°C , resulted in a shear strength $\sim 1 \text{ MPa}$. So, in comparison to metal-coordination, hydrogen bonding provided weaker cohesive strength but, in both cases, debonding was possible in a few seconds using UV-light or heating.

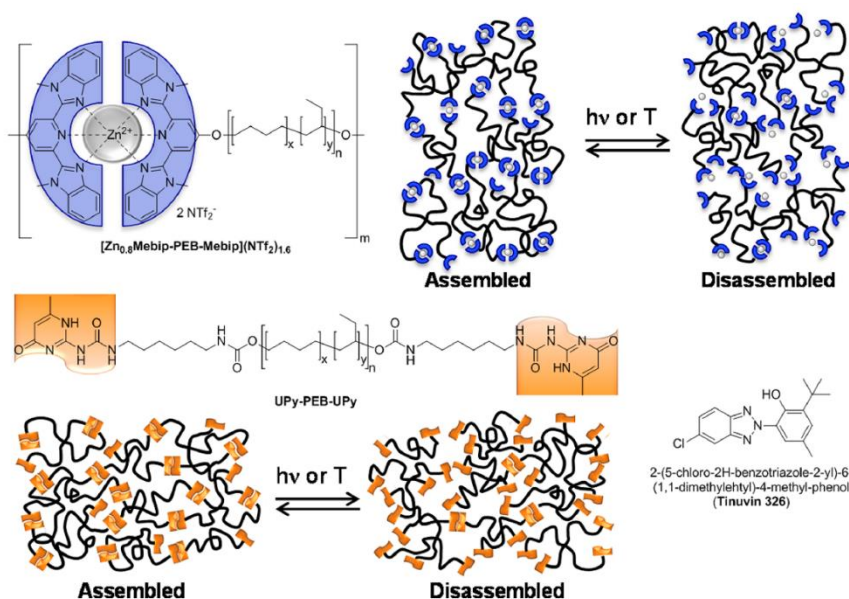


Figure 5. “Chemical structures for the components of the $[\text{Zn}_{0.8}(\text{Mebip-PEB-Mebip})(\text{NTf}_2)_{1.6}]$ and Upy-PEB-UPy supramolecular polymers, and the UV absorber (Tinuvin 326). Also shown are schematic representations of the stimuli-responsive assembly and disassembly of supramolecular polymers using light or heat.” Reprinted with permission of the ACS[70], further permissions related to the material excerpted should be directed to the ACS, <https://pubs.acs.org/doi/10.1021/am405302z>.

Further studies report the use of urea groups for crosslinking via hydrogen interactions [71, 72, 80-83]. Another publication by Weder's group proposes reversible interactions by modification with urea groups[72]. Macromonomers containing Upy groups were synthesized by first functionalizing 2-hydroxyethyl methacrylate (HEMA) with Upy but with hexamethylenediisocyanate (HMDI) as spacer. Varying amount of Upy-HMDI-HEMA monomers were copolymerized with hexyl methacrylate or butyl methacrylate to give poly(Upy-HMDI-HEMA-co-hexyl-MA) and poly(Upy-HMDI-HEMA-co-butyl-MA) polymers with different amount of crosslinker (0, 2.5, 5 and 10 mol%) as illustrated in Figure 6[72].

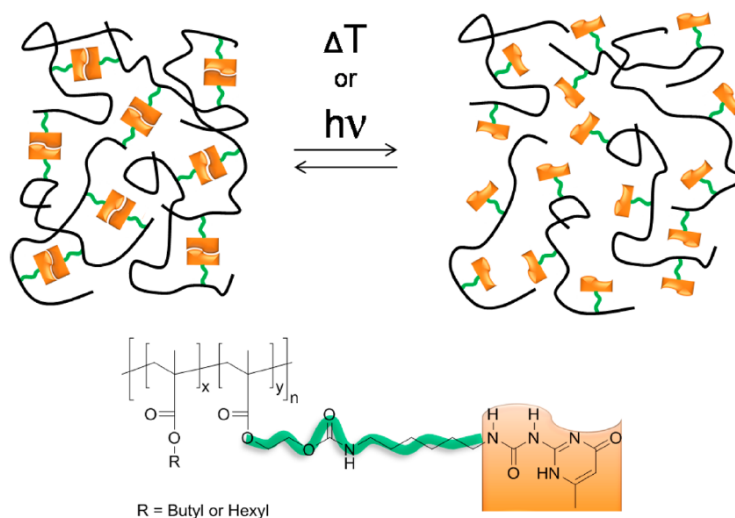


Figure 6. "Schematic representation of the heat or UV-light triggered disassembly of methacrylic copolymers functionalized with UPy side-chains from a crosslinked to a linear state (top). Chemical structure of the (co)polymers investigated in this study (bottom)" Reprinted with permission from *Supramolecular Cross-Links in Poly(alkyl methacrylate) Copolymers and Their Impact on the Mechanical and Reversible Adhesive Properties*, C. Heinzmann et al., *ACS Applied Materials and Interfaces*, 2015, 7, 24, 13395-13404[72]. Copyright © 2015 American Chemical Society

With Dynamic Mechanical Analysis (DMA), butyl-MA polymers were seen more rigid but both butyl-MA and hexyl-MA polymers showed dissociation of crosslinker at $\sim 100^\circ\text{C}$. The increase of Upy-HMDI-HEMA content increased the T_g and the polymers became glassy and the toughness increased; it was even more pronounced for butyl-MA polymers.

To investigate the reversible adhesion of the materials, lap shear tests were realized at different temperatures[72]. The shear resistance of poly(Upy-HMDI-HEMA-co-hexyl-MA) increased linearly with Upy molar fraction and the trend was kept at higher temperature. For 10 mol% of Upy, the resistance to shear was improved with increasing temperature. The results obtained for poly(Upy-HMDI-HEMA-co-butyl-MA) were mainly influenced by its glassy behaviour. The polymer with 0 mol% of crosslinker showed the best shear resistance as with higher content of Upy, the contact between the polymer and the substrate may be weaker. The lap shear tests did not fail from poor cohesive strength but rather from poor adhesive contact due to high stiffness and it was seen by adhesive failure of the tests. However, the values of shear resistance were still high and were maintained at for 40 and 60°C. At 60°C, the polymer itself was more viscous and the improvement of shear resistance with Upy content was seen. Finally, both poly(Upy-HMDI-HEMA-co-hexyl-MA) and poly(Upy-HMDI-HEMA-co-butyl-MA) showed debonding by heating above 80°C and could rebind to the substrate. The adhesion of the polymers crosslinked with Upy was fully recovered.

Another example of hydrogen bonding by urea was reported for acrylic PSA by Callies et al.[81]. bis-urea center-functionnalized poly(butyl acrylate) (PnBAX) were prepared by atom transfer radical polymerization. Two polymers were prepared with different number average molecular weight: PnBAX5 ($M_n=5.4 \text{ kg.mol}^{-1}$) and PnBAX8 ($M_n=7.5 \text{ kg.mol}^{-1}$). It was seen that the centred supramolecular motifs self-assemble to modify the viscoelastic properties of the polymers[80, 84]. In Callies's study[81], both hydrogen bonds and covalent crosslinks were introduced to balance viscoelasticity and favour energy dissipation for high adhesion. Copolymers of butyl acrylate and glycidyl methacrylate poly(butyl acrylate-co-glycidyl methacrylate) were synthesized; 1,5-amino-2-methylpentane was used as crosslinker to form covalent bonds by opening of the epoxy rings of glycidyl methacrylate moieties.

The ratio of epoxy groups was changed to increase the covalent crosslinking density: E4-PnBAX (3.5 epoxy groups per chain) and E7-PnBAX (7.1 epoxy groups per chain). A random poly(butyl acrylate-co-glycidyl methacrylate) E8-PnBA (not urea functionalized) was taken as comparison to observe the effect of supramolecular and covalent interactions on the mechanical and adhesive properties. Frequency sweeps measured in linear rheology showed that E7-PnBAX, E4-PnBAX and PnBAX5 exhibited viscoelastic behaviours with rubbery region $G' > G''$ and transition to flowing at low frequencies. PnBAX8 and E8-PnBA were more viscous and no rubbery region was observed. The work of adhesion W_{adh} of the materials were tested by probe-tack with a steel probe. Without addition of diamine, E4-PnBAX and E7-PnBAX showed already higher W_{adh} than PnBAX5 and PnBAX8 ($\sim 90 \text{ J.m}^{-2}$ for $\sim 30 \text{ J.m}^{-2}$), suggesting that the presence of glycidyl methacrylate monomer increased the stability of extended fibrils[81]. The role of diamine concentration over the adhesive behaviour was then studied and showed that when no supramolecular interactions were present (i.e. in E8-PnBA), the work of adhesion increased with diamine content as the polymer could sustain higher stresses. However, for urea containing polymers E4-PnBAX and E7-PnBAX, the addition of covalent crosslinks decreased the adhesion as they became too stiff[81]. The trend was even more pronounced for the longer acrylate chains E7-PnBAX. Observations of the contact area between the adhesive layer and the probe have shown the debonding mechanism goes from bulk cavitation to interfacial cracks.

The dynamics of supramolecular bonds are interesting for adhesion and can be implemented with covalent cross-linking; but it should be well balanced so that the mobility of the polymer chains still dominate the viscoelastic properties.

ii. Ionic interactions in adhesive systems

- The sandcastle worm's glue

Sandcastle worms are marine polychaete worms forming the Sabellariidae family. They mostly live in warm coastal regions of oceans on the shores. They assemble sand beads to obtain tube structures in which they live as seen in Figure 7[85]. The castles sustain the forces of the waves during high and low tides. Due to their architectural skills, the sandcastle worms have been widely studied and scientists have managed to identify the key elements of the worm's cement.

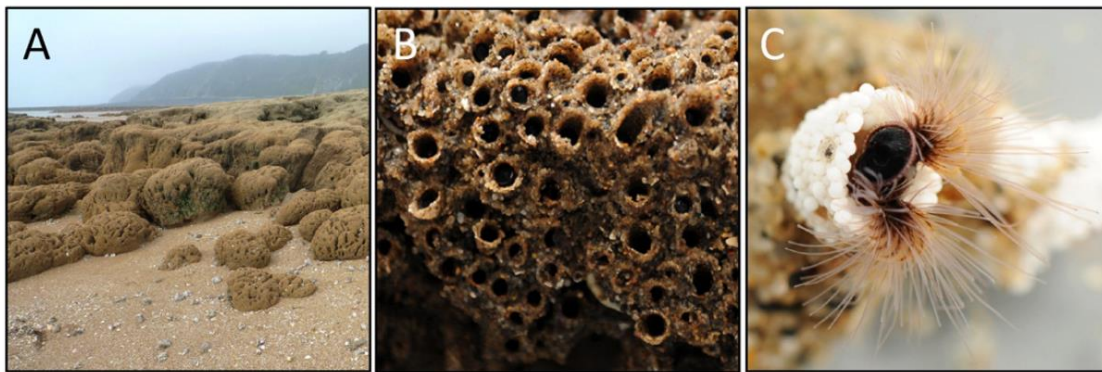


Figure 7. "Reef-building sabellariid tubeworms. (A) Lowtide. Dome-shaped colonies of *S. alveolata* (foreground) fuse into a tabular surface covering the beach. Photo courtesy of, (B) Close up view of a *P. californica* colony. Each tube was built by an individual worm. (C) A worm glues zirconium oxide beads onto the anterior end of its natural tube in a lab aquarium"

Reprinted with permission from [85]. Copyright © 2016 Elsevier B.V.

The worm secretes a glue thanks to a gland and can assemble the sand grains with a building organ. The secreting gland is formed of two types of cell producing two types of granules which are kept separated until secretion. Both homogenous and heterogenous granules are composed of densely charged macromolecules but the proteins involved differ[86-88].

Homogenous granules are made of sulphated polysaccharides, polybasic proteins (Pc2 and Pc5) and catechol oxidase. Heterogenous granules are more complex and are a formulation of polyphosphate proteins (Pc3B), polyampholyte proteins (Pc3A), polybasic proteins (Pc1, Pc4), Mg^{2+} and catechol oxidase.

The polybasic proteins Pc1, Pc2, Pc4 and Pc5 are mainly based on lysine (K), histidine (H), glycine (G) and tyrosine (Y) residues. For which the tyrosine residues are hydroxylated into dopa. Pc3B is composed mainly of phosphorylated serine (S) and dopa hydroxylated tyrosine residues, while Pc3A is formed from S, K, Y and arginine (R) residues[86-88].

While the glue is secreted in seawater of high ionic strength and $pH > 8$, it undergoes coacervation [85, 89]. It is a phase separation mechanism of polyelectrolyte solutions; resulting in a dense polymer phase and a dilute phase. The two phases state is usually reversible and equilibrium can be found back at the right conditions (of pH and ionic strength). In the case of the sandcastle worm, coacervation is triggered by complexation of the phosphorylated residues with Mg^{2+} and Ca^{2+} . The setting of the glue between sand beads is reached within less than a minute but further curing of the adhesive is allowed by covalent crosslinking between quinones catalysed by the catechol oxidase enzymes[90, 91].

- Ionic interactions for setting and cohesive strength underwater

The stiffness and efficiency of the sandcastle worm glue has inspired synthetic mimicking systems to design underwater adhesives based on the key feature of complex coacervation. The polymers involved in the phase-separation are usually water-soluble but the coacervate is not but remain processable for application.

An applicable water-borne adhesive was obtained by synthesizing polymers mimicking the interacting proteins of the sandcastle worm glue[92-95]. On one hand, a statistical copolymer of 88.4 mol% monoacryloxyethyl phosphate (MAEP), 9.7 mol% dopamine methacrylate (DMA) and 1.9 mol% acrylamide (Aam) was obtained as the polyacid Pc3B.

The polybase Pc1 was replaced by a copolymer based on Aam with various molar fraction of N-(3-aminopropyl)methacrylamide hydrochloride (APMA)[92]. Mixing the two polyelectrolytes with a stoichiometric ratio between phosphate and amine side-chains resulted in a pH dependent phase behaviour.

At pH below 5, the mixture formed a solution of colloidal polyelectrolyte complexes (PECs), phase separation was observed for $5.1 < \text{pH} < 9.5$ but cohesive coacervate phase were recognized only at pH=7.2 and 8.3. At pH=10, a liquid-phase was observed but it simultaneously formed a hydrogel by crosslinking through dopaquinone and primary amines. Complex coacervation was also obtained by introducing Mg^{2+} and Ca^{2+} divalent cations in the solutions; but was highly dependent on their concentration.

Coacervates were obtained for respectively high/intermediate amine to phosphate ratios and low/high cations to phosphate ratios[92]. The more stable coacervate phases were used to glue wet bones. The bond strength measured by the fracture stress in pure shear and underwater, was above 50 kPa and increased with the divalent ions fraction to 100 kPa. It was suspected by the authors that adhesion was improved by the interactions of dopa with the bone through electrostatic interactions and quinone-mediated covalent coupling; while cohesive strength was obtained by covalent crosslinking of dopa residues with the amine side-chains. To optimize the properties of the coacervate adhesive, a second network of polyethylene glycol-diacrylate (PEG-dA) was introduced and the research was reported in another publication[96]; the adhesive bonds were strengthened and the viscosity at high shear rate was lowered, making possible the application of such system through thine tubes like catheters. Even stronger adhesive bonds were reported for coacervates prepared from mixing poly(MAEP)-co-dopamide with a poly-aminated collagen hydrolysate[95].

Another mechanism of coacervation was investigated by Zhao, Lee et al. through solvent exchange[97]. They mixed in DMSO a cationic polyelectrolyte, a quaternized chitosan ion-paired with bis(trifluoromethane-sulphony)imide (Tf_2N^-) (QCS- Tf_2N), and a polyanion, a poly(acrylic acid) modified with catechols (30% mol, PAAcat).

In view of the dielectric constant of DMSO, the ionization of the polyanion is suppressed, thus allowing the mixing of both polycation and polyanion. They successfully deposited the mixture under water (Figure 8). As the water replaced the DMSO, the poly(acrylic acid) was ionized and allowed the coacervation to proceed to result in a fluidic complex. It was proven that the mixing of QCS and unmodified PAA resulted in poor adhesion, thus catechol groups played a role in the adhesion on the glass surface.

After a minimum setting time $t_s \approx 1.5$ min, the adhesion force obtained was $F_{\text{adh}} \approx 200$ mN but after $t_s > 1$ h, poor or no adhesion was found. The complex was stable under water, withstood water blasts depending on the setting time and re-immersion in DMSO, but could be removed by the rubber gloves.

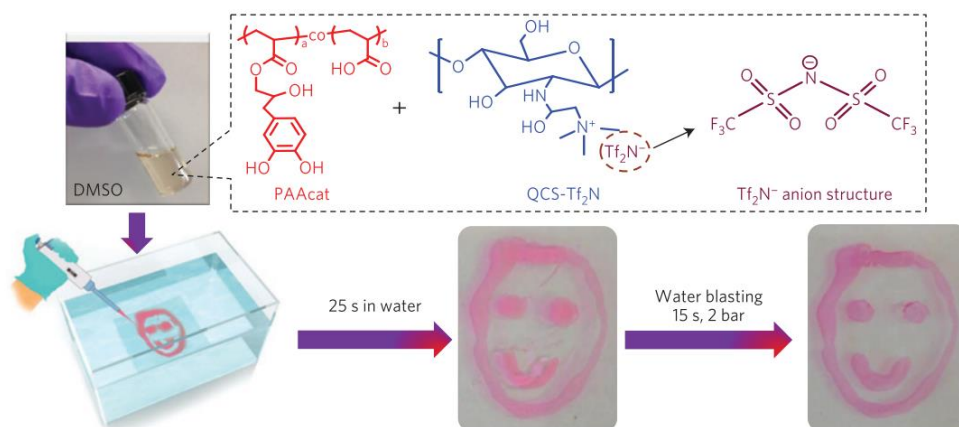


Figure 8. “Wet adhesion mediated by solvent exchange: from left to right: QCS- Tf_2N and PAAcat were dissolved in DMSO and the mixture was extruded onto a glass slide immersed in water. After setting 25 s in water (20°C, no applied pressure), adhesion to substrate withstood water blasting (2 bar, 15 s)” Reprinted by permission from Springer Nature: Nature Materials[97].

Copyright © 2016 Springer Nature.

Coacervation of an underwater adhesive can also be thermally induced as proposed by a recent publication[98]. Thermo-responsiveness was introduced by grafting of poly(N-isopropyl acrylamide) (PNIPAM) on poly(acrylic acid) (PAA) and poly(dimethyl aminopropylacrylamide) (PDMAA) chains; with a ratio between backbone and PNIPAM of 70:30. PNIPAM is known to collapse via physical interactions upon a certain lower critical solution temperature (LCST). The two oppositely charged polyelectrolytes were mixed in a 0.75 M solution of NaCl to control the coacervation induced by interactions of ionic charges.

Yet, phase transition was obtained by bringing the solution to temperatures above 35°C (above PNIPAM LCST) as displayed in Figure 9; the liquid and transparent solution stiffened and gave a white solid-like material. No transition was seen by mixing the homopolymers of PAA and PDMAA.

Rheological experiments have helped assess that the PNIPAM grafted coacervate heated at $T > 26^{\circ}\text{C}$, turned indeed into an elastic-like material as the cross-over frequency was decreased and both elastic and loss moduli increased. The underwater adhesion of coacervate prepared from the homo- and grafted polymers was tested using a probe-tack. At 20°C , both systems showed no resistance to strain due to their fluid-like behaviours and no adhesion could be measured. The same was observed at 50°C for the homopolymer coacervate; however, the PNIPAM grafted material could sustain higher stress and elongation thanks to the collapsed PNIPAM clusters. The work of adhesion W_{adh} thus reached $\sim 1.7 \text{ J.m}^{-2}$ with both anionic and cationic probe surfaces. High adhesion ($W_{\text{adh}} \sim 3.5 \text{ J.m}^{-2}$) was also obtained on glass and poly(tetrafluoroethylene) surfaces.

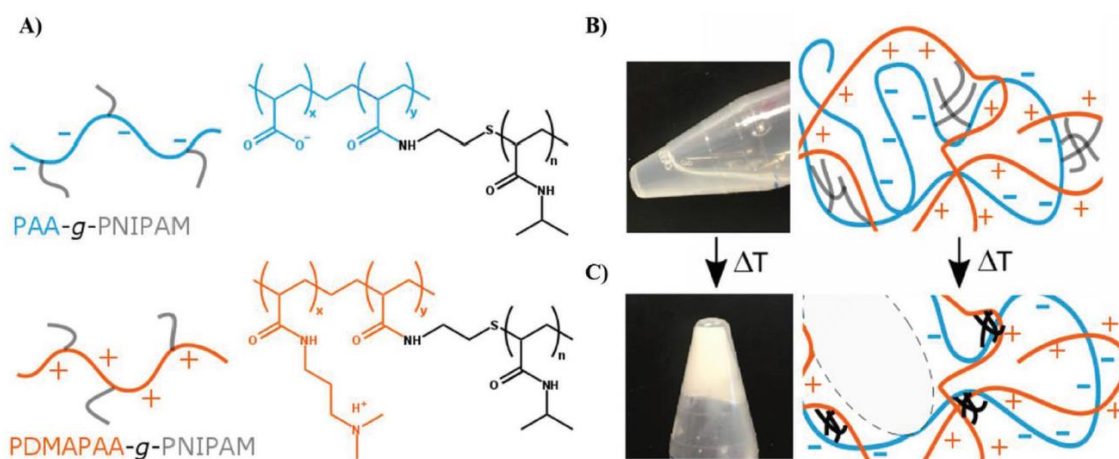


Figure 9. “Composition and temperature responsiveness of the complex coacervate phase. A) Molecular structure of PAA-g-PNIPAM and PDMAA-g-PNIPAM. B) Picture and schematic representation of the complex coacervate structure below the LCST. C) Picture and schematic representation of the solidification triggered by increasing the temperature above PNIPAM LCST.”

Reprinted with permission from Open Access of [98]. Copyright © 2019 Wiley-VCH.

The adaptability and performance of the PAA-g-PNIPAM/PDMAA-g-PNIPAM coacervate makes it a promising material for injectable adhesive. Thanks to the inspiration given by the sandcastle worm, adhesives for medical applications such as embolitic agent[99], suture of foetal membrane[100] and healing of bone defects[101] have emerged.

- Ionic interactions as physical crosslinks

In most research, the use of ionic interactions for adhesives relate to underwater and biological adhesives. However, a few examples exist where ionic interactions have been used as physical crosslinkers for PSAs, as shown by Feldstein and his group[102-104]. They were the firsts to study the viscoelastic and adhesive properties of polyacid and polybase blends. The polybase was prepared from the tertiary amine N,N-dimethylaminoethyl methacrylate (DMAEMA), methyl methacrylate (MMA) and butyl methacrylate (BMA) with a 2:1:1 molar ratio, giving PDMAEMA-co-MMA-co-BMA.

The polyacid was synthesized from the copolymerization of methacrylic acid (MAA) and ethyl acrylate (EA), with a molar ratio 1:1 giving PMAA-co-EA. Triethyl acetate (TEC) was used as plasticizer. The structures of the 3 components can be found in Figure 10. The polybase and polyacid were individually liquid-like polymers and were blended to obtain interpolymer complexes from interactions between the oppositely charged ionic groups. PDMAEMA-co-MMA-co-BMA was considered as the film-forming polymer and PMAA-co-EA as the crosslinker. The crosslinked structure expected by the authors is given in Figure 11.

Different phase behaviours were observed for compositions of the blends. Blending with a 1:1 concentration ratio gave separation of sol and gel fractions. Non-stoichiometric blends gave so-called "scrambled egg" structure and according to the authors, the best polymer conformation to optimize a ratio between free volume of the polymer chains and intermolecular cohesion. No adhesion was found for the stoichiometric blend and research was continued for the blends with polybase:polyacid ratios 20:1 and 10:1.

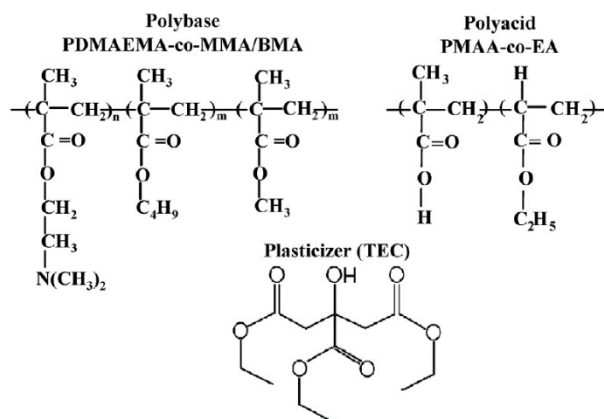


Figure 10. Chemical structures of PDMAEMA-co-MMA-BMA, PMAA-co-EA and TEC. Reprinted and adapted with permission from [102]. Copyright © Wiley Periodicals, Inc.

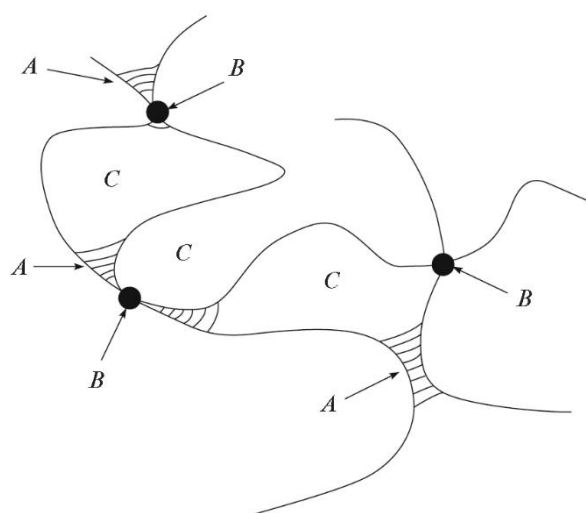


Figure 11. Crosslinked structure of the polymer network via interpolymer complexation. Zone A represents non-covalent crosslinks consisting of sequences of hydrogen, electrostatic or ionic bonds.

Zone B represents the entanglements points and zone C the loops of polymer segments. Reprinted by permission from Springer Nature: Polymer Science, Series A[102-104].

Copyright © 2009, Pleiades Publishing, Ltd.

Under uniaxial stress (tensile tests), the polybase alone showed liquid-like behaviour but the 10:1 blend (polybase:polyacid) with 25 wt% of TEC showed increased resistance to stress and a yield point suggesting the intermolecular cohesion was improved; PMAA-co-EA thus acted as a crosslinker due to local ionic complexations. By adding more plasticizer, the elasticity of the polymer was shielded as more free-volume was “created” in the network.

The adhesive behaviour of the blends was analysed by probe-tack and a similar trend was observed. With 25 wt% TEC, the work of adhesion decreased inversely with PMAA-co-EA content as the polymer was strengthened and the elongation of fibrils lowered. Increasing TEC content to 35 wt% increased the work of debonding W_{deb} by 5 for the 20:1 blend plus cohesive failure was seen, which signifies free volume was predominant. W_{deb} increased by 10 for the 10:1 blend but adhesive failure was observed.

The best adhesive performance (i.e. optimization between free-volume and intermolecular strength) was measured for the 10:1 blend with 50 wt% plasticizer. Cohesive strength was further doped by causing ionization of the ionic groups by adding an acid (hydrochloric acid HCl) or a base (sodium hydroxide NaOH). According to the authors, improvement of the adhesive properties was seen as the crosslinker points (ionic complexes) were strengthened and “free” groups of the same charges were contributing to the free-volume via electrostatic repulsion of the polymer chains.

Academic research has shown the high potential of using ionic interactions for their mechanical and adhesive properties in different applications: bio, electro-conducting and stimuli-responsive adhesives. This thesis aims to report methods of preparation of ionically crosslinked adhesives. This kind of PSA is fairly uncommon (except for studies realized by Feldstein and his group) and is, to the author’s knowledge, not available in the industry. Therefore, in this thesis, the ionic crosslink points are brought by introducing oppositely charged functional groups in a polymer, as proposed by Feldstein[102]; the crosslinks are then formed by electrostatic interactions during the film formation. Although, the blending of polyions has shown interesting features to balance the cohesive strength and “free-volume”, for this project it was chosen to introduce both anionic and cationic charges in the same polymer as a single product. Therefore, the link between polymer structure and mechanical properties of the adhesive films were investigated as well as their aptitude for an improved adhesion-cohesion balance.

D. Synthesis of PSAs

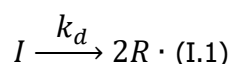
Two types of chain-growth polymerization were used in this project and are hereby introduced; but as mentioned previously, very few literatures report the preparation of polyampholytes for PSAs. Although the functional monomers (ionic) used in this PhD are commercially available, they are usually used for other applications (cosmetics, stabilizers, flocculants, rust prevention...) and thus in other conditions. Also, the literature describing the syntheses of highly charged polyions may not be relevant as in this work, the weight content of charged group doesn't exceed 15 wt% of an acrylate-based polymer. Therefore, the specific systems described in this work cannot be theoretically introduced, the following paragraphs summarize general knowledge on free radical solution polymerization and emulsion polymerization.

iii. Free radical polymerization

Free-radical polymerization is one of the most used method to synthesize polymers[105]. In this technique, the addition of monomers to the polymer chains is carried out by opening of a double bond. The reaction can progress as with each addition of monomer, a new radical active site is produced. The mechanism of free-radical polymerization involves three steps: initiation, propagation and termination[105-108].

- Initiation:

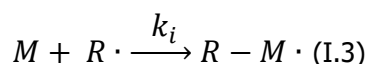
During initiation, radicals are produced by the decomposition of the initiator, with a decomposition rate k_d as followed:



The decomposition can be induced thermally or by red-ox reaction. The rate of the radical production can be calculated from:

$$\frac{d[R\cdot]}{dt} = 2 k_d [I] \quad (I.2)$$

The radicals formed then initiate a polymer chain by reacting with a monomer unit with an initiation rate k_i ; creating a new C-C bond and another active site:

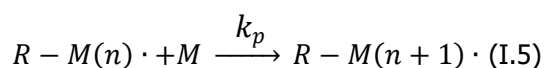


The rate of initiation can thus be written:

$$R_i = 2 f k_d [I] \quad (I.4)$$

- Propagation:

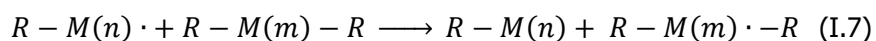
During propagation, the polymer chains grow by successive addition of monomer units with a constant rate k_p and the rate of propagation is then given by R_p .



$$R_p = k_p [M\cdot] [M] \quad (I.6)$$

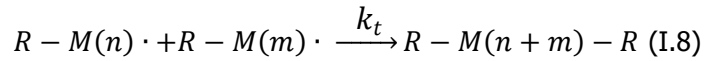
$[M\cdot]$ represents the concentrations of radical chains in the reaction.

Free polymerizations are in most cases not perfectly linear and transfer to polymer can occur anywhere in the chains if sites are available to radical formation:



- Termination:

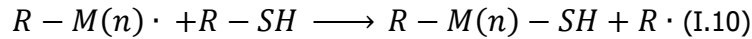
Once all the monomers are converted, termination of polymer chain can either occur from coupling with a free radical from the initiator and/or by combination with another growing polymer chain:



The termination rate constant is thus given by k_t and the rate by R_t :

$$R_t = 2k_t[M \cdot]^2 \quad (I.9)$$

Termination and propagation can become competitive mechanisms, and if so, polymer chains of small molecular weight will be obtained. In regular cases, the average molecular weight can be adjusted by changing the reaction temperature and the amount of initiator. It can also be controlled by adding a chain transfer[109] agent (CTA, e.g. mercaptans) which terminates a growing chain and releases another radical:

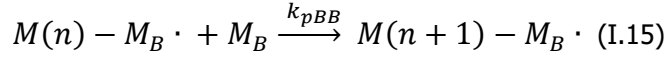
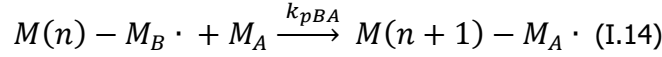
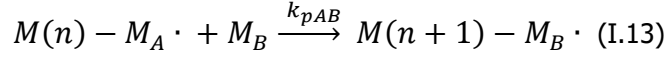
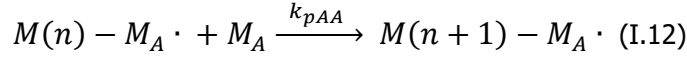


The number average degree of polymerization[110] indicates the number of monomer introduced in the polymerized chains. It is calculated from the ratio between monomer consumption rate and production of polymer chains:

$$\overline{DP}_n = -\frac{d[M]}{dt} / \frac{d[polymer]}{dt} \quad (I.11)$$

Copolymerization of monomers complicates the system. Each monomer has its own reactivity to the system[107, 111, 112]. The polymerization depends thus on the reactivity of each monomer towards themselves and to the comonomers.

The propagation in a two monomers system can thus be summarized as:



The rate of copolymerization under a steady-state is then given by [112, 113]:

$$R = \frac{(r_A[M(n)M_A \cdot]^2 + 2[M_A][M_B] + r_B[M_B]^2)R_i^{1/2}}{(r_A^2\delta_A^2[M_A]^2 + 2\phi\delta_A\delta_B r_A r_B[M_A][M_B] + r_B^2\delta_B^2[M_B]^2)^{1/2}} \quad (\text{I.16})$$

By defining the reactivity ratios of a monomer as r_{ii} and termination ratio as δ_{ii} :

$$r_i = \frac{k_{pii}}{k_{pij}} \quad (\text{I.17}) \quad \text{and} \quad \delta_i = \frac{k_{tii}^2}{k_{pii}} \quad (\text{I.18})$$

The reactivity ratios are determinant for the conversion and composition of the final polymer.

If the reactivity of one or both monomers is too high, it is likely that no statistical copolymer will be formed.

Perfectly statistical co-polymers are obtained if each monomer propagates preferentially with the other than with itself. Random copolymers are produced if the reactivities of all monomers are close to 1 and the addition of one monomer to a chain is statistical.

iv. Emulsion polymerization

Polymer dispersions have become nowadays important materials to prepare coatings, inks, primers, adhesives, flooring... and represent around 4% of the total polymer production[114]. Syntheses by emulsion polymerization have become popular as they are more environmentally friendly, can reach high conversions and can produce polymers of high molecular weight with an efficient energy input and low viscosity. It is also a versatile technique as many monomers can be used but also different particle sizes and morphologies[115, 116] can be obtained to vary the end-polymers properties.

The polymerization follows the free-radical polymerization and the three main intervals of reaction[114, 117-119]. The initiator decomposes and initiate the reaction in the water phase. As the oligo-radicals become insoluble in water with increasing molar mass, they migrate inside the emulsifier micelles and polymer particles are formed.

Diffusion of monomers through the water-phase from reserve droplets, allow further polymerization as illustrated in Figure 12.

The polymerization requires that the monomer(s) are slightly soluble in water for the initiation step but also for the propagation.

Although, the surfactant provides stabilization to the polymer particles [114, 117], either by steric hinderance or by electrostatic repulsion, a minimum amount should be used to reach micellization. This is known as the critical micelle concentration (cmc). With concentrations above cmc, the number of micelles increases and free surfactant might be available for adsorption on growing particles. However, the amount of available surfactant influences the particle size as the more amphoteric species there are, the higher can be the stabilized surface and the smaller can be the particles. To have even higher control of the particle size, a seeded polymerization can be carried out. The seed is added to the initial charge to have pre-formed particles of narrow size distribution. They constitute then the nucleation site of the polymerization.

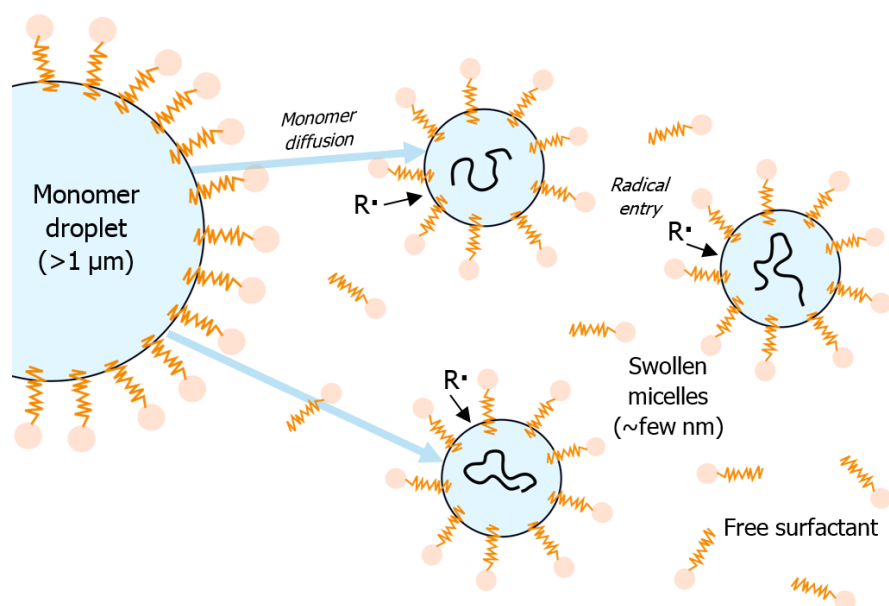


Figure 12. Scheme of emulsion polymerization inspired from Urban & Takamura[114].

Adapted with permission. Copyright © 2003, Society of Chemical Industry

E. Testing adhesion of PSAs

Several tests have been developed for measuring the adhesive performance of PSA, mainly by measuring the detachment force. The sample preparation, the relevant adhesion tests and the main adhesive failures are introduced in the following paragraphs.

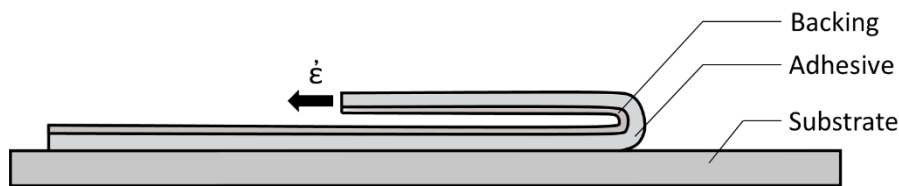
i. Sample preparation

In Peel and Shear tests, the PSA is coated with a specific thickness (\sim hundreds μm) or grammage ($\sim 10\text{-}100 \text{ g.m}^{-2}$), on backing materials (paper, PET, PP, PVC, non-woven textiles...). To obtain the desired thicknesses, coatings are made with doctor blades. The films are then cured with heat (oven) for a few minutes, a protective silicon sheet is applied, and the film is stored under controlled humidity and temperature. The final samples are typically cut into strips of 2.5 mm width and around 20 cm length.

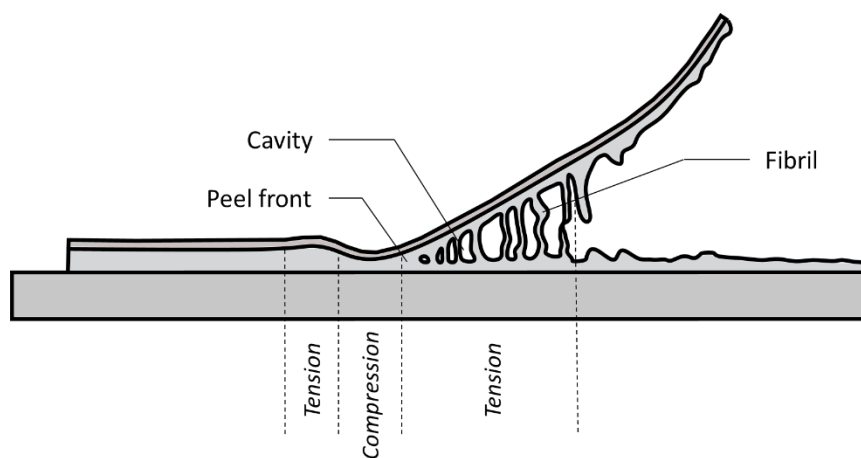
For probe-tack tests, the adhesives are coated on glass microscope slides with adaptable doctor blades; to thicknesses of around 50-200 μm . Curing is also carried out by heat in an oven and the coated glass slides are protected from dust deposition by storing in boxes or with protective silicon sheets.

ii. Peel test

Peel tests are realized by applying a sample strip on a clean substrate (steel, glass, polyethylene, rubber, PVC...). A certain application force is applied ($F_c \sim 2 \text{ kg}$) to ensure repeatable contact formation between the adherends. After a certain contact time t_c (i.e. dwelling time), the strip is peeled off with a tensile machine, at a certain angle (90 or 180°) and cross-head velocity at a given strain rate $\dot{\epsilon}$, as illustrated in Figure 13. The peel force F is recorded by the load cell and represents the resistance of the adhesive bond towards debonding.

Figure 13. Illustration of Peel 180°

The removal of the adhesive creates a peeling front and an uneven distribution of the normal stress in the adhesive layer as summarized in Figure 14.

Figure 14. Illustration of peeling of PSA

The maximum stress is recorded at the peel front, Kim et al.[120] also refer to this region as the boundary of the bond, because the debonding is localized in this area. However as the PSA backing is rather flexible and because the adhesive layer is dissipating energy, a compressive transition zone is observed (as seen in Figure 14). The dissipation of the energy starts by cavitation at the bond boundary, when the strain increases, and the compliance of the adhesive allows it, fibrils form and elongate under normal stress. This means that when measuring peel, we don't only measure the adhesive resistance to debonding but also the resistance of the backing and the adhesive to deformation.

The adhesive fracture energy G_c can be described by[120]:

$$G_c = G_0 + \Psi \quad (\text{I.19})$$

Where G_0 is the energy required to propagate a crack and Ψ is the viscoelastic energy dissipated by the adhesive and the backing. When considering the dimensions of the peel measurement, the fracture energy G can be written as follows, with F the adhesion force, b the width of the PSA and θ the peel angle:

$$G_c = \frac{F}{b} (1 - \cos \theta) \quad (\text{I.20})$$

The final value obtained from a measurement is usually given in N.inch^{-1} or N.25 mm^{-1} .

iii. Shear test

Shear test measures the resistance of the PSA to a steady load and records the time needed to obtain fracture of the adhesive bond. It is a way to determine the creep behaviour of the polymeric material under shear stress. This information is crucial in applications where the adhesive joins two objects and one of them is loaded for an unlimited time during application, for example in construction. For these purposes, PSA can also be reinforced with structured fibres or fillers like silica particles.

To measure the shear strength (i.e. holding power, time needed to obtain bond fracture with a certain shear load), the PSA is applied over a specific area (usually 1 inch \approx 2.5 cm) to connect two surfaces together. One surface is attached to an immobile bench, the other bears a load with a weight that is adaptable, as illustrated in Figure 15.

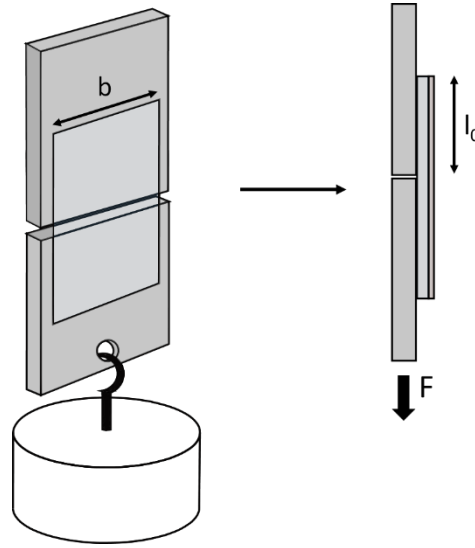


Figure 15. Illustration of the shear test with associated parameters

During the measurement the weight applies a constant shear force F to the maximum adhesive area A_0 which result in a displacement of a given point in the adhesive layer of Δl , and the shear strain ε is then given as followed with d the thickness of the adhesive[121]:

$$\varepsilon = \frac{\Delta l}{d} \quad (\text{I.21})$$

While shear stress σ is defined as[121]:

$$\sigma = \frac{F}{A} \quad (\text{I.22})$$

When the adhesive moves away from its original position l_0 , the area of contact changes as function of displacement Δl , giving a new contact area A [121]:

$$A = A_0 \left(1 - \frac{\Delta l}{l_0}\right) \quad (\text{I.23})$$

To obtain the evolution of the shear stress according to time, and observe the cold flow of the polymer, the displacement can be measured by a linear differential transducer as explained by Zosel[122] and σ is calculated with equation (I.22).

iv. Probe-tack

Probe-tack measurements are not systematic in industry but present some advantages like removing the effect of backing and controlling the strain history of the sample. In a probe-tack test a cylindrical probe is brought into contact with a layer of adhesive coated on a microscope slide[123]. The surface of the probe is flat and the alignment between probe and adhesive surfaces is adjusted to optimize their maximal contact area A_{\max} (cannot be higher than area of the probe). A certain compression force can be loaded onto the adhesive and after a certain contact time t_c , the probe is detached at a constant debonding velocity V_{deb} . The Force F needed to detach the probe and the displacement Δl are recorded. A stress-strain curve is obtained from calculating the nominal stress σ_N and the strain ε , as followed[124]:

$$\sigma_N = \frac{F}{A_{\max}} \text{ and } \varepsilon = \Delta l / l_0 \quad (\text{I.24})$$

The final value of adhesion is extracted from the area under the curve and thus gives a work of debonding W_{deb} [124]:

$$W_{\text{deb}} = h_0 \int_0^{\varepsilon_{\max}} \sigma(\varepsilon) d\varepsilon \quad (\text{I.25})$$

Usually a camera is placed underneath the glass plate to first calculate the actual contact area between the adhesive and the probe but also to observe the macroscopic debonding mechanism. The microscopic understanding of the debonding process is given by the dependence of the stress on the strain.

Three main behaviours can be recognized: viscous flowing, partially crosslinking and brittleness. The typical curves are displayed in Figure 16. The relevant parameters extracted from the stress-strain curves can be found in Figure 17.

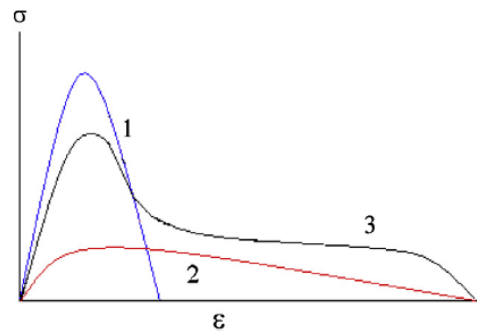


Figure 16. Typical probe-tack curves for brittle(1), partially crosslinked(2) and viscous(3) polymers.

Reprinted with permission from [103]. Copyright © 2014 Elsevier Ltd.

- Pure viscous materials exhibit a low peak stress written σ_{peak} or σ_{max} but is followed by a gradual decrease until the force recorded approaches zero with high elongation.
- Brittle materials show only a stress at peak because they bear more load which is usually high and the stress sharply decreases to zero $\sigma_{\text{peak/max}}=0$ Pa for low maximum elongation ϵ_{max} .
- For partially crosslinked materials, a stress peak is also observed but after the stress stabilizes to a plateau σ_{plateau} , elongation increases until fracture or detachment is obtained.

For the 3 cases the values of W_{deb} might be similar and it is why it is almost more important to take a look at the stress-strain curves in Probe-tack rather than the adhesive value obtained. The peak stress and plateau stress have been explained by observation of the adhesive layer during debonding.

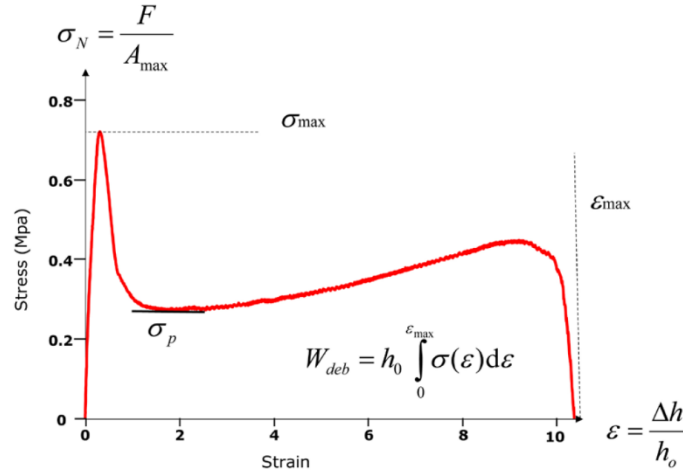


Figure 17. Typical stress-strain curve obtained in probe-tack test and definition of the various parameters that can be extracted[123]. Copyright © IOP Publishing. Reproduced with permission. All rights reserved. <https://iopscience.iop.org/article/10.1088/0034-4885/79/4/046601>

During the removal of the probe (as illustrated in Figure 18 and Figure 19), first cavitation is observed inside the adhesive layer (Figure 19 image C). On the stress-strain curve, this event corresponds to σ_{peak} (σ_p). This last gives an indication of how compliant is the polymer to cavitation.

The cavities can form from existing air pockets trapped in the surface roughness of the probe and between the adhesive layer but also in the bulk of the adhesive layer. In the case of PSA, their rather low elastic modulus G' allow them to be deformed enough to undergo cavitation but the cavities growth is highly dependent on the polymer network. Indeed, with further pulling of the probe, the cavities deform, as explained by Creton and Shull[125], if the released elastic energy G is higher than the critical energy release rate G_c .

When the Young's modulus E and the elastic modulus G' of the adhesive are low enough, the cavity will grow in the bulk and with further applied strain, fibrils will form from the cavity wall (Figure 19 image A). In another case where E is high, $G' > G_c$ and that the local dissipation energy rate is too low, the cavities will grow at the interface between the two adherends and detachment will take place with cracks as seen in Figure 19 image B.

The cavitation and fibrillation mechanisms are thus dependent on the mechanical properties of the polymer and will be discussed in paragraph I.2.G.

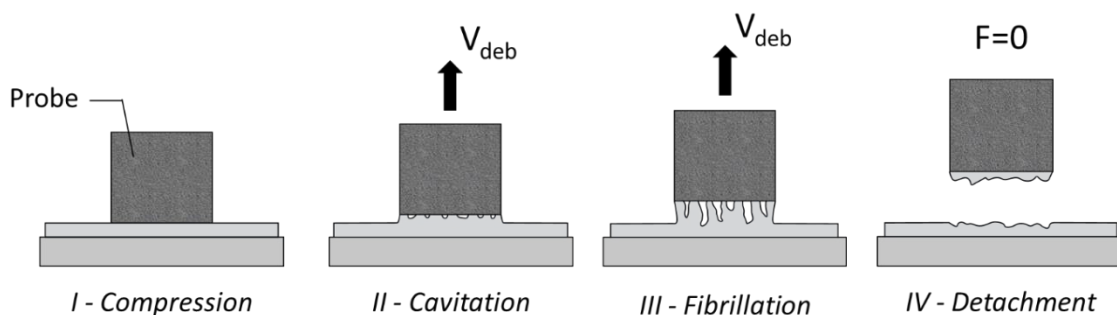


Figure 18. Illustration of the different stages of Probe-tack test

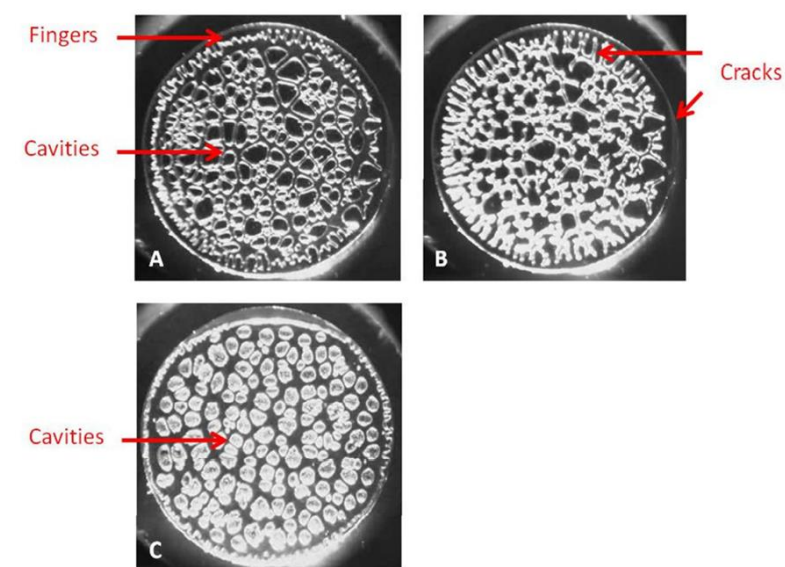


Figure 19. Images of detachment of the probe from an adhesive layer (view below the adhesive).

Reprinted with permission from Combined Effect of Chain Extension and Supramolecular Interactions on Rheological and Adhesive Properties of Acrylic Pressure-Sensitive Adhesives, ACS Applied Materials and Interfaces, 2016, 8, 48, 33307-33315[81]. Copyright © 2016 American Chemical Society.

v. Adhesion failures

Failure modes give valuable information and are relevant in adhesive testing. The failure mechanism gives information on the limiting parameters of an adhesive and helps to optimize the formulations and/or chemistries. Three main failure modes can occur: Adhesive A, Cohesive K and Glassy G. An illustration of those is given in Figure 20.

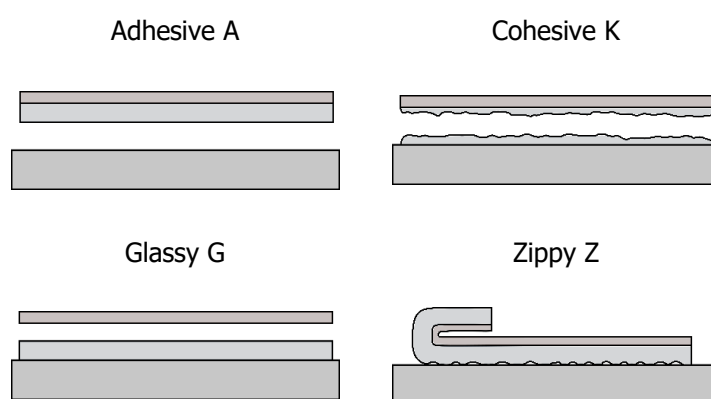


Figure 20. Illustration of adhesion failure modes

Adhesive fracture A: Fracture between the interface of the two adherends suggests poor interfacial interaction and results in a so-called adhesive failure.

Glassy fracture G: It takes place at the interface between adhesive and backing if the adhesive shows higher affinity with the substrate or if the polymer layer is too stiff and didn't wet the backing properly during film formation.

Cohesive fracture K: It occurs inside the adhesive layer. In that case, it is likely that proper contact with substrate and backing is reached but the adhesive exhibits poor structural solidarity.

Zippy failure Z: It is observed in peel tests when extremely poor or at least very inhomogeneous interaction with the substrate takes place.

F. Adhesion theory of PSAs

The adhesion mechanisms described in I.1.B. suggest certain requirements for adherence to take place. Tackiness (i.e. stickiness) is not sufficient to describe the behaviour of PSAs[126-128]. PSAs are viscoelastic materials and while they can bear functional groups to influence interfacial interactions, the wettability and viscoelastic mechanism are the most relevant to describe adhesion of PSAs.

Tackiness of the polymer is provided mainly by its glass transition temperature (T_g) and the polymer chain mobility. They are necessary to form fast and good contact with one substrate. However, materials owning high tack are usually very viscous and present no resistance to debonding. This compliance can be counteracted with a moderate elasticity; in this way the polymer can deform to higher elongation and dissipate higher levels of energy during debonding[128].

Better understanding of the viscoelastic parameters influencing the adhesion and obtain their direct relation, has been the goal of different studies throughout the years. Feldstein and his group have developed a model system[103, 104, 129] to understand the relation structure-properties of the PSAs viscoelasticity. They showed the direct linearity between the peel force and the work of deformation measured by uniaxial elongation; which gives[103,128]:

$$P = k \cdot b \cdot l \cdot \int_0^{\varepsilon_b} \sigma \cdot d\varepsilon \quad (I.26)$$

With b the width, l the thickness of the adhesive layer, σ the stress, ε the elongation and k the constant relative to the backing layer and which was approximated to 1. It thus appears the peel is a direct measurement of a stress over the strain.

Furthermore, considering the linear elastic law, the peel force can be written as[128]:

$$P = \frac{b \cdot l \cdot \sigma_b^2}{4E} \quad (I.27)$$

With σ_b the stress measured at the point of fracture during debonding and E the Young's modulus. This relation given by Feldstein[103, 104, 129] is similar to the one reported by Kaelble[130-133]; who studied the mechanics involved in the peeling of a PSA. He recognized that different stresses were involved in the process: tensile, compressive and shear stresses. The tensile stress is usually predominant as fibrils undergo high elongation and the polymers can show high strain-hardening. He also showed that the peel force is dependent on the systems dimension.

PSAs are viscoelastic materials and respond to the Maxwell law. This law predicts that the polymer can be considered as an installation in series of a pure viscous and a pure elastic polymer. From this law, the Young's modulus can be written as a ratio between the viscosity η and the relaxation time τ [128]:

$$E = 3 \cdot \frac{\eta}{\tau} \quad (I.28)$$

But the viscosity of a reptating (i.e. flowing) polymer can directly be expressed with the self-diffusion coefficient D of one polymer chain following Brownian motion[128]:

$$\eta = \frac{kT}{D \cdot a \cdot N} \quad (I.29)$$

With k the Boltzmann constant, T the temperature, N the number of monomer units in the chain and a their size. The peel force can thus be written as followed[128]:

$$P = b \cdot l \cdot \frac{a \cdot D \cdot \tau}{3kT} \cdot \sigma_b^2 \quad (I.30)$$

In equation (I.30), the dependence of the peel on the materials viscoelastic parameters is clear: the self-diffusion parameter D , the relaxation time τ and the elasticity measured by σ_b . The diffusion is a direct measure of the movement available to the polymer chains, and D can be written[134, 135]:

$$D = A \cdot e^{-B/f_v} \quad (I.31)$$

With A and B constants and f_v the free volume fraction, which represents the unoccupied (by the polymer chains) volume.

Deducing from the relation in (I.31), a high peel would be favoured with high mobility of the polymer chains (i.e. high f_v), as it would provide tackiness. A high peel would also require long τ and high σ_b which are given by restricting the polymer chain movements with crosslinking and are thus conflicting with the free volume. A delicate balance between these properties should thus be fulfilled to optimize the adhesion of a PSA.

G. Mechanical properties and viscoelastic behaviour of PSAs

In this section, the connection between the adhesive and mechanical properties of a PSA is discussed. We hereby differentiate between bonding and debonding events. Bonding refers to the formation of the contact between adhesive and substrate, this stage involves a variety of characteristics (both chemical and mechanical) of the adhesive polymer. Debonding refers to the removal of the adhesive from the substrate. This step involves the viscoelasticity of the polymers, their deformability and dissipative features.

- Bonding stage

The formation of good contact between adhesive and substrate depends on interfacial interactions, contact time t_c , contact force F_c , the roughness and viscoelastic properties of both adherends. In most cases, the substrate has an infinite toughness in comparison to the adhesive and is not considered, while dependence on t_c , F_c and roughness actually derive from the mechanical properties of the adhesive.

The deformations involved in a bonding process are small and fall within the linear viscoelastic regime of the polymer. For this reason, only the relationship between adhesion and linear rheology measurements in dependence of frequency is discussed. Zosel[136] has shown that the elasticity of the polymer network have a high influence on the bonding behaviour and thus on tack. If the shear modulus G is increased, the fracture energy (from tack measurement) is dependent of the surface roughness because the indentation depth is changed due to the low compliance (high G) of the polymer. For a softer polymer (lower G), the dependence of adhesion on roughness surface is not sharp but in both cases the contact time is crucial for better bonding.

Zosel[136] has shown that the fracture energy G_a (i.e. energy required to separate the two adherends) is proportional to the relaxation modulus G^{-1} and that full contact should be attained with contact times superior to the relaxation time of polymer samples. The relaxation time τ in linear rheology corresponds to the time required by the adhesive to fully relax after application of a shear stress with a certain amplitude.

It is given by the inverse of the cross-over frequency ω_c to flowing region (i.e. when storage G' and loss G'' moduli are equal). As $\tau = 1/\omega_c$, the characteristic can be referred also as ω_c .

Another work of Zosel[137] has shown the same dependency with covalent crosslinking. If the crosslinking density is increased, the ability to come in contact with the adherend by viscous flow decreases and G_a is lowered.

The ability of the adhesive to adapt to the substrate's roughness has been given by Dahlquist with the Dahlquist criterion and can be related to the tackiness of the adhesive. The elastic plateau modulus G' should be lower than 3.3×10^5 Pa. Above that value, the bonding cannot be optimum. This value only considers a certain contact time, the Dahlquist criterion should be fulfilled for the bonding frequency of 1 Hz, which refers to a time of contact of 1 s and at 25°C.

vi. Debonding stage

During the debonding stage, the constraints put on the material are mainly tensile strains, and resistance to those will be mainly governed by the mechanical features of the polymer both in linear and non-linear regimes.

The viscoelasticity of PSAs was studied by Zosel[137]. The elastic and loss moduli (respectively G' and G'') were varied by crosslinking density and the effect on tack and peel strength was measured. For a starting soft PSA (non-crosslinked and low T_g for high tack) the sample showed a viscous behaviour in dependence of angular frequency ω with $G' < G''$, G' being proportional to $\sim \omega^2$ and $G'' \sim \omega^1$. Afterwards G' increased gradually with the crosslinking density with the formation of a covalently bonded polymer network. At the gel point, $G' \approx G''$ as the storage of energy by the polymer is favoured thanks to the network. When the network becomes even tighter, the storage modulus G' becomes independent of ω and the dissipative behaviour of the material becomes irrelevant in comparison its high elasticity $G' > G''$.

The peel strength was seen to increase and fail cohesively until the gel point, then be constant until G'' was maximal. The optimum tack was obtained between those two points, until $G' > G''$ the stress-strain curves showed the plateau for fibrillation[137]. Yet until $G' = G''$, we can consider that the material will relax in the time-frame of the contact time t_c and that full/optimum contact between the two adherends is obtained. It thus suggests that the increased crosslinking density in that range influences the fibrillation in peel and tack to increase the adhesion. The optimum between storage and dissipation of energy is reached, the fibrils are slightly crosslinked to bear a higher stress but still dissipate enough energy to comply to strain during the debonding, which results in higher adhesion[137]. Once the crosslinking prevents the elongation of fibrils, brittle-like behaviour is seen in the curves, also low adhesion and adhesive failures are observed. The dependence of crosslinking density on the viscoelastic properties and thus the debonding mechanism of the adhesive i.e. cavitation and adhesion failure, was also discussed by Yamaguchi and co-authors[138], Poivet et al.[139] as they observed the morphologies of cavities and fibrils during removal of the PSA. The ability for fibril formation and the detachment mechanisms have also been connected to the rheological properties of the adhesive. As discussed in I.2.E.iv., the "crack-propagation" of cavities, leading either to detachment or fibrils formation, depends on the ratio between the critical energy release rate G_c and the elastic modulus G' of the adhesive.

Last but not least, it was also recognized that when fibrils are formed, each one undergoes similar high-strain deformation than the material in tensile test. In that way, the behaviour of the fibrils from the tensile measurements of the adhesive can be predicted.

vii. Window of PSA applications

Studies on both bonding and debonding stages of an adhesive by linear rheology have shown that we can relate both stages to a frequency. The frequencies relate to the time scale of each event, by definition $f=1/t$ or $\omega=2\pi/t$. The stated bonding time between two adherends was given for ~ 15 s thus bonding frequency is considered as 10^{-2} rad.s $^{-1}$; and debonding time was stated for ~ 1.5 ms meaning a debonding frequency of 10^2 rad.s $^{-1}$.

Depending on the mechanical response (elastic and loss modulus) at these frequencies, Chang[140] has developed a relative scheme that summarizes the windows of applications as seen in Figure 21; each end application is connected to a range of G' and G'' values, which the PSA should fulfil.

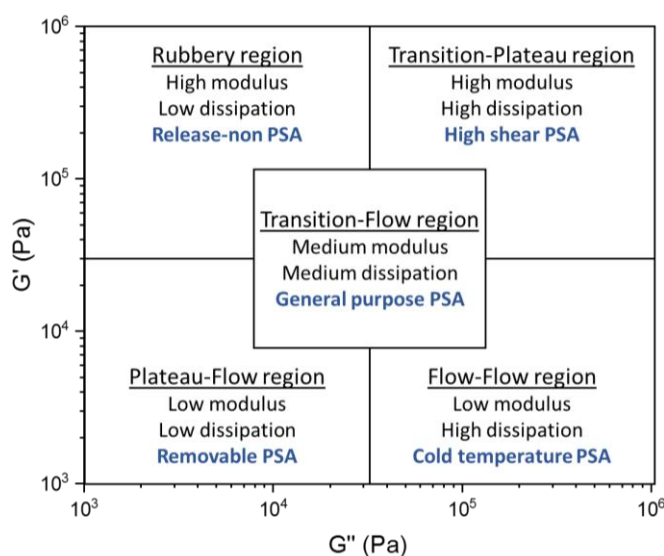


Figure 21. Windows of PSA applications. Reprinted and adapted with permission from [140].

Copyright © Taylor & Francis.

I.3. Thesis outline

High performance PSAs should combine two opposite properties: tackiness and cohesive strength. Regular designs of PSA products involve low glass transition temperature T_g for polymer mobility and tackiness; in addition to covalent crosslinking of the chains to procure bulk cohesion. Yet, the permanent character of covalent bonds does not allow stress dissipation effectively during debonding. Reversible interactions are regarded as interesting alternative crosslink mechanism for designing adhesives with optimized tackiness and cohesion.

This thesis aimed to find suitable formulation to obtain PSA polymers comprising ionic interactions. Inspiration of relevant ionic groups were taken from sandcastle's worm glue. As additional challenge, the synthesis method should be relevant for industrial scale applications, and therefore based on one-pot systems and commercially available precursors. Three preparation techniques were investigated. Another objective was the characterization of the mechanical and adhesive properties of the formulations based on these polymers, in order to connect the polymers structure with the performance of the derived materials.

This Thesis is organized as follows:

In Chapter I, an introduction to adhesion and pressure-sensitives is given; the general adhesion theories and the challenges of pressure-sensitive adhesion were reviewed. The basic chemistry of PSA, the polymerization techniques and adhesive tests used for this thesis were discussed. The state-of-the-art on the application of reversible interactions for increasing adhesion performance of PSAs is described.

Chapter II reports the polymerization of low T_g acrylates comprising quaternary ammonium groups and methacrylic acid as physical crosslinkers using emulsion polymerization. The parameters influencing the stability of the emulsions were studied. The content of functional (i.e. crosslinking) groups was varied and the consequences on the polymers' mechanical and adhesive properties were discussed.

Chapter III is devoted to the use of solution polymerization to prepare acrylates with quaternary ammonium and phosphate side-groups. The number of crosslinker groups was altered, the stoichiometry between ionic moieties was changed and different ionic moieties were used (carboxylic acid and tertiary amine). The mechanical and adhesive properties as function of composition are analysed, and also compared with commercial adhesives. To improve the adhesive performance, a study for molecular weight optimization is described.

Chapter IV describes the preparation of secondary dispersions from the polymers prepared by solution polymerization from Chapter III. The polymers were dispersed in water to avoid the presence of organic solvent in the final product. The characteristics of the dispersions are described. The mechanical and adhesive properties of the dispersed polymers are compared with those of the solutions and commercialized products.

Chapter V summarizes the most relevant conclusions of this thesis.

A detailed description of the materials, characterization method, additional graphs and figures are given in Appendixes.

I.4. References

1. Mazza, P.P.A., et al., *A new Palaeolithic discovery: tar-hafted stone tools in a European Mid-Pleistocene bone-bearing bed*. Journal of Archaeological Science, 2006. **33**(9): p. 1310-1318.
2. Kashuba, N., et al., *Ancient DNA from chewing gums connects material culture and genetics of Mesolithic hunter-gatherers in Scandinavia*. bioRxiv, 2018: p. 485045.
3. Wilson, C., *Chewing gum tells of Stone Age life*. New Scientist, 2019. **241**(3211).
4. Malek, J., P.T. Nicholson, and I. Shaw, *Ancient Egyptian Materials and Technology*. American Journal of Archaeology, 2001. **105**(2).
5. Pocius, A.V., *Adhesion & Adhesives Technology - An Introduction*. Third ed. 2012.
6. S. Ebnesajjad, A.H.L., *Adhesives Technology Handbook - Chapter 1: Introduction and Adhesion Theories*. 2015: Elsevier Inc.
7. Good, R.J., *On the definition of adhesion*. The Journal of Adhesion, 1976. **8**: p. 1-9.
8. Wake, W.C., *Theories of Adhesion and uses of adhesives*. Polymer, 1978. **19**: p. 291-308.
9. Kendall, K., *Molecular Adhesion and Its Applications - The Sticky Universe*. 2004: Kluwer Academic Publishers.
10. Kinloch, A.J., *Adhesion and adhesives: science & technology*. 1987: Chapman & Hall, London.
11. McBain, J.W. and D.G. Hopkins, *On adhesives & adhesive action*. Journal of Physical Chemistry, 1925. **29**: p. 188-204.
12. Voyutskii, S.S., *The diffusion theory of adhesion*. Rubber Chemistry & Technology, 1960. **33**: p. 748-756.
13. Deryaguin, B.V. and V.P. Smilga, *Electronic theory of adhesion*. The Journal of Applied Physics, 1967. **38**: p. 4609-4616.
14. Deryaguin, B.V. and V.P. Smilga, *Adhesion, fundamentals and practice*. 1969: MacLaren and Son, London.
15. Buchan, S. and W.D. Rae, *Chemical nature of the rubber to glass bond*. Transactions of the Institution of the Rubber Industry, 1946. **20**: p. 205-216.
16. Sharpe, L.H. and H. Schonhorn, *Thermodynamic adhesion*. Chemical & Engineering News, 1963. **41**(67-88).

17. Schonhorn, H., *Adhesion fundamental and practice*. 1970: Elsevier Ltd.
18. Gent, A.N. and J. Schultz, *Effect of wetting liquids on the strength of adhesion of viscoelastic material*. The Journal of Adhesion, 1972. **3**: p. 281-294.
19. Carré, A. and J. Schultz, *Polymer-Aluminium adhesion II. Role of the adhesive and cohesive properties of the polymer*. The Journal of Adhesion, 1984. **17**: p. 135-155.
20. Raphael, E. and P.-G.D. Gennes, *Rubber-rubber adhesion with connector molecules*. Journal of Physical Chemistry, 1992. **96**: p. 4002-4007.
21. Brochard-Wyart, F. and P.-G.D. Gennes, *Adhesion between rubbers and grafted solids*. The Journal of Adhesion, 1996. **57**: p. 21-30.
22. *The Global Adhesives Industry 2014-2019 - A Multiclient Study*, n.G. Kusumgar, Inc., Editor. 2015.
23. *Pressure Sensitive Adhesives Market by Chemistry (Acrylic, Rubber, EVA), Technology (Water-based, Solvent-based, Hot Melt), Application (Labels, Tapes, Graphics), End-Use Industry (Packaging, Automotive, Medical), Region - Global Forecast to 2021*, M.a. Markets, Editor. 2016.
24. Yadav, A., *World Pressure Sensitive Tapes - Current Overview and Future Growth*. 2013, Freedonia Group: Scapa Group plc.
25. *Pressure-sensitive Tapes and Labels Market - Industry Share Report 2024*, G.M. Insights, Editor. 2019, Global Market Insights.
26. Ebnesajjad, S. and A.H. Landrock, *Characteristics of Adhesive materials*, in *Adhesives Technology Handbook*. 2015, Elsevier Inc. p. 85159.
27. Urban, D. and L. Egan, *Applications in the adhesives and construction industries*, in *Polymer Dispersions and their industrial applications*, D. Urban and K. Takamura, Editors. 2002, Wiley-VCH. p. 191-252.
28. Creton, C., *Pressure-Sensitive Adhesives: An Introductory Course*. MRS Bulletin, 2013. **28**(6): p. 434-439.
29. Benedek, I., *Pressure-Sensitive Raw Materials*, in *Technology of Pressure-Sensitive Adhesives and Products - Handbook of Pressure-Sensitive Adhesives and Products*, I. Benedek and M.M. Feldstein, Editors. 2009, CRC Press.
30. Ahn, B.K., et al., *Surface-initiated self-healing of polymers in aqueous media*. Nat Mater, 2014. **13**(9): p. 867-72.
31. Dahlke, J., et al., *A New Approach Toward Metal-Free Self-Healing Ionomers Based on Phosphate and Methacrylate Containing Copolymers*. Macromolecular Chemistry and Physics, 2017. **218**(23).

32. Das, A., et al., *Ionic modification turns commercial rubber into a self-healing material*. ACS Appl Mater Interfaces, 2015. **7**(37): p. 20623-30.
33. Hohlbein, N., et al., *Self-healing dynamic bond-based rubbers: understanding the mechanisms in ionomeric elastomer model systems*. Physical Chemistry Chemical Physics, 2015. **17**(32): p. 21005-21017.
34. Kalista, S.J., J.R. Pflug, and R.J. Varley, *Effect of ionic content on ballistic self-healing in EMAA copolymers and ionomers*. Polymer Chemistry, 2013. **4**(18).
35. Krogsgaard, M., V. Nue, and H. Birkedal, *Mussel-Inspired Materials: Self-Healing through Coordination Chemistry*. Chemistry, 2016. **22**(3): p. 844-57.
36. Stukalin, E.B., et al., *Self-Healing of Unentangled Polymer Networks with Reversible Bonds*. Macromolecules, 2013. **46**(18).
37. Hennink, W.E. and C.F. van Nostrum, *Novel crosslinking methods to design hydrogels*. Advanced Drug Delivery Reviews, 2012. **64**: p. 223-236.
38. Li, J., et al., *Tough adhesives for diverse wet surfaces*. Science, 2017. **357**: p. 378-381.
39. Yin, R., et al., *Glucose and pH dual-responsive concavalin A based microhydrogels for insulin delivery*. International Journal of Biological Macromolecules, 2011. **49**: p. 1137-1142.
40. Qiu, Y. and K. Park, *Environment-sensitive hydrogels for drug delivery*. Advanced Drug Delivery Reviews, 2001. **53**: p. 321-339.
41. Yim, N., et al., *Exosome engineering for efficient intracellular delivery of soluble proteins using optically reversible protein-protein interaction module*. Nature Communications, 2016. **7**.
42. Chung, J., et al., *Thermo-responsive drug delivery from polymeric micelles constructed using block copolymers of poly(N-isopropylacrylamide) and poly(butylmethacrylate)*. Journal of Controlled Release, 1999. **62**: p. 115-127.
43. Saito, G., J.A. Swanson, and K.-D. Lee, *Drug delivery strategy utilizing conjugation via reversible disulfide linkages: role and site of cellular reducing activities*. Advanced Drug Delivery Reviews, 2003. **55**: p. 199-215.
44. Appel, E.A., et al., *Self-assembled hydrogels utilizing polymer-nanoparticle interactions*. Nature Communications, 2015. **6**.
45. Northen, M.T., et al., *A gecko-inspired reversible adhesive*. Advanced Materials, 2008. **20**(20): p. 3905-3909.

46. Paretkar, D., et al., *Bioinspired pressure actuated adhesive system*. Materials Science and Engineering C, 2011. **31**: p. 1152-1159.
47. Kamperman, M., et al., *Functional adhesive surfaces with "Gecko" effect: the concept of contact splitting*. Advanced Engineering Materials, 2010. **12**(5): p. 335-348.
48. Bini, E., D.P. Knight, and D.L. Kaplan, *Mapping domain structures in silks from insects and spiders related to protein assembly*. Journal of Macromolecular Biology, 2004. **335**: p. 24-40.
49. Hakimi, O., et al., *Spider and mulberry silkworm silks as compatible biomaterials*. Composites Part B: Engineering, 2007. **38**: p. 324-337.
50. Adlassnig, W., et al., *Deadly Glue — Adhesive Traps of Carnivorous Plants*, in *Biological Adhesive Systems*. 2010. p. 15-28.
51. Gowda, D.C., G. Reuter, and R. Schauer, *Structural studies of an acidic polysaccharide from the mucin secreted by Drosera capensis*. Carbohydrate Research, 1983. **113**: p. 113–124.
52. Jefree, C.E., *The fine structure of the plant cuticle*, in *Biology of the plant cuticle*, M. Riederer and C. Müller, Editors. 2006, Blackwell Publishing, Oxford. p. 11-125.
53. Simoneit, B.R.T., P.M. Medeiros, and E. Wollenweber, *Triterpenoids as major components of the insect-trapping glue of Roridula species*. Zeitschrift für Naturforschung, 2008. **63**.
54. Waite, J.H., et al., *Mussel adhesion: finding the tricks worth mimicking*. The Journal of Adhesion, 2005. **81**: p. 297-317.
55. Maugh, K.J., et al., *Bioadhesive coding sequence*. 1991: USA.
56. Waite, J.H. and X.X. Qin, *Polyphosphoprotein from the adhesive pads of Mytilus edulis*. Biochemistry, 2001. **40**: p. 2887-2893.
57. Holten-Andersen, N., H. Zhao, and J.H. Waite, *Stiff coatings on compliant biofibers: the cuticle of Mytilus californianus byssal threads*. Biochemistry, 2009. **48**: p. 2752-2759.
58. Zhao, H., et al., *Probing the adhesive footprints of Mytilus californianus byssus*. The Journal of Biological Chemistry, 2006. **281**: p. 11090-11096.
59. Wei, W., et al., *Hydrophobic enhancement of Dopa-mediated adhesion in a mussel foot protein*. J Am Chem Soc, 2013. **135**(1): p. 377-83.
60. Lu, Q., et al., *Adhesion of mussel foot proteins to different substrate surfaces*. J R Soc Interface, 2013. **10**(79): p. 20120759.

61. Lee, B.P., et al., *Mussel-Inspired Adhesives and Coatings*. Annu Rev Mater Res, 2011. **41**: p. 99-132.
62. Zhang, K., et al., *Recent Progress of Mussel-Inspired Underwater Adhesives*. Chinese Journal of Chemistry, 2017. **35**(6): p. 811-820.
63. Kim, H.J., et al., *Mussel adhesion-employed water-immiscible fluid bioadhesive for urinary fistula sealing*. Biomaterials, 2015. **72**: p. 104-111.
64. Feldstein, M.M. and A.P. Moscalets, *Bio-inspired pressure-sensitive adhesives and their applications*, in *Innovations in Pressure-Sensitive Adhesives Products*. 2016, Smithers Rapra Technology Ltd.
65. Matos-Pérez, C.R., J.D. White, and J.J. Wilker, *Polymer composition and substrate influences on the adhesive bonding of a biomimetic, cross-linking polymer*. Journal of the American Chemical Society, 2012. **134**: p. 9498-9505.
66. White, J.D. and G.J. Wilker, *Underwater bonding with charged polymer mimics of marine mussel adhesive proteins*. Macromolecules, 2011. **44**: p. 5085-5088.
67. Krogsgaard, M., et al., *Self-healing mussel-inspired multi-pH-responsive hydrogels*. Biomacromolecules, 2013. **14**(2): p. 297-301.
68. Narkar, A.R. and B.P. Lee, *Incorporation of anionic monomer to tune the reversible catechol-boronate complex for pH-responsive, reversible adhesion*. Langmuir, 2018. **34**(32): p. 9410-9417.
69. Wang, J., et al., *Complex coacervate core micelles from iron-based coordination polymers*. The Journal of Physical Chemistry B, 2010. **114**: p. 8313-8319.
70. Heinzmann, C., et al., *Light-induced bonding and debonding with supramolecular adhesives*. ACS Appl Mater Interfaces, 2014. **6**(7): p. 4713-9.
71. Heinzmann, C., C. Weder, and L.M. de Espinosa, *Supramolecular polymer adhesives: advanced materials inspired by nature*. Chem Soc Rev, 2016. **45**(2): p. 342-58.
72. Heinzmann, C., et al., *Supramolecular cross-links in poly(alkyl methacrylate) copolymers and their impact on the mechanical and reversible adhesive properties*. ACS Appl Mater Interfaces, 2015. **7**(24): p. 13395-404.
73. Bunworth, M., et al., *Optically healable supramolecular polymers*. Nature, 2011. **472**: p. 337-337.
74. Fiore, G.L., S.J. Rowan, and C. Weder, *Optically healable polymers*. Chemical Society Reviews, 2013. **43**: p. 7278-7288.

75. Coulibaly, S., et al., *Reinforcement of optically healable supramolecular polymers with cellulose nanocrystals*. *Macromolecules*, 2014. **47**: p. 152-160.
76. Biyani, M.V., E.J. Foster, and C. Weder, *Light-healable supramolecular nanocomposites based on modified cellulose nanocrystals*. *ACS Macro Letters*, 2013. **2**: p. 236-240.
77. Nicharat, A., et al., *Thermally-activated shape memory behavior of melt-mixed polyurethane/cellulose nanocrystal composites*. *Journal of Applied Polymer Science*, 2017.
78. Calvino, C., et al., *Approaches to polymeric mechanochromic materials*. *Journal of Polymer Science Part A*, 2017. **55**: p. 640-652.
79. Vadrucci, R., et al., *Nanodroplet-containing polymers for efficient low-power light upconversion*. *Advanced Materials*, 2017. **29**.
80. Courtois, J., et al., *Supramolecular soft adhesive materials*. *Advanced Functional Materials*, 2010. **20**(11): p. 1803-1811.
81. Callies, X., et al., *Combined Effect of Chain Extension and Supramolecular Interactions on Rheological and Adhesive Properties of Acrylic Pressure-Sensitive Adhesives*. *ACS Appl Mater Interfaces*, 2016. **8**(48): p. 33307-33315.
82. Lewis, C.L., K. Stewart, and M. Anthamatten, *The influence of hydrogen bonding side-groups on viscoelastic behavior of linear and network polymers*. *Macromolecules*, 2014. **47**: p. 729-740.
83. Faghihnejad, A., et al., *Adhesion and surface interactions of a self-healing polymer with multiple hydrogen-bonding groups*. *Advanced Functional Materials*, 2014. **24**: p. 2322-2333.
84. Pensec, S., et al., *Self-assembly in solution of a reversible comb-shaped supramolecular polymer*. *Macromolecules*, 2010. **43**: p. 2529-2534.
85. Stewart, R.J., et al., *The role of coacervation and phase transitions in the sandcastle worm adhesive system*. *Adv Colloid Interface Sci*, 2017. **239**: p. 88-96.
86. Endrizzi, B. and R.J. Stewart, *Glueomics, an expression survey of the adhesive gland of the sandcastle worm*. *The Journal of Adhesion*, 2009. **85**: p. 546-559.
87. Waite, J., R. Jensen, and D. Morse, *Cement precursor proteins of the reef-building polychaete *Phragmatopoma californica* (Fewkes)*. *Biochemistry*, 1992. **31**: p. 5733-5738.
88. Zhao, H., et al., *Cement proteins of the tube-building polychaete *Phragmatopoma californica**. *The Journal of Biological Chemistry*, 2005. **280**: p. 42938-42944.
89. Stewart, R.J., et al., *The tube cement of *Phragmatopoma californica* - a solid foam*. *The Journal of Experimental Biology*, 2004. **216**: p. 4727-4734.

90. Stevens, M.J., et al., *Multiscale structure of the underwater adhesive of Phragmatopoma californica: a nanostructured latex with a steep microporosity gradient*. Langmuir, 2007. **23**: p. 5045-5049.
91. Wang, C.S. and R.J. Stewart, *Multipart copolyelectrolyte adhesive of the sandcastle worm, Phragmatopoma californica (Fewkes): catechol oxidase catalyzed curing through peptidyl-DOPA*. Biomacromolecules, 2013. **14**: p. 1607-16017.
92. Shao, H., K.N. Bachus, and R.J. Stewart, *A water-borne adhesive modeled after the sandcastle glue of P. californica*. Macromolecular Bioscience, 2009. **9**: p. 464-471.
93. Stewart, R.J., C.S. Wang, and H. Shao, *Complex coacervates as a foundation for synthetic underwater adhesives*. Advances in Colloid and Interface Science, 2011. **167**: p. 85-93.
94. Stewart, R.J., *Protein-based underwater adhesives and the prospects for their biotechnological production*. Applied Microbiology and Biotechnology, 2011. **89**: p. 27-33.
95. Shao, H. and R.J. Stewart, *Biomimetic underwater adhesives with environmentally triggered setting mechanisms*. Adv Mater, 2010. **22**(6): p. 729-33.
96. Kaur, S., G.M. Weerasekare, and R.J. Stewart, *Multiphase adhesive coacervates inspired by the sandcastle worm*. Applied Materials and Interfaces, 2011. **3**: p. 941-944.
97. Zhao, Q., et al., *Underwater contact adhesion and microarchitecture in polyelectrolyte complexes actuated by solvent exchange*. Nat Mater, 2016. **15**(4): p. 407-12.
98. Dompé, M., et al., *Thermoresponsive complex coacervate-based underwater adhesive*. Advanced Materials, 2019(Online 1808179).
99. Jones, J.P., et al., *Water-borne endovascular embolics inspired by the undersea adhesive of marine sandcastle worms*. Advanced Healthcare Materials, 2016. **5**: p. 795-801.
100. Mann, L.K., et al., *Fetal membrane patch and biomimetic adhesive coacervates as a sealant for fetoscopic defects*. Acta Biomaterialia, 2012. **8**: p. 2160-2165.
101. Winslow, B.D., et al., *Biocompatibility of adhesive complex coacervates modeled after the Sandcastle glue of P. californica for craniofacial reconstruction*. Biomaterials, 2010. **31**: p. 9373-9381.
102. Feldstein, M.M., et al., *Mechanisms of molecular interactions in polybase-polyacid complex formed by copolymers of N,N-dimethylaminoethylmethacrylate with alkylmethacrylates and methacrylic acid with ethylacrylate*. Journal of Applied Polymer Science, 2009. **112**(3): p. 1142-1165.
103. Feldstein, M.M., E.E. Dormidontovad, and A.R. Khokhlov, *Pressure-sensitive adhesives based on interpolymers complexes*. Progress in Polymer Science, 2015. **42**: p. 79-153.

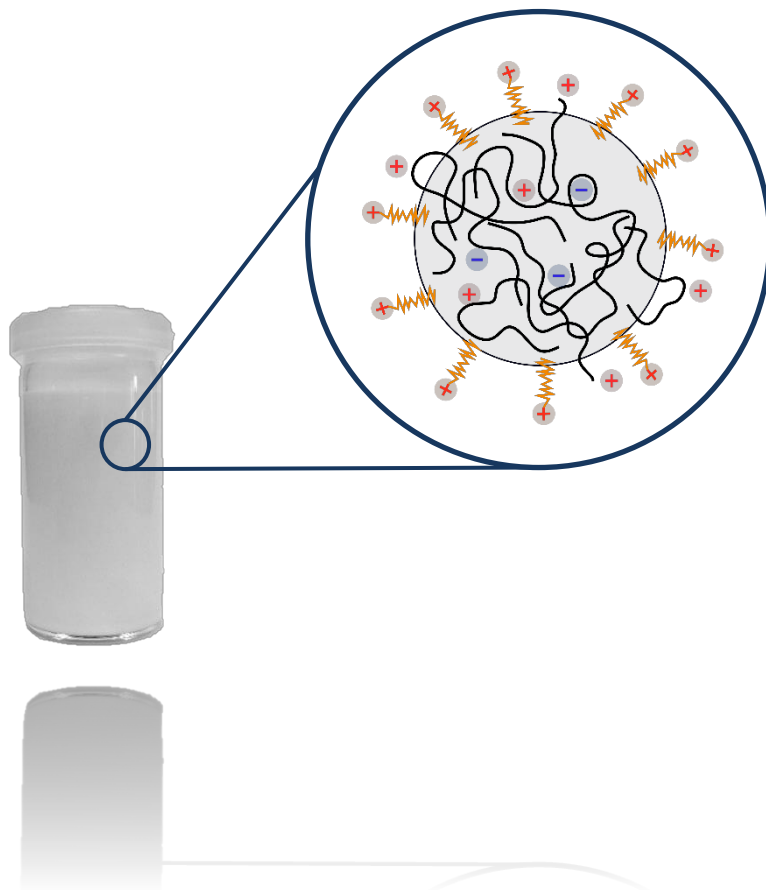
104. Feldstein, M.M., et al., *A new class of pressure-sensitive adhesives based on interpolymer and polymer-oligomer complexes*. Polymer Science Series A, 2009. **51**(7): p. 799-814.
105. Vana, P., et al., *Radical Polymerization*, in *Encyclopedia of Polymer Science and Technology*. 2003, John Wiley & Sons, Inc. .
106. Russell, G.T., *Kinetics of radical polymerization*, in *Encyclopedia of Polymer Science and Technology*. 2010, John Wiley & Sons, Inc. Al.
107. Rudin, A. and P. Choi, *Free-Radical Polymerization*, in *The Elements of Polymer Science & Engineering*. 2013, Elsevier Inc.
108. Bevington, J.C., *Overall Mechanisms*, in *Free-radical Polymerization*, G. Allen and J.C. Bevington, Editors. 1996, Elsevier Ltd.
109. Palit, S.R., S.R. Chatterjee, and A.R. Mukherjee, *Chain Transfer*, in *Encyclopedia of Polymer Science and Technology*. 2011, John Wiley & Sons, Inc. .
110. Rudin, A., *Molecular weight distributions*, in *Free-radical polymerization*, G. Allen and J.C. Bevington, Editors. 1996, Elsevier Ltd.
111. Barner-Kowollik, C., et al., *Copolymerization*, in *Encyclopedia of Polymer Science and Technology*. 2003, John Wiley & Sons, Inc. Al.
112. Braun, D. and W.K. Czerwinski, *Rates of Copolymerization*, in *Free-radical Polymerization*. 1996.
113. Melville, H.W., B. Noble, and W.F. Watson, *Copolymerization. I. Kinetics and some experimental considerations of a general theory*. Journal of polymer Science, 1947. **2**: p. 229-245.
114. Urban, D. and K. Takamura, *Polymer Dispersions and their industrial applications*. 2002: Wiley-VCH.
115. Gonzalez-Ortiz, L.J. and J.M. Asua, *Development of particle morphology in emulsion polymerization. 1. Cluster dynamics*. Macromolecules, 1995. **28**: p. 3135-3145.
116. Okubo, M., *Control of particle morphology in emulsion polymerization*. Macromolecular Symposia, 1990. **35-36**: p. 307-325.
117. Asua, J.M., *Emulsion polymerization: from fundamental mechanisms to process developments*. Journal of Polymer Science Part A: Polymer Chemistry, 2004. **42**: p. 1025-1041.
118. Nomura, M., H. Tobita, and K. Suzuki, *Emulsion polymerization: kinetic and mechanistic aspects*, in *Polymer Particles*, M. Okubo, Editor. 2005, Springer.

119. Smith, W.V. and R.H. Ewart, *Kinetics of emulsion polymerization*. The Journal of Chemical Physics, 1948. **16**.
120. H-J. Kim, D.-H.L., Y-J. Park, *Fundamentals of Pressure-Sensitivity - Chapter 7: Peel Resistance*. Handbook of Pressure-Sensitive Adhesives and Products, ed. M.M.F. I. Benedek. 2009: CRC Press.
121. S. V. Antonov, V.G.K., *Fundamentals of Pressure Sensitivity - Chapter 8: Shear Resistance*. Handbook of Pressure-Sensitive Adhesives and Products, ed. M.M.F. I. Benedek. 2009: CRC Press.
122. Zosel, A., *Shear Strength of Pressure Sensitive Adhesives and its Correlation to Mechanical Properties*. The Journal of Adhesion, 1994. **44**(1-2): p. 1-16.
123. Creton, C. and M. Ciccotti, *Fracture and adhesion of soft materials: a review*. Rep Prog Phys, 2016. **79**(4): p. 046601.
124. C. Creton, K.R.S., *Fundamentals of Pressure Sensitivity - Chapter 6: Probe Tack*. Handbook of Pressure-Sensitive Adhesives and Products, ed. M.M.F. I. Benedek. 2009: CRC Press.
125. Shull, K.R. and C. Creton, *Deformation behavior of thin, compliant layers under tensile loading conditions*. Journal of Polymer Science Part B: Polymer Physics, 2004. **42**(22): p. 4023-4043.
126. Feldstein, M.M. and C. Creton, *Pressure-sensitive adhesion as a material property and as a process*, in *pressure-sensitive design, theoretical aspects*, I. Benedek, Editor. 2006, VSP.
127. Feldstein, M.M., *Molecular fundamentals of pressure-sensitive adhesion*, in *Developments in pressure-sensitive products*, I. Benedek, Editor. 2006, CRC-Taylor & Francis.
128. Feldstein, M.M., *Molecular Nature of Pressure-Sensitive Adhesion*, in *Fundamentals of Pressure-Sensitive Adhesives*, I. Benedek and M.M. Feldstein, Editors. 2009, Taylor & Francis Group, LLC
129. Feldstein, M.M., et al., *Free volume adhesion and viscoelastic properties of model nanostructured pressure-sensitive adhesive based on stoichiometric complex of poly(N-vinyl pyrrolidone) and poly(ethylene glycol) of disparate chain lengths*. Journal of Applied Polymer Science, 2011. **119**: p. 2408-2421.
130. Kaelble, D.H., *Theory and analysis of peel adhesion: mechanisms and mechanics*. Transactions of the Society of Rheology, 1959. **3**: p. 161-180.
131. Kaelble, D.H., *Theory and analysis of peel adhesion: rate-temperature dependence of viscoelastic interlayers*. Journal of Colloid Science, 1964. **19**: p. 413-424.
132. Kaelble, D.H., *Theory and analysis of peel adhesion: bond stresses and distributions*. Transactions of the Society of Rheology, 1960. **4**: p. 45-73.

133. Kaelble, D.H., *Theory and analysis of peel adhesion: adhesive thickness effects*. The Journal of Adhesion, 1992. **37**: p. 205-214.
134. Fujita, H., *Diffusion on polymer-diluent systems*. Advances in Polymer Science, 1961. **3**: p. 1-47.
135. Lipatov, Y., *The iso-free-volume state and glass transitions in amorphous polymers*, in *Advances in Polymer Science - Polymer Chemistry*, Polymer, Editor. 1978. p. 63-104.
136. Zosel, A., *The effect of bond formation on the tack of polymers*. Journal of Adhesion Science and Technology, 1997. **11**(11): p. 1447-1457.
137. Zosel, A., *Effect of crosslinking on tack and peel strength of polymers*. Journal of Adhesion, 1991. **34**(1-4): p. 201-209.
138. T. Yamaguchi, K.K., M. Doi, *In situ observation of stereoscopic shapes of cavities in soft adhesives*. Europhysics Letters, 2007. **77**(6): p. 64002-64006.
139. S. Poivet, F.N., C. Gay, P. Fabre, *Cavitation-induced force transition in confined viscous liquids under traction*. Europhysics Letters, 2003. **62**(2): p. 244-250.
140. Chang, E.P., *The Viscoelastic Window of PSAs*. The Journal of Adhesion, 1991. **34**(1-4): p. 189-200.

II.

Adhesive polyampholyte particles prepared by emulsion polymerization



II. Adhesive polyampholyte particles prepared by emulsion polymerization.....83

II.1.	Introduction	85
II.2.	Results.....	87
A.	Selection of surfactant	88
B.	Selection of initiating system	90
C.	Selection of cationic monomer	91
D.	Effect of the ionic monomer ratio on emulsion stability	93
E.	Effect of a chain transfer agent on the gel content	94
F.	Effect of the amount of ionic comonomers and pH on the polymer structure and physical properties of the films.....	96
II.3.	Discussion	120
II.4.	Conclusion	125
II.5.	References	126

II.1. INTRODUCTION

The aim of this thesis was to find an efficient synthetic route to physical (reversible) polymer network, based on oppositely charged polyions to obtain PSA with improved adhesion properties. The ionic complexation in polymers is an effective crosslinking mechanism that can lead to improved material properties such as ultra-stretchability[1] or self-healing[2-6]. Adhesives containing interpolymer complexes are expected to show high shear resistance coupled with improved dissipative character during debonding[7, 8].

Emulsion polymerization is one of the most common techniques used in industry to prepare performance materials[9, 10]. It allows to produce polymers of high molar masses while keeping reasonable viscosity and good heat transfer. Water-based products are also safer to manufacture and for the environment[11, 12]. Yet, successful emulsion polymerization relies on achieving a stable dispersion of the particles in the supernatant, and on the homogenous diffusion of the monomers in these particles. The kinetics of the copolymerization depend also on the solubility of the monomers and on the different reactivity ratios[13, 14]. Furthermore, colloidal stabilization is insured by micellization of surfactant which can be non-ionic or ionic in nature[9]. As a result, emulsions are sensitive to addition of salts and to change in pH. The introduction of oppositely charged monomer groups in polymers using emulsion polymerization is therefore challenging. The functional groups should be chosen in accordance, not to disturb the steric and/or electrostatic stabilization, but to allow diffusion of the charged comonomers into the particles and copolymerization with the hydrophobic monomers.

The emulsion copolymerization of styrene with ionic comonomers has been used in a few examples to prepare highly charged colloids for flocculant and paper industries[15-18]. Similar syntheses were disclosed with polymerizable ionic surfactants[19, 20]. These techniques give monodisperse particles, but the colloidal stabilization is only insured by the ionic comonomers, hence only the preparation of cationic or anionic latexes is permitted.

Amphoteric copolymers have been obtained using inverse emulsion polymerization (water-in-oil)[21-23] yet the oil supernatant makes this synthesis irrelevant for PSA applications (dried polymer films). Ionically crosslinked coatings from polyampholytes have been reported by Tiggelman and Hartmann[24]. Separate anionic and cationic dispersions were obtained by emulsion polymerization. Ionic crosslinking was obtained during film formation after blending the two complementary charged emulsions. However, the crosslinking took place at the interface of the polymer particles which decreased adhesion and water resistance.

G. D. Rose et al.[25] studied the seeded copolymerization in emulsion of acrylates, methacrylic acid (MAA) and a cationic comonomer stabilized by a cationic surfactant. Although this work gives an insight to the introduction of both strong cationic and weak acid groups in the same dispersion, the aim was to induce particle-particle coacervation (polyelectrolyte phase-separation) by deprotonation of MAA. In other words, the goal of their study was to generate particle flocculation (particle destabilization) for water treatment, the effect of ionic crosslinking through complexation between the charged groups was never mentioned.

In this chapter, the system proposed by G. D. Rose et al.[25] was further developed and the presence of ionic crosslinking in the final polymer was investigated. The polymers obtained should form an ionic network upon film formation from inter and intramolecular complexes. This requires increasing the pH over the pKa of the weak acid comonomer. To prevent the phase separation described in Rose's work, it was hypothesized that an excess of cationic monomer would be required. The influence of the molar ratio between cationic and anionic groups on the stability of the emulsion at pH 2 and 8 was therefore studied. Towards understanding the adaptability and limits of the system, the impacts of surfactant, initiator and cationic monomer types on the emulsion stability were studied. Finally, polymers with increased content of ionic moieties, and by extension higher ionic crosslinking density were prepared and their mechanical and adhesive properties were compared depending on the pH.

II.2. RESULTS

A polymer backbone of n-Butylacrylate (n-BA) and styrene (St) was copolymerized with oppositely charged ionic moieties: methacrylic acid (MAA) as the weak anionic moiety and 2-(Methacryloyloxy)ethyl trimethylammonium chloride (MAETAC) as strong cationic moiety. The structures of the monomers can be found in Figure 1.

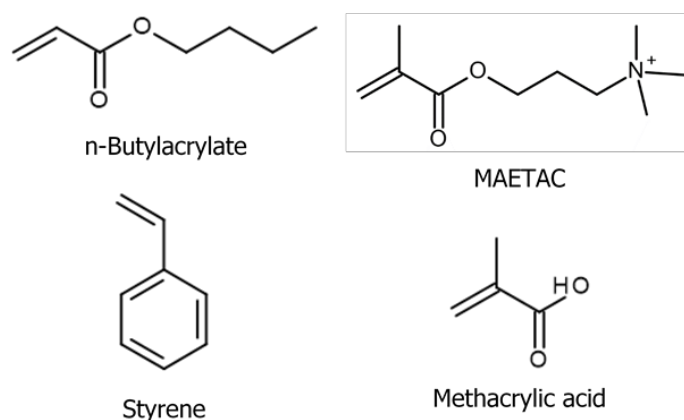


Figure 1. Chemical structures of the monomers used in this PhD thesis

All samples were prepared at 2 L scale by seeded emulsion polymerization. After preliminary optimization experiments (described in sections from II.2.A. to II.2.E.), Dodecyltrimethyl ammonium chloride (DTMACI) was selected as surfactant and tert-Butyl Hydroperoxide (t-BHP)/Rongalit® C was selected as red-ox couple for the initiation of polymerization. To reduce the content of volatile organic compounds (VOCs) and to work in industrial conditions, the polymerization of residual monomers was performed with a second feed of initiator (chemical deodorization). After cooling, the latexes were filtered through a 125 μm mesh and the amount of coagulum (destabilized particles) obtained was measured. A scheme of the expected emulsion is given in Figure 2.

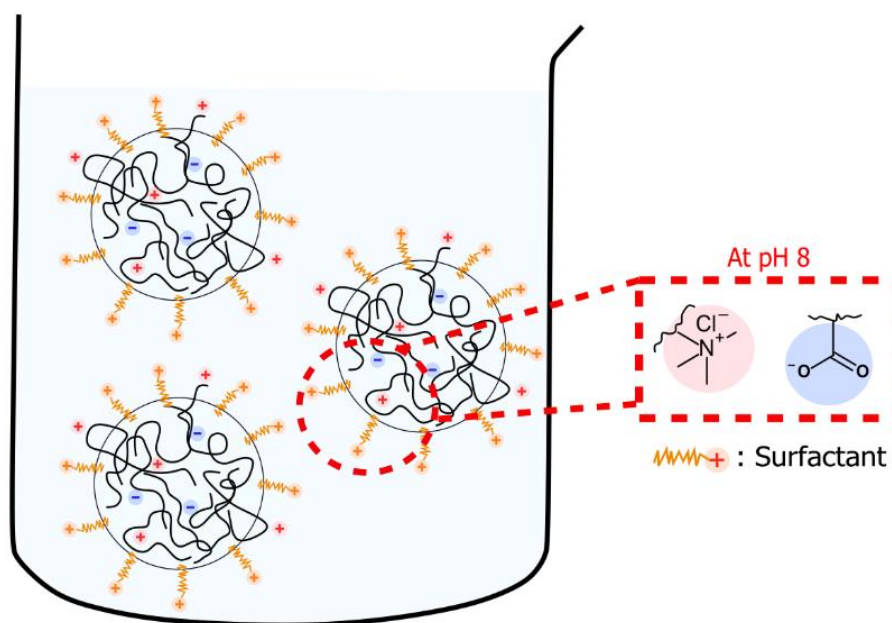


Figure 2. Expected emulsified system of a copolymer from n-BA/St/MAETAC/MAA

A. Selection of surfactant

In emulsion polymerization, the surfactant plays a key role for the colloidal stabilization and thus for the polymerization. In most cases, ionic stabilization (i.e. ionic surfactant) is preferred rather than steric stabilization (i.e. non-ionic surfactant or protective colloid) as it allows better control over the particle size and a fast particle nucleation[26]. The nature of the surfactant is also likely to impact the stability of the emulsion when copolymerizing a quaternary ammonium monomer. The influence of the nature and charge of surfactant on the stability of the emulsion was thus investigated. Latexes were prepared using different surfactants: three cationic ones with different length of alkyl groups (DTMACI, Stepanquat[®] BC 40, Petrostep[®] Q5018), a non-ionic one (Lutensol[®] AT18) and a mixture of anionic ones (Disponil[®] FES 77, Dowfax[®] 2A1). A summary of the experiments can be found in Table 1.

Table 1. Summary of used surfactants for emulsion stability trials; the particle size modi correspond to the mean particle sizes obtained for the different particle populations

Surfactant	Chemical nature	Charge	Amount (pphm)	Particle size modi (nm)	Result and remarks
DTMACI	C ₁₂ Alkyltrimethyl ammonium chloride	+	1	152, 228 + t*	Stable emulsion with cationic seed & coagulum < 0.5 wt%
Stepanquat® BC 40	C ₁₆ C ₁₈ Alkyldimethyl Benzyl ammonium chloride	+	1	157, 265 + t, 600	Stable emulsion with cationic seed & 1 wt% coagulum
Petrostep® Q 5018	C ₁₈ Alkyltrimethyl ammonium chloride	+	1	150, 279 + t, 511	Stable emulsion with cationic seed & 1 wt% coagulum
Lutensol® AT 18	C ₁₆ C ₁₈ -fatty alcohol + 18 EO	Non ionic	1	156, 275 + t, 594	Stable emulsion with cationic seed & 1 wt% coagulum
Disponil® FES 77 / Dowfax® 2 A1	Fatty alcohol ether sulfate + 30 EO / Alkyldiphenyloxide disulfonate	-	0.6/0.4	-	Unstable emulsion with cationic or anionic seed and with different initiator

*t=tailing

Stable emulsions were obtained using all three cationic surfactants, with particle sizes between 150 and 500 nm. The emulsions with longer alkyl chains C₁₆ or C₁₈, showed larger particle size (c.a. 550 nm) and coagulum (small amount of particle precipitation) up to 10 g on an overall 1 kg of emulsion meaning 1 wt%; which suggests a weaker stabilization than with the shorter (C₁₂) surfactant DTMACI.

The same was observed when a non-ionic surfactant was used; the emulsion was stable with 1 wt% of residue recovered but collapsed as consequence of increasing the pH to 8 with ammonia. Therefore, in comparison to cationic, steric stabilization gave lower emulsion stability and control of particle size at pH 2; plus, it was insufficient to prevent particles aggregation at pH 8. The experiment using a mixture of anionic surfactants resulted in an unstable emulsion with polymer precipitation even when using an anionic seed and Sodium Persulfate (NaPS) as initiator.

B. Selection of initiating system

Water-soluble initiators used in emulsion polymerization carry frequently charged groups; therefore, charged initiators might disturb the stability of the emulsion and consequently the conversion of the reaction when polymerizing charged monomers. Ionic interactions (attractive or repulsive) between the initiator and MAETAC might be competitive towards the propagation of the polymerization. Therefore, different initiators were tested in preliminary experiments: neutral (t-BHP/Rongalit® C), anionic (Sodium Persulfate NaPS and t-BHP/Sodium Acetone Bisulphite) and cationic (Wako V50). The other reaction parameters were kept constant unless otherwise specified: DTMACI was used as surfactant and the amounts for MAA and MAETAC were 95 and 100 mmol respectively. The structures of the initiators investigated are found in Figure 3 and a summary of the experiments can be found in Table 2.

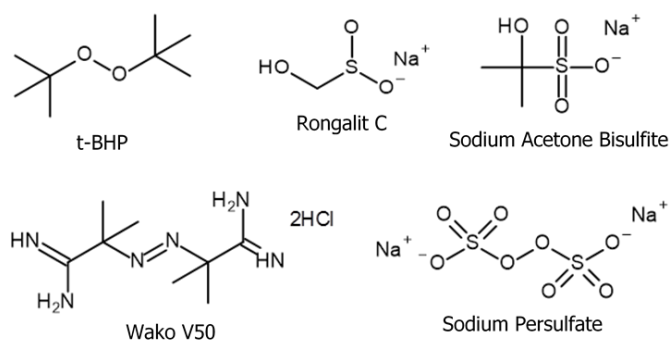


Figure 3. Structures of the investigated initiators

The combination of t-BHP/Rongalit® C for reaction feed and chemical deodorization (initiator feed for removal of residual monomer) was successful and resulted in stable emulsions only when using cationic seed and surfactant. The use of the anionic counterparts resulted in coagulation. The latex was also stable using a cationic initiator Wako V50 during the feed and t-BHP/Rongalit® C for the chemical deodorization. The experiment prepared in an anionic system (i.e. using anionic surfactant) showed high instability during polymerization. The same was observed in the case of NaPS/t-BHP-Sodium Acetone Bisulfite for both cationic and anionic surfactants.

These results suggest that ionic interactions between the initiator and MAETAC and/or DTMACI take place. In combination with the cationic surfactant DTMACI selected in II.2.A., t-BHP/Rongalit® C was chosen as initiating system (feed and chemical deodorization) for the rest of the experiments.

Table 2. Summary of the experiments ran with different initiating system

Initiator Feed	Chemical deodorization	Result and remark
t-BHP/Rongalit® C	t-BHP/Rongalit® C	Stable emulsion with cationic seed and surfactant Unstable with anionic seed and anionic surfactant
Wako V50	t-BHP/Rongalit® C	Stable with cationic surfactant 5 wt% coagulum with non-ionic surfactant and anionic seed
NaPS	t-BHP/Sodium Acetone Bisulfite	Unstable weither cationic/anionic seed and surfactant

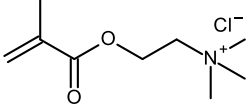
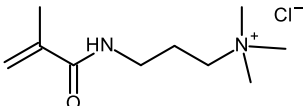
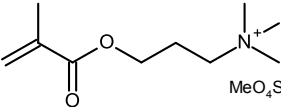
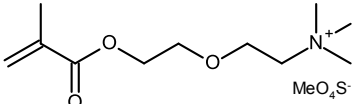
C. Selection of cationic monomer

The acrylate moiety of MAETAC is sensitive to hydrolysis. In order to provide an extended portfolio of viable monomers (i.e. stable and already available in industry from flocculants and cosmetics segments), the stability of the emulsion was tested and compared using the following comonomers: 3-(methacryloylamino)propyl trimethylammonium chloride (MAMPTAC), (3-(2-methylprop-2-enoyloxy)propyl)trimethylammonium methylsulfate (MAPTAMS), and (2-(2-(2-methylprop-2-enoyloxy)ethoxy)ethyl)trimethylammonium methylsulfate (MAEEOAMS).

In comparison to MAETAC, MAMPTAC contains an acrylamide group and a propyl chain, MAPTAMS contains a propyl chain and a methyl sulfate counter-ion and MAEEOAMS contains an ethoxy group between the acrylate and the ammonium plus a methyl sulfate counter-ion. The different structures are available in Table 3.

All monomers were successfully polymerised, although an excess of coagulum (particle aggregation) ~ 3 wt% was observed for MAPTAMS and MAEEOAMS. Only a small instability (measured by the amount of coagulum) of the emulsion was seen when MeSO_4^{2-} was present as a counter-ion. Overall, the emulsions were stable with the four monomers, though smaller amounts of coagulum were measured when using MAMPTAC. Being less prone to hydrolysis due to the acrylamide group (instead of acrylate), MAMPTAC would be an appropriate candidate to replace MAETAC.

Table 3. Monomers structures and results of the experiments

Monomer	Structure	Amount (mmol)	Result and remark
MAETAC		100	Stable and coagulum < 0.5 wt%
MAMPTAC			Stable and coagulum < 0.5 wt%
MAPTAMS			Stable but coagulum > 3 wt%
MAEEOAMS			Stable but coagulum > 3 wt%

D. Effect of the ionic monomer ratio on emulsion stability

For the following sections, it was chosen to use DTMACI as surfactant, t-BHP/Rongalit® C as initiating system and MAETAC as cationic monomer as the combination showed good emulsion stability. In this case, the overall ionic charge of the dispersion is cationic. In consequence, the ionic crosslinks (from interactions of the oppositely charged monomers) should be triggerable by increasing the latex pH from 2 to 8 (over the $pK_a(\text{MAA}) = 4.65$ [27]). A higher pH, ionic interactions might destabilize the polymer particles. To prevent instabilities, it was hypothesised that an excess of the cationic monomer was required.

The stability of latexes at pH 2 and 8 as function of MAA:MAETAC ratio was studied by preparing a set of samples with a fixed amount of MAA (95 mmol) and increasing amount of MAETAC from 0 to 100 mmol. The pH was then increased to 8 by addition of NH_3 (10wt%) under agitation. The stability of the latex was optically and qualitatively assessed (macro-aggregation of particles or precipitation). A description of the set is available in Table 4.

Table 4. Summary of emulsion stability experiments with different MAA:MAETAC ratio

Amount of MAA (mmol)	Amount of MAETAC (mmol)	pH	Stable
95	0	2	N*
		8	
	10	2	Y
		8	N
	20	2	Y
		8	N
	30	2	Y
		8	N
	50	2	Y
		8	N
	100	2	Y
		8	

*Y=Yes
N=No

All latexes obtained were stable at pH 2 and the same particle size was found of around 100 nm with a tailing at ~230 nm, except for the procedure with 0 mmol of MAETAC. Upon increasing the pH of the products to pH 8, the latexes containing 10 to 50 mmol of MAETAC collapsed and only the sample with 100 mmol MAETAC showed stability to ammonia. It seems, the slight excess of cationic charges prevented particle coacervation at pH=8.

Consequently, the excess of MAETAC was required to obtain stable dispersions with deprotonated acid groups and this configuration was required to form adhesive films.

E. Effect of a chain transfer agent on the gel content

The aim of this chapter was also to produce ionically crosslinked polymers, free of covalent crosslinks, to study the effects of the physical network on the adhesive properties of the dried latex films. However, covalent crosslinking can occur during radical polymerization due to grafting (or backbiting) reactions[28]. To control grafting reactions (i.e. secondary reactions from transfer to polymer chains), a chain-transfer agent (CTA) can be used[10]. A CTA reacts with a propagating chain for termination; this releases another radical that will preferably initiate a new growing chain instead of transferring to a polymer chain and produce grafting.

To evaluate the amount of covalent crosslinking in the polymer, the gel content in the dried polymer film is determined[29]. The gel content is the percentage of the dried polymer film that is insoluble in a solvent and gives a measure of the formation of covalent crosslinks during polymerization. If the polymer chains are free of covalent crosslinks and can be solubilized in the solvent, no gel is measured. On the other hand, fully crosslinked particles should cause a gel content of 100%.

Two series of polymers were synthesized using DTMACI as surfactant, a cationic seed, t-BHP/Rongalit® C as initiating couple, a constant ratio n-BA/St, a constant amount of MAA (95 mmol) and 50 or 100 mmol of MAETAC. The first series was polymerised as described above, while in the second series, tert-dodecyl mercaptan (t-DMK) was used as CTA. The gel contents in Ethanol (EtOH) were measured and are shown in Table 5.

Table 5. Series of samples and measured gel contents

Amount of MAA (mmol)	Amount of MAETAC (mmol)	Amount of t-DMK (mmol)	Gel% in EtOH
95	50	0	84
	100		85
	50	2	0.5
	100		1

It is worth mentioning that, the gel content can take into account the physical network formed from the ionic interactions if these are not soluble in the solvent. Therefore, all measurements were done with films from dispersions at acidic pH.

The polymers synthesized in the absence of t-DMK gave gel contents of about 85%. However, for the polymers synthesized in the presence of the chain transfer agent t-DMK, the gel contents dropped to zero considering the error range (~5%). These results indicate that covalent crosslinks between polymer chains were formed during the polymerization reaction, most likely due to grafting with H abstraction on n-BA moieties on the backbone. Addition of a CTA could prevent the proton abstraction, and avoided the formation of a covalent network. The amount of MAETAC had no influence on the gel content in EtOH.

F. Effect of the amount of ionic comonomers and pH on the polymer structure and physical properties of the films

i. Preparation and characterization of the emulsion polymers with increasing ionic content

A set of dispersions, seen in Table 6, was prepared with increasing content of both ionic functional groups. The samples names are abbreviated to EP for Emulsion Polymer, the abbreviation of the monomer is used and followed by the amount of each in mmol (e.g. M stands for MAETAC, e.g. EP-MAA₉₅M₁₀₀ contains 95 mmol of MAA and 100 mmol of MAETAC). The amount of ionic crosslinker group in the polymer is referred to ionicX in wt%.

To prevent instability of the emulsion, several conditions were kept constant: the n-BA/St ratio, the use of DTMACI surfactant to avoid attractive interactions with MAETAC, the red-ox couple of t-BHP and Rongalit® C because it showed the best stability, 2 mmol of t-DMK. The cationic monomer was always used in a small excess (~5 mmol) in respect to the acid to be able to increase the pH of the dispersion to 8.

To characterize the obtained polymers, the particle size was measured by Hydrodynamic Chromatography (HDC) and the gel contents were measured by the method described in paragraph II.2.E. The molecular weight distributions were obtained by Size Exclusion Chromatography (SEC) with Refractive Index (RI) detector. The results are available in Table 7.

Table 6. Set of samples with increasing amount of MAETAC and MAA

Experiment	MAA (mmol)	MAETAC (mmol)	ionicX (wt%)
EP-M₁₀₀	0	100	0
EP-MAA₄₅M₅₀	45	50	3.5
EP-MAA₉₅M₁₀₀	95	100	5.9
EP-MAA₁₁₅M₁₂₀	115	120	9.1
EP-MAA₁₉₅M₂₀₀	195	200	12.4

Samples with a weight average molecular weight $M_w \approx 220\,000\text{ g.mol}^{-1}$, a number average molecular weight $M_n \approx 40\,000\text{ g.mol}^{-1}$ and a polydispersity index $PDI \approx 6$, were obtained.

The particle size increased with pH and with the fraction of ionic moieties from 155 nm to 250 nm with tailing (Table 7). The particle sizes of EP-MAA₁₁₅M₁₂₀ and EP-MAA₁₉₅M₂₀₀ at pH 8 are not available because larger than the filters pore size (1200 nm). These results suggest that the particles swell or aggregate with increasing ionicX and increasing pH and, therefore, larger hydrodynamic radii are obtained at those conditions.

Table 7. Molecular weights of the polymers measured by SEC and particle size modi of the dispersions measured by HDC

Experiment	pH	Particle size (nm)	SEC		
			M_w (g.mol ⁻¹)	M_n (g.mol ⁻¹)	PDI
EP-M₁₀₀	2	155	206 000	44 200	4.7
	8	147 + t*			
EP-MAA₄₅M₅₀	2	117, 198	220 000	41 700	5.3
	8	175, 284 + t			
EP-MAA₉₅M₁₀₀	2	152, 228 + t	222 000	35 800	6.2
	8	258 + t			
EP-MAA₁₁₅M₁₂₀	2	200 + t	259 000	35 500	7.3
	8	n.a.			
EP-MAA₁₉₅M₂₀₀	2	189 + t	237 000	38 100	6.2
	8	n.a.			

*t=tailing

ii. Gel content of the polymer films

The gel content of the different polymer films was evaluated. Results are specified in Table 8 (a summary of the physicochemical properties of the samples is given in Appendix 1). It is expected that swelling and crosslinking density correlate inversely.

However, in low crosslinked polymers the immiscibility of charges might also contribute to swelling differences. Curiously, increasing the pH of the dispersions (i.e. triggering the formation of ionic crosslinks) did not have an influence on the gel fraction measured in MEK and EtOH. It suggests that either the ionically crosslinked network was not measured by the gel content method, or the ionic interactions did not form in the organic solvents.

Table 8. Gel contents measured in MEK and EtOH for the series of sample at pH 2 and 8

Experiment	pH	Gel%	
		in MEK	in EtOH
EP-M₁₀₀	2	52	83
	8	51	87
EP-MAA₄₅M₅₀	2	46	81
	8	47	84
EP-MAA₉₅M₁₀₀	2	36	59
	8	38	73
EP-MAA₁₁₅M₁₂₀	2	32	1
	8	35	2
EP-MAA₁₉₅M₂₀₀	2	28	2
	8	26	1

Higher swelling ratios were measured for EP-M₁₀₀, EP-MAA₄₅M₅₀ and EP-MAA₉₅M₁₀₀ with respect to EP-MAA₁₁₅M₁₂₀ and EP-MAA₁₉₅M₂₀₀ in MEK, indicating that an increased ionicX decreased swelling in MEK. The gel content measured in a more polar solvent like EtOH (i.e. that might dissolve better the polyampholyte) also decreased from 81 % to 1 and 2 % for respectively EP-MAA₄₅M₅₀, EP-MAA₁₁₅M₁₂₀ and EP-MAA₁₉₅M₂₀₀. This suggests that EP-MAA₁₁₅M₁₂₀ and EP-MAA₁₉₅M₂₀₀ did not contain covalent crosslinks. The swelling ratios for EP-M₁₀₀, EP-MAA₄₅M₅₀ and EP-MAA₉₅M₁₀₀ in EtOH were respectively 83, 81 and 59 %, indicating formation of covalent networks in samples with low ionicX through secondary reactions. The architecture of the polymer chains might thus vary with the MAETAC and MAA molar fractions; and induce composition drifts in the reactions for high ionicX content.

iii. Morphology of the polymer films

Good film forming ability of latexes and dispersions is an important feature for coated applications and is crucial for high adhesive performance. In order to form a film, dispersions are coated or poured in a mould, water evaporates and the polymer particles stack on one another within the remaining solid film. If during drying the polymer chains contained in the core of the particles do not interpenetrate and form an entangled network, this can result in low cohesiveness (low resistance to shear) and/or polymer ordering and decrease of tackiness[30, 31].

To examine the homogeneity of the dispersion films, cross-cuts of films from the different latexes were imaged by Atomic Force Microscopy (AFM) in tapping mode. Latexes were disposed on droplet holders. The holders were positioned backwards during the drying of the film to form smooth polymer droplets. The dried droplets were cut with a diamond knife to obtain cross-sections.

The AFM phase pictures obtained for EP-MAA₉₅M₁₀₀ and EP-MAA₁₁₅M₁₂₀ in tapping mode, can be seen in Figure 4. The samples showed a biphasic structure with areas of lower phase contrast (brown) representing a soft polymer matrix while yellow points were made of harder material. A possible reason for the appearance of this biphasic structure is polymer or particle phase-separation due to a difference in composition. The black areas are likely due to the migration of surfactant to the film surface. This hypothesis was confirmed by treating the samples with water, which washed off the dark areas (seen in Appendix 2).

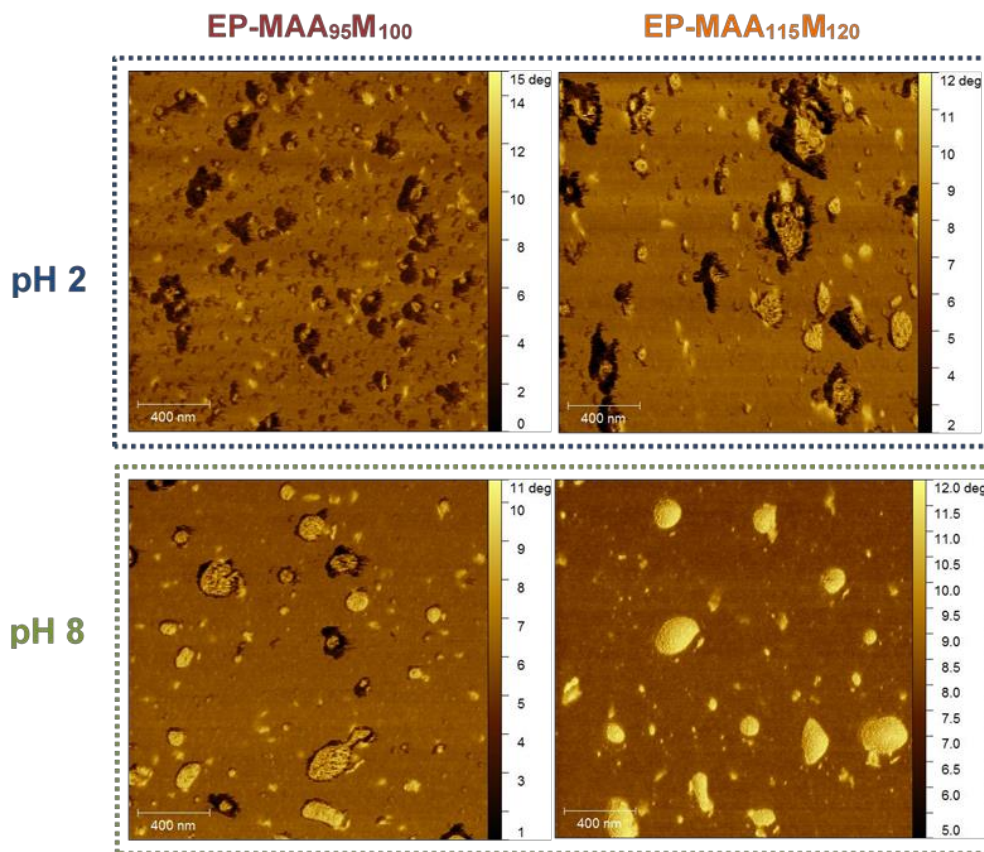


Figure 4. AFM phase cross-cut pictures of EP-MAA₉₅M₁₀₀ and EP-MAA₁₁₅M₁₂₀ at pH 2 and pH 8

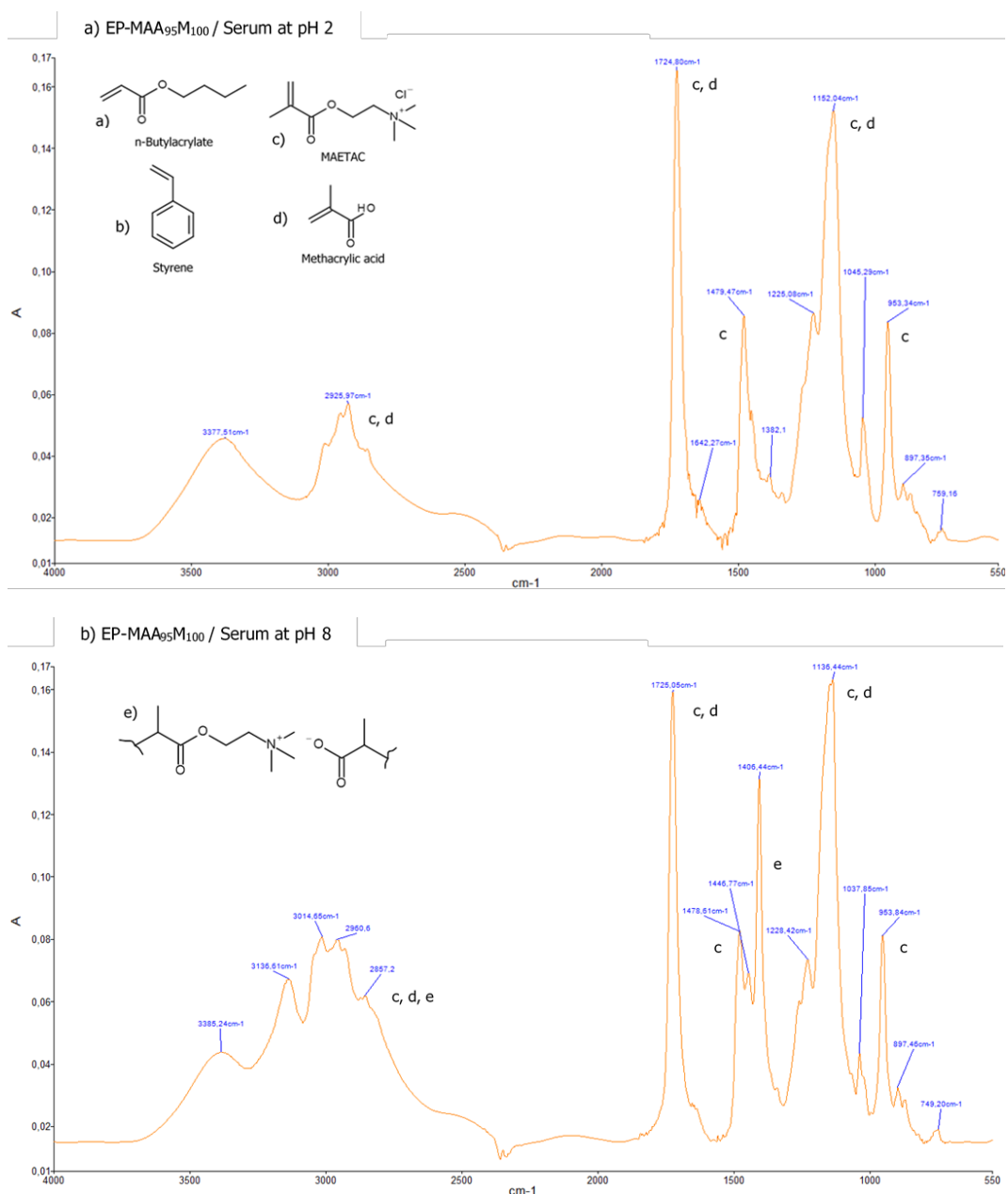
To understand if these white dots come from phase-separation of polymer chains or from polymer particles, separation of the water phase (serum) and the particles (sediment) from the emulsion was carried out using an Analytical Ultracentrifuge (AUC) for EP-MAA₉₅M₁₀₀ and EP-MAA₁₁₅M₁₂₀. The Infrared (IR) spectra of the two collected phases were dried and measured with Diamond Attenuated Total Reflectance Spectrometer (ATR). The spectra were compared to those of MAETAC and are available in Appendix 3 to 6. Spectra of the serum phase of EP-MAA₉₅M₁₀₀ at pH 2 and 8 are displayed in Figure 5.

The serum phases at pH 2 and 8, showed the same absorptions characteristic of MAETAC: $\nu(\text{C}=\text{O})$ at 1724 cm^{-1} , $\nu(\text{C}-\text{O})$ at 1148 cm^{-1} which corresponds to the carbonyl of the acrylate part, plus $\nu(\text{C}-\text{N})$ at 1476 cm^{-1} for the ammonium, $\nu(\text{C}-\text{H})=953, 1038\text{ cm}^{-1}$ of the ethyl and water is also present with a broad shoulder around 3400 cm^{-1} .

In this region another shoulder is observed with four peaks 2858, 2960, 3016 and 3143 cm^{-1} which could be an overlapping of $\nu(\text{Csp}^3\text{-H})=2800 \text{ cm}^{-1}$ of the N-CH_3 groups and the $\nu(\text{O-H})$ of a carboxylic acid, here only Methacrylic acid is conceivable. The band for C=O and C-O would overlap with the one of the acrylate of MAETAC. No band for the alkene C=C of the monomer is found in the serum ($\nu(\text{C=C})=1650 \text{ cm}^{-1}$). At pH 8, an increase of the bands at 3132 and 2959 cm^{-1} and new peaks at 1447 and 1407 cm^{-1} were observed. If considering that at this pH the MAA and MAETAC would interact, this could correspond respectively to the C-H and the C=O in the complex $\text{R}(\text{CH}_3)_2\text{N}^+\text{OOC-CH}_3$ [32].

The analysis of the sediment (at both pH) showed bands that correspond to the groups of acrylates of n-BA with $\nu(\text{C=O})=1729 \text{ cm}^{-1}$, $\nu(\text{C-O})=1160 \text{ cm}^{-1}$, $\nu(\text{C-H})=1470\text{-}1420 \text{ cm}^{-1}$ and aromatic of styrene $\nu(\text{C=C})=1450 \text{ cm}^{-1}$, $\delta(\text{Csp}^2\text{-H})=1250\text{-}900 \text{ cm}^{-1}$ and $\nu(\text{Csp}^2\text{-H})=3080\text{-}3010 \text{ cm}^{-1}$. The band of MAA with $\nu(\text{OH})$ around 2900 cm^{-1} should also overlap in this region, another indication for MAA is given by the peak at 1240 cm^{-1} for an additional C-O stretch.

The IR analysis thus suggested that two distinct polymers were synthesized, and correlate with AFM images. It appears that n-BA-co-MMA-co-MAA (soft polymer, brown matrix) was formed inside the particles while MAETAC-co-MAA (hard polymer, yellow areas) was polymerized in the water phase; and that the polymers could not mix during film formation giving the biphasic structure.

Figure 5. IR spectra of the Serum phase of EP-MAA₉₅M₁₀₀ at a) pH 2 and b) pH 8

iv. Characterization of the thermal and mechanical properties of the polymer films

The glass transition temperature (T_g) of the polymers was measured by Differential Scanning Calorimetry (DSC) and found to be around -20°C (available in Appendix 1). The fraction of ionic groups did not have any influence in the T_g of the polymers.

The mechanical properties of the polymer films were measured by oscillatory rheology and uniaxial tensile tests. Dried films of thickness ~ 1.2 mm of the samples set, were analysed by linear rheology with a plate-to-plate geometry of 25 mm. Frequency sweep tests were carried out with an amplitude of 1%. The curves of the elastic G' and loss G'' modulus as function of the angular frequency ω for films prepared at pH 2 and 8 and measured at $T=25^\circ\text{C}$, are available in Appendix 7. The loss tangent as function of ω are displayed in Figure 6.

The rheological curves of all samples showed a rubbery plateau with $G' > G''$ at high frequency (rubbery region) and $G' \sim 0.1\text{-}0.3$ MPa, and a $\tan \delta = G''/G'$ between 0.5 and 1, both at pH 2 and 8. This rheological behaviour is characteristic of low crosslinked materials. At frequencies below 0.1 rad.s^{-1} the transition to the flowing regime ($G'' > G'$, $\tan \delta > 1$) was observed in EP-MAA₁₁₅M₁₂₀ and EP-MAA₁₉₅M₂₀₀. Although these polymers contain a higher ionicX, the interactions between the chains seem to be weaker.

The pH did not affect the shape of the rheological curves, indicating that the observed rheological response at the measured frequency range was not dominated by ionic interactions to a significant extent. Entanglements or non-ionic intermolecular interactions between the polymer chains would be responsible for the observed transitions. Only in the case of EP-MAA₉₅M₁₀₀, the values of $\tan \delta$ are shifted between 0.75 and 0.5 (Figure 7) from pH 2 to 8. This suggests that the interactions between polymer chains in EP-MAA₉₅M₁₀₀ were reinforced upon the deprotonation of acid groups.

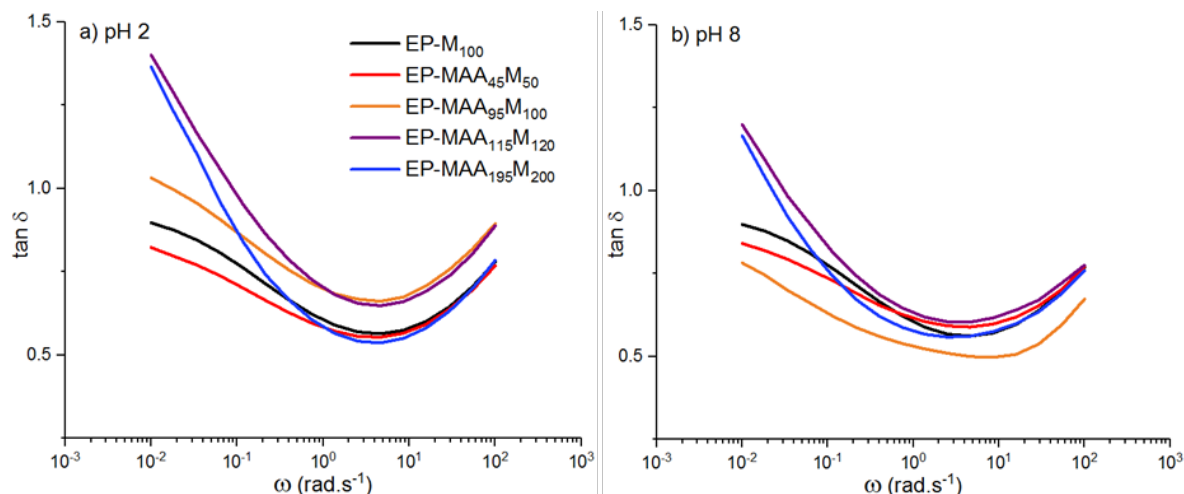


Figure 6. Loss tangent $\tan \delta$ as function of angular frequency ω for a) pH 2 and b) pH 8

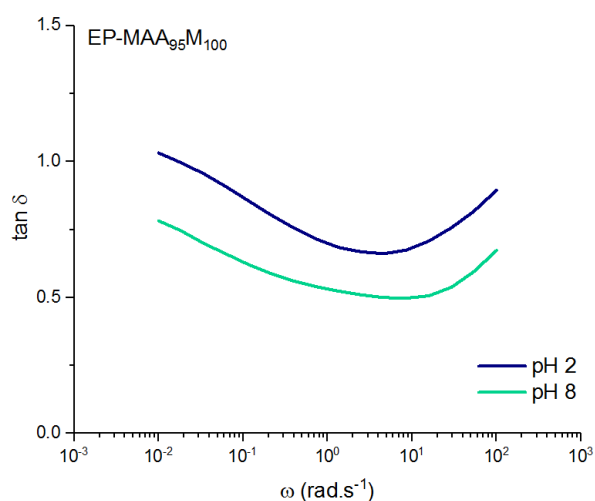


Figure 7. Comparison of $\tan \delta$ at pH 2 and 8 for EP-MAA₉₅M₁₀₀

The behaviour of a polymer at low frequencies can be correlated to its behaviour at higher temperature on a shorter range of frequency. Time-Temperature Superposition measurements were realized for all samples with temperatures starting from 25 then 30 to 180°C, in 10°C steps, with an amplitude of 1% and a frequency range from 1 to 100 rad.s⁻¹.

By compiling measurements on short range frequency at different temperature by shifting factors a_T and b_T , a master curve for G' and G'' for a larger frequency range can be obtained. The samples master curves for $T=25^\circ\text{C}$ are shown in Figure 8.

A rubbery plateau is observed at high frequency, as expected for viscoelastic polymers. A cross-over of the G' and G'' curves was observed at $10^{-3} < \omega < 10^{-1} \text{ rad.s}^{-1}$ (i.e first transition, the cross-over frequency, ω_{c1}). The cross-over was not followed by a classical flowing regime with $G'' \gg G'$ (i.e. terminal relaxation). Instead, a transitive regime with $G' \approx G''$ was observed. At lower frequencies, $\omega < 10^{-3} \text{ rad.s}^{-1}$, a second cross-over point was seen (i.e. second transition for ω_{c2}), which was followed by a second rubbery plateau with $G' > G''$. This rubbery plateau is indicative of a loose network (i.e. high molecular weight between crosslinks M_c). It was observed in all samples, including those at pH 2 where no ionic crosslinks should be present, and therefore it should be associated to a covalent network.

The nature of the molecular interactions responsible for the first rubbery plateau at high frequency was also observed in samples at pH 2 and 8. Therefore, it can be assumed that it is associated to entanglements and likely covalent crosslinks between chains, at least for EP-M₁₀₀, EP-MAA₄₅M₅₀ and EP-MAA₉₅M₁₀₀ for which high gel contents were measured. This hypothesis would imply that the polymer films have complex architectures which can resemble to a double network: one network is rather dense (low molecular weight between crosslinks M_c), formed from a combination of different molecular interactions (entanglements and/or covalent crosslinks and/or branches); and can be seen with the first rubbery plateau at high frequency. The second network is loose, likely formed from covalent crosslinks and can be seen by the second elastic plateau at very low frequencies.

To further understand the impact of the concentration of ionic groups on the polymers responses; the cross-over frequencies ω_c for the first ($10^{-3} < \omega_{c1} < 10^{-1}$ rad.s⁻¹) and second transition ($\omega_{c2} < 10^{-3}$ rad.s⁻¹) are displayed as function of ionicX in Figure 9 and a table of data in Appendix 9. For the first transition ω_c increased one degree of magnitude from $\sim 2.10^{-3}$ to 5.10^{-2} rad.s⁻¹ with increasing ionicX from 0 to 12.4 wt%. This trend was observed at pH 2 and 8. These results indicate that the samples with higher ionic co-monomer concentration contained less or weaker molecular interactions between polymer chains and could transit to flowing regime more easily (i.e. at higher frequency). However, the polymer with 5.9 wt% ionicX (i.e. EP-MAA₉₅M₁₀₀) was toughened by the increase of pH as ω_c decreased to 2.10^{-3} rad.s⁻¹, suggesting that ionic interpolymer interactions also affected this transition.

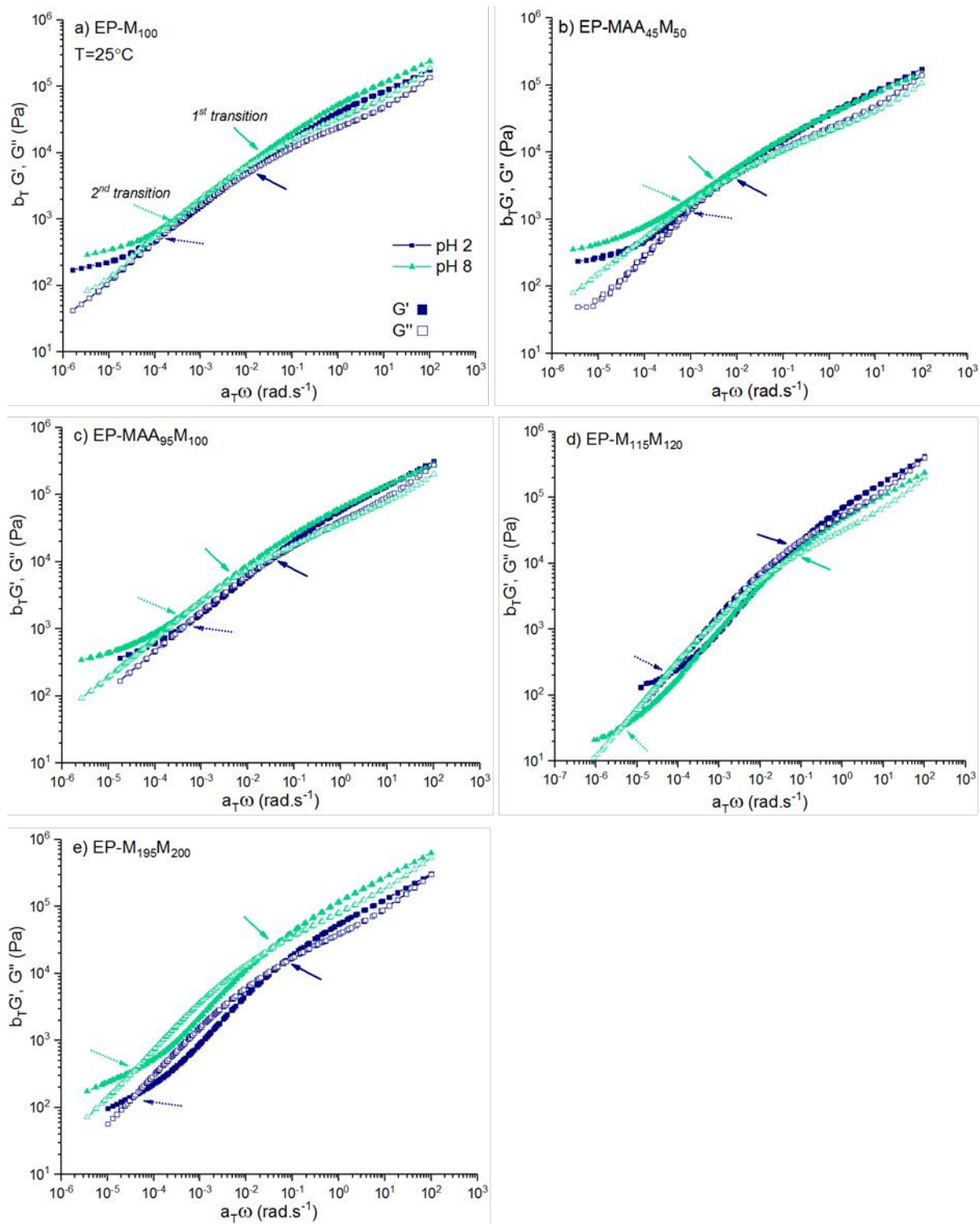


Figure 8. Master curves at $T=25^\circ\text{C}$ obtained for the set of samples with increasing ionicX;
an enlargement of the master curves is given in Appendix 8

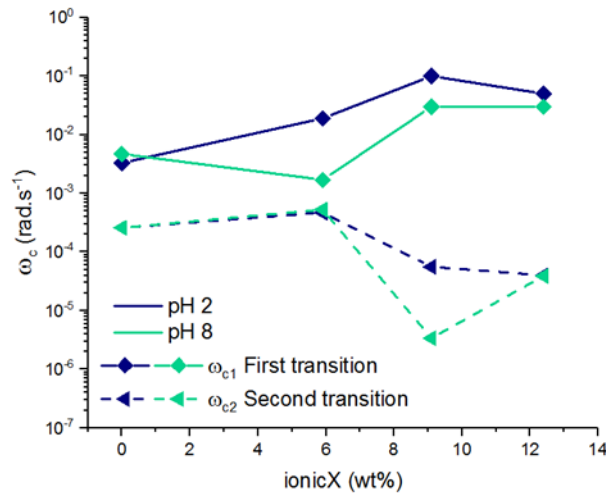


Figure 9. Evolution of cross-over frequency ω_c as function of ionicX for the first and second transitions

The influence of ionicX on ω_c of the second transition was antagonist. From 0 to 12.4 wt% ionicX, ω_c decreased by an order of magnitude to $\sim 4 \cdot 10^{-5} \text{ rad.s}^{-1}$. At pH 8, ω_{c2} shifted to $\sim 3 \cdot 10^{-6} \text{ rad.s}^{-1}$ for EP-MAA₁₁₅M₁₂₀ (i.e. 9.1 wt% ionicX) as the polymer gained in stiffness. Overall, the difference between ω_{c1} and ω_{c2} increased with ionicX, the transitive regime is thus longer for EP-MAA₁₁₅M₁₂₀ and EP-MAA₁₉₅M₂₀₀.

Although two structures (i.e. networks) are recognized in the rheological measurements, it is difficult to connect the results with the film morphologies discussed in paragraph II.2.F.iii. One could assume that the inclusions of MAETAC-co-MAA inside the n-BA-co-MAA-co-MAA matrix act as fillers in the films, and the responsible for the observed second elastic plateau. However, in this case, an increase of stiffness would be expected with increasing ionicX (increased plateau modulus and high cross-over frequency ω_{c2}). But the data show the inverse trend: ω_{c2} decreased with ionicX. Therefore, no conclusive molecular scenario can be associated to the molecular nature of the relaxations.

Tensile tests were carried out on the set of samples to study the behaviour of the polymers at large strains. The latexes films were carefully dried to obtain thicknesses of ~ 1.2 mm and cut to the dimensions of DIN-53504 S3A of 4 mm width and 16 mm measuring length. The stress-strain curves at pH 2 and at pH 8 are compared in Figure 10, individual curves are available in Appendix 10. The related values of stress at yield σ_y , maximum stress σ_{\max} and elongation ϵ_{\max} , stress σ_B and elongation ϵ_B at break can be found in Appendix 12. The dependence of σ_{\max} and ϵ_B as function of ionicX can be found in Figure 11.

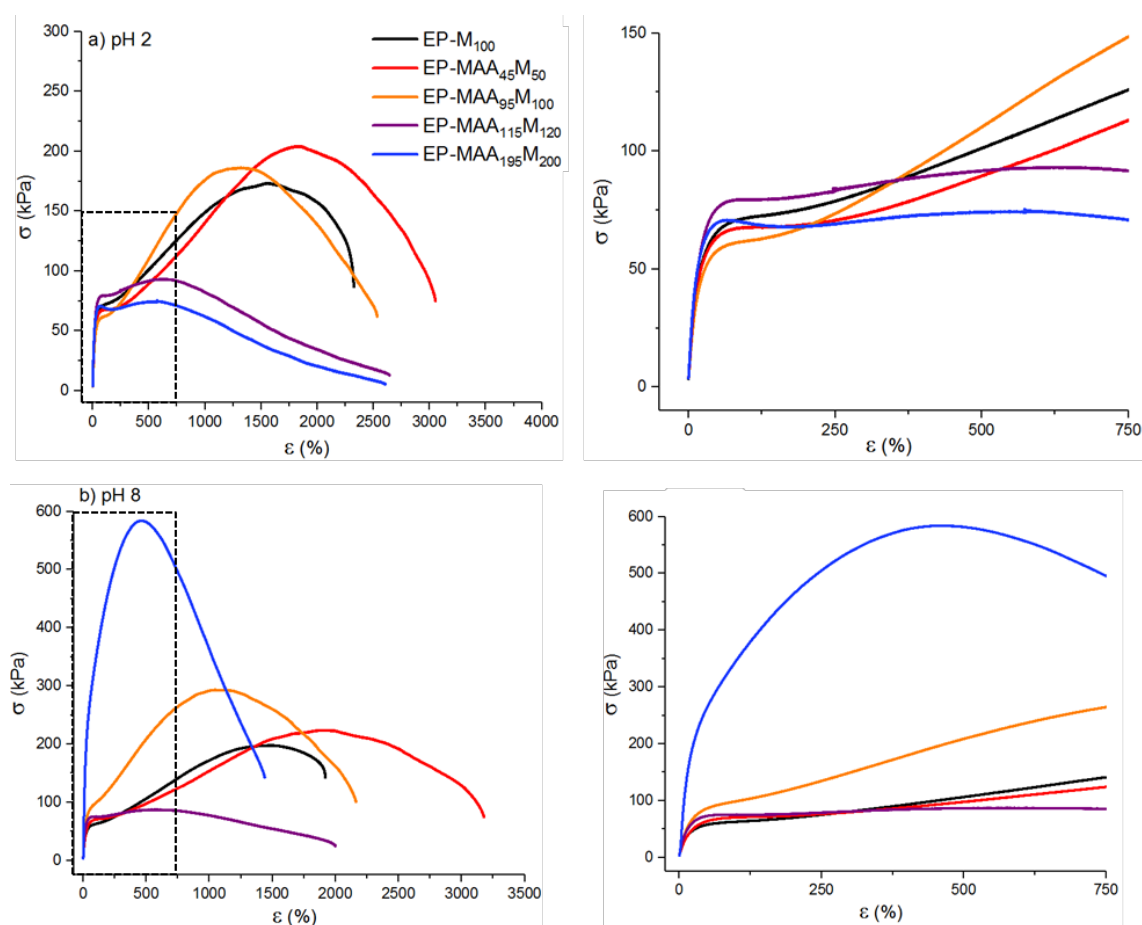


Figure 10. Stress-strain curves of all samples for a) pH 2 and b) pH 8

The stress-strain curves obtained for EP-M₁₀₀, EP-MAA₄₅M₅₀ and EP-MAA₉₅M₁₀₀ are consistent with the characteristics of crosslinked materials: first a shoulder was observed corresponding to the yield stress and the end of the elastic deformation of the polymer.

Then, strain-hardening was observed (sharp increase of stress); it is caused by the orientation of the polymer chains and resistance to the directional force by presence of branching, entanglements and crosslinks. Afterwards, the stress decreased and the sample broke.

The trend of the stress-strain curves for EP-MAA₁₁₅M₁₂₀ and EP-MAA₁₉₅M₂₀₀ was similar, but no strain-hardening was seen and the stress at break σ_B was low (<20 kPa). This suggests the two polymers were only slightly crosslinked in comparison to EP-M₁₀₀, EP-MAA₄₅M₅₀ and EP-MAA₉₅M₁₀₀ and that high ionicX decreases the number of branching and/or entanglements and/or crosslinks responsible for the strength of the polymer networks.

Increasing the pH 8 only had an effect on EP-MAA₉₅M₁₀₀ and EP-MAA₁₉₅M₂₀₀. The strain-hardening increased further for EP-MAA₉₅M₁₀₀ and the stress-strain curve for EP-MAA₁₉₅M₂₀₀ only showed a large peak, characteristic of brittle polymers.

At pH 2, for EP-M₁₀₀, EP-MAA₄₅M₅₀ and EP-MAA₉₅M₁₀₀ σ_{max} reached 200 kPa with strain-hardening for $\epsilon > 1250\%$; while σ_{max} reached 94 and 76 kPa for respectively EP-MAA₁₁₅M₁₂₀ and EP-MAA₁₉₅M₂₀₀. As σ_{max} is a measure of the maximal force that can be sustained by the sample, it appears the mechanical resistance of EP-M₁₀₀, EP-MAA₄₅M₅₀ and EP-MAA₉₅M₁₀₀ is higher than for EP-MAA₁₁₅M₁₂₀ and EP-MAA₁₉₅M₂₀₀, although they contain high ionicX.

As seen in Figure 11, at pH 8 σ_{max} remained unchanged for most samples but increased for EP-MAA₉₅M₁₀₀ and EP-MAA₁₉₅M₂₀₀. This indicates a higher crosslinking density in comparison to the same polymers at pH 2, by triggering the ionic interactions. But it also shows that σ_{max} increased with ionicX as EP-MAA₉₅M₁₀₀ and EP-MAA₁₉₅M₂₀₀ became mechanically stronger than EP-M₁₀₀ and EP-MAA₄₅M₅₀, apparently due to more ionic crosslinks.

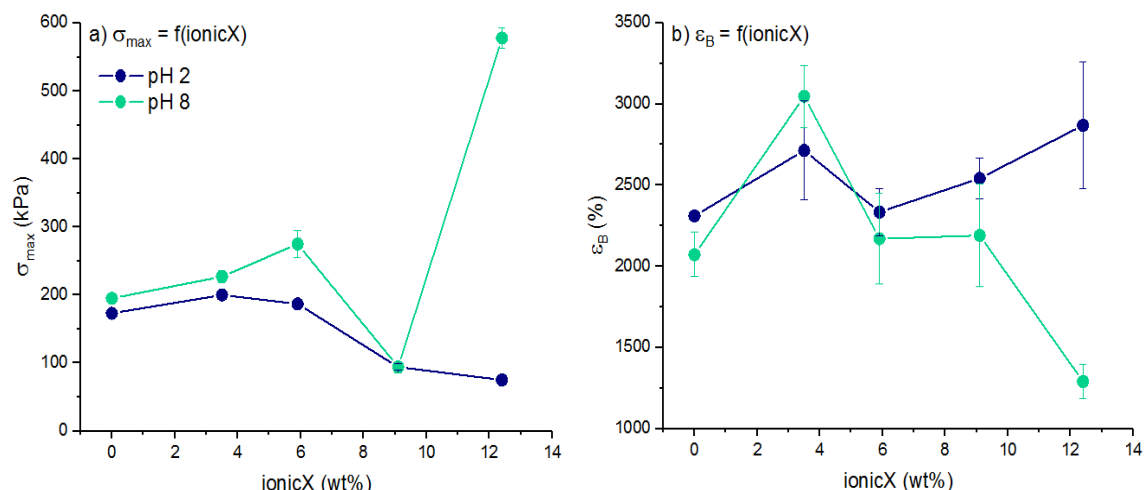


Figure 11. Evolution of σ_{\max} and ϵ_B as function of ionicX measured by tensile test

Although, EP-MAA₉₅M₁₀₀ exhibited stronger resistance to strain at pH 8, a similar elongation at break $\epsilon_B \sim 2500$ % was measured, suggesting the density of ionic crosslink points was still low so that the material was still dissipative (could dissipate the energy to deform with applied stress). On the other hand, from pH 2 to 8, ϵ_B decreased by a factor of 2 for EP-MAA₁₉₅M₂₀₀. In this case, the physical network was dense and more elastic due to high ionicX, which lowered its deformability. For low ionicX compounds, no significant change of ϵ_B was observed with the increase of pH.

It is important to note that the increase of crosslinking density induced by higher amounts of ionic moieties and increase of pH was seen with 5.9 and 12.4 wt% of ionicX (i.e. EP-MAA₉₅M₁₀₀ and EP-MAA₁₉₅M₂₀₀), but EP-MAA₁₁₅M₁₂₀ was unaffected by the pH. The sample cannot be considered, and its inconsistency will be discussed in the next section.

The results given by the tensile tests are in accordance with the measurements of the gel contents in II.2.F.ii. The differences in the strain-hardening behaviours at pH 2 can be associated to a lack of covalent crosslinks for EP-MAA₁₁₅M₁₂₀ and EP-MAA₁₉₅M₂₀₀ and this correlates well with the absence of gel contents measured in EtOH.

To relate to the polymers compositions discussed in II.2.F.iii. the strain-hardening feature of the polymer films would be given by the n-BA-co-St-co-MAA as it is more likely to undergo side-reactions for grafting and crosslinking. On the other hand, the increase of σ_{\max} at pH 8 is due to the formation of inter and intra-polymer (between MAETAC-co-MAA itself and with n-BA-co-St-co-MAA) ionic interactions that toughen the films.

v. Adhesive properties of the polymer films

The adhesive properties were first tested by probe-tack on films of thickness ~ 0.15 mm. The stress-strain curves obtained for the series of samples are available in Appendix 13 as well as the images taken of the detaching probe in Appendix 14. A comparison of all samples is given in Figure 12 at both pH and failure modes were recorded.

As introduced in Chapter I paragraph 2.B.iii., the stress-strain curves are important to understand the debonding mechanism involved in the adhesive layers. The parameters σ_{peak} , σ_{\max} , ϵ_{\max} and the work of debonding W_{deb} extracted from the curves were used to compare the samples with increasing ionicX and are displayed in Figure 13; a summary of the data obtained from the measurements is shown in Appendix 16.

At pH 2 the stress-strain curves of samples with low MAA and MAETAC content (EP-M₁₀₀, EP-MAA₄₅M₅₀, EP-MAA₉₅M₁₀₀ and EP-MAA₁₁₅M₁₂₀) showed characteristics of low crosslinked materials: with increased strain, the stress first reached a sharp maximum σ_{peak} , then decreased and stabilized to a plateau region with σ_{plateau} ; after that, σ decreased slowly to σ_{\max} when the probe detached from the adhesive.

The σ_{peak} fall in the same range ~ 600 -900 kPa for all samples, but the behaviour at higher strains differed among them. Samples with higher ionic monomer content, i.e. EP-M₁₀₀, showed a short plateau, low $\epsilon_{\max}=4$ and formation of fibrils (seen in Appendix 13) which detached via an adhesive failure mode (i.e. no adhesive residue left on the substrate).

EP-MAA₄₅-M₅₀ showed a plateau followed by a sharp decrease of σ , which can be associated to an entering of air in the cavities (i.e. equilibrium of pressure)[33]. Adhesive failure was obtained in this case, and no elongated fibrils were seen, suggesting that the polymer was too stiff (most likely crosslinked) for energy dissipation.

EP-MAA₉₅M₁₀₀ showed a long plateau with $\sigma_{\text{plateau}}=153$ kPa, with stable fibrils observed on the camera (seen in Appendix 14) which sustained load to $\epsilon_{\text{max}}=19$, dissipating efficiently energy.

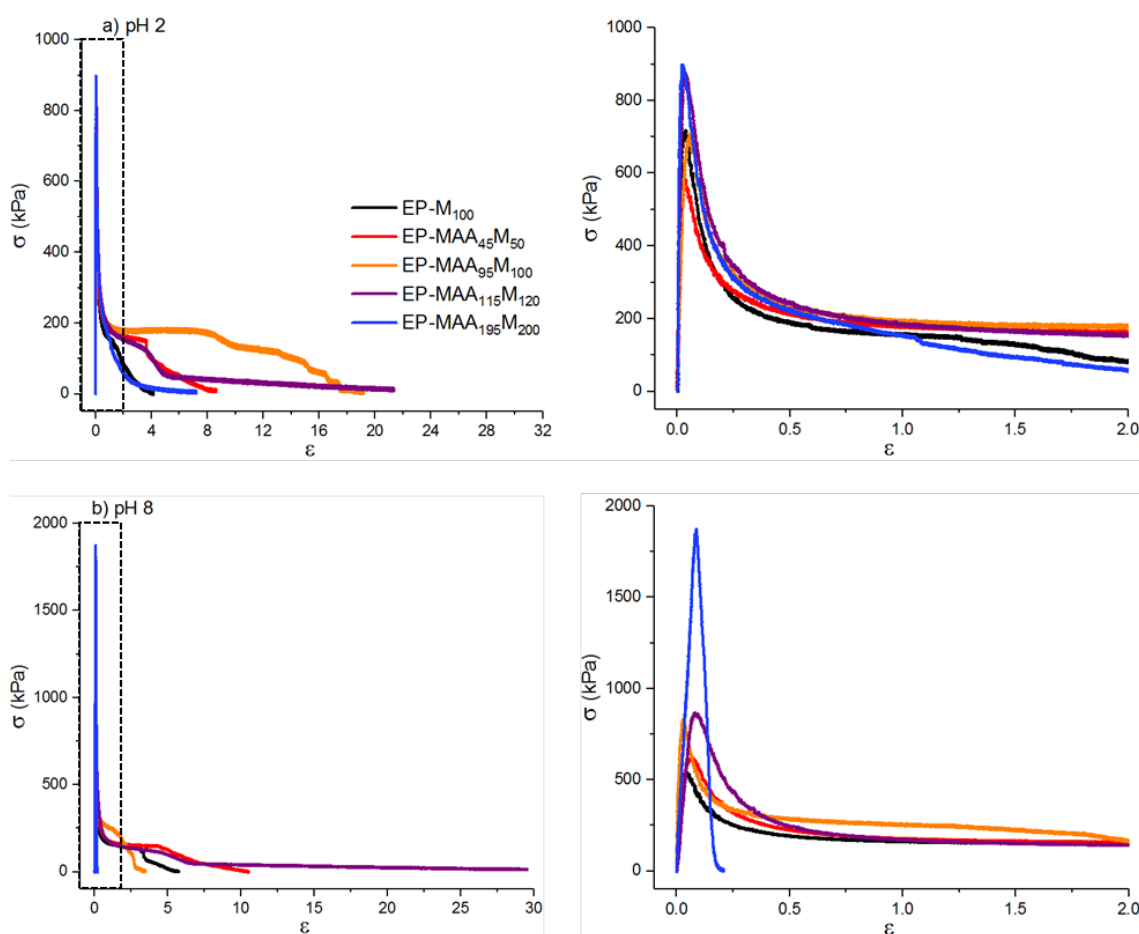


Figure 12. Comparison of tack stress-strain curves of samples at a) pH 2 and b) pH 8

While EP-MAA₁₁₅M₁₂₀ showed a plateau as well but full debonding at shorter strain $\epsilon_{\text{max}}=4$ suggesting viscous polymer as cohesive failure was observed. EP-MAA₁₉₅M₂₀₀ showed a viscous behaviour as no fibrillation plateau and cohesive failure (failure in adhesive bulk) were observed.

No clear influence of ionicX was seen on the probe-tack measurements at pH 2, as the two samples with the higher amount of ionicX (i.e. EP-MAA₁₁₅M₁₂₀ and EP-MAA₁₉₅M₂₀₀) showed the weakest resistance to debonding by viscous dissipation and contained thus fewer crosslinks.

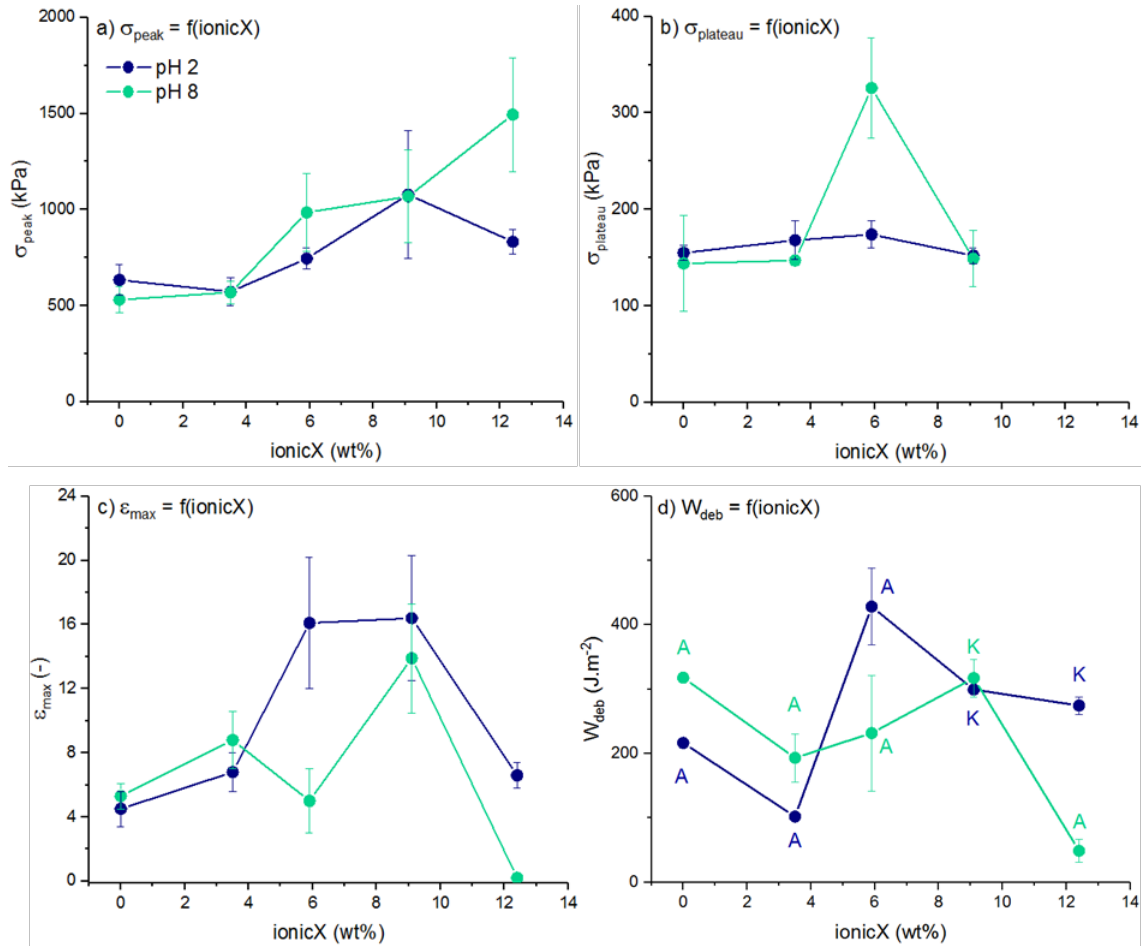


Figure 13. Evolution of a) σ_{peak} b) σ_{plateau} c) ϵ_{max} and d) W_{deb} as function of ionicX for pH 2 and 8

At pH 8 similar trends were observed. The same curve was observed for EP-M₁₀₀ plus stable fibrils and adhesive failure were obtained. No influence of pH was seen on the curve of EP-MAA₄₅M₅₀ yet fibrils were observed and still resulted in adhesive detachment.

The opposite was seen for EP-MAA₉₅M₁₀₀, the plateau stress had the same value as at pH 2, but ϵ_{max} was divided by 3; no stable fibrils were observed but a depletive front at the surface of the probe, this change in failure can be seen in Figure 14.

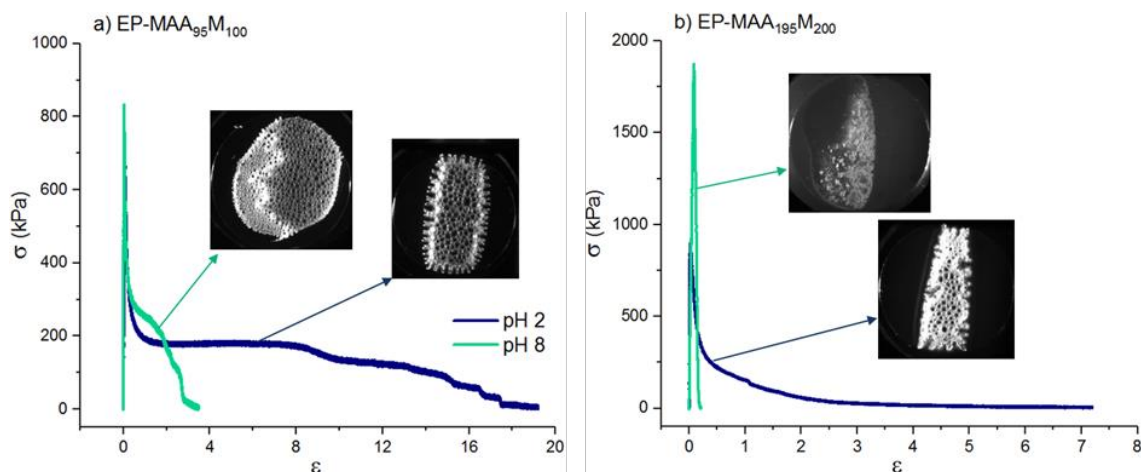


Figure 14. Comparison of tack stress-strain curves at pH 2 and pH 8 for a) EP-MAA₉₅M₁₀₀
and b) EP-MAA₁₉₅M₂₀₀

On the other hand, EP-MAA₁₁₅M₁₂₀ showed no effect of a change of pH, ϵ_{\max} even increased to ~ 30 but the polymer was viscous as the observed fibrils were flowing and sustained low σ . On the contrary, the behaviour of EP-MAA₁₉₅M₂₀₀ switched from viscous to brittle-like with σ_{peak} multiplied by 2 and ϵ_{\max} decreased to 0.2, no fibrils were observed, detachment took place without formation of defined cavities as seen in Figure 14. The density of ionic crosslinking was therefore high and made the polymer too elastic.

The influence of increased ionicX and pH is unclear, the values of the work of debonding W_{deb} illustrated in Figure 13 scattered and did not reflect the expected trend where adhesion measured with W_{deb} should increase at intermediate ionicX (i.e. crosslinking density) due to more inter/intrapolymer interactions which improve energy dissipation. With higher ionicX, W_{deb} should then decrease as the elastic character of the polymer chains prevail and favour energy storage.

In connection to previous mechanical properties, the behaviours of the polymer films in probe-tack were similar to tensile tests. At pH 2 for EP-MAA₁₁₅M₁₂₀ and EP-MAA₁₉₅M₂₀₀, a lack of covalent crosslinks was reflected at large strains, as the samples showed characteristics of flowing polymers and no fibrillation plateaus were formed.

By increasing the pH to 8, the inter and intrapolymer interactions between n-BA-co-St-co-MAA and MAETAC-co-MAA stiffened the whole polymer films and cracks propagation were observed rather than fibrillation resulting in lower adhesion.

The adhesive performance of the latexes was also measured by Peel tests on steel with dried films of grammage 20 g.m^{-2} (20 g of dried polymer per m^2) coated on Polyethylene terephthalate (PET) backing. Films strips of 25 mm width were cut, and tests were carried out over a length of 150 mm, at 180° angle and for different contact times of $t_c=2 \text{ min}$ and $t_c=24 \text{ h}$. The Peel mean forces F_{mean} and the failure modes are shown in Figure 15 for pH 2 and 8 as function of ionicX, the table of values is available in Appendix 17.

For short contact times ($t_c=2 \text{ min}$) and pH 2, the ability of the polymers to wet the substrate (low strain behaviour) was not influenced by the concentration of ionic moieties as F_{mean} was constant $\sim 8 \text{ N.25 mm}^{-1}$ and adhesive failures modes were observed. However, at pH 8 the peel force was slightly decreased for 5.9 wt% ionicX (i.e. EP-MAA₉₅M₁₀₀) which could be due to the strengthening of the polymer network likely with ionic crosslinks. On the contrary, a higher pH increased F_{mean} for 12.4 wt% ionicX, but adhesive failure was also observed so the polymer was more resistant to debonding than at pH 2.

A prolonged contact time favoured overall the adhesion at pH 2 and pH 8, but especially for EP-MAA₉₅M₁₀₀ and EP-MAA₁₉₅M₂₀₀ at pH 8. The wetting of the samples was improved by letting the polymer chains relax and optimize the penetration depth of the adhesive layer in the substrate. The same adhesive/filmic (A/F) detachment (thin residual layer left on the steel substrate) was observed for all samples which means that the crack propagation for debonding happened at the near interface between the adhesive layer and the steel substrate.

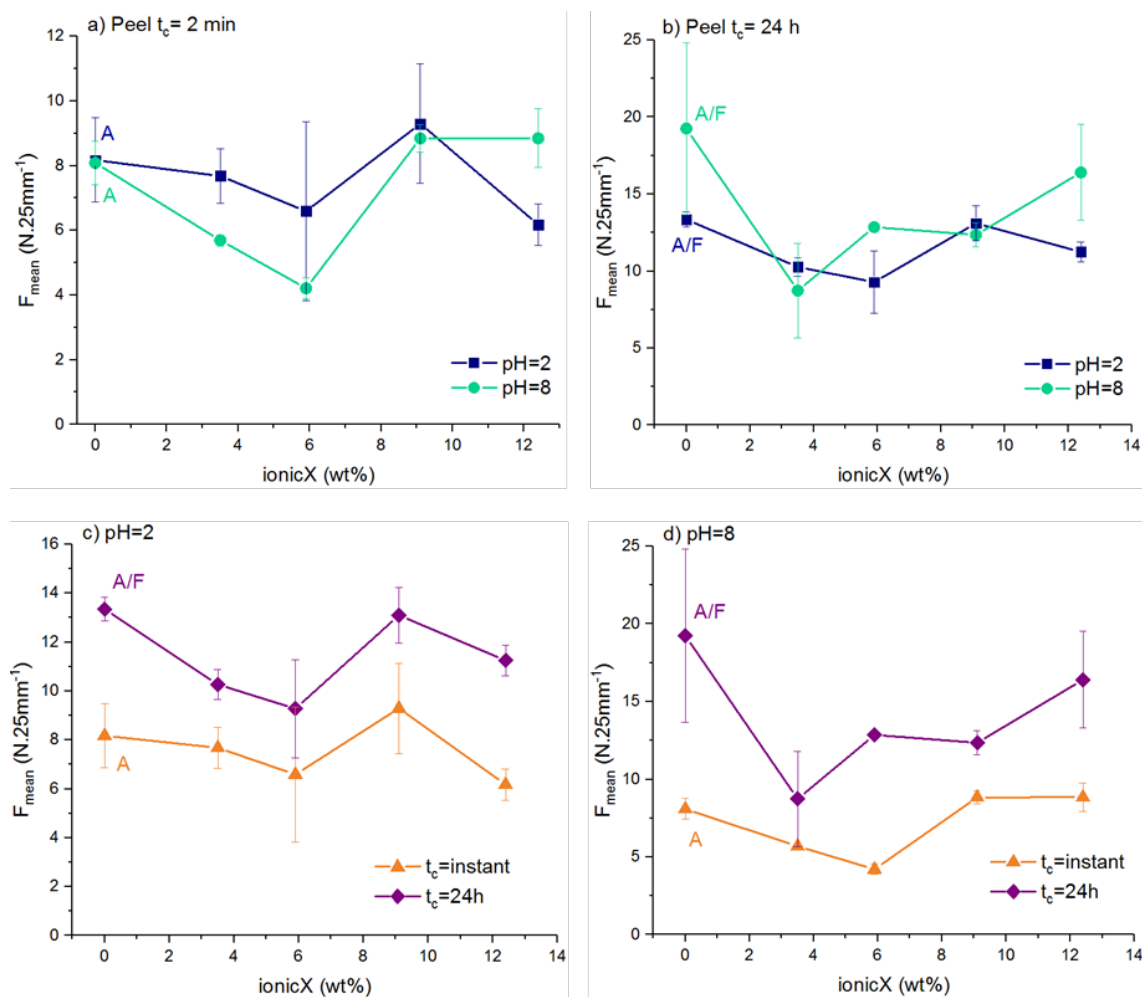


Figure 15. Comparison of F_{mean} at pH 2 and 8, for $t_c=2$ min and 24 h as function of ionicX

At higher pH, the peel forces increased respectively to 13 and 16 N.25 mm^{-1} for EP-MAA₉₅M₁₀₀ and EP-MAA₁₉₅M₂₀₀. This suggested that the samples with higher ionicX content had stronger intermolecular interactions.

Static shear test was carried out with a 1.5 kg weight, on contact area of 25 mm^2 with steel plates and with a dwelling time of 10 minutes. The holding power (i.e. shear strength), recorded as the time needed for the adhesive joint to fail under shear load; is represented in Figure 16 as function of ionicX.

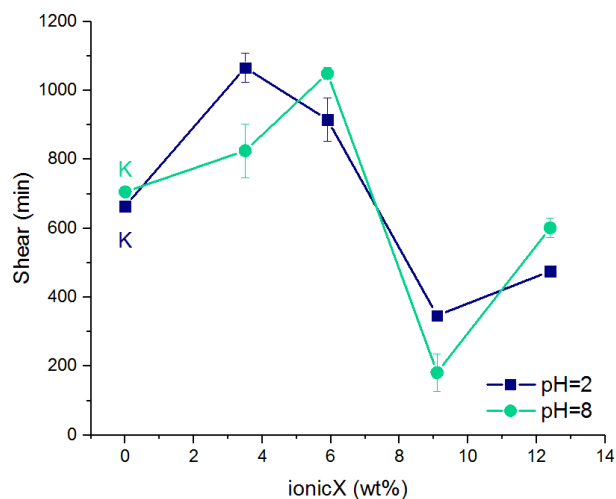


Figure 16. Comparison of shear holding power at pH 2 and 8 as a function of ionicX

Although shear strength is expected to increase at higher crosslinking density, the holding power increased to ~1000 min until ionicX=5.9 wt%. and dropped to ~300-500 min for higher content of ionic functionalities, suggesting that the polymers with 9.1 and 12.4 wt% ionicX, are more viscous materials.

The effect of pH 8 was not obvious, differences are noticeable but can be considered in the error bar for a shear measurement.

II.3. DISCUSSION

The aim of this chapter was to produce polyampholyte copolymers by emulsion polymerization. Several components in the polymerization mixture were changed to study how the molecular design affects the emulsion stability. Starting with the surfactant, the latexes obtained were stable using quaternary ammonium and a non-ionic surfactant. A slight excess of coagulum was seen for the cationic emulsifiers when the alkyl part of the emulsifier was higher than C₁₂. This result suggests that longer hydrophobic tails may induce more steric hindrance inside the particles which increases their size and might lead to more emulsion instabilities. Latexes prepared with non-ionic surfactants were stable but collapsed at pH 8. This suggests the overall ionic charge of the dispersion should be cationic and that the isoelectric point should be higher than 8. Using an anionic surfactant resulted in strong destabilization due to attractive interactions between emulsifier and cationic monomer. It is therefore suggested that critical micelle concentration was not met, and the system could not be dispersed[9].

Different types (neutral, cationic and anionic) of initiators were also investigated. Polymerizations carried out with Wako V50, a cationic water-soluble azo initiator; and a reductive-oxidative system of tert-Butyl hydroperoxide/Rongalit® C gave stable dispersions. The latexes prepared with sodium persulfate collapsed. It has been reported[34] that the entry efficiency of an initiator (Potassium Persulfate and Wako V50) in polymer particles was independent of the charge of both initiator and surfactant (anionic and cationic). The strong sulfate ions of NaPS may therefore not interact with the surfactant but rather the cationic monomer and induce instability during the polymerization.

Four cationic monomers were tested, all dispersions were stable and medium amounts 3 wt% (~30 g for 1 L latex) of coagulum were found when using MAPTAMS and MAEEOAMS. It is believed that if the cationic monomer group of the polymer particles points towards the water-phase and MeSO₄⁻ binds stronger to the ammonium as Cl⁻, it might slightly compress the electrical double layer and create emulsions instabilities[35, 36].

Using a stable system with a cationic surfactant and t-BHP/Rongalit® C as initiator and a constant fraction of MAA (95 mmol) polymers with increasing MAETAC concentrations from 0 to 100 mmol were prepared. The experiment carried out without MAETAC was highly unstable, but increasing the amount of MAETAC to 10 mmol was sufficient to obtain stable latexes. Yet the emulsions obtained for fractions of MAETAC ranging from 10 to 50 mmol did not remain stable upon increasing pH. The slight excess of cationic monomers charges $R_1NMe_3^+$ over anionic charges R_2COO^- of MAA seems to play a key role to counter balance inter and intra molecular interactions upon deprotonation of acid moieties.

To study the isolated effect of ionic crosslinks in the network on the adhesive properties of PSAs, it was necessary to assess that the polymers did not contain covalent crosslinking. Using t-DMK as CTA no gel content was obtained in the polymers, while a gel content of 80 % was measured without t-DMK. Covalent networks were thus formed during the polymerization due to secondary reactions[28, 37] but could be avoided by adding t-DMK as chain transfer agent.

The influence of ionic monomer fraction ionicX and pH on the chemical, mechanical and adhesive properties of the final polymer was investigated. The polymer morphologies observed by AFM in (Figure 4) and the separation of serum and sediment by ultra-centrifugation evidenced that two polymers of different compositions were obtained during the syntheses. From our experimental design, we expected a polyampholyte copolymer containing n-BA, St, MAETAC and MAA to be buried inside the particles (Figure 2). Instead, we found that a copolymer of n-BA, St and eventually MAA was polymerized inside the particles, while a polymer of MAETAC and MAA was formed in the water phase to give a morphology presented Figure 17. This is attributed to the high affinity of the cationic monomer for the water-phase in comparison to particle diffusion. Brouwer et al.[38] have reported that seeded polymerization of styrene and a cationic monomer led to migration of the hydrophobic monomer in the seed particles resulting in separate polymerization of the monomers. Regarding MAA, as the polymerizations were carried out at acidic pH, it was expected to be buried in the particles[39] but the presence of MAETAC in the water phase might have hindered its diffusion to the hydrophobic phase.

Due to the heterogeneous polymers partition illustrated in Figure 17, the particle size measured by HDC increased with ionicX and pH as seen in Table 7. This can be explained by a higher swelling of the outer layer of the particles (formed from the hydrophilic polymer) by increasing ionicX. The resulting increase of the hydrodynamic radius would result in a higher particle size. With the addition of ammonia at pH 8, the particle size increased with the increased swelling. The tailing was likely induced by instabilities of the emulsion.

No covalent network was detected in the measurement of the gel content with increasing ionic X, i.e. for EP-MAA₁₁₅M₁₂₀ and EP-MAA₁₉₅M₂₀₀ (Table 8). Yet, with increased ionicX, the fraction of n-BA and St decreased. This would suggest that the CTA limits grafting/transfer reactions to polymer, but only acts on the n-BA/St/MAA (hydrophobic) fraction, probably due to its high hydrophobicity. Grafting or covalent crosslink points should increase the molecular weight M_w and the PDI measured by SEC. But in reality, only the molecular weight distribution of the polymer soluble part (low or un-crosslinked) is determined and justifies that no difference was seen for the series of samples (Table 7).

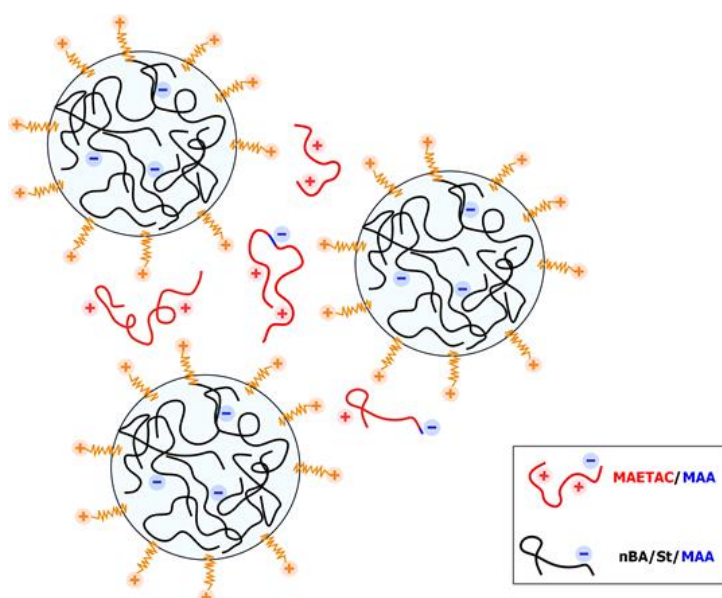


Figure 17. Possible structure of the two polymers system observed

The disappearance of gel fraction with high content of ionic monomers is both in agreement and contradiction with the mechanical properties of the samples. Although the analysis of $\tan \delta$ showed that EP-MAA₁₁₅M₁₂₀ and EP-MAA₁₉₅M₂₀₀ were dissipative materials, the master curves showed in all cases a second transition at low angular frequency $\omega < 10^{-3} \text{ rad.s}^{-1}$ where $G' > G''$ and $G' \approx 300 \text{ Pa}$ (Figure 8), indicating the existence of an elastic polymer network with low M_c and stiffness. The origin of this network is unclear, since the film architectures are complex. Although all samples appeared slightly crosslinked in linear rheology, tensile tests pointed the lack of covalent crosslinking at larger deformation of EP-MAA₁₁₅M₁₂₀ and EP-MAA₁₉₅M₂₀₀. First in tensile tests at pH 2, by their lower tendency for strain-hardening but also in probe-tack as flowing fibrils and low adhesive bulk cohesion were seen (Appendix 14). Finally, their dissipative behaviour was also recognized by low shear resistance [30, 40] $< 500 \text{ min}$ in comparison to EP-M₁₀₀, EP-MAA₄₅M₅₀ and EP-MAA₉₅M₁₀₀.

Given the poor linearity of the properties obtained for experiments with increasing fraction of ionic monomers, it would be complex to deduce the overall effect of ionicX on mechanical and adhesive properties. Only an assumption of the effect of pH 8 on the mechanical and adhesive properties excluding EP-MAA₁₁₅M₁₂₀ was clearly visible.

At pH 8, with deprotonation of the acidic moieties, the interpolymer ionic complexes led to more elastic materials for samples containing higher amount of ionicX. This was first seen at low strains (i.e. in linear rheology) for EP-MAA₉₅M₁₀₀ by the decrease of the first cross-over (rubbery region) frequency ω_{c1} (Figure 9). But the effect of the pH was more pronounced at long elongations.

In tensile tests, EP-MAA₉₅M₁₀₀ and EP-MAA₁₉₅M₂₀₀, showed stiffer behaviour with increased maximal stress σ_{\max} and decreased elongation at break ϵ_B (Figure 11). The impact of increased network density resulted in more resistant mechanisms to debonding in probe-tack. Comparing EP-MAA₉₅M₁₀₀ and EP-MAA₁₉₅M₂₀₀ at pH 8, ionicX is multiplied by 2 and by extension the ionic crosslink density, lower adhesion (determined by W_{deb} in Figure 13) was measured due to stiffening of the adhesive. This is not in accordance with the peel strength shown in Figure 15 and the shear resistance in Figure 16.

However, the peel forces and holding power should be interpreted with caution because are highly influenced by the apparent lack of covalent crosslinking even at high pH.

The dependency of the physical crosslinking only over high strains is similar to what was observed in different studies on percolating networks[41, 42] and nanostructured adhesives[43-45]. They reported similar results over which the dissipative mechanism during peeling was unchanged by the crosslinked network but that the shear resistance was improved.

In this chapter, the presence of a complex polymeric structure (like a percolating network or double network formed by the two different polymers) on the shear properties was not seen and cannot be discussed due to the poor linearity of the films mechanical properties observed at high ionicX.

II.4. CONCLUSION

The preparation by emulsion polymerization of polyampholyte particles of n-butylacrylate and styrene containing a strong base and a weak acid was challenging. The system was sensitive to emulsifiers, initiators and monomers. For a stable system using dodecyl trimethylammonium chloride as surfactant, tert-butyl hydroperoxide and Rongalit® C as initiating system and MAETAC as cationic monomer, the morphology of the films indicated that polymerization occurred in the two phases of the emulsion. A copolymer of MAETAC and MAA was found in the water-phase while nBA-co-St-MAA was positioned in the particles.

The results obtained for a varying ionicX were contrary to what was expected; the samples with higher ionicX content showed a more viscous behaviour by mechanical testing at higher strains. The overall effect of ionicX on the properties was difficult to understand, since the effect of pH i.e. the expected triggering of ionic interactions with increased ionization, was only noticed for the samples with ionicX= 5.9 and 12.4 wt%. The expected interpolymer complexes formed by increasing pH raised the mechanical resistance of the polymers at higher deformations. This effect was also noticed in probe-tack and tensile testing; but not in the peel tests.

Physical crosslinks were likely obtained by introducing oppositely charged moieties in the polymer. However, studying their effect on the adhesion of PSAs requires homogeneous distribution of the ionic groups in the polymer. Attempts to obtain these systems are presented in the next Chapter.

II.5. REFERENCES

1. Miwa, Y., et al., *Dynamic ionic crosslinks enable high strength and ultrastretchability in a single elastomer*. Communications Chemistry, 2018. **1**(1).
2. Stukalin, E.B., et al., *Self-Healing of Unentangled Polymer Networks with Reversible Bonds*. Macromolecules, 2013. **46**(18).
3. Dahlke, J., et al., *A New Approach Toward Metal-Free Self-Healing Ionomers Based on Phosphate and Methacrylate Containing Copolymers*. Macromolecular Chemistry and Physics, 2017. **218**(23).
4. Kalista, S.J., J.R. Pflug, and R.J. Varley, *Effect of ionic content on ballistic self-healing in EMAA copolymers and ionomers*. Polymer Chemistry, 2013. **4**(18).
5. Das, A., et al., *Ionic modification turns commercial rubber into a self-healing material*. ACS Appl Mater Interfaces, 2015. **7**(37): p. 20623-30.
6. Hohlbein, N., et al., *Self-healing dynamic bond-based rubbers: understanding the mechanisms in ionomeric elastomer model systems*. Physical Chemistry Chemical Physics, 2015. **17**(32): p. 21005-21017.
7. Feldstein, M.M., E.E. Dormidontov, and A.R. Khokhlov, *Pressure-sensitive adhesives based on interpolymer complexes*. Progress in Polymer Science, 2015. **42**: p. 79-153.
8. Levada, T.I. and M.M. Feldstein, *Relationship between intermolecular bonding, nanostructure, phase behavior, and macroscopic physical properties of pressure-sensitive adhesives based on polyelectrolyte complexes*. Journal of Applied Polymer Science, 2012. **125**: p. 448-470.
9. Urban, D. and K. Takamura, *Polymer Dispersions and their industrial applications*. 2002: Wiley-VCH.
10. Asua, J.M., *Emulsion polymerization: from fundamental mechanisms to process developments*. Journal of Polymer Science Part A: Polymer Chemistry, 2004. **42**: p. 1025-1041.
11. Penzel, E., *Polyacrylates*, in *Ullmann's Encyclopedia of Industrial Chemistry*. 2005, Wiley-VCH.
12. Herk, A.M.v., *Chemistry and technology of emulsion polymerization* 2013: John Wiley & Sons Ltd.
13. Noël, L.F.J., et al., *Model prediction of batch emulsion copolymerization as a function of conversion: a sensitivity analysis*. Journal of Polymer Science: Part A - Polymer Chemistry, 1994. **32**(11): p. 2161-2168.
14. Nomura, M., H. Tobita, and K. Suzuki, *Emulsion polymerization: kinetic and mechanistic aspects*, in *Polymer Particles*, M. Okubo, Editor. 2005, Springer.

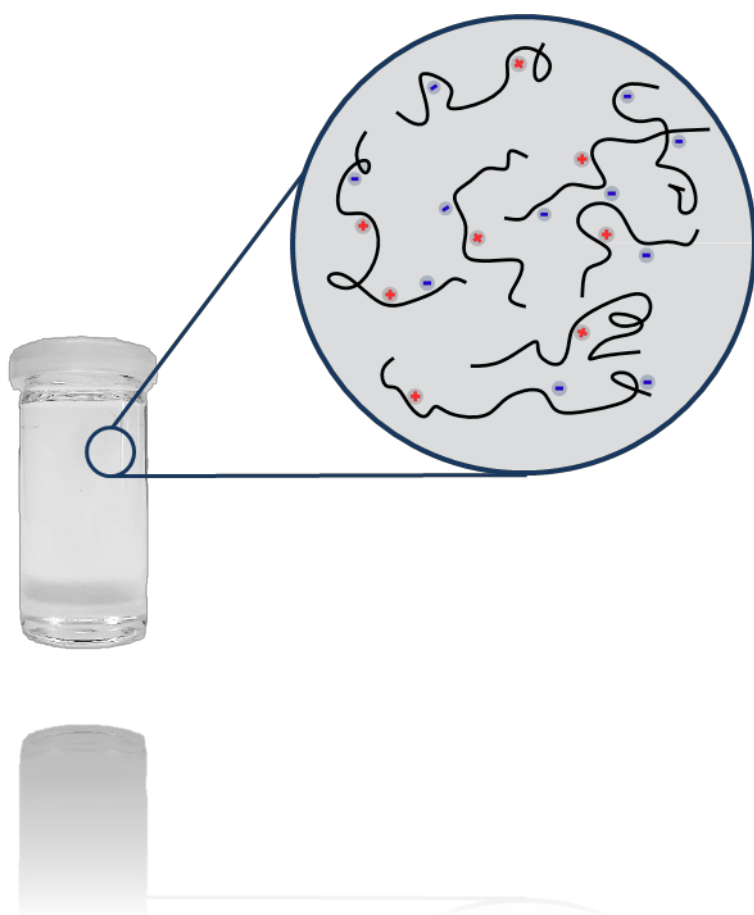
15. Liu, Z., H. Xiao, and N. Wiseman, *Emulsifier-free emulsion copolymerization of styrene with quaternary ammonium cationic monomers*. Journal of Applied Polymer Science, 1999. **76**(2000): p. 1129–1140.
16. Juang, M.S.-D. and I.M. Krieger, *Emulsifier-free emulsion polymerization with ionic comonomer*. Journal of Polymer Science Polymer Chemistry Edition, 1976. **14**: p. 2089-2107.
17. Krieger, Y.C.I.M., *Emulsion polymerization of styrene with ionic comonomer in the presence of methanol*. Journal of Applied Polymer Science, 1981. **26**: p. 1819-1827.
18. Zhang, J., et al., *Soap-Free Cationic Emulsion Copolymerization of Styrene*. Journal of Applied Polymer Science, 2002. **89**: p. 2791–2797.
19. He, M. and Q. Zhang, *Application of ammonium α -allyl alkyl phenol polyoxyethylene ether sulfonate in acrylic emulsion pressure-sensitive adhesive*. Polymer-Plastics Technology and Engineering, 2011. **50**(15): p. 1570-1575.
20. Fang, C., Y. Jing, and Z. Lin, *The application research of environment-friendly reactive surfactants in acrylate emulsion pressure sensitive adhesives*. International Journal of Adhesion and Adhesives, 2017. **73**: p. 1-7.
21. A., L.S. and M.J. J., *Amphoteric water-in-oil self-inverting polymer emulsion*. 1985.
22. A., L.S. and M.J. J., *Amphoteric water-in-oil self-inverting polymer emulsion*. 1979.
23. Lu, S., R. Liu, and X. Sun, *A study on the synthesis and application of an inverse emulsion of amphoteric polyacrylamide as a retention aid in papermaking*. Journal of Applied Polymer Science, 2002. **84**: p. 343-350.
24. Tiggelman, I. and P.C. Hartmann, *Ionic autocrosslinking of water-based polymer latices: a new concept of acid–base interaction occurring upon film formation*. Progress in Organic Coatings, 2010. **67**: p. 76-83.
25. Rose, G.D., et al., *Rapid gel-like latex film formation through controlled ionic coacervation of latex polymer particles containing strong cationic and protonated weak acid functionalities*. Langmuir, 2005. **21**: p. 1192-1200.
26. Meconi, G.M., et al., *Shedding light on the different behavior of ionic and nonionic surfactants in emulsion polymerization: from atomistic simulations to experimental observations* Physical Chemistry Chemical Physics, 2017. **19**: p. 31692-31705.
27. Dong, H., H. Du, and X. Qian, *Theoretical prediction of pKa values for methacrylic acid oligomers using combined quantum mechanical and continuum solvation methods*. The Journal of Physical Chemistry A, 2008. **112**: p. 12687–12694.

28. Peck, A.N.F. and R.A. Hutchinson, *Secondary reactions in the high-temperature free radical polymerization of butyl acrylate*. *Macromolecules*, 2004. **37**: p. 5944-5951.
29. Flory, P.J., *Principles of polymer chemistry*. 1964: Springer.
30. Zosel, A. and G. Ley, *Influence of crosslinking on structure, mechanical properties, and strength of latex films*. *Macromolecules*, 1993. **26**: p. 2222-2227.
31. Aradian, A., E. Raphael, and P.-G.d. Gennes, *A scaling theory of the competition between interdiffusion and cross-linking at polymer interfaces*. *Macromolecules*, 2002. **35**: p. 4036-4043.
32. J. Max, C.C., *Infrared spectroscopy of aqueous carboxylic acids: comparison between different acids and their salts*. *The Journal of Physical Chemistry A*, 2004. **108**(16): p. 3324-3337.
33. C. Creton, K.R.S., *Fundamentals of Pressure Sensitivity - Chapter 6: Probe Tack*. *Handbook of Pressure-Sensitive Adhesives and Products*, ed. M.M.F. I. Benedek. 2009: CRC Press.
34. Berkel, K.Y.v., G.T. Russell, and R.G. Gilbert, *Entry in emulsion polymerization effects of initiator and particle*. *Macromolecules*, 2003. **36**: p. 3921-3931.
35. Marra, J., *Effects of counterion specificity on the interactions between quaternary ammonium surfactants in monolayers and bilayers*. *Journal of Physical Chemistry*, 1986. **90**: p. 2145-2150.
36. Nevea, L.D., et al., *Quantification of counterion binding to and its effects on aqueous dispersions of dialkyl cationic surfactants*. *Colloids and Surfaces*, 2017. **532**: p. 458-463.
37. Plessis, C., et al., *Seeded semibatch emulsion polymerization of butyl acrylate effect of the chain-transfer agent on the kinetics and structural properties*. *Journal of Polymer Science Part A: Polymer Chemistry*, 2001. **39**(7): p. 1106-1119.
38. Brouwer, W.M., M.v.d. Vegt, and P.v. Haeren, *Particle surface characteristics of permanently charged poly(styrene-cationic comonomer) latices*. *European Polymer Journal*, 1990. **26**(1): p. 35-39.
39. Tripathi, A.K. and D.C. Sundberg, *Partitioning of functional monomers in emulsion polymerization: distribution of carboxylic acid monomers between water and monomer phases*. *Industrial & Engineering Chemistry Research*, 2013. **52**: p. 3306-3314.
40. Zosel, A., *Shear Strength of Pressure Sensitive Adhesives and its Correlation to Mechanical Properties*. *The Journal of Adhesion*, 1994. **44**(1-2): p. 1-16.
41. Deplace, F., et al., *Controlled Sparse and Percolating Cross-Linking in Waterborne Soft Adhesives*. *Applied Materials and Interfaces*, 2009. **1**(9): p. 2021-2029.
42. Deplace, F., et al., *Deformation and adhesion of a periodic soft-soft nanocomposite designed with structured polymer colloid particles*. *Soft matter*, 2009. **5**(7): p. 1440-1447.

43. Bellamine, A., et al., *Design of nanostructured waterborne adhesives with improved shear resistance*. Macromolecular Materials and Engineering, 2011. **296**(1): p. 31-41.
44. Yamamoto, Y., et al., *Soft polymer-silica nanocomposite particles as filler for pressure-sensitive adhesives*. Polymer, 2015. **70**.
45. Wang, N., et al., *Preparation of a silica/poly(*n*-butyl acrylate-co-acrylic acid) composite latex and its pressure-sensitive properties*. Journal of Applied Polymer Science, 2009. **113**.

III.

Adhesive polyampholyte polymers prepared by solution polymerization



III. Adhesive polyampholyte polymers prepared by solution polymerization.....131

III.1. Introduction	133
III.2. Results & discussion	135
A. Variation of ionic crosslinking density of the polymers and the effects on the mechanical and adhesive properties of the resulting films.....	136
B. The role of stoichiometry between ionic groups on the mechanical and adhesive properties of polymer films.....	160
C. Effect of the nature of ionic groups on the mechanical and adhesive properties of the polymer films	171
D. Comparison of adhesive performance to commercialized products	186
E. Optimization of the molecular weight using a batch process	189
III.3. General conclusion.....	209
III.4. References	211

III.1. INTRODUCTION

In Chapter II, the preparation of polyampholytes by emulsion polymerization was described; yet the reaction products with increasing ionic monomer concentration showed compositional drifts due to different monomers solubilities. Free radical polymerization in homogenous phase would therefore be preferable. The homogenous phase (i.e. solvent) should be capable of dissolving both hydrophobic and hydrophilic monomers. Most importantly, it should be close to a theta solvent for the end polymers bearing hydrophobic and ionic species, to produce good polymer films with well distributed ionic moieties. The accomplishment of all these solubility conditions is challenging. Most reported synthesis of polyampholytes have been carried out in water[1-3], also in the case of polyampholyte block-copolymers [4-7]. However, water is not a good solvent for non-ionic acrylate copolymers. Moreover, complexation of the oppositely charged monomers might occur.

To allow miscibility of all comonomers and avoid intramolecular interactions and the formation of macro-gel in solution, a solvent with high dielectric constant ϵ_r should be used[8, 9] (dependent on the monomer mixture, in this chapter $\epsilon_r > 10$). Zhao et al.[10] demonstrated that dimethyl sulfoxide (DMSO), being a solvent with high dielectric constant, could be used to produce synthetic underwater adhesives based on ionic complexes. A polybase (quaternized chitosan) and a polyanion (catechol functionalized polyacrylic acid) were mixed successfully in DMSO. They showed that equilibrium between the polyelectrolytes was brought by the solvent as complex coacervation (phase separation) was triggered by solvent exchange with water.

For the polymers prepared by emulsion polymerization described in chapter II, the ionic feature was brought by a strong cationic moiety (MAETAC) in combination with a weak acid (MAA). Such strong/weak combination was necessary for the stability of the emulsion. In the case of solution polymerization, a strong base/strong acid combination of the ionic comonomers could be possible and would increase the strength of ionic interactions for potentially higher mechanical and adhesive performance.

Such system was introduced by Stewart' group. Inspired by the coacervation of the charged proteins occurring in the glue secreted by the sandcastle worm[11-15], they developed synthetic systems based on the same principle [16-18]. The natural system is driven by the strong interactions between phosphorylated serine and lysine and histidine (quaternary ammonium groups) amino acids. The phosphate and quaternary ammonium interactions were reproduced in synthetic polymer mixtures and showed great adhesion performance in wet environments [11, 18-20], they were therefore chosen for the system studied hereby.

This chapter describes the free radical copolymerization in isopropanol (high permittivity medium) of n-BA, methyl methacrylate (MMA), a phosphate ester methacrylate as strong anionic group, and MAETAC as cationic moiety. Based on this copolymer, the influence of several parameters on the mechanical and adhesive properties of the PSA was studied: concentration, stoichiometry and nature of the ionic comonomers. The most performant adhesives were compared to commercialized products. Finally, an optimization of the molecular weight was carried out using a batch process to improve further the shear resistance.

III.2. RESULTS & DISCUSSION

This chapter aimed at copolymerizing a polyampholyte by free radical polymerization in solution. This polyampholyte comprised an acrylate backbone of n-Butyl acrylate (n-BA), Methyl methacrylate (MMA) and charged functional groups. A strong acid moiety was introduced with 2-hydroxyethyl methacrylate ester phosphoric acid (Polystep® HPE), as well as a strong base with 2-(methacryloyloxy)ethyl trimethyl ammonium chloride (MAETAC). The structures of the monomers can be found in Figure 1.

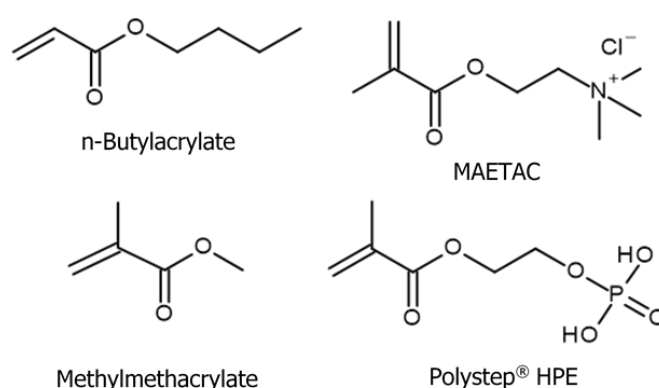


Figure 1. Structures of the copolymerized monomers

The polymers were prepared in Isopropanol (iPrOH) as described in the experimental section in Appendix (Chapter VI). The reactions were carried out at 2 L scale and 70°C. After 3 hours in semi-batch polymerization with tert-butyl peroxyphosphate (t-BPPV) as initiator, the temperature was increased to 90°C and a second feed of t-BPPV was added within 30 min to polymerize residual monomers.

Four different series of polymers were synthesized. In the first series, the content of ionic comonomers was varied but their ratio kept constant, whereas in the second series the stoichiometry was changed. Different functional groups were introduced in the third series and the fourth series focuses on changing the process parameters. The characterization of the polymers and the resulting properties of their films will be described in the next paragraphs.

A. Variation of ionic crosslinking density of the polymers and the effects on the mechanical and adhesive properties of the resulting films

i. Preparation of the polymers by solution polymerization

In this first series of samples, the role of ionic species fraction, meaning ionic crosslinking density, on the mechanical and adhesive properties was studied. Polymers with an increasing amount of ionic comonomers (Polystep® and MAETAC) were synthesized. The concentrations of Polystep® and MAETAC was increased from 0 to 100 mmol while keeping a stoichiometric molar ratio between the ionic species. A summary is given in Table 1. The name of experiments was abbreviated to SP for Solution Polymer, P stands for Polystep®, M for MAETAC and each are followed by their amount used in mmol (e.g. SP-P₂₂M₂₂ contains 22 mmol of Polystep® and MAETAC). The amount of both monomers in the polymerization mixture is referred as ionicX in wt% for convenience (weight fraction of ionic crosslink points in the polymer).

Table 1. Description of the series of samples 1 with increasing ionicX

Series #	Experiment	Polystep® (mmol)	MAETAC (mmol)	ionicX (wt%)
1	SP-P₀M₀	0	0	0
	SP-P₂₂M₂₂	22	22	1.9
	SP-P₄₄M₄₄	44	44	3.8
	SP-P₆₆M₆₆	66	66	5.8
	SP-P₈₈M₈₈	88	88	7.6
	SP-P₁₀₀M₁₀₀	100	100	8.7

To trigger all sites for ionic interaction (i.e. ionic crosslink points) where available, the phosphate acid groups RPO₄H₂ of Polystep® were deprotonated to RPO₄H⁻ +K by addition of 1 equivalent (regarding acid moiety) of Potassium hydroxide (KOH).

To avoid any gelation upon addition of KOH (also change in viscosity), the solutions were diluted to 30 wt% with isopropanol. In order to prepare polymer films, the solution was poured in moulds or coated with a doctor blade (for thin films). The ionic crosslinks were therefore formed during film formation with the evaporation of iPrOH by counter-ions exchange Cl^- and K^+ . An illustration of the solutions and dried polymer films with and without KOH is given in Figure 2.

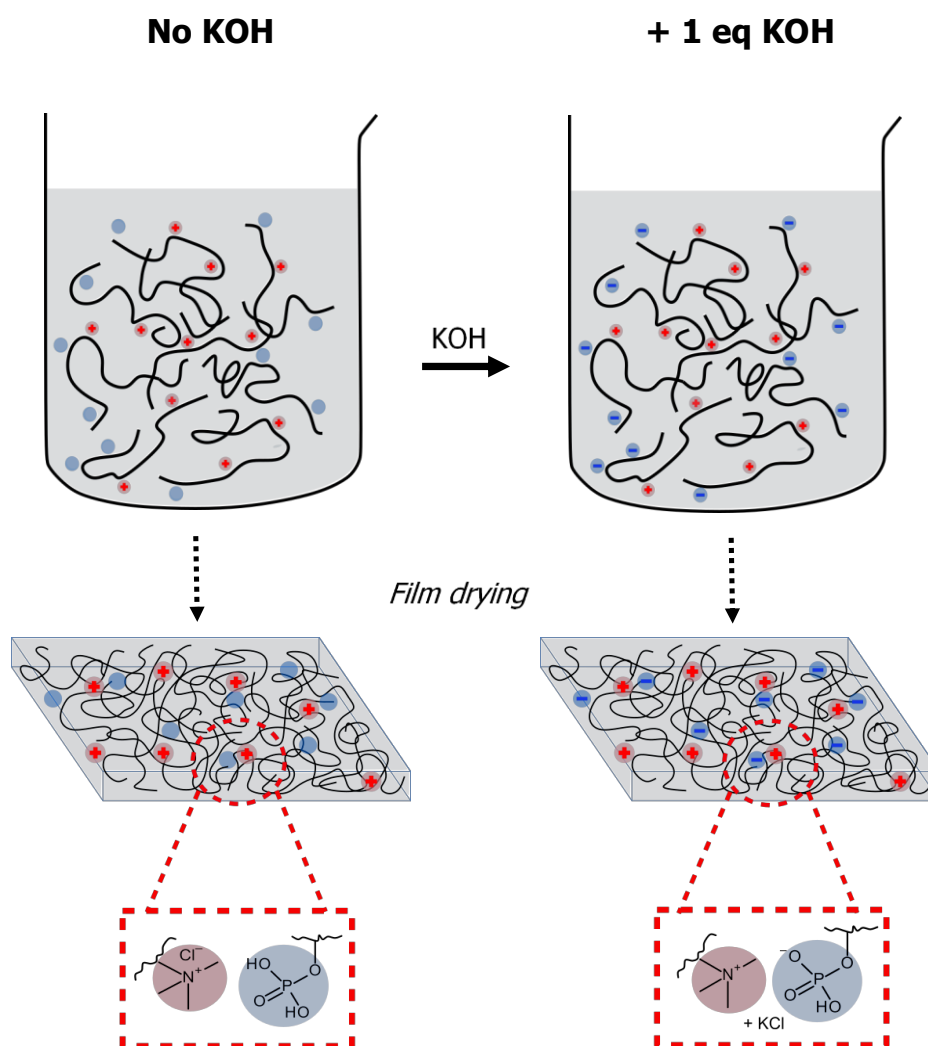


Figure 2. Illustration of the polymer in isopropanol and the dried films with or without prior addition of 1 equivalent of KOH

Theoretically, the maximal ionic crosslinking density should be reached after addition of KOH and relate directly to ionicX (i.e. total weight fraction of ionic comonomers).

The polymers characteristics, mechanical and adhesive performance were compared before and after addition of KOH.

ii. Physicochemical properties of the polymers

The molecular weight distribution of the polymers was measured by Size Exclusion Chromatography (SEC) in hexafluoroisopropanol (HFIP) using refractive index (RI) and multi-angle light scattering (MALLS) detectors, the values are given in Appendix 18. To ensure that the molecular structure and M_w were unaffected by the addition of KOH, SEC measurements of SP-P₂₂M₂₂ and SP-P₁₀₀M₁₀₀ before and after addition of KOH were performed (the different values are found in Appendix 18). No differences were found for M_n , PDI and M_w values in RI and MALLS before and after the addition of KOH. In both cases, the weight average molecular weight M_w and PDI increased by 2 from SP-P₀M₀ to SP-P₁₀₀M₁₀₀ while M_n remained constant. This implies that copolymerization at higher ionicX was less controlled and polymer chains with higher M_w and linear, grafted or branched geometries could be present. This was seen by a shoulder in high M_w region on the relative molar mass distributions obtained by RI in Appendix 19.

Overall, M_w values obtained by RI were higher than $\sim 40\,000\text{ g.mol}^{-1}$. RI detection measures the hydrodynamic radius of the polymer coils using neutral Polymethyl methacrylate PMMA as standard. The higher M_w values obtained vs. MALLS detection could be due to the presence of charged moieties. It was proposed in the literature[21] that if a polymer coil presents a large hydrodynamic radius due to repulsion of ionic groups, the M_w could be overestimated when compared to an uncharged standard. In that way, the absolute M_w measured by MALLS might be more accurate.

The conformation factor can be extracted from MALLS data using the linear fitting of $\log(R_g)=f(\log(M))$ [22]. The conformation of polymer chains is rod-like for $v=1$, coil-like for $v=0.5$ and sphere-like for $v=0.33$. The conformation factor was calculated for the series and was displayed as function of ionicX in Figure 3. The $\log(R_g)=f(\log(M))$ curves and fitting are available in Appendix 20.

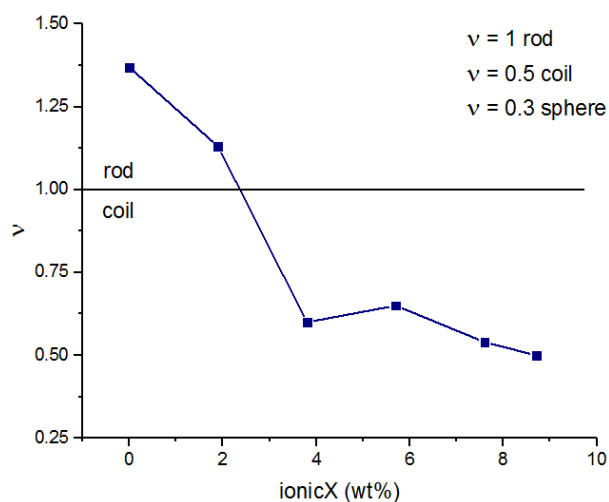


Figure 3. Conformation factor v obtained by SEC-MALLS as function of ionicX

The conformation of the polymers was highly dependent on the ionicX. At low content of ionic comonomers the polymer chains were rod-like and more linear, whereas above 1.9 wt% ionicX, the chains became coil-like. This was coupled with an increased PDI, indicating that grafting reactions could be taking place during polymerization and might be driven by one of the ionic monomers (i.e. MAETAC or Polystep®).

iii. Physicochemical properties of the polymer films

The gel content, T_g and morphology of the polymer films were measured as described in Chapter II.2.F. Results are given in Appendix 18. The gel content measured in Methyl ethyl ketone (MEK) and Ethanol (EtOH) were in the error range of zero, indicating that all polymer films were free of covalent crosslinks. After addition of KOH no gel was measured suggesting the polymer and ionic network could be dissolved by both solvents.

The glass transition temperature T_g (Appendix 18) was influenced by the fraction of ionic comonomers, but not by the addition of KOH. The T_g of pure n-BA/MMA was -29°C and increased to -25°C with 1.9 and 3.8 wt% ionicX, to -22°C with 5.8 and 7.6 wt% and to -18°C for 8.7 wt% ionicX. Although the T_g of MAETAC and Polystep® homopolymers are not yet referenced in the literature, they are expected to be higher than the T_g of the n-BA/MMA copolymer as the ionic moieties might reduce the polymer chain mobility.

The presence of ionic units in an organic copolymer might affect the morphology of the polymer dried films and thus their mechanical properties, as ionic moieties tend to aggregate in clusters[23, 24]. The morphologies of the dried polymer films were thus examined by AFM phase imaging. Cross-cut images of SP-P₆₆M₆₆, SP-P₈₈M₈₈ and SP-P₁₀₀M₁₀₀ are shown in Figure 4. Images of SP-P₈₈M₈₈ and SP-P₁₀₀M₁₀₀ with addition of KOH are available in Appendix 21. The polymer films observed were homogeneous and no micro structures were seen. To confirm the homogeneity of the films, other imaging methods such as Transmission Electron Microscopy (TEM) with and without contrasting stain and Energy Dispersive X-ray Spectroscopy (EDX) specific for Nitrogen and Phosphor were carried out for SP-P₁₀₀M₁₀₀. The images are available in Figure 5. SP-P₁₀₀M₁₀₀ film showed high homogeneity and no micro-structures were observed with the different techniques.

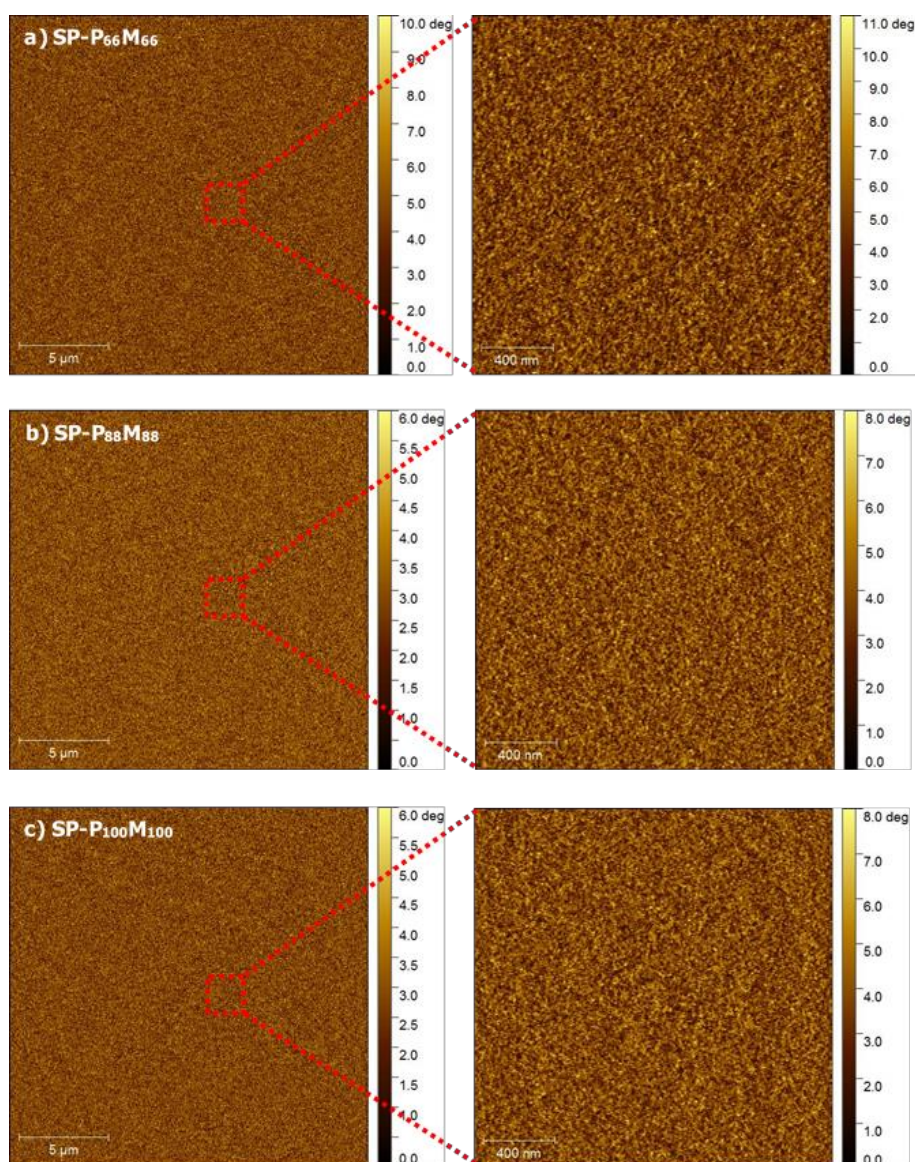


Figure 4. AFM phase images in tapping mode at 20 μm scale with enlargement at 2 μm of a) SP-P₆₆M₆₆,

b) SP-P₈₈M₈₈ and c) SP-P₁₀₀M₁₀₀

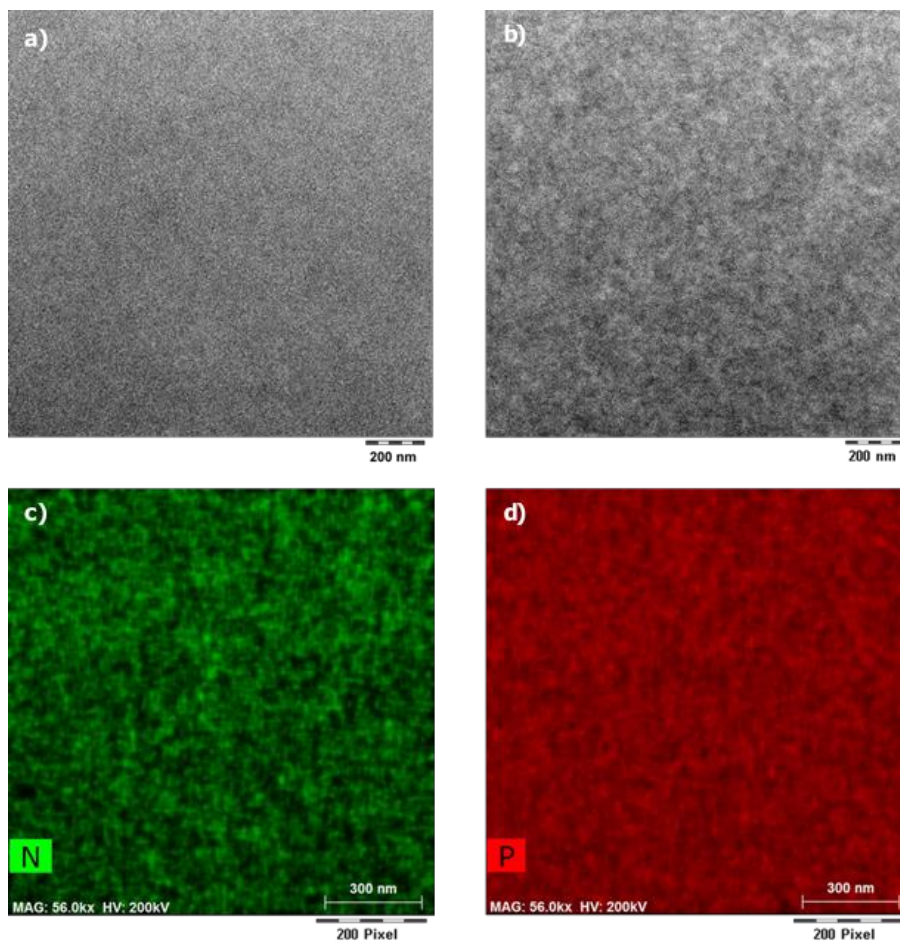


Figure 5. Images of SP-P₁₀₀M₁₀₀ obtained by a) TEM, b) TEM with Uranyl acetate stain, c) EDX-Nitrogen and d) EDX-Phosphor

iv. Mechanical behavior of the polymer films

To study the effect of intra and interpolymer ionic interactions and their density on the mechanical properties of the materials, oscillatory rheology and tensile tests were performed on dried polymer films as described in Chapter II.2.F.

A classical frequency sweep test was performed for SP-P₀M₀, as it showed characteristics of an uncrosslinked (viscous) polymer (loss modulus $G'' \sim \omega^1$ and storage modulus $G' \sim \omega^2$) over the angular frequency range of 0.01 to 100 rad.s⁻¹. For the other samples, TTS measurements were performed using the same method described in Chapter II.2.F and in experimental section in Appendix. The master curves at T=25°C of elastic and loss moduli as function of angular frequency are given in Figure 6 and the tan δ in Figure 7.

In the high frequency region ~ 100 rad.s⁻¹, all samples containing ionic comonomers showed a rubbery-like behavior with $G' > G''$, $G' \sim 10^5$ Pa and $\tan \delta < 1$, followed by a terminal relaxation (fully viscous/flowing polymer) at lower frequencies. Terminal relaxation indicates that the intermolecular forces/interactions (permanent and non-permanent crosslinks and entanglements) do not prevent the polymer chains to flow under strain. The $\tan \delta = f(\omega)$ curves were compared between samples containing increasing number of ionic comonomers (Appendix 22). A decrease in $\tan \delta$ values with increasing ionicX was measured in the rubbery region for $\omega > 1$ rad.s⁻¹, suggesting the polymers stiffened with increasing density of ionic interactions. Also, the transitions to viscous region with $G'' > G'$ shifted to lower frequencies with ionicX.

The influence of KOH addition, i.e. the triggering of the ionic network, can be seen with $\tan \delta$ in Figure 7. For the samples containing KOH, the cross-over point (i.e. after which $\tan \delta > 1$) shifted to lower frequencies, at low ionicX content (i.e. SP-P₂₂M₂₂ and SP-P₄₄M₄₄). The shift of the terminal transition to lower frequency with increasing ionicX is an indication for higher crosslinking of the sample as consequence of the electrostatic attraction between the opposite charged ionic groups in the chain.

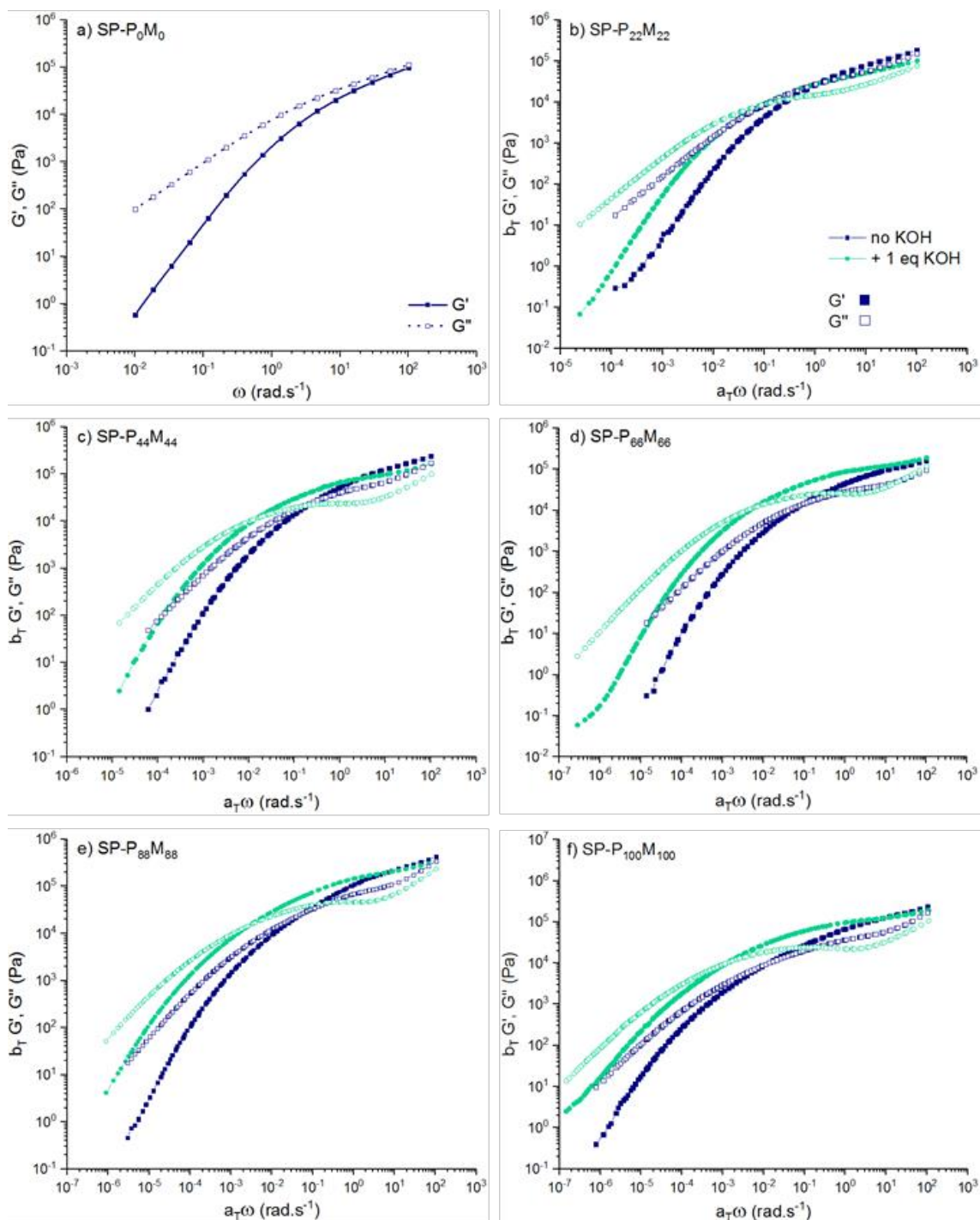
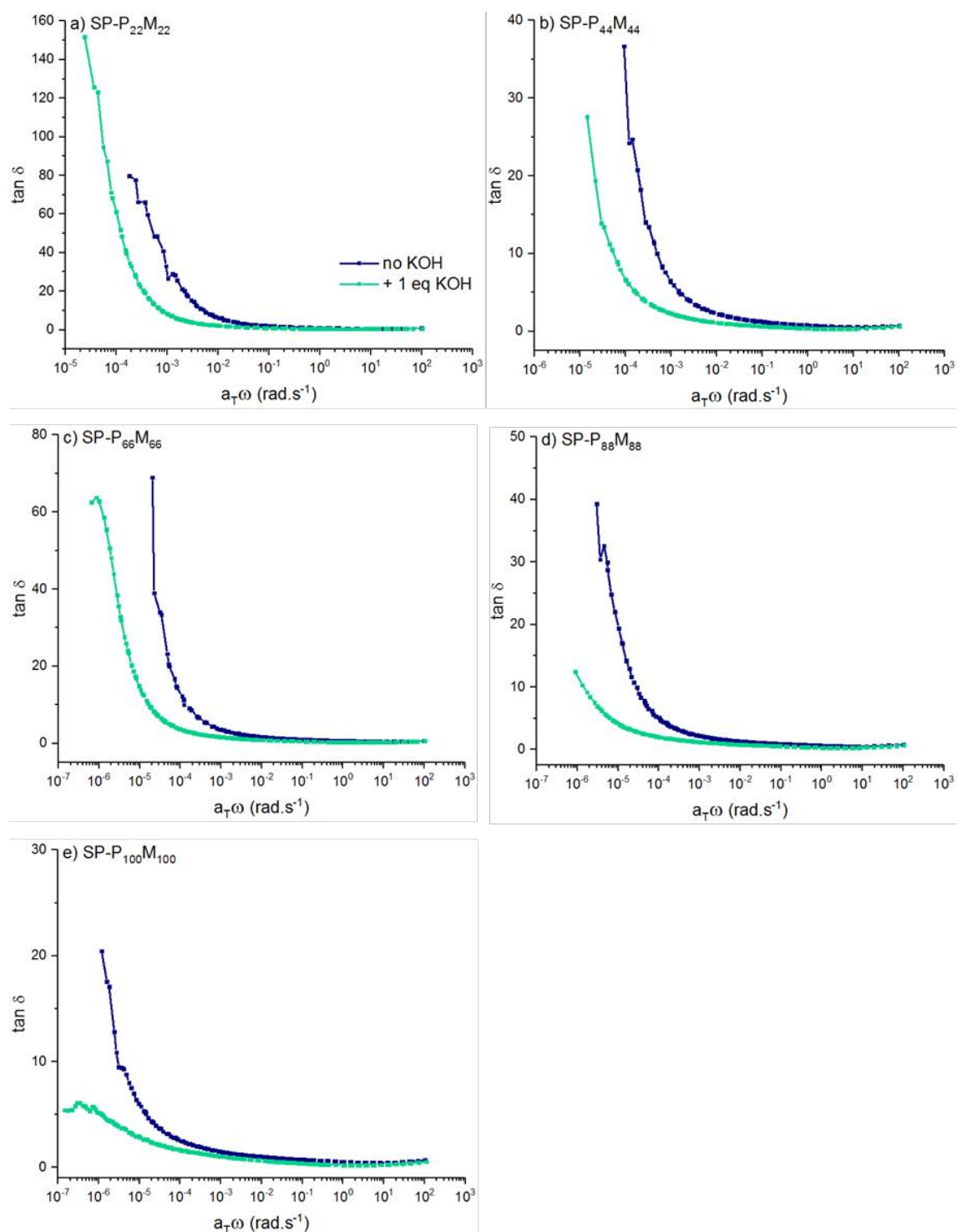


Figure 6. Master curves at 25°C of the elastic G' and Loss G'' moduli as function of the angular frequency obtained by Time-Temperature Superposition measurements

Figure 7. Tan δ as function of the corrected angular frequency for the series of sample 1

The correlation between ion content, addition of KOH and polymer toughening was also reflected in the dependence of cross-over frequency and the flow viscosity, over ionicX given in Figure 8. The values are available in Appendix 23. The cross-over frequency range with increasing ionicX was found between 1 and 0.01 rad.s⁻¹, while with the addition of KOH it was shifted to one degree of magnitude lower between 0.1 and 0.001 rad.s⁻¹, even for low ionicX with SP-P₂₂M₂₂ and SP-P₄₄M₄₄; indicating further stiffening of the polymer network due to higher ionic crosslinking density.

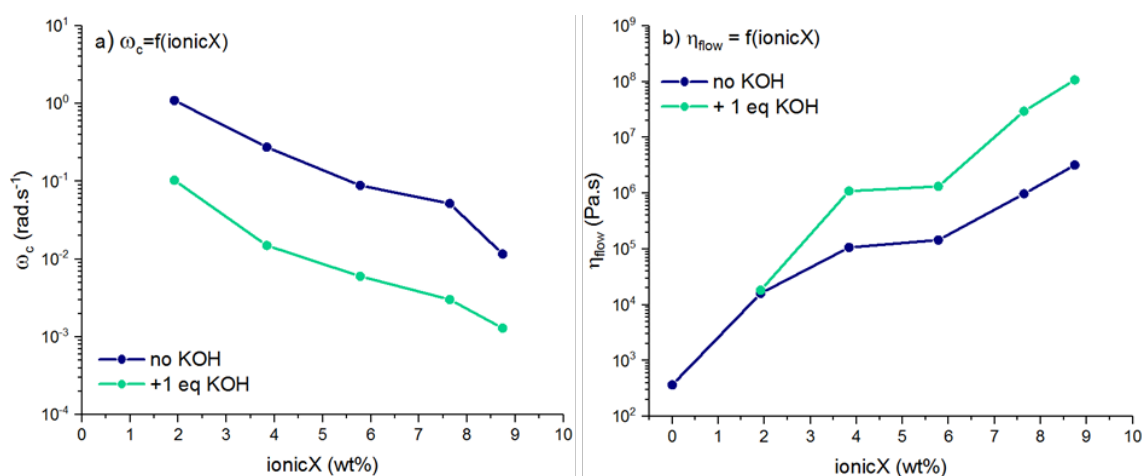


Figure 8. a) Cross-over frequency ω_c and b) flow viscosity η_{flow} as function of ionicX for samples with and without added KOH

The viscosity of the free-flowing polymer can be obtained from the value of G' at low frequencies by the relation $\eta = G'/\omega$. To calculate the flow viscosity η_{flow} , the lowest values of G' and ω were taken. Already with no KOH, η_{flow} was directly increased with ionicX, suggesting that without triggering the ionic crosslinks, the ionizable monomers strengthen interactions between the polymer chains. The flow viscosity was further increased after triggering the ionic network by adding the base.

v. Predicting adhesion with data from linear rheology

As introduced in Chapter I.2.C., the behavior of polymers in linear rheology can be used to predict their adhesive performance[25-29]. The two events that are crucial for PSA adhesion are bonding and debonding. During bonding stage, the PSA should deform fast and easily, to optimize its contact with the substrate (high penetration depth regarding substrate rugosity).

During the debonding stage, the adhesive should sustain fibrillation but dissipate high amount of energy to postpone fracture/detachment.

A time scale for the two stages was proposed in relation to frequencies in linear rheology with respectively bonding and debonding angular frequencies $\omega_{\text{Bonding}}=0.01 \text{ rad.s}^{-1}$ and $\omega_{\text{Debonding}}=100 \text{ rad.s}^{-1}$. The elastic and loss moduli at these bonding and debonding frequencies are reported in Appendix 24 and are illustrated as function of ionicX in Figure 9.

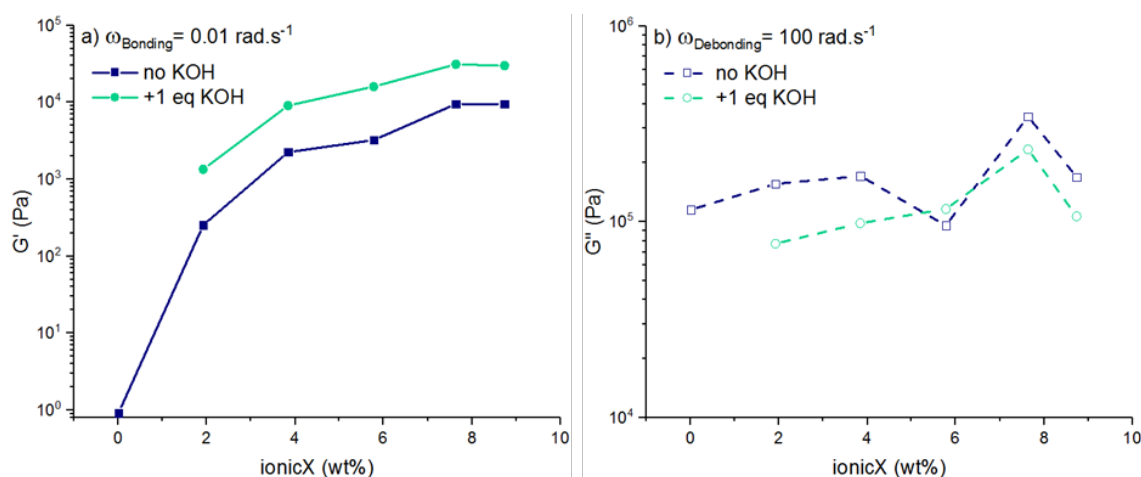


Figure 9. Dependence of ionicX on a) G' at bonding frequency and b) G'' at debonding frequency

The elastic modulus at $\omega=0.01 \text{ rad.s}^{-1}$ increased by 3 decades from SP-P₀M₀ to SP-P₂₂M₂₂ i.e. 0 to 2 wt% ionicX and by another decade between SP-P₂₂M₂₂ and SP-P₁₀₀M₁₀₀ without addition of KOH. Triggering the ionic network (with KOH) increased the storage modulus over the whole ionicX range but had more influence at low ionicX 1.9-5.8 wt% for which G' increased by 5 and by 3 for 7.6 and 8.7 wt% ionicX.

At the debonding frequency of $\omega=100 \text{ rad.s}^{-1}$, the loss modulus remained almost constant with increasing ionicX around 10^5 Pa while the addition of KOH lowered G'' for SP-P₂₂M₂₂ and SP-P₄₄M₄₄ by almost 2 and its effect was weaker for higher ionicX.

The calculation of $\tan \delta = G''/G'$ gives information of the dissipation behavior of the polymer and might play a higher role than the value of the elastic modulus G' on the ability of an adhesive to bond to a surface. $\tan \delta$ at ω_{Bonding} as function of ionicX is therefore displayed in Figure 10. It was seen that $\tan \delta$ decreased drastically with ionicX until ionicX=3.8 wt%, from this point to 8.7 wt%, $\tan \delta$ was kept between 2 and 1. The addition of KOH lowered the calculated $\tan \delta$ and the effect was even more important for samples containing low ionicX.

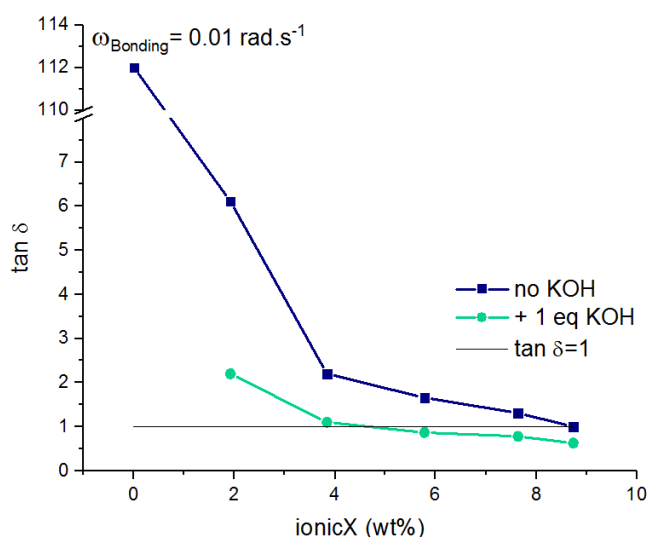


Figure 10. Evolution of $\tan \delta$ measured at ω_{Bonding} as function of ionicX with a reference line of $\tan \delta=1$

The observations made on G' and $\tan \delta$ at bonding frequencies suggest that adhesion for short contact time will be decreased with ionicX and addition of KOH, most likely because of polymer stiffening with increased ionic comonomers content and ionic network density.

vi. Mechanical behavior of the polymer films in tensile testing

The stress-strain curves obtained from tensile tests are available in Figure 11 and a table of the data can be found in Appendix 25. Single stress-strain curves of each sample are given in Appendix 26. No measurement could be done on SP-P₀M₀ as the film was too amorphous/viscous to be cut in a dog bone form and thus should be considered a fully flowing polymer.

All three SP-P₂₂M₂₂, SP-P₄₄M₄₄ and SP-P₆₆M₆₆ exhibited a flowing behaviour with a peak for maximum stress and slow decrease of σ with ϵ ; while semi-crosslinked characteristics were observed for SP-P₈₈M₈₈ and SP-P₁₀₀M₁₀₀, as they both showed a yield peak followed by an increase of σ as strain-hardening and large deformation. Increasing the number of ionic moieties in the polymers was followed by an increase of the yield stress of the films, by 10 from 2 to 7.6 wt% ionicX, and made the materials more elastic. With SP-P₈₈M₈₈, increasing ionicX to 7.6 wt% resulted in the appearance of a stress-hardening behaviour at higher elongation $\sim 1000\%$ but the elongation at break of 3500% was maintained suggesting the material was still dissipative; whereas SP-P₁₀₀M₁₀₀ showed a greater strain-hardening attaining a maximal stress of 234 kPa but a decreased elongation at break of 1943%.

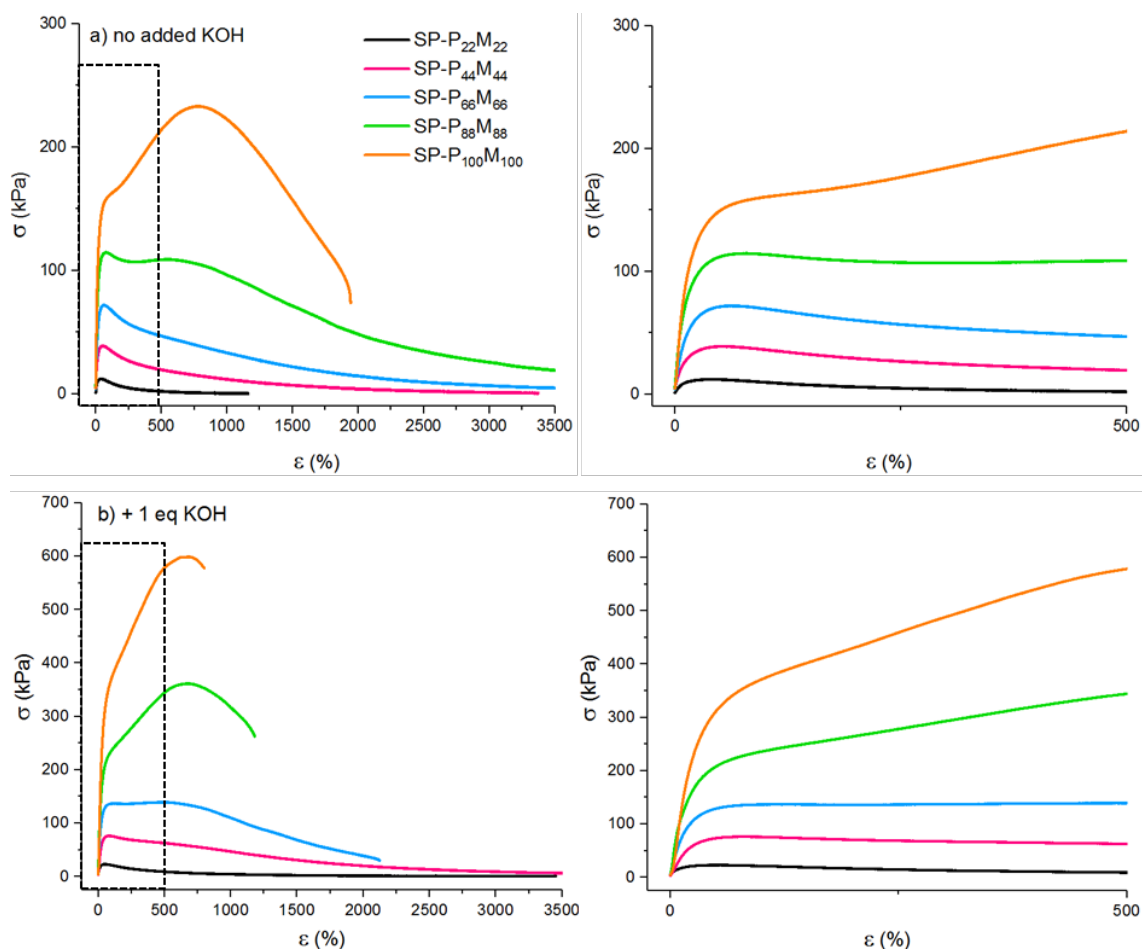


Figure 11. Stress-strain curves of all samples for a) no added KOH and b) 1 equivalent of KOH

Higher ionic crosslinking induced by the addition of KOH also stiffened the polymer films. At low ionicX, SP-P₂₂M₂₂ could sustain larger deformation and ϵ_B of was increased by 3 (Figure 12). For 3.8 wt% ionicX (SP-P₄₄M₄₄), σ_Y was increased by 2 and high elongation at break was maintained. SP-P₆₆M₆₆ showed slight strain-hardening and reduced ϵ_B suggesting already at 5.8 wt% ionicX with addition of KOH, the material starts storing more energy than dissipating under uniaxial stress. Over 7.6 wt% ionicX, SP-P₈₈M₈₈ and SP-P₁₀₀M₁₀₀ were densely crosslinked and showed brittle-like behaviors with σ_{max} increased respectively to 362 and 600 kPa and ϵ_B decreased by half.

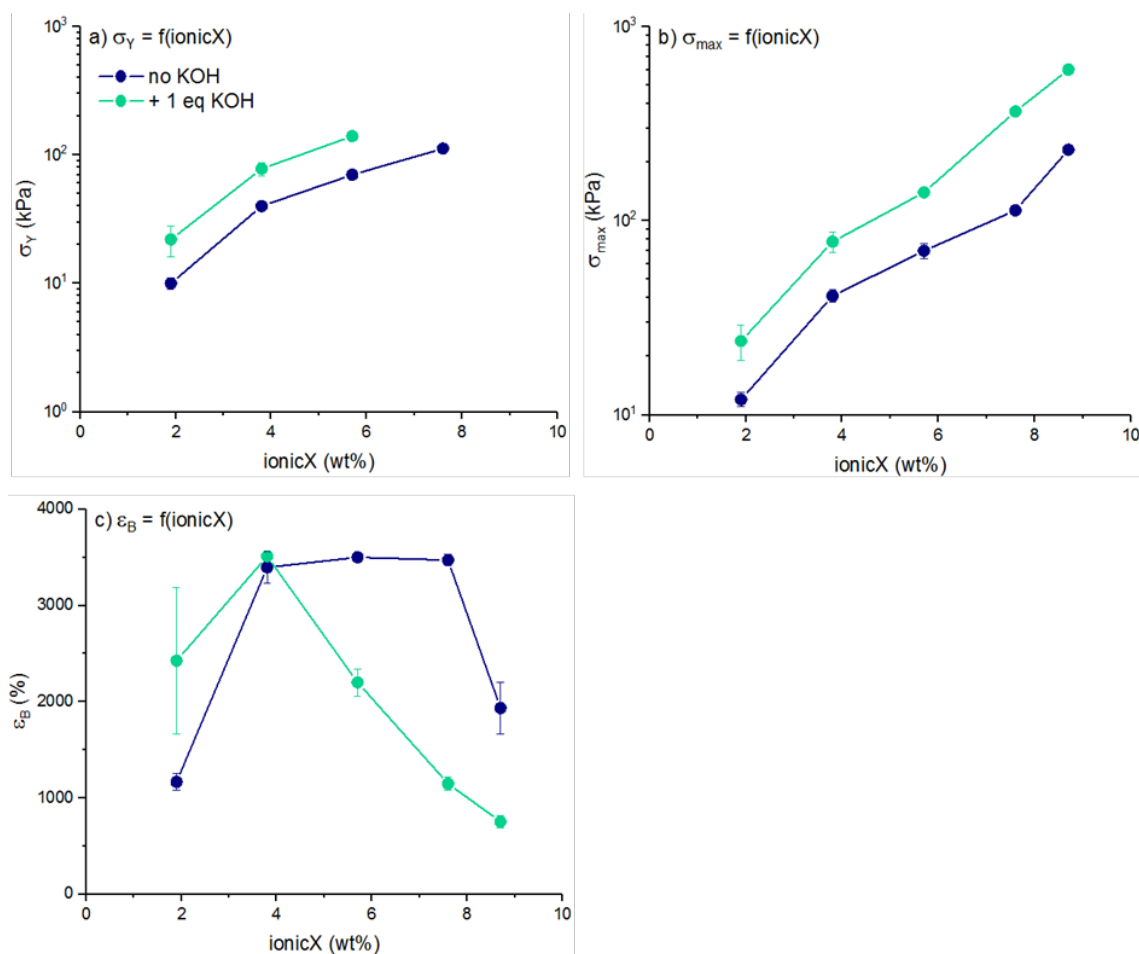


Figure 12. Evolution of a) yield stress σ_Y , b) maximal stress σ_{max} and c) elongation at break ϵ_B as function of ionicX

The yield stress increases with the stiffness of the polymer film and delimitates the transition from elastic (linear) to plastic (non-linear) regime. σ_Y should be proportional to the toughness of the films measured in linear rheology. The yield stress obtained by tensile test and the cross-over frequency measured by oscillatory rheology were compared and are displayed in Figure 13. σ_Y increased with the toughness by increasing ionicX and adding KOH while ω_c was lowered. The two methods correlated therefore very well.

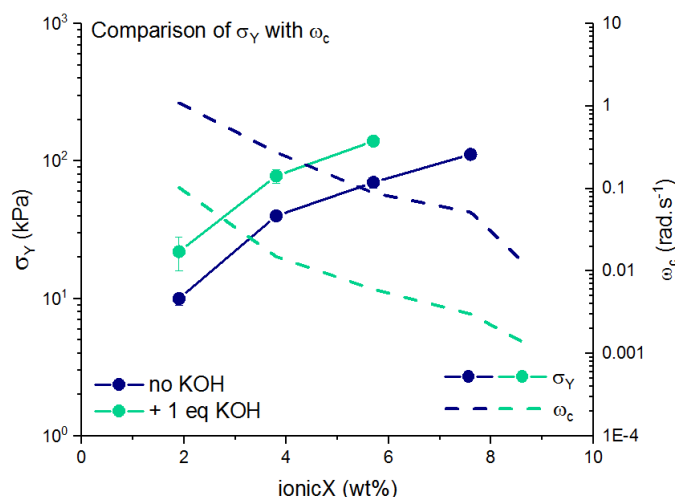


Figure 13. Comparison of the yield stress σ_Y obtained by tensile test and the cross-over frequency obtained by oscillatory rheology as function of ionicX

vii. Adhesive properties of the polymer films

Using the same experimental procedure as in Chapter II.2.F, the adhesive properties were measured by shear and peel tests on steel substrate. The failure modes were recorded and reported as A (adhesive) or K (cohesive). All values can be found in Appendix 27.

Peel tests at 180° were realized for dwelling times of 2 minutes, 24 hours and 48 hours to ensure the adhesion could be measured after the polymer had fully relaxed during contact with the substrate. The dependence of each measurement on ionicX is illustrated in Figure 14. For 2 min contact time and SP-P₂₂M₂₂, the presence of ionic monomers increased the resistance to debonding by better energy dissipation in comparison to SP₀M₀ as both exhibited cohesive failures and the peel mean force F_{mean} increased first from 0 to 1.9 wt% ionicX from 3 to 12 N.25 mm⁻¹. With higher ionicX, the adhesives were too elastic to form good adhesion in short contact time and the mean force was decreased until $F_{\text{mean}} \sim 1$ N.25 mm⁻¹ for 8.7 wt% ionicX and the failures obtained were adhesive. The samples with added KOH followed the same trend and resulted in the same failure modes.

For longer contact time of 24 hours, cohesive failures were observed suggesting the adhesive was able to relax and optimize contact with the substrate and failure in the bulk was obtained. F_{mean} increased with the number of functional groups and was constant $\sim 19 \text{ N.25 mm}^{-1}$ for SP-P₄₄M₄₄, SP-P₆₆M₆₆ and SP-P₈₈M₈₈, but for SP-P₁₀₀M₁₀₀ the force was decreased by half and the sample was detached with an adhesive failure. The effect of KOH was negligible, and the same trend of results were obtained.

Finally, after 48 hours all samples exhibited cohesive failures, peel force increased with ionicX from 0 to 3.8 wt% ionicX and reached $F_{\text{mean}} \approx 19 \text{ N.25 mm}^{-1}$. F_{mean} stayed constant with increasing the content of ionic comonomers, suggesting the samples were able to dissipate the same amount of energy during debonding. However, with the addition of KOH and ionicX > 7.8 wt%, the peel mean force was decreased to 12 N.25 mm^{-1} for SP-P₈₈M₈₈ (7.6 wt% ionicX) and 8 N.25 mm^{-1} for SP-P₁₀₀M₁₀₀ (8.7 wt% ionicX). This is likely to be due to high ionic crosslinking density turning the material to low dissipative adhesive. The adhesive failures observed, also signified that the polymers were elastic and detached more easily from the steel substrate.

Overall, the adhesive values were improved with longer dwelling time due to polymer relaxation. Yet, the peel forces for SP-P₈₈M₈₈ and SP-P₁₀₀M₁₀₀ were lowered after 48 h. In addition, failure mode of SP-P₈₈M₈₈ switched from cohesive to adhesive suggesting the same adhesive gained in stiffness over time. This might be due to migration of salts to the surface and reducing the adhesion or due to reorganization of the ionic interactions to the detriment of surface contact.

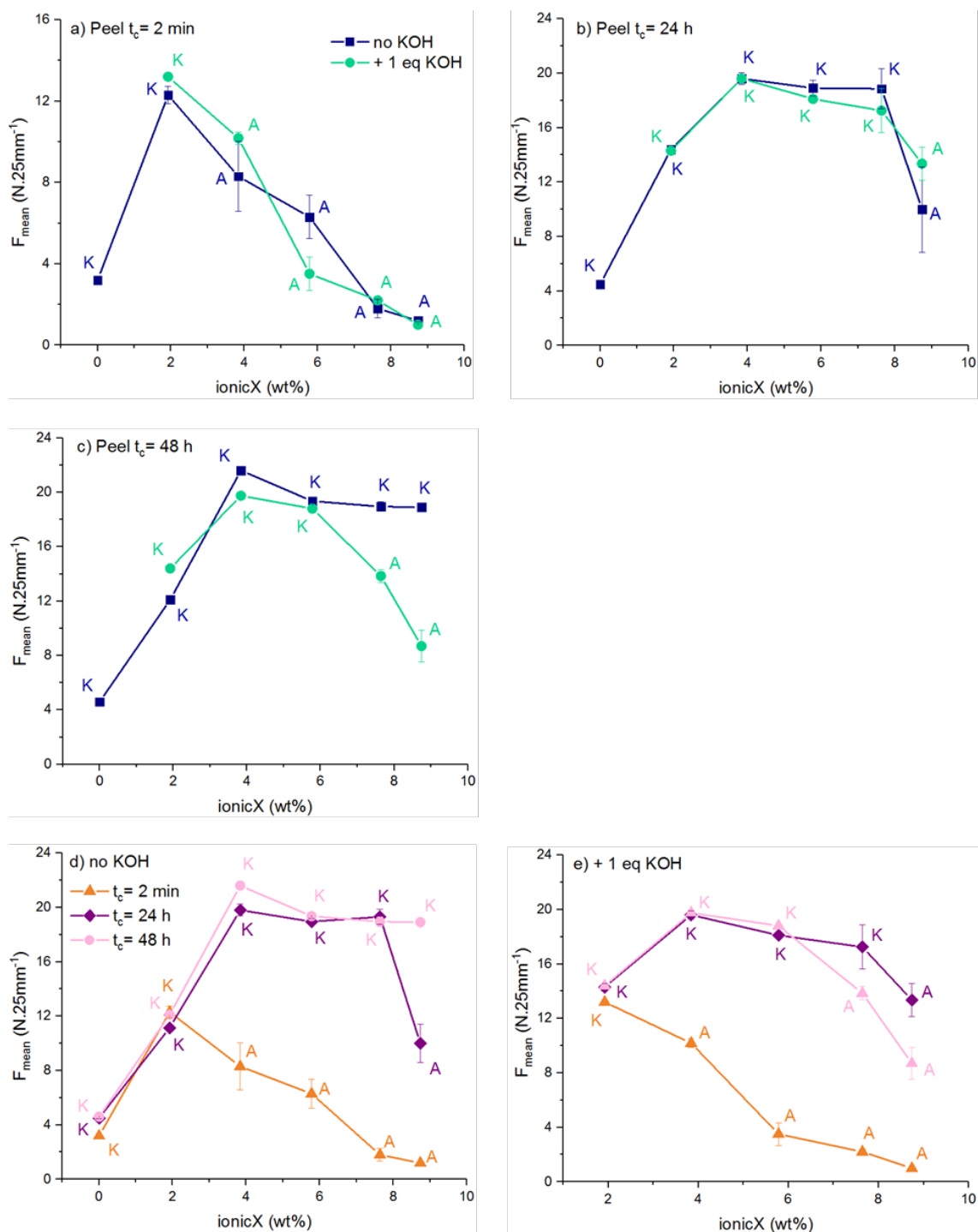


Figure 14. Peel mean force F_{mean} as function of ionicX for a) 2 min, b) 24 h and c) 48 h dwelling times; and F_{mean} as function of ionicX for all dwelling times with d) no KOH and e) 1 eq of KOH

Static shear holding time/power obtained for the set of samples were displayed as function of ionicX in Figure 15. Holding time showed strong dependence on the content of ionic moieties; it increased up to 1000 min with 8.9 wt% ionicX. The dependence was even stronger with the addition of KOH, as ionicX was increased. Shear strength was increased by almost two with ionicX > 5.9 wt%. Overall, SP-P₈₈M₈₈ exhibits the best compromise between high adhesion (F_{mean}) and high cohesion (Holding power).

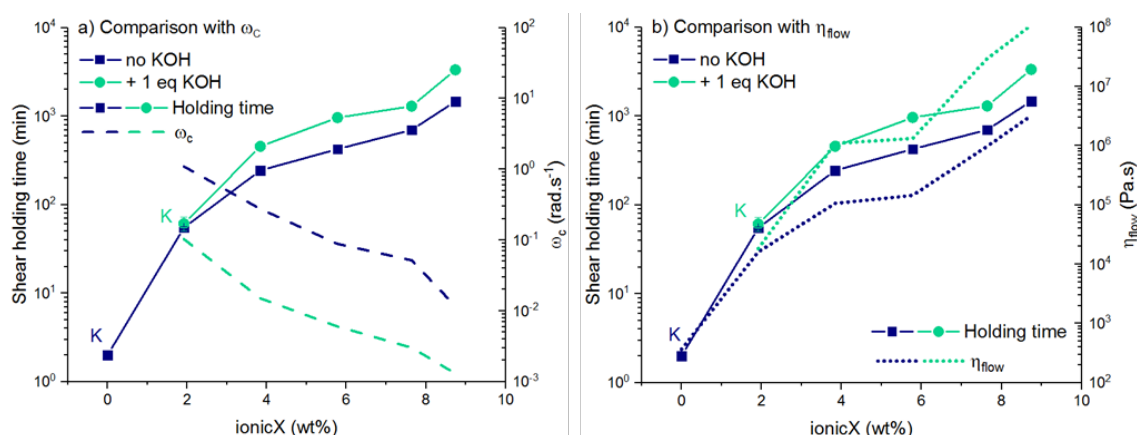


Figure 15. Dependence of shear strength over ionicX for samples with and without added KOH and comparison with a) cross over frequency and b) flow viscosity

The comparisons with cross-over frequency and the flow viscosity obtained in linear rheology are also displayed in Figure 15. Shear resistance (i.e. holding time) showed expected trends towards ω_c and η_{flow} . It is inversely proportional to ω_c as the cohesive strength increases with ionicX (and KOH) and cross-over frequencies are decreased.

But shear holding power is directly related to η_{flow} (as seen in Figure 15 b) due to the high time scale of the static shear experiment. The polymer has time to rearrange and behaves as viscoelastic materials under low frequency shear stress. Therefore, the linear rheology and adhesive measurements correlate very well.

viii. Discussion

This chapter describes the influence of the ionic crosslinking density, as function of the concentration of the charged monomer or the pH, on the mechanical and adhesive properties of the polymer films. Firstly, it is important to note that the synthesized polymers incorporated the ionic comonomers statistically in the chain and no phase separation into a microstructure was observed in the polymer films characterized by AFM, TEM and EDX (Figure 4 and Figure 5). Formation of ionic aggregates and multiplets in ionomers usually requires a minimum amount of ionic moieties [23, 30-32]. However, this is highly dependent on the polymer chain mobility and thus on the properties of the entire system such as M_w , T_g , comonomers, molecular weight between entanglements, grafted architectures... Therefore, no general rule can be defined [33, 34].

Toughening of the polymer was observed at higher ionic content of the polymer chains, even when the ionic groups were protonated. This was reflected in oscillatory rheology (Figure 6, Figure 7 and Figure 8) by the decrease of ω_c with ionicX and the differences in dissipative behavior showed by $\tan \delta > 1$. It was also reflected in the higher strain on the stress-strain curves obtained by tensile tests. Strain hardening appeared at high ionicX (Figure 11), and σ_y , σ_{max} increased while ϵ_B decreased. Adhesive performance was also influenced by ionicX. The peel force at low contact time decreased and shear strength increased with high ionicX. Although, the polymers clearly showed sign of increased intermolecular interactions (crosslinking, higher M_w , branching) [26, 35, 36], as peel forces increased with time.

These results could be explained by the model developed by Villey et al.[37]. They showed that the fracture energy (by extension the peel force) measured in peel is a direct quantification of the adhesive rheological parameters: average stress (i.e. relative to stiffness measured by σ_y and G') and maximum extensibility (i.e. deformation, ϵ_B).

However, stiffness increased with ionicX while the maximum elongation (as seen in tensile test) was decreased. It is therefore possible that constant peel values were obtained as the increase of toughness and the loss of extensibility are counterbalancing each other, for SP-P₄₄M₄₄, SP-P₆₆M₆₆ and SP-P₈₈M₈₈ after 24h. And after optimization of the interfacial interactions between adhesive and substrate, the adhesive parameters (toughness and extensibility) of SP-P₁₀₀M₁₀₀ also equilibrate each other.

As no gel content was measured and M_w was seen to increase with incorporation of ionic comonomers, the strengthening of polymer films can have several explanations. Firstly, M_w and PDI increased highly with ionicX and the polymers conformation changed to coil-like with ionicX; thus, stiffening might be due branching[38] introduced by Polystep[®] on growing polymer chains. Long polymer branches usually decrease the flexibility of polymer chains[39], thus increasing resistance to shear and the normal stress in tensile tests. Phosphoric acid esters monomers are usually provided not pure and contain a certain amount of dimer. ³¹P NMR given in Appendix 28, showed Polystep[®] contained a 50/50% ratio of mono- and dimer. The structure of the dimer is given in Figure 16.

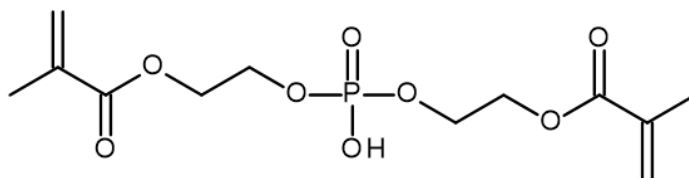


Figure 16. Structure proposed for the dimer contained in Polystep[®] HPE

Secondly, ionic clustering can act as fillers in the polymer films and could have not been characterized by the methods used i.e. AFM and TEM. Even though, the polymers were most likely not linear, ionic complexation triggered with addition of KOH acted as regular covalent crosslinks[26, 35, 36] and further toughened the materials even for low ionicX. Cross-over frequencies seen in Figure 8, were further decreased and rubbery plateau were lengthened as crosslinking density increased. This is described in the Sticky Rouse model[40].

This phenomenon takes place for ionomers where the ionic moieties act as 'sticky' points and delay the relaxation of polymer chains. In this paragraph, it was illustrated by the delay of the cross-over between storage and loss moduli, with and without addition of KOH. As ω_c decreased without addition of KOH, the ionic clusters acted as the 'sticky' points and after the addition of KOH, ω_c was further decreased as the ionic clusters might have been bigger and stronger with ionic interactions.

To summarize, three different phenomena could be at the origin of the increased stiffness of the polymers with ionicX and are illustrated in Figure 17. At first, the grafting density might be increased with the content of Polystep. Then, the ionic moieties are likely to aggregate during film formation and form ionic clusters acting as fillers. Also, with addition of KOH, the clusters get stronger and might coexist with additional ionic crosslinks between polymer chains (outside of the clusters).

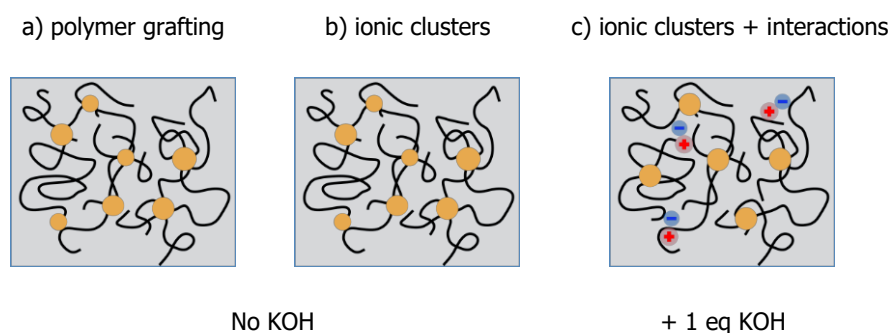


Figure 17. Illustration of the phenomena leading to increased film toughness: a) polymer grafting, b) ionic clustering and c) ionic clustering coupled with ionic interactions

The toughening of the polymers was also observed at higher strains, the films got brittle-like for high amounts of ionic comonomers (ionicX > 7.6 wt%). However, the peel resistance was unchanged which suggests the ionic interactions were not hindering the ability of the polymer to relax within that time scale and with these weight fractions. But after 48 h peel force decreased and led to adhesive failure.

Yet resistance to static shear increased with ionic crosslinking as with covalent crosslinks[41, 42] in addition to polymer grafting with high amount of Polystep®; and increased further for samples containing high ionicX.

The balance between mechanical resistance at low strain (shear strength), network mobility to insure good contact formation and optimum energy dissipation for high adhesion, has been reported for self-healing ionomers[43-45] and largely show the potential of ionic crosslinks for adhesive applications (e.g. repositionable labels).

Finally, the values extracted from linear rheology measurements at bonding and debonding frequencies correlated well with the results obtained by peel. At bonding frequency i.e. short contact time, $\tan \delta$ decreased while G' increased with ionicX (Figure 9 and Figure 10) as the peel mean force and thus adhesion decreased. And no dependence of G'' over ionicX was seen at debonding frequencies and could connotate with the constant peel force obtained for samples with different content of ionic moieties, even with added KOH.

B. The role of stoichiometry between ionic groups on the mechanical and adhesive properties of polymer films

i. Preparation of the polymers by solution polymerization

The weight fraction of ionic comonomers in the polymers described in the previous section was low (max. 9 wt% in the whole polymer). The probability for each ionic group to find its counterpart was therefore small. It was also disclosed in the literature that polycations and polyanions alone present improved mechanical properties due to ionic aggregation and not necessarily through complexation[46-48]. The importance of stoichiometry between ionic groups to obtain the same performance, was thus questionable and investigated in this paragraph.

In comparison to SP-P₁₀₀M₁₀₀ containing 100 mmol of each ionic comonomer, two polymer variants were prepared: one with an excess of the cationic group and another one with an excess of anionic group. The description of the series of samples (set 2) is given in Table 2.

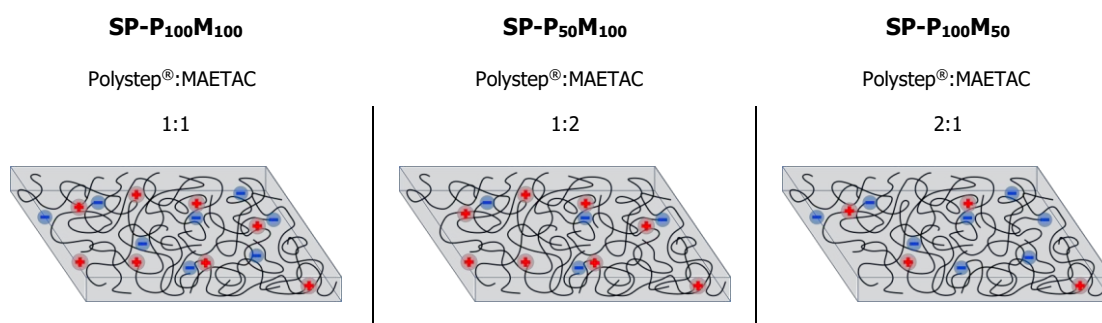
The syntheses and the polymers characterization were carried out as described in III.2.A.

An illustration of the 3 dried polymer films relevant in this paragraph can be found in Figure 18.

Table 2. Summary of the series of samples 2 with corresponding amount of functional groups

Series #	Experiment	Anionic monomer (mmol)	Cationic monomer (mmol)	-/+ ratio
2	SP-P₁₀₀M₁₀₀	Polystep® 100	MAETAC 100	1/1
	SP-P₅₀M₁₀₀	Polystep® 50	MAETAC 100	1/2
	SP-P₁₀₀M₅₀	Polystep® 100	MAETAC 50	2/1

In this section, the chemical and physical properties of the polymers were also studied in comparison to the samples containing 1 equivalent of KOH.

Figure 18. Illustration of the dried films for the sample series 2ii. Characteristics of the polymers and their films

The polymers characteristics were measured as reported in the previous paragraph and are given in Appendix 29.

The molecular weight of SP-P₁₀₀M₅₀ was $\sim 145\,000\text{ g.mol}^{-1}$ as measured by RI and MALLS, and was in accordance with the value measured for SP-P₁₀₀M₁₀₀ ($\sim 145\,000\text{ g.mol}^{-1}$). Yet, different values of M_w were found for SP-P₅₀M₁₀₀ using the two detection methods. With RI, $M_w = 138\,000\text{ g.mol}^{-1}$ while $M_w = 90\,000\text{ g.mol}^{-1}$ with MALLS. As mentioned in III.2.A., this may be due to differences in hydrodynamic radius which thus appeared to be dependent on the content of Polystep®, due to polymer grafting. The conformations of the three polymers were determined by MALLS data treatment (described in III.2.A.ii.) and are given in Table 3 with the conformation factors, the linear fits are available in Appendix 30.

Table 3. Conformation factor for series 2 obtained by SEC-MALLS and relative polymer conformation

Series #	Experiment	ν	Conformation
2	SP-P ₁₀₀ M ₁₀₀	0.50	coil
	SP-P ₅₀ M ₁₀₀	0.69	coil/rod
	SP-P ₁₀₀ M ₅₀	0.51	coil

SP-P₅₀M₁₀₀ conformation was found more rod-like than SP-P₁₀₀M₁₀₀ and SP-P₁₀₀M₅₀ and further supports the hypothesis that it had a lower grafting density.

Gel contents of the polymers in MEK and EtOH were lower than 3.5%. They are thus considered gel free. The glass transition temperatures T_g measured by DSC, was similar for the whole series around -22°C.

iii. Mechanical characterization of the polymer films

The master curves obtained from TTS measurements are displayed in Figure 19, the cross-over frequencies extracted from the master curves are displayed in Figure 20 and the data is available in Appendix 31.

Generally, the curves of SP-P₁₀₀M₅₀ and SP-P₁₅₀M₁₀₀ showed the same trend as for SP-P₁₀₀M₁₀₀ with a rubbery region $G' > G''$ at $\omega > 1 \text{ rad.s}^{-1}$. However, the cross-over to flowing region took place at higher frequencies for the non-stoichiometric samples, suggesting less interchain interactions in these samples.

The cross-over frequencies ω_c was lowered by 4 for SP-P₁₀₀M₅₀ and by one degree of magnitude for SP-P₁₀₀M₁₀₀ and SP-P₅₀M₁₀₀, it indicates the addition of KOH increased the density of interactions. Although SP-P₅₀M₁₀₀ contained less acidic moieties ω_c was lower than for SP-P₁₀₀M₅₀ suggesting the polymer was more elastic.

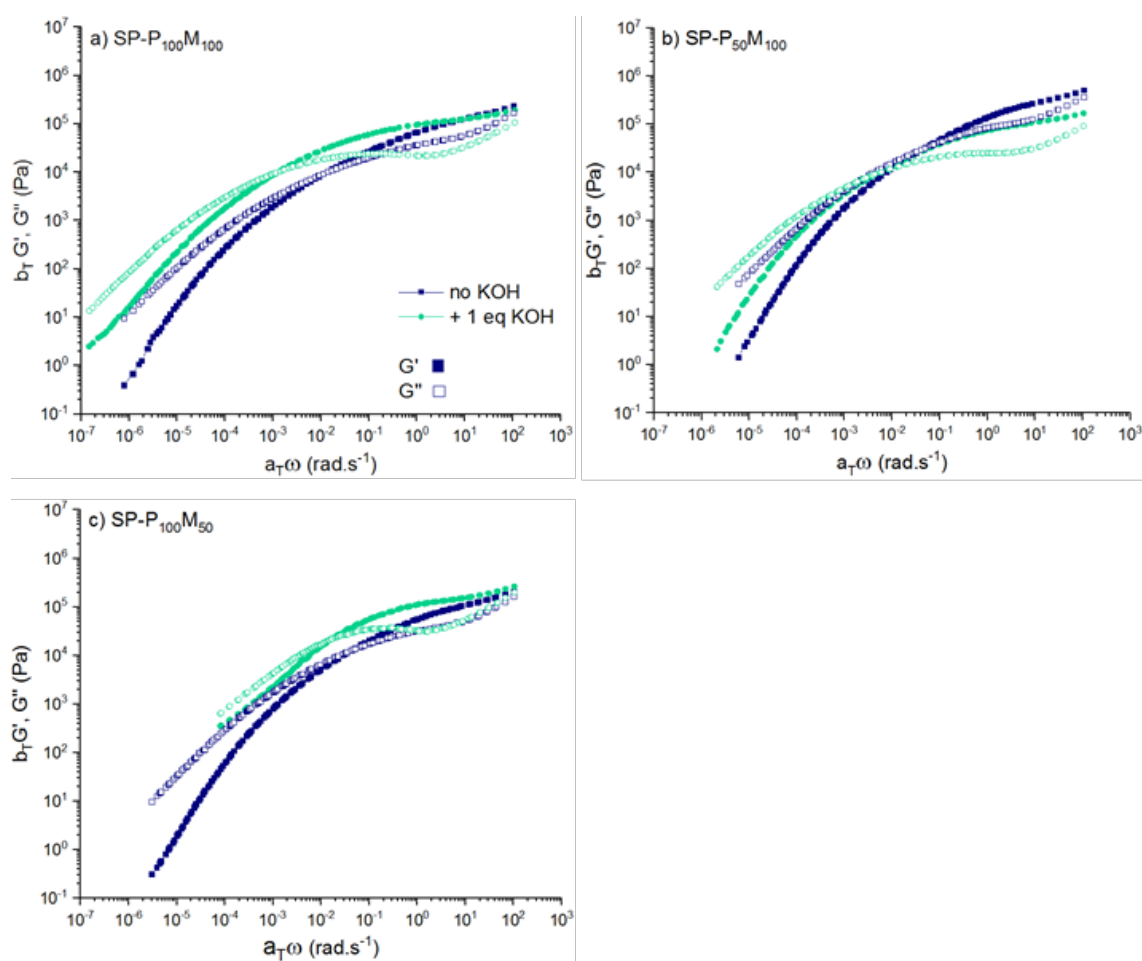


Figure 19. Master curves at 25°C of the elastic G' and Loss G'' moduli as function of the angular frequency obtained by Time-Temperature Superposition measurements

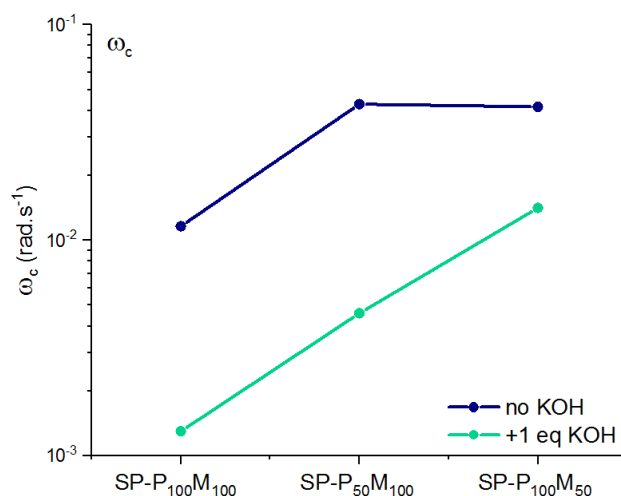


Figure 20. Cross-over frequency ω_c as function of the samples with and without added KOH

Tan δ were calculated from the master curves and are displayed in Figure 21, the comparison between the three samples first without and secondly with addition of KOH are given. Without KOH, SP-P₅₀M₁₀₀ and SP-P₁₀₀M₅₀ behaved in a similar manner and were more dissipative at low frequency than SP-P₁₀₀M₁₀₀ as tan δ increased more rapidly. However, after KOH addition, SP-P₁₀₀M₅₀ and SP-P₁₀₀M₁₀₀ were toughened by the ionic interactions. This was seen especially at low frequencies $\omega < 10^{-3} \text{ rad.s}^{-1}$ where tan δ was constant, suggesting that the residual intermolecular frictions/interactions delayed slightly terminal relaxation and thus full dissipative behaviour.

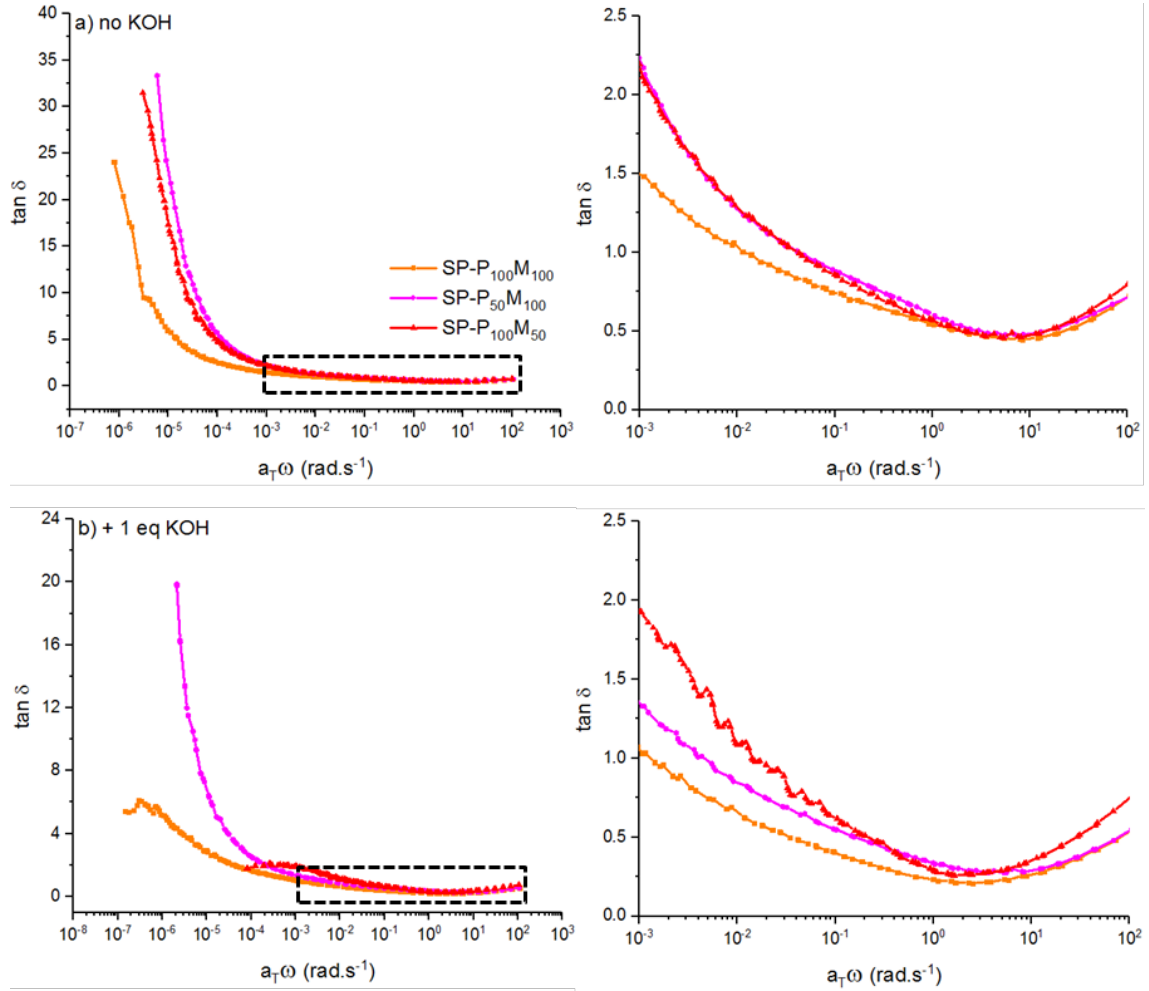


Figure 21. $\tan \delta$ as function of the corrected angular frequency for the series of sample 2 with
enlargement for $10^{-3} < \omega < 10^2$

Tensile measurements were also carried out, the stress-strain curves obtained are shown in Figure 22, individual curves are available in Appendix 32. The relevant parameters from the stress-strain curves were extracted from the graphs and displayed in Figure 23 for the different samples, the values can be found in Appendix 33.

With no KOH, all 3 materials showed characteristics of crosslinked materials.

Yet, SP-P₁₀₀M₁₀₀ exhibited a prominent strain-hardening with $\sigma_{\max}=234$ kPa and a lower elongation at break of $\varepsilon_B=1943$ %. Therefore, the number of intra/interpolymer interactions was likely to be much higher than for the non-stoichiometric polymers. This would be in accordance with the stoichiometry of the ionic groups as more ionic complexes can be formed.

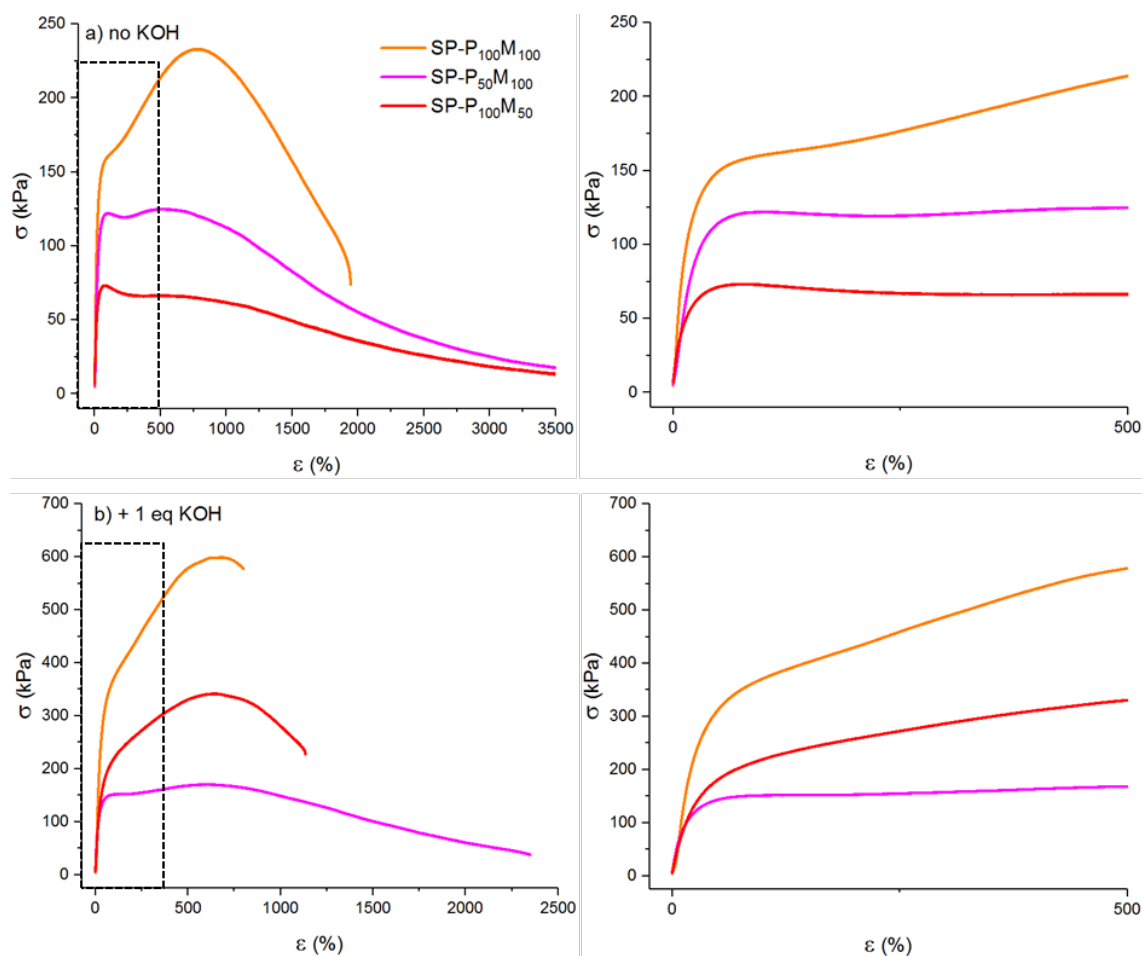


Figure 22. Stress-strain curves of all samples for a) no added KOH and b) 1 equivalent of KOH

Concerning the non-stoichiometric polymers (i.e. containing a non-stoichiometric amount of ionic groups), SP-P₅₀M₁₀₀ appeared more crosslinked than SP-P₁₀₀M₅₀ as for the same $\varepsilon_B=3500\%$, it obtained higher yield stress and showed a slight strain-hardening. It might be due to the presence of a higher number of ionic clusters with 100 mmol of MAETAC (permanently charged).

However, with the deprotonation of the acidic moieties, the trend inverted and SP-P₁₀₀M₅₀ showed more strength than SP-P₅₀M₁₀₀ with a strong strain-hardening with σ_{\max} =341 kPa and lower ϵ_B =1134%. SP-P₁₀₀M₁₀₀ was also strengthened by the addition of KOH as σ_{\max} was increased by almost 3 and ϵ_B was reduced by half, signifying the polymer lost its ability to elongate when triggering the ionic interactions, as they act as crosslinks.

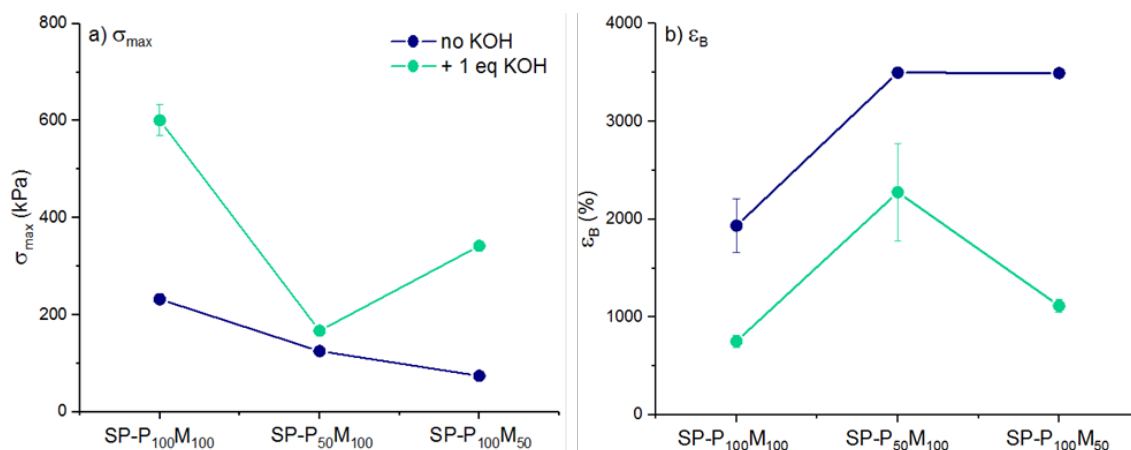


Figure 23. Evolution of a) maximal stress and c) elongation at break as function of the series 3

iv. Adhesive performance of the polymer films

The peel forces for different contact times t_c (2 min, 24 and 48 h) are displayed in Figure 24 and the related data in Appendix 34. First of all, the peel mean forces F_{mean} for short t_c and no KOH, were comparable $\sim 3 \text{ N.25 mm}^{-1}$, and all samples failed adhesively. The addition of KOH mainly lowered the peel strength of SP-P₁₀₀M₅₀. The samples had most likely a too high stiffness to create a good contact with the surface in this time scale.

Overall after 24 hours, F_{mean} values increased; the non-stoichiometric samples obtained higher peel forces $\sim 15 \text{ N.25 mm}^{-1}$ and cohesive detachments, in comparison to SP-P₁₀₀M₁₀₀; suggesting the intra and intermolecular interactions were weaker. Considering the error range, KOH had no influence on the adhesion.

At 48 hours of contact, F_{mean} reached $\sim 17 \text{ N.25 mm}^{-1}$ with cohesive failures. The addition of KOH influenced the adhesion of SP-P₅₀M₁₀₀ and SP-P₁₀₀M₁₀₀ (already reported in III.2.A). With 50 mmol of Polystep®, F_{mean} increased over 20 N.25 mm^{-1} and cohesive failure was still observed suggesting the fibrils strength was improved with more ionic interactions. On the other hand, the crosslinking density may be too high for SP-P₁₀₀M₁₀₀ so the peel force was decreased. But in general, adhesion was improved with dwelling time as the contact with the substrate was optimized.

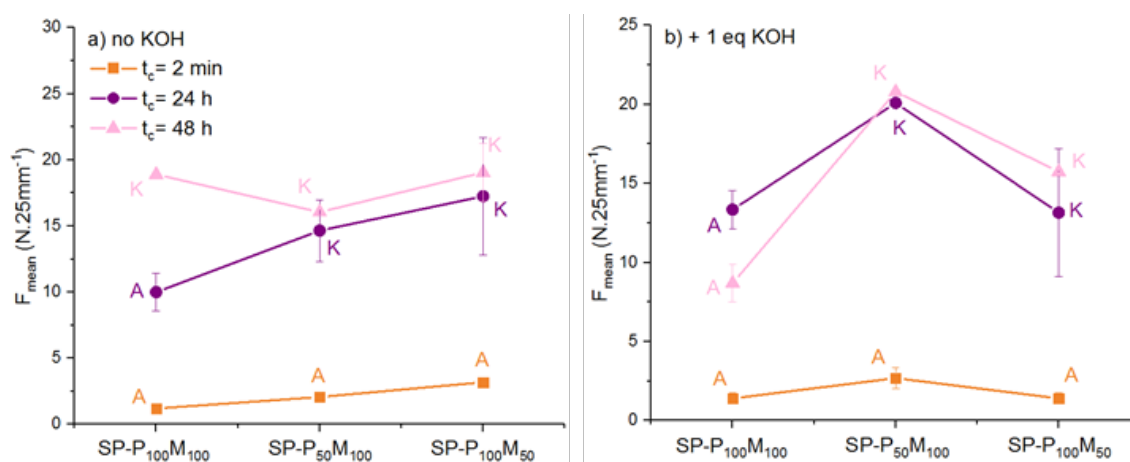


Figure 24. Peel mean force F_{mean} as function of ionicX for all dwelling times with d) no KOH and e) 1 eq of KOH

The shear holding times are available in Appendix 34 and displayed in Figure 25. The holding times were high but SP-P₁₀₀M₁₀₀ showed overall better performance and no difference between the non-stoichiometric samples was found. However, the addition of KOH increased by more than 2 the static shear strength of SP-P₁₀₀M₁₀₀ (3336 min) and SP-P₁₀₀M₅₀ (2623 min). This indicates that high amount of deprotonated phosphate improved the resistance to flow for small deformations. The difference found for SP-P₅₀M₁₀₀ with KOH can be considered in the error range.

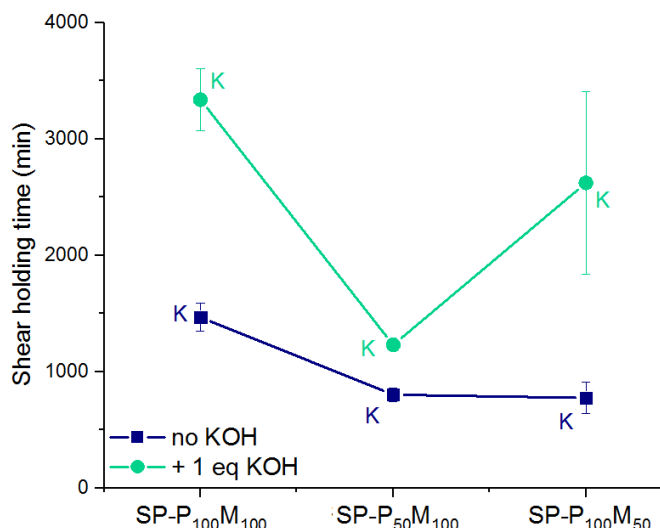


Figure 25. Dependence of shear holding time over sample series 2 with and without added KOH

v. Discussion

The objective of this section was to study the role of ionic comonomers stoichiometry on the mechanical and adhesive properties of the samples. The stoichiometric sample SP-P₁₀₀M₁₀₀ contains the highest number of possible sites for ionic complexation. The samples SP-P₅₀M₁₀₀ and SP-P₁₀₀M₅₀, on the other hand, have a lower number of possibilities to form ionic crosslinks and ionic clusters. These two assemblies are expected to largely affect the mechanical and adhesive behavior of the films.

As expected, SP-P₁₀₀M₁₀₀ showed more elastic characteristics. However, SP-P₅₀M₁₀₀ showed a higher stiffness than SP-P₁₀₀M₅₀ without KOH, in tensile tests (Figure 22). The stiffness of SP-P₅₀M₁₀₀ was further enhanced by KOH: lower cross-over frequency in linear rheology (Figure 20) and increased peel forces suggesting a better energy dissipation during debonding (Figure 24). The sample containing the excess of Polystep® i.e. SP-P₁₀₀M₅₀ was highly stiffened (in comparison to SP-P₅₀M₁₀₀) by the addition of KOH. This was unexpected as the two materials contained the same theoretical number of ionic crosslinks (defined by the molar fraction of the limiting monomer: 50 mmol for both samples).

The effect of KOH on SP-P₁₀₀M₅₀ was emphasized at high degree of deformation in tensile test where the material showed brittle fracture (Figure 22) and could be compared to SP-P₁₀₀M₁₀₀. It also outperformed the stoichiometric sample in shear strength. This could suggest that with the deprotonation of the phosphate groups, the sample with ionic comonomers stoichiometry (SP-P₁₀₀M₁₀₀) or the one with excess of Polystep® (SP-P₁₀₀M₅₀) reached about the same crosslinking density. This might be possible thanks to the excess of deprotonated phosphate groups which arrange to form complexes as proposed by Feldstein et al.[48, 49] and illustrated in Figure 26.

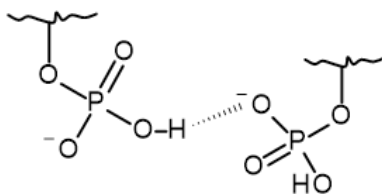


Figure 26. Proposed interactions between phosphate groups in the case of an excess of Polystep® and deprotonation with KOH

SP-P₅₀M₁₀₀ without KOH, seemed to have a lower grafting density (lower amount of Polystep®) but was still tougher than SP-P₁₀₀M₅₀. A larger number of ionic clusters could be at the origin of such observation. SP-P₅₀M₁₀₀ contained twice more MAETAC than SP-P₁₀₀M₅₀, and an excess of the cationic monomer (ionized even without KOH) may create more ionic clusters in the film. Upon addition of KOH, SP-P₁₀₀M₅₀ became more elastic than SP-P₅₀M₁₀₀ thanks to more physical crosslinks (from phosphate to phosphate) which thus prevailed on the stiffening by clustering in SP-P₅₀M₁₀₀. But it lowered slightly the adhesion (F_{mean}) for SP-P₁₀₀M₅₀. Therefore overall, SP-P₅₀M₁₀₀ showed the best balance of adhesive and cohesive performance.

C. Effect of the nature of ionic groups on the mechanical and adhesive properties of the polymer films

The advantage of ionic complexes as crosslinker lies in the possibility to tune the bonding force by selecting ionic pairs with different dissociation constants; such groups are referred as weak acid/base groups or strong acid/base[50, 51]. In that way, polymers can be designed to answer to external triggers such as pH and ionic strength[52] or “permanent” ionic bonds can be obtained combining both strong base and acid moieties.

In this section, different combinations of oppositely charged monomers were used to study the effect of the strength of ionic interactions on the adhesive performance. To do so, polymers containing ionic couples formed from weak acid/strong base, strong acid/weak base and weak acid/weak base were compared to the combination of strong acid/strong base (Polystep®/MAETAC) reported in paragraph III.2.A. Methacrylic acid (MAA) was chosen as weak acid and 2-(Dimethylamino)ethyl methacrylate (DMAEMA) as weak base.

i. Preparation of the polymers by solution polymerization

The structures of the different monomers are shown in Table 4. The polymers were prepared using the same procedure than in preceding paragraphs and the molar fraction of each monomer was fixed to 88 mmol. Table 5 summarizes the experiments (sample series #3) studied in this section while Table 6 summarises the expected ionic interactions before and after addition of KOH to deprotonate the acid groups and an illustration in the polymer films is given in Figure 27.

Table 4. Abbreviations and structures of the different ionic monomers studied in this section

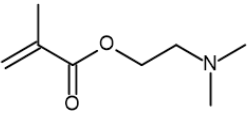
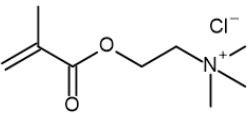
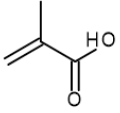
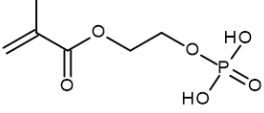
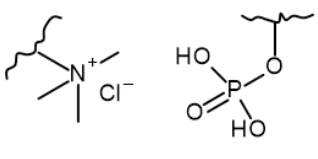
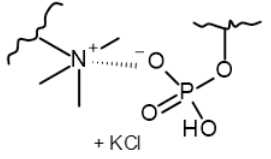
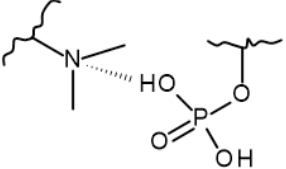
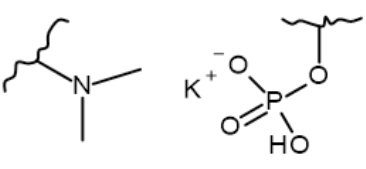
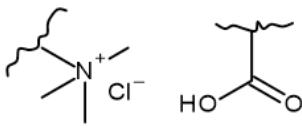
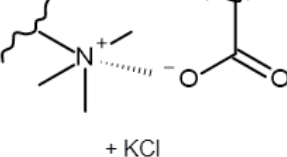
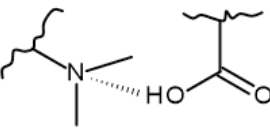
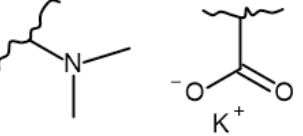
	Name	Structure
Cationic monomers	DMAEMA	
	MAETAC	
Anionic monomers	MAA	
	Polystep®	

Table 5. Description of the ionic comonomers composition for the sample series 3

Series #	Experiment	Anionic monomer (mmol)	Cationic monomer (mmol)
3	SP-P₈₈M₈₈	Polystep® 88	MAETAC 88
	SP-P₈₈D₈₈	Polystep® 88	DMAEMA 88
	SP-MAA₈₈M₈₈	MAA 88	MAETAC 88
	SP-MAA₈₈D₈₈	MAA 88	DMAEMA 88

Table 6. Summary of the expected ionic interacting groups with and without addition of KOH in the different samples of series 3

Experiment	no KOH	+ 1 eq KOH
SP-P ₈₈ M ₈₈		
SP-P ₈₈ D ₈₈		
SP-MAA ₈₈ M ₈₈		
SP-MAA ₈₈ D ₈₈		

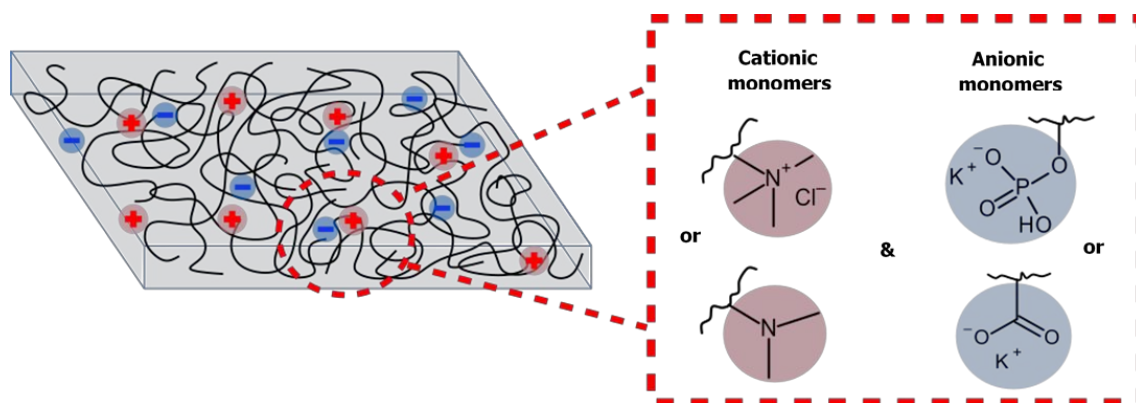


Figure 27. Illustration of the interacting groups present in the polymer films studied in this section

ii. Characterization of the polymers and the film properties

The polymers and their films were characterized with the same techniques described in the previous paragraphs III.2.A. and B. The molecular weight distributions, gel contents and T_g can be found in Appendix 35, and the relative molar mass distributions in Appendix 19.

M_w obtained by MALLS was higher in samples containing Polystep®, with $M_w \sim 105\,000\text{ g.mol}^{-1}$ vs. $M_w \sim 40\,000\text{ g.mol}^{-1}$ for samples containing MAA. The same was observed in the value obtained by RI. The polydispersity index was reduced by half as M_w decreased and M_n increased slightly to $\sim 21\,700\text{ g.mol}^{-1}$. This would suggest the polymerization was more controlled with MAA as anionic comonomer, possibly because no dimers (from Polystep®, as discussed in III.2.A.viii.) were introduced.

The conformation factor for the four polymers are available in Table 7 and the $\log(R_g)=f(\log(M))$ curves are given in Appendix 36. The two polymers containing Polystep® had coil-like conformations, while MAA containing samples were more rod-like. This further implicates that the grafting of polymers with Polystep® occurs and change the polymers conformations and induce shifts in M_w measurements. Or that stronger attractive interactions between Polystep® and MAETAC (in comparison to MAA with MAETAC or DMAEMA) would make the polymer conformation more coil-like.

Table 7. Conformation factor for series 3 obtained by SEC-MALLS and relative polymer conformation

Series #	Experiment	ν	Conformation
3	SP-P₈₈M₈₈	0.54	coil
	SP-P₈₈D₈₈	0.49	coil
	SP-MAA₈₈M₈₈	0.72	coil/rod
	SP-MAA₈₈D₈₈	0.97	rod

iii. Mechanical characteristics of the polymer films

The master curve calculated for $T=25^{\circ}\text{C}$ of the different samples and obtained from linear oscillatory rheology, can be found in Figure 28. The cross-over frequencies extracted from the curves are displayed in Figure 29 and the values are available in Appendix 37. $\tan \delta$ were calculated from the master curves and are displayed in Figure 30, comparisons of the samples are given for samples containing no or 1 eq KOH separately.

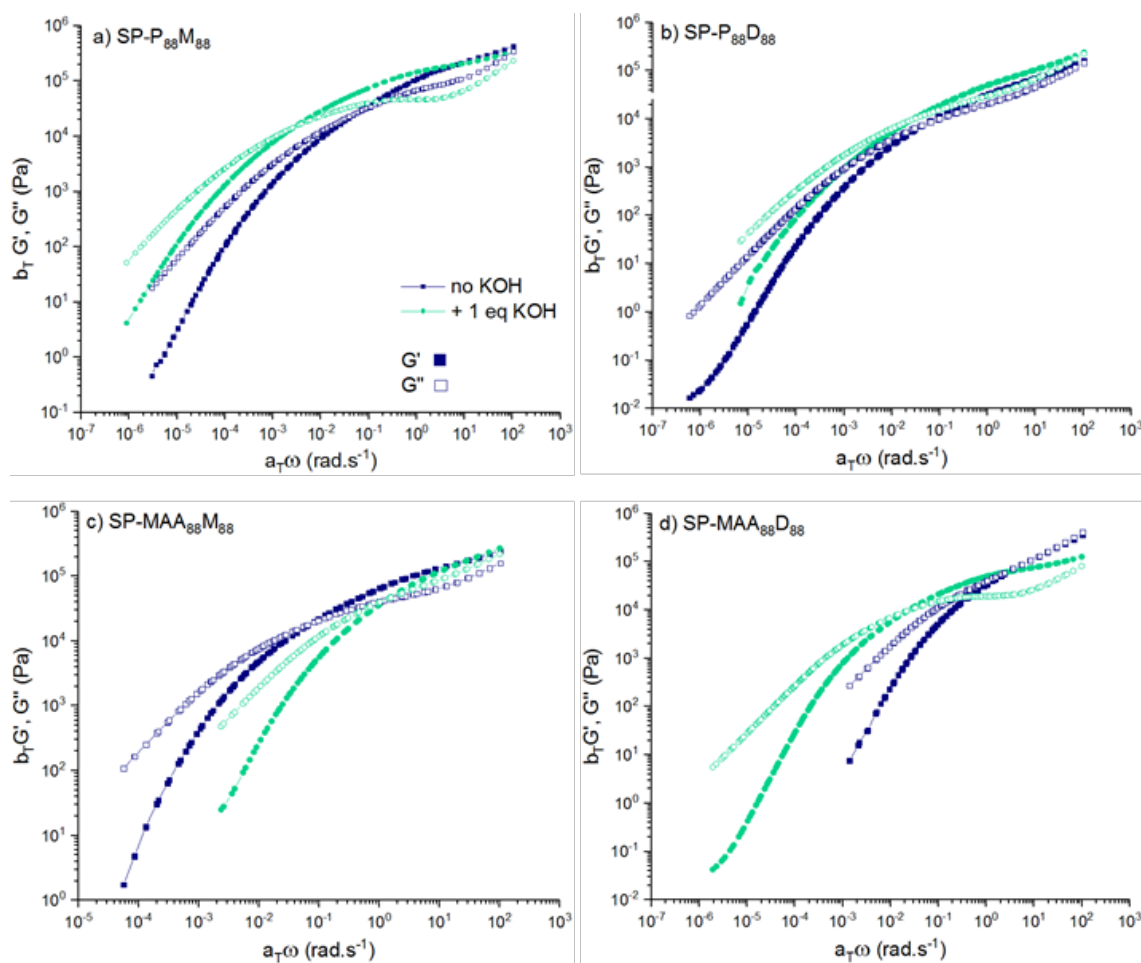


Figure 28. Master curves at 25°C of the elastic G' and loss G'' moduli as function of the angular frequency obtained by Time-Temperature Superposition measurements

SP-P₈₈M₈₈, SP-P₈₈D₈₈ and SP-MAA₈₈M₈₈ showed a behavior characteristic of weakly crosslinked samples. The samples containing Polystep® were less dissipative (i.e. more elastic) than MAA containing materials. Tan δ of SP-MAA₈₈D₈₈ was lower in comparison to SP-MAA₈₈M₈₈, but it showed a flowing behavior as $\tan \delta \geq 1$ over the range of frequency.

After deprotonation of the acid groups, SP-P₈₈M₈₈ and SP-MAA₈₈D₈₈ were stiffened (most likely due to higher crosslinking density) as at $\omega > 0.1 \text{ rad.s}^{-1}$, tan δ was lowered and ω_c decreased by one order of magnitude for SP-P₈₈M₈₈ and almost two for SP-MAA₈₈D₈₈ (without KOH, $\omega_c > 100 \text{ rad.s}^{-1}$).

On the contrary, SP-P₈₈D₈₈ did not show strong change but SP-MAA₈₈M₈₈ seemed to be plasticized by the presence of salts; indeed, tan δ increased over 1 for the whole range of frequencies and ω_c increased by one order of magnitude.

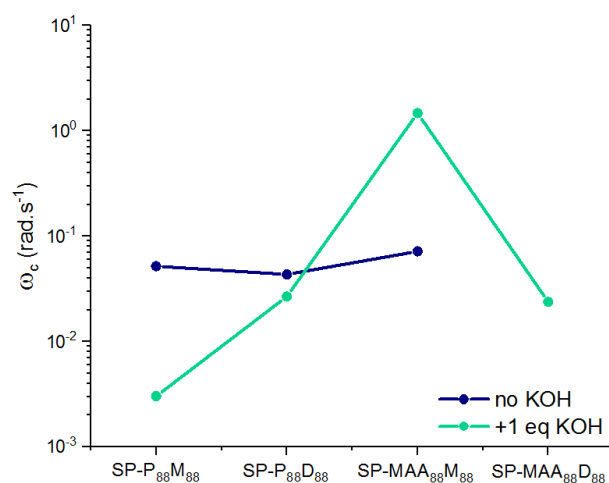


Figure 29. Cross-over frequency ω_c as function of the samples with and without 1 eq KOH

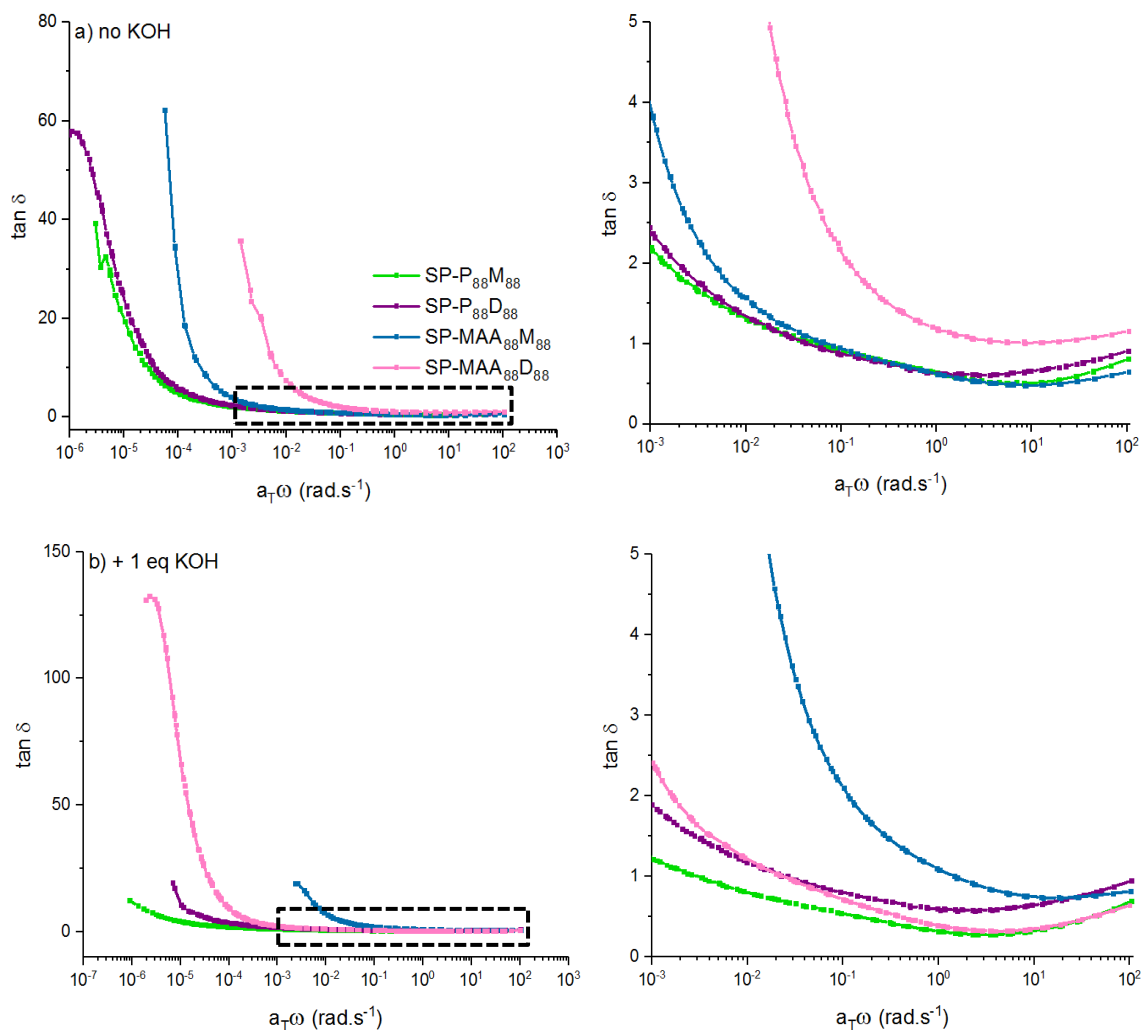


Figure 30. $\tan \delta$ as function of the corrected angular frequency for the series of sample 3 with
enlargement for $10^{-3} < \omega < 10^{-2}$

SP-P₈₈M₈₈ and SP-P₈₈D₈₈ showed similar trends (slightly crosslinked polymers) without KOH; however, upon addition of the base ω_c for SP₈₈M₈₈ was decreased and a longer rubbery plateau was observed while SP-P₈₈D₈₈ was unchanged. This would imply that ionic interactions were formed in SP-P₈₈M₈₈ between Polystep® and MAETAC and stiffened the polymer; but no attractive interactions took place between Polystep® and DMAEMA.

Comparing SP-MAA₈₈M₈₈ and SP-MAA₈₈D₈₈ differences were observed already without deprotonation of the acids. SP-MAA₈₈D₈₈ showed viscous characteristics ($\omega_c > 100 \text{ rad.s}^{-1}$) when SP-MAA₈₈M₈₈ exhibited a viscoelastic behavior. Upon deprotonation with KOH, ω_c increased for SP-MAA₈₈M₈₈ as it was plasticized by the presence of salts and ω_c decreased to $\sim 3.10^{-2} \text{ rad.s}^{-1}$ for SP-MAA₈₈D₈₈; a rubbery plateau also appeared on the master curve (Figure 28) and highlights the formation of attractive interactions between polymer chains.

The responses of the materials at higher strains were measured by tensile tests, the resulting stress-strain curves can be observed in Figure 31, individual curves are given in Appendix 38. The most important parameters extracted from the graphs are displayed in Figure 32 and are available in Appendix 39. SP-P₈₈M₈₈ exhibited a more elastic behavior than the three other samples, coupled with a doubled stress at yield while a high elongation at break was maintained $\epsilon_B \approx 3500 \%$. Its stiffness was enhanced by the deprotonation of the acid groups, a brittle-like stress-strain curve was obtained with KOH as $\sigma_{\max} = 362 \text{ kPa}$, $\sigma_B = 263 \text{ kPa}$ and $\epsilon_B = 1183 \%$.

Prior addition of KOH, SP-P₈₈D₈₈ and SP-MAA₈₈M₈₈ were comparable, yet it seems SP-P₈₈D₈₈ was highly crosslinked after deprotonation of the phosphate groups; σ_{\max} reached 270 kPa and polymer fracture was obtained for high $\sigma_B = 194 \text{ kPa}$ and low $\epsilon_B = 468 \%$. On the other hand, SP-MAA₈₈M₈₈ was softened by KOH as seen by decreased σ_Y and ϵ_B . In comparison, SP-MAA₈₈D₈₈ was found to be more resistant to elongation with KOH as σ_Y and ϵ_B were improved by a factor of 4.

The differences between SP-P₈₈M₈₈ and SP-P₈₈D₈₈ were highlighted by tensile test. The stress-strain curve of SP-P₈₈M₈₈ showed a trend of semi-crosslinked material but the curve of SP-P₈₈D₈₈ exhibited the characteristics of a viscous material. But upon addition of KOH to activate the ionic network, SP-P₈₈M₈₈ was reinforced as its stress-strain curves showed strong strain-hardening; the stress-strain curve of SP-P₈₈D₈₈ indicated a brittle-like fracture suggesting SP-P₈₈D₈₈ was also strengthened by KOH.

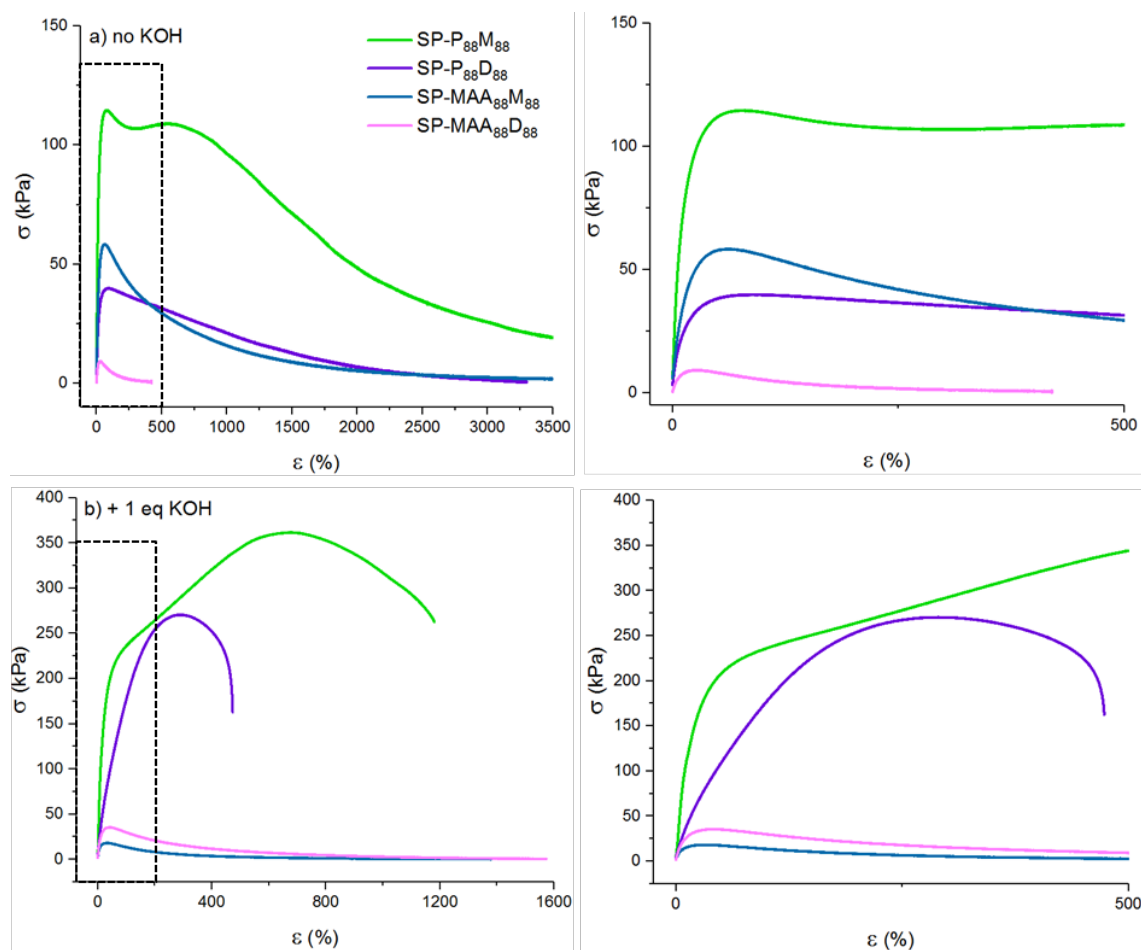


Figure 31. Stress-strain curves of all samples for a) no added KOH and b) 1 equivalent of KOH

Before the addition of KOH, SP-MAA₈₈D₈₈ exhibited a truly flowing behaviour with a small σ_Y (7.3 kPa) and short ϵ_B (<500%). SP-MAA₈₈M₈₈ also showed the characteristics of a flowing polymer but with higher σ_Y (61 kPa) and longer ϵ_B (~3500%). With the addition of Potassium hydroxide, σ_Y dropped to 16 kPa and ϵ_B was decreased by half, SP-MAA₈₈M₈₈ film was thus plasticized by the salts and did not show resistance to uniaxial elongation. The stress at yield and elongation at break ($\sigma_Y=33$ kPa and $\epsilon_B=1700$ %) for SP-MAA₈₈D₈₈ on the other hand, were increased and signify the polymer was toughened by the addition of the base; most likely by formation of molecular interactions between the polymer chains.

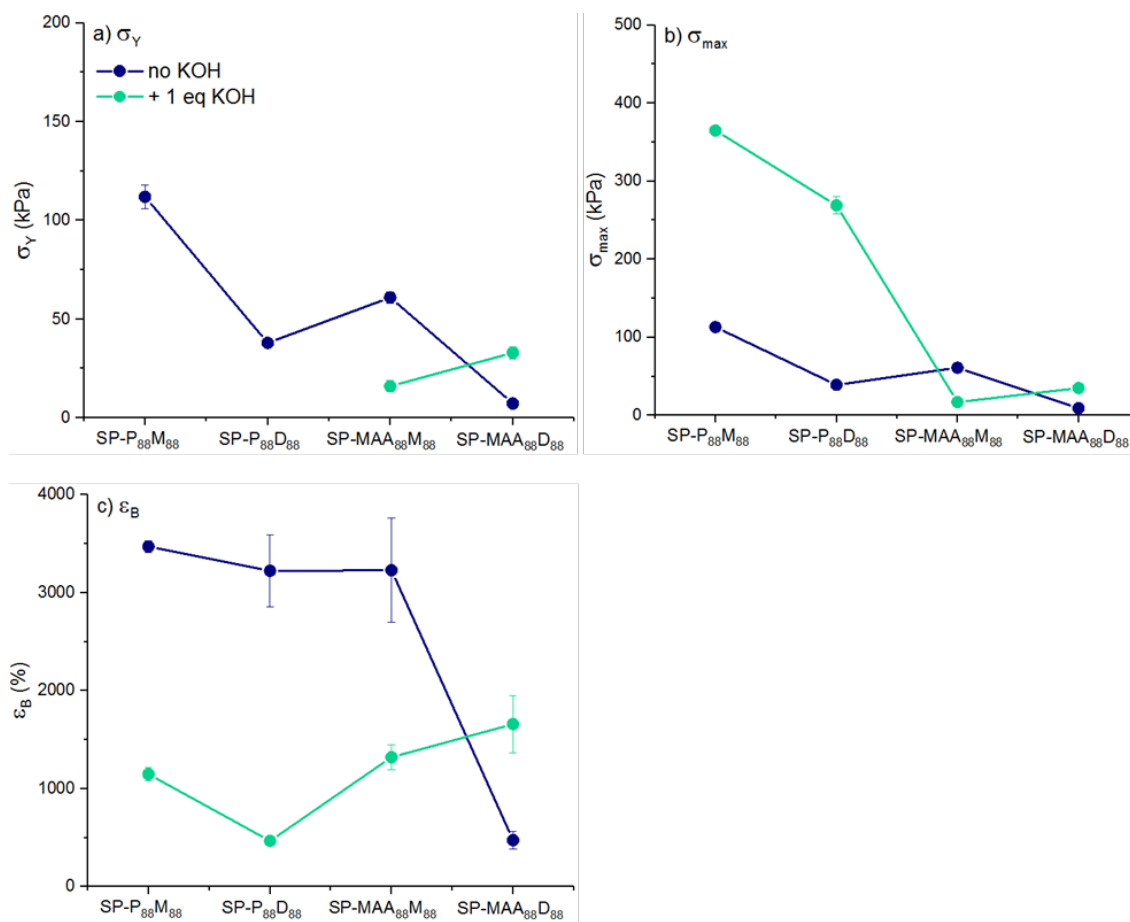


Figure 32. Evolution of a) yield stress, b) maximal stress and c) elongation at break as function of series 3

iv. Adhesive properties of the polymer films

The adhesive performance of the materials was also compared, the peel mean forces F_{mean} are displayed in Figure 33 and the values in Appendix 40.

At short contact time ($t_c=2$ min), the adhesion measured by peel mean force F_{mean} was largely influenced by the stiffness of the polymers. The highest tackiness $F_{mean}=19.6$ N.25 mm⁻¹ was measured and cohesive failure was observed for the weak acid/weak base couple (SP-MAA₈₈D₈₈). $F_{mean} \sim 11$ N.25 mm⁻¹ with adhesive failure, was comparable for SP-P₈₈D₈₈ and SP-MAA₈₈M₈₈; low adhesion $F_{mean}=1.8$ N.25 mm⁻¹ was found for SP-P₈₈M₈₈.

As observed in tensile tests, the addition of KOH resulted in different behaviours. Interactions of Polystep® or MAA with DMAEMA (i.e. SP-P₈₈D₈₈ and SP-MAA₈₈D₈₈) decreased the adhesion while most probably no complexation between MAA and MAETAC was obtained, SP-MAA₈₈M₈₈ was plasticized by the KOH salts instant peel force increased and cohesive failure was observed.

After 24 and 48 hours of dwelling time, all samples showed high adhesion to the steel substrate and the cohesive failures suggest the contact to the substrate was optimized. The peel force was increased to $F_{\text{mean}} \sim 20 \text{ N.25 mm}^{-1}$ for SP-P₈₈M₈₈, SP-P₈₈D₈₈ and SP-MAA₈₈D₈₈, and $F = 25.5 \text{ N.25 mm}^{-1}$ for SP-MAA₈₈D₈₈. KOH slightly lowered F_{mean} , especially for SP-P₈₈M₈₈ after $t_c = 48 \text{ h}$. Overall, the combination of weak acid and weak base MAA/DMAEMA showed the highest adhesion.

Similar F_{mean} were measured for SP-P₈₈M₈₈ and SP-P₈₈D₈₈ except at t_c of 2 min, at which the mean peel force was higher for SP-P₈₈D₈₈ thus suggesting that it was tackier than SP-P₈₈M₈₈ with and without addition of KOH.

Between SP-MAA₈₈M₈₈ and SP-MAA₈₈D₈₈, F_{mean} was almost higher for SP-MAA₈₈D₈₈ suggesting it was more adhesive and probably a more viscous material. However, at $t_c = 2 \text{ min}$, the addition of KOH decreased F_{mean} to $\sim 10 \text{ N.25 mm}^{-1}$ with triggering interpolymer interactions; but with longer dwelling time, the adhesion was recovered and F_{mean} doubled.

As illustrated in Figure 34, the highest performance in static shear strength were obtained for the combination of strong Polystep®/MAETAC (i.e. SP-P₈₈M₈₈) and Polystep®/DMAEMA (SP-P₈₈D₈₈) with deprotonation of the phosphate. The shear resistance of SP-MAA₈₈-M₈₈ and SP-MAA₈₈-D₈₈ were low and unchanged with triggering of the interactions suggesting poor cohesiveness of the polymer networks.

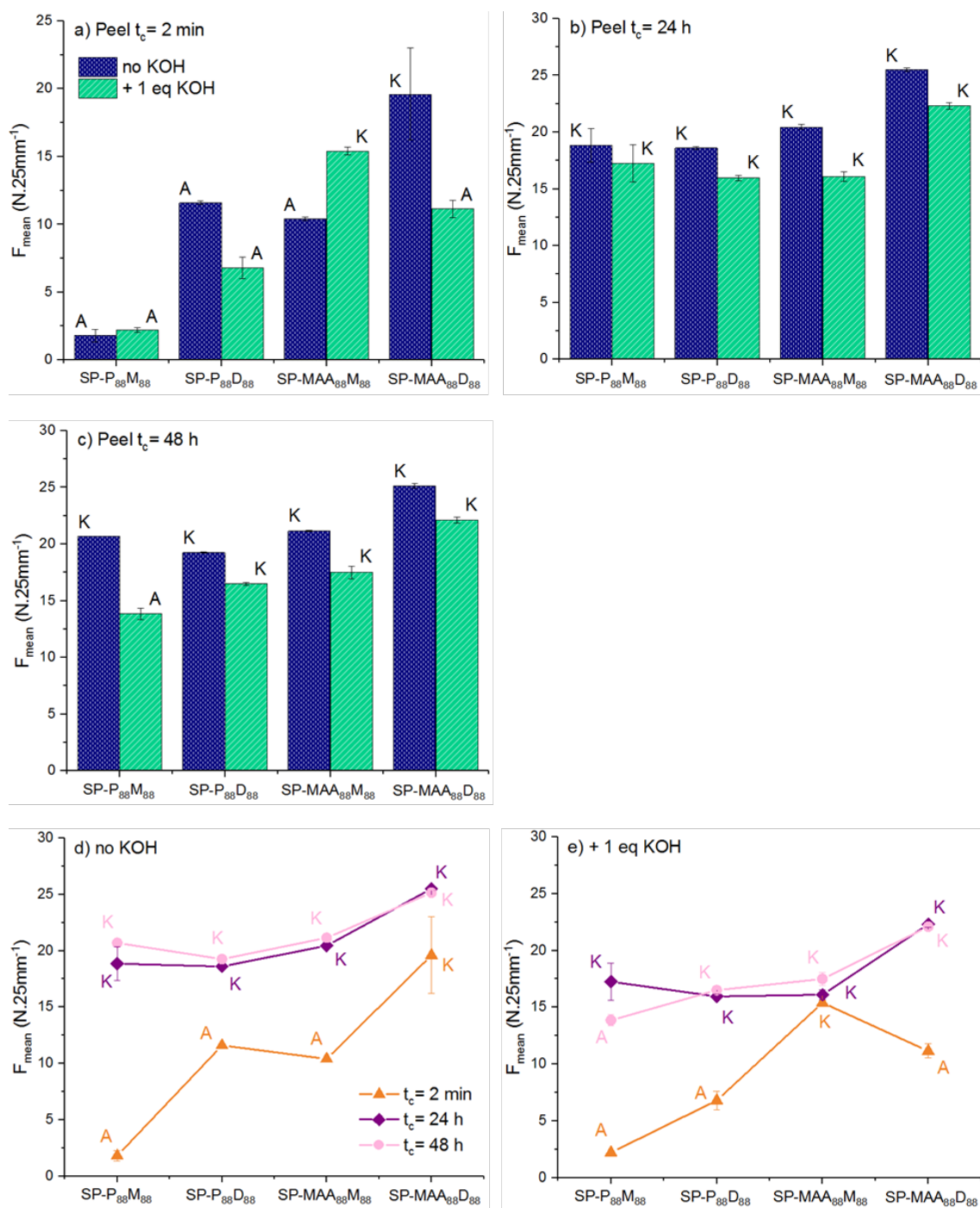


Figure 33. Peel mean force F_{mean} as function of ionicX for a) 2 min, b) 24 h and c) 48 h dwelling times; and F_{mean} as function of ionicX for all dwelling times with d) no KOH and e) 1 eq of KOH

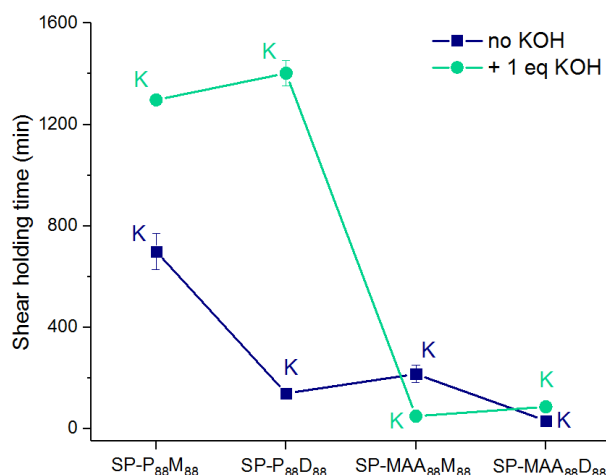


Figure 34. Dependence of shear holding time over sample series 3 with and without added KOH

v. Discussion

The purpose of this section was to assess the possibility of tuning the mechanical and adhesive properties of the adhesives (based on ionic crosslinks) by changing the nature of the interacting groups. Overall, the sample containing the strong/strong combination of interactions with Polystep® and MAETAC was more elastic than the others. The presence of Polystep® and KOH in SP-P₈₈M₈₈ and SP-P₈₈D₈₈ was seen as they exhibited characteristics of highly crosslinked materials: brittle fractures were observed in tensile tests with strong strain-hardening and short elongation at break (Figure 31). It was also seen by a strong increase in shear resistance (Figure 34). Although SP-P₈₈D₈₈ with KOH, showed very high cohesion, the linear rheology was not influenced by the deprotonation of the phosphate groups. This is similar to what was observed in II.2.B. with SP-P₁₀₀M₅₀; interactions between deprotonated acids were proposed as crosslink points[48, 49] leading to improvement of strain and shear resistance. It could also come from high grafting density and ionic clustering produced by aggregation of the Polystep® groups in the film.

SP-P₈₈M₈₈ and SP-P₈₈D₈₈ contained the same amount of Polystep® (theoretically by extension, the same number of dimers introduced) but no ionic interactions should take place without addition of KOH. Then ionic clusters might form (discussed in III.2.A.) by aggregation of ionic groups in the n-BA/MMA matrix; and as MAETAC is ionized unlike DMAEMA, it would tend to form bigger and/or more clusters in SP-P₈₈M₈₈, making it tougher than SP-P₈₈D₈₈.

Contrary to expectations, the combination between methacrylic acid and MAETAC (SP-MAA₈₈M₈₈) didn't lead to ionic crosslinking after deprotonation. Although it showed characteristics of low crosslinked materials against small and high strains (Figures 28 and 31), the dissipative component increased highly with addition of KOH. The cross-over frequency in linear rheology was increased and $\tan \delta$ was measured above or equal to 1 for the whole range of frequencies; cohesive failure was also obtained for short contact time in peel tests and holding power was lowered. The origin of such behaviour is blurry as such ionic couple should form ionic complexation upon acid deprotonation.

For the weak acid/weak base combination SP-MAA₈₈D₈₈, the effect of KOH was strong for small strains as a rubbery plateau was observed and ω_c decreased. For high strains, the polymer was slightly more crosslinked and could sustain longer deformation before breaking. Also, the ability of the adhesive to form fast contact with the substrate was slightly lowered as peel force after 2 min was lowered, and adhesive failure was observed. These suggest the deprotonation of MAA induced short range interactions that could resist to short deformation but didn't influence the viscoelastic properties in the non-linear regime.

The direct effect of changing the base from MAETAC to DMAEMA (i.e. comparing SP-MAA₈₈M₈₈ and SP-MAA₈₈D₈₈), is difficult to assess as the polymers showed antagonist behaviors upon deprotonation of the methacrylic acid groups. Their mechanical properties differed but the overall adhesive performance was similar. A small difference of the peel mean force was recorded at short contact time; F_{mean} was higher for SP-MAA₈₈D₈₈ (19.6 N.25 mm⁻¹ against 10.4 N.25 mm⁻¹ for SP-MAA₈₈M₈₈) and could be explained by the higher tackiness of the sample.

SP-MAA₈₈M₈₈ might be less tacky as it might form ionic clusters due to a high content of charged MAETAC groups as proposed in the above paragraph.

Once again, the different properties of the polymer films were influenced by the polymer grafting for Polystep[®] containing samples and the ionic clustering which may not have similar organization (cluster size or even clustering minimal concentration) by changing the ionic groups. The comonomers could also be incorporated differently in the polymers according to their nature and their reactivity ratios with the other monomers. This could lead to composition drifts therefore differences in the polymer architectures and mechanical properties.

It is also important to mention that the effect of grafting might anyway prevail on the effect of ionic clustering and have higher impact on the polymers mechanical properties rather than the ionic network.

D. Comparison of adhesive performance to commercialized products

In order to comprehend the potential of the adhesives presented in the previous paragraphs, the best performers were compared to products commercialized by BASF.

SP-P₈₈M₈₈, SP-P₅₀M₁₀₀ and SP-P₈₈D₈₈ were selected as they presented good adhesive and cohesive balance. Acronal® V 215 and Acronal® 3633 are widely used acrylic water-based dispersions for PSA. They show high adhesive performance, water resistance and can easily be formulated with tackifiers or wetting agents. Their characteristics can be found in Table 8. In these products, resistance to shear and deformation is obtained by a certain degree of covalent crosslinking (i.e. gel content) while high tack is provided by a low $T_g \sim 40^\circ\text{C}$.

Table 8. Characteristics of commercialized acrylic dispersions Acronal®

Product	Application	T_g (°C)	Gel% in MEK	Gel% in EtOH
Acronal® V 215	Various (labels, tapes)	- 43	65.6	85.2
Acronal® 3633	Tapes & flooring adhesives	- 35	52.0	79.5

The peel and shear properties on steel of the two Acronal® were measured using the same procedure previously introduced. The comparison of the Peel mean force F_{mean} for dwell times of 2 minutes and 24 hours are given in Figure 35, and the comparison of shear resistance for 1.5 kg in Figure 36. The values are given in Appendix 41.

Acronal® 3633 showed the highest tackiness at low contact time and F_{mean} already reached $18.3 \text{ N.25 mm}^{-1}$ with cohesive failure. SP-P₈₈D₈₈ showed higher peel force (with $F_{\text{mean}}=11.6 \text{ N.25 mm}^{-1}$) than Acronal® V 215 and similar with added KOH.

Although low adhesion was found for SP-P₈₈M₈₈ and SP-P₅₀M₁₀₀ for $t_c=2$ min, after 24 h they reached the same performance, with and without KOH, as both Acronal®. SP-P₈₈D₈₈ also reached high peel forces and could compete with the commercial products.

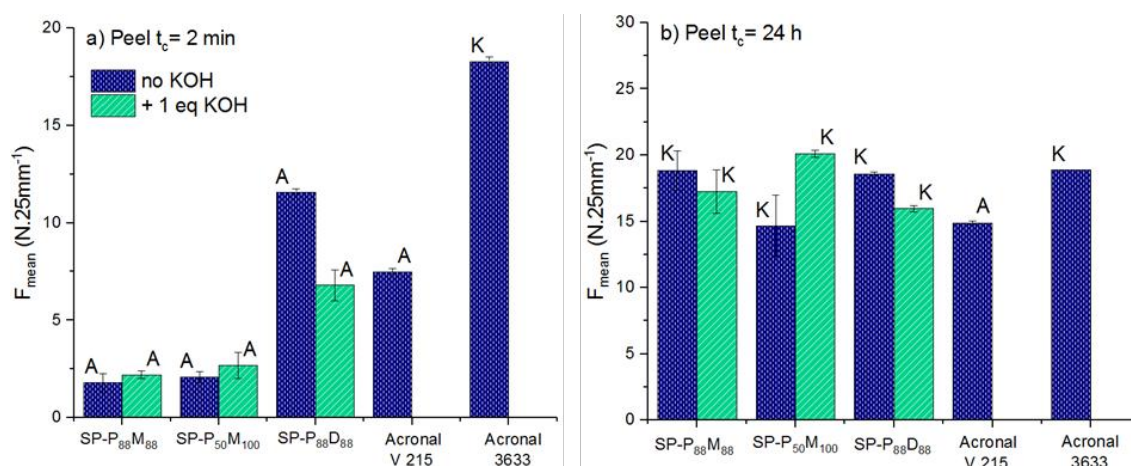


Figure 35. Comparison of Peel mean force F_{mean} on steel for a) $t_c=2$ min and b) $t_c=24$ h

Given the error range of the shear holding time (shear resistance), the solution polymers (SP) reached (SP-P₈₈D₈₈) or outperformed (SP-P₈₈M₈₈ & SP-P₅₀M₁₀₀) Acronal 3633 while Acronal V 215 showed the highest shear resistance with 1170 min. However, with the addition of KOH, the shear holding time of all three SP was over 1200 min.

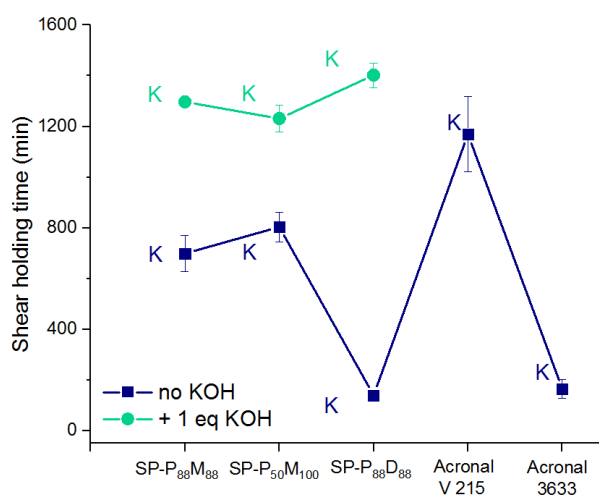


Figure 36. Comparison of the shear holding time on steel with a 1.5 kg load

To evaluate the products with the best adhesion/cohesion balance, shear strength as function of the peel mean force for $t_c=24$ h is given in Figure 37.

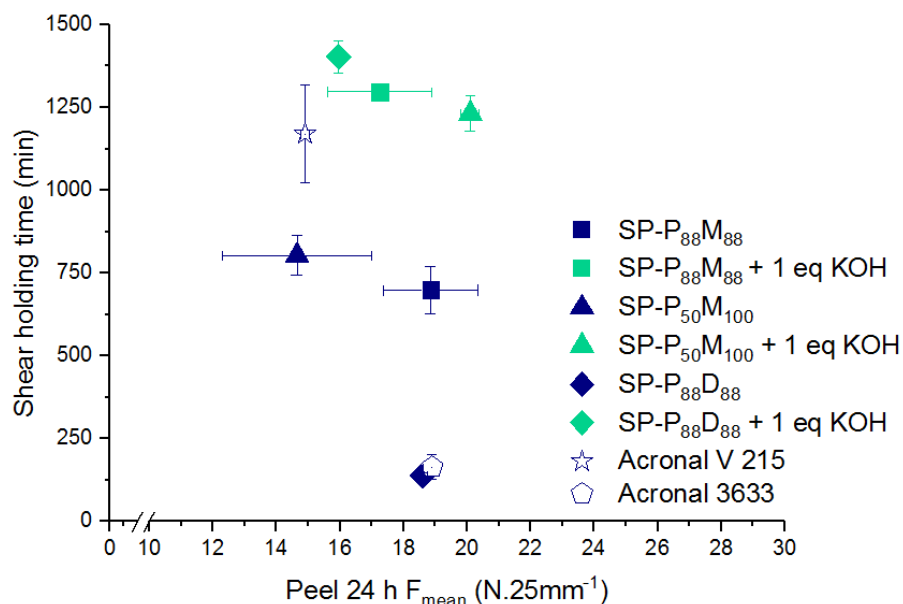


Figure 37. Evolution of the shear strength as function of the 24 h F_{mean}

In Figure 37, it was observed that triggering the ionic network of the SP by addition of KOH, improved further the adhesion/cohesion balance. The adhesion was not lost by the creation of ionic interactions (even increased in some cases) and shear resistance highly improved. Generally speaking, they performed therefore better than both Acronal®.

It is also important to note that the glass transition temperatures of SP-P₈₈M₈₈, SP-P₅₀M₁₀₀ and SP-P₈₈D₈₈ are around 20°C higher which should highly lower their peel performance.

E. Optimization of the molecular weight using a batch process

i. Synthesis and characteristics of the polymers

The samples synthesized in the previous paragraphs are promising products and compete with commercialized products while having higher glass transition temperatures. To improve further the shear holding power of the samples while keeping high peel forces, the optimization of their molecular weight[41, 42] was investigated by changing the types of feeding process. A moderate M_w of $\sim 400\,000 - 500\,000 \text{ g.mol}^{-1}$ was targeted; a too high molecular weight ($>700\,000 \text{ g.mol}^{-1}$) might turn the polymer unfavourable to substrate wetting (lowered chain mobility) and lower adhesion[42].

In free radical polymerization, the number-average degree of polymerization DP_n indicates the average number of monomer units introduced per polymer chain[53, 54]. The number M_n and weight M_w average molecular weights are more likely to increase if DP_n is high. Yet, DP_n depends directly on the growing chains kinetics and correlates to the instantaneous concentration of monomers and is inversely proportional to the instantaneous concentration of radicals. In other words, $DP_n \sim [\text{Monomers}]$ but $DP_n \sim [I\cdot]^{-1/2}$.

Based on the synthesis of SP-P₈₈M₈₈ (described in III.2.A.), the molecular weight distribution was increased first using a batch process to increase $[\text{Monomers}]$ and decrease $[I\cdot]$.

In a second step, the instantaneous initiator concentration was also lowered by using tert-Butyl peroxy-2-ethylhexanoat (t-BP2EH) as initiator. t-BP2EH has a higher half-life temperature (73°C for $t_{1/2}=10 \text{ h}$) than tert-Butyl peroxy-pivalate (t-BPPVT used for the synthesis of SP-P₈₈M₈₈, 57°C for $t_{1/2}=10 \text{ h}$). Used at the same reaction temperature $T=70^\circ\text{C}$, the low decomposition rate of t-BP2EH further decreases $[I\cdot]$. An illustration of the semi-batch and batch processes is available in Figure 38. The monomers (n-BA, MMA, Polystep® and MAETAC) conversions were followed during the polymerizations by High Performance Liquid Chromatography (HPLC) while the molecular distributions were measured by SEC-RI and MALLS.

To make sure the ionic comonomers would not induce compositions drifts due to higher or lower copolymerization rates, reference reactions were carried out with pure n-BA/MMA compositions (P_0M_0 i.e. 0 mmol of Polystep® nor MAETAC). A summary of the samples synthesised by semi-batch and batch using t-BPPVT and batch using t-BP2EH is given in Table 9.

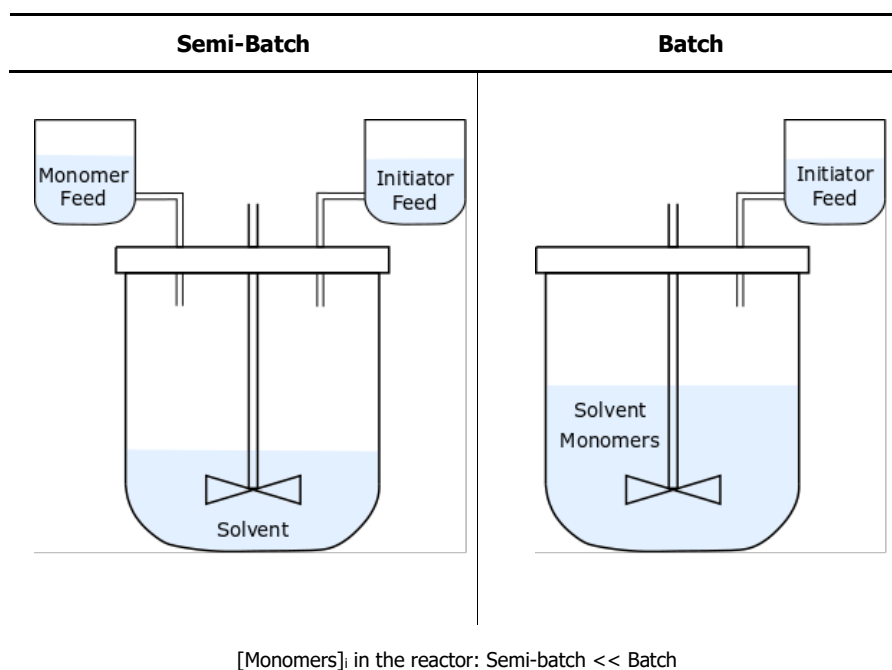


Figure 38. Illustration of Semi-batch and batch processes

All detailed procedures are available in the experimental section in Chapter VI; yet, it is important to recall all reactions were carried out at 70°C. The reaction time of the 3 syntheses were adjusted to obtain the maximum conversion of monomers but the temperature in the reactors was increased to 90°C and a second feed of initiator (chemical deodorization) was added to remove all residual monomers.

Table 9. Description of the samples series 4 using different processes to increase the polymer molecular weight

Series #	Experiment	Feeding type	Initiator	Composition
4	SP-SemiB	Semi Batch	t-BHPV	$P_{88}M_{88}$
				P_0M_0
	SP-B	Batch		$P_{88}M_{88}$
				P_0M_0
	SP-B-tBP2EH	Batch		$P_{88}M_{88}$
				P_0M_0

The instantaneous conversion of the individual monomers, C_i , and the molecular weight M_w are displayed in Figures 39-41 as function of the reaction time for SP-Semi B, SP-B and SP-B-tBP2EH. All values can be found in Tables 10 to 16. The relative molar mass distributions obtained by RI signal for the different reaction times are available in Figure 42.

As seen for SP-SemiB $P_{88}M_{88}$, Polystep® was converted faster than other monomers and total conversion almost was reached after 3 hours of reaction. MAETAC and MMA are converted more slowly but most importantly, a high increase of 20% in conversion was seen after the increase of reaction temperature to 90°C (indicated by the first straight black line) that would suggest fast incorporation of the two monomers. n-BA showed much slower conversion and almost 50% of it was unconverted before the temperature increase (prior second feed of initiator); total conversion was obtained after an hour of post-polymerization.

The weight average molecular weight increased with conversion of the monomers until the chemical deodorization after which it decreased.

As only the M_w of the sol part of the polymer is measured in SEC, this decrease in M_w should be an indication that during the second initiator feed many radicals were formed due to high amounts of residual monomers. Due to prior increase in temperature, the initiator decomposition was fast, and many radicals were created. Yet, the residual monomer concentration was low so small chains were formed. Moreover, due to slower chain propagation, some radicals or oligoradicals were grafted onto the polymer chains and led to covalent crosslinking. This is illustrated on the relative molar mass distributions in Figure 42, with the appearance of a shoulder of high M_w but a broadening at low M_w was also observed suggesting new chains were also formed.

Similar monomers conversions were observed for the pure n-BA/MMA copolymer but the maximal M_w (from MALLS detection) reached $\sim 40\,000\text{ g.mol}^{-1}$ after 1 h and was stable until increasing reactor temperature to 90°C and the chemical deodorization where a broadening of M_w was seen in Figure 42 for low M_w ; suggesting generations of new chains.

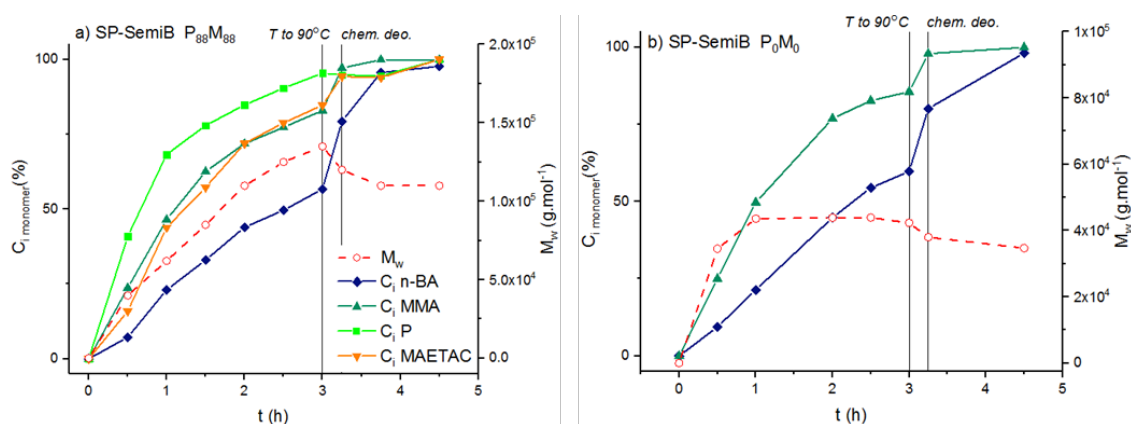


Figure 39. Instant monomer conversion C_i and M_w over reaction time for SP-SemiB

Table 10. Table of molecular weights obtained by SEC as function of the reaction time for
SP-SemiB P₈₈M₈₈

Experiment	Reaction time	M _w (g.mol ⁻¹)	M _n (g.mol ⁻¹)	PDI	M _w MALLS (g.mol ⁻¹)
SP-SemiB P ₈₈ M ₈₈	1 h	80 600	25 900	3.1	40 000
	1 h 30	108 000	47 900	2.3	62 000
	2 h	138 000	47 700	2.9	85 000
	2 h 30	161 000	38 300	4.2	110 000
	3 h	169 000	53 300	3.2	125 000
	3 h 15	181 000	53 400	3.4	135 000
	3 h 45	161 000	36 500	4.4	120 000
	4 h 30	148 000	22 300	6.7	110 000
	5 h 30	145 000	16 900	8.6	110 000

Table 11. Table of molecular weights obtained by SEC as function of the reaction time for
SP-SemiB P₀M₀

Experiment	Reaction time	M _w (g.mol ⁻¹)	M _n (g.mol ⁻¹)	PDI	M _w MALLS (g.mol ⁻¹)
SP-SemiB P ₀ M ₀	30 min	40 500	6 880	5.9	34 500
	1 h	50 700	12 000	4.2	43 600
	2 h	53 000	13 500	3.9	43 900
	2 h 30	52 000	15 800	3.3	43 900
	3 h	50 500	14 900	3.4	42 300
	3 h 15	45 100	11 500	3.9	38 000
	4 h 30	40 700	8 910	4.6	34 700

Looking at the conversions of SP-B $P_{88}M_{88}$ in Figure 40, the individual conversions of MMA, Polystep® and MAETAC were similar throughout the reaction. After 4h and before the final initiator feed conversions were complete, 15% of n-BA was left to polymerize.

M_w increased sharply after 2 h (simultaneously with n-BA conversion) and increased during the reaction to reach $\sim 900\,000\text{ g}\cdot\text{mol}^{-1}$. It was observed on the relative molar mass distributions obtained by RI signal (Figure 42), directly a broadening to $M_w > 10^7\text{ g}\cdot\text{mol}^{-1}$ and after the chemical deodorization a broadening of low M_w .

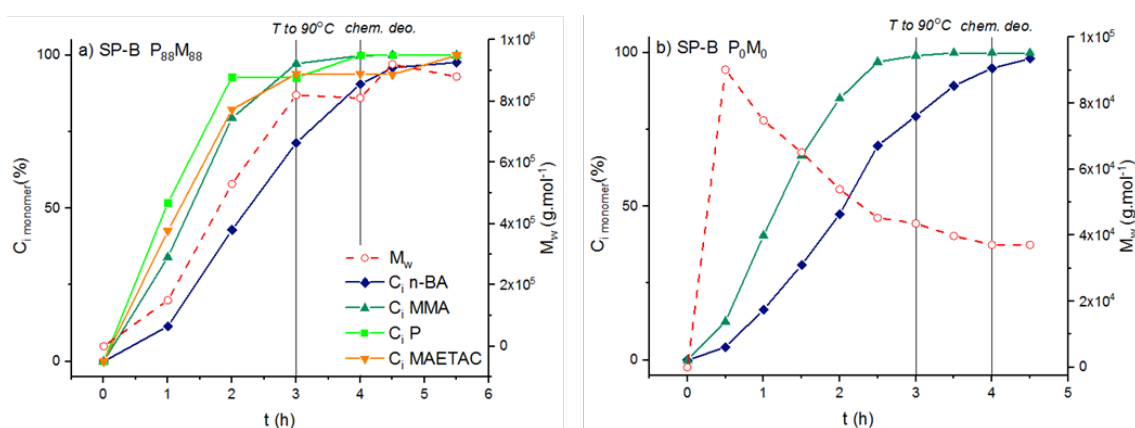


Figure 40. Instant monomer conversion C_i and M_w over reaction time for SP-B

Table 12. Table of molecular weights obtained by SEC as function of the reaction time for SP-B P₈₈M₈₈

Experiment	Reaction time	M _w (g.mol ⁻¹)	M _n (g.mol ⁻¹)	PDI	M _w MALLS (g.mol ⁻¹)
SP-B P ₈₈ M ₈₈	1 h	203 000	97 500	2.1	150 000
	2 h	398 000	63 400	6.3	530 000
	3 h	508 000	27 700	18.3	820 000
	4 h	449 000	15 100	29.7	810 000
	4 h 30	462 000	13 700	33.7	920 000
	5 h 30	448 000	12 700	35.3	880 000

Table 13. Table of molecular weights obtained by SEC as function of the reaction time for SP-B P₀M₀

Experiment	Reaction time	M _w (g.mol ⁻¹)	M _n (g.mol ⁻¹)	PDI	M _w MALLS (g.mol ⁻¹)
SP-B P ₀ M ₀	30 min	104 000	37 900	2.8	90 200
	1 h	87 400	22 500	3.9	74 800
	1 h 30	75 100	31 400	2.4	65 100
	2 h	65 500	21 900	3.0	53,900
	2 h 30	56 800	17 200	3.3	45 300
	3 h	52 800	14 300	3.7	43 600
	3 h 30	48 500	10 000	4.9	39 800
	4 h	45 500	7 660	5.9	37 100
	4 h 30	43 900	6 250	7.0	37 100

For SP-B P_0M_0 , n-BA was converted more slowly than MMA. After 2 h, ~80% of MMA was converted while only ~50% of n-BA was. The molecular weight increased sharply readily after 30 min to ~90 000 g.mol⁻¹ and gradually decreased to ~37 000 g.mol⁻¹. This, added to the gradual increase of the shoulder on the molar mass distribution (Figure 42) for $M_w < 10^4$ g.mol⁻¹, suggests that new and shorter chains of polymer were synthesised instead of adding monomer units to existing growing chains.

Concerning SP-B t-BP2EH $P_{88}M_{88}$, the conversions of MMA, Polystep® and MAETAC were similar. Total conversions were reached after 6 hours before the chemical deodorization. After this reaction time, the conversion of n-BA was measured to be around 75 %. M_w increased sharply after 4 hours of polymerization. M_w reached 2 700 000 g.mol⁻¹ after 6 hours and decreased afterwards until 1 800 000 g.mol⁻¹. It is likely that the true M_w could not be measured by SEC, due to microgel formation from some covalent crosslinking.

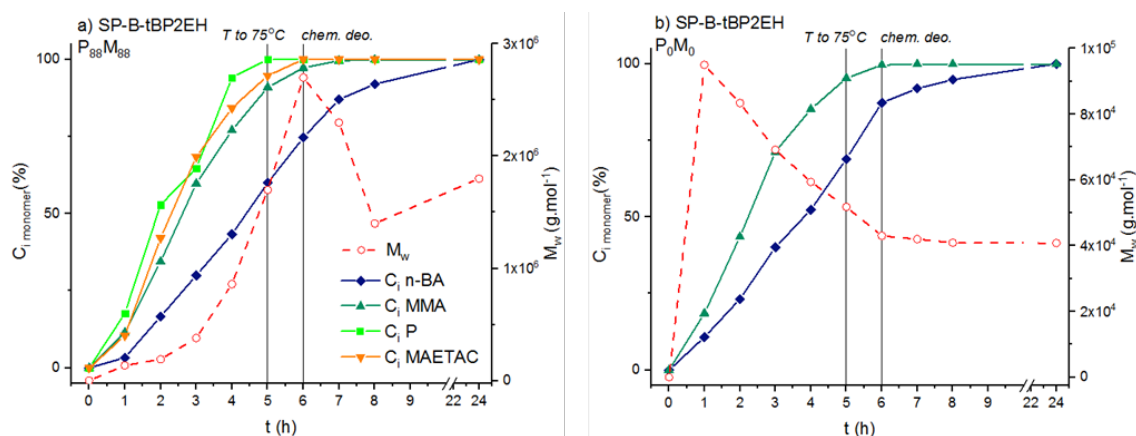


Figure 41. Instant monomer conversion and M_w over reaction time for SP-B-tBP2EH

Regarding P_0M_0 sample, differences in conversion between MMA and n-BA were seen. The maximum M_w was found also directly after 1 hour of reaction and decreased sharply afterwards to ~40 000 g.mol⁻¹.

It is most likely due to reactions competition between the initiation of new polymer chains and chain growth; and it is accentuated by the last initiator feed and the high amount of residual monomers.

The final values of M_w for all samples are available in Table 17.

For $P_{88}M_{88}$ samples, M_w increased by more than one degree of magnitude from 110 000 g.mol^{-1} (SP-SemiB) to 880 000 and 1 800 000 g.mol^{-1} for respectively SP-B and SP-B t-BP2EH. Therefore, the molecular weight of SP-SemiB was successfully increased by using a batch process. However, M_w for the pure n-BA/MMA polymers were not increased using batch polymerization.

Table 15. Table of molecular weights obtained by SEC as function of the reaction time for SP-B t-BP2EH $P_{88}M_{88}$

Experiment	Reaction time	M_w (g.mol^{-1})	M_n (g.mol^{-1})	PDI	M_w MALLS (g.mol^{-1})
SP-B-tBP2EH $P_{88}M_{88}$	1 h	104 000	9 240	11.3	135 000
	2 h	233 000	38 500	6.1	190 000
	3 h	353 000	66 900	5.3	380 000
	4 h	584 000	81 900	7.1	860 000
	5 h	695 000	26 800	25.9	1 700 000
	6 h	656 000	20 000	32.7	2 700 000
	7 h	658 000	21 100	31.1	2 300 000
	8 h	522 000	16 600	31.5	1 400 000
	24 h	592 000	13 200	44.7	1 800 000

Table 16. Table of molecular weights obtained by SEC as function of the reaction time for SP-B t-BP2EH P₀M₀

Experiment	Reaction time	M _w (g.mol ⁻¹)	M _n (g.mol ⁻¹)	PDI	M _w MALLS (g.mol ⁻¹)
SP-B-tBP2EH P ₀ M ₀	1 h	108 000	20 300	5.3	95 000
	2 h	97 400	26 200	3.7	83 400
	3 h	80 500	19 000	4.2	69 200
	4 h	72 100	17 600	4.1	59 400
	5 h	63 300	17 000	3.7	51 800
	6 h	55 100	12 300	4.5	43 000
	7 h	52 400	9 090	5.8	42 000
	8 h	49 900	8 140	6.1	40 900
	24 h	49 500	7 010	7.1	40 800

Table 17. Final values of of molecular weights obtained by SEC-RI and MALLS for the sample series 4

Series #	Experiment	Composition	M _w (g.mol ⁻¹)	M _n (g.mol ⁻¹)	PDI	M _w with MALLS (g.mol ⁻¹)
4	SP-SemiB	P ₈₈ M ₈₈	148 000	23 000	6.5	110 000
		P ₀ M ₀	69 100	14 900	4.6	34 700
	SP-B	P ₈₈ M ₈₈	448 000	12 700	35.3	880 000
		P ₀ M ₀	73 100	14 200	5.1	37 100
	SP-B-tBP2EH	P ₈₈ M ₈₈	611 000	14 000	43.4	1 800 000
		P ₀ M ₀	74 800	13 500	5.5	40 800

The polymer chains conformations indicated by ν and given in Table 18 (R_g vs M curves fitting given in Appendix 42), were much more linear (rod-like) for P_0M_0 samples due to the absence of Polystep® (for $P_{88}M_{88}$, coil-like). But no differences in polymer conformation were seen between the types of processes.

Table 18. Conformation factor for series 4, obtained by SEC-MALLS and relative polymer conformation

Series #	Experiment	ν	Conformation	
4	SP-SemiB	$P_{88}M_{88}$	0.46	coil
		P_0M_0	1.42	rod
	SP-B	$P_{88}M_{88}$	0.52	coil
		P_0M_0	1.49	rod
	SP-B-tBP2EH	$P_{88}M_{88}$	0.46	coil
		P_0M_0	1.03	rod

As in previous paragraphs, the gel contents and T_g of the final polymers were measured (available in Appendix 43). No gel was measured for all polymers ($P_{88}M_{88}$ and P_0M_0) in MEK and EtOH and thus should not contain covalent networks. The T_g (given in Appendix 43) of SP-B and SP-B t-BP2EH were slightly lower (-24.0 and -26.6°C) than for SP-SemiB, most likely due to higher polymer chains length. And as reported in III.2.A., the T_g n-BA/MMA copolymers were increased by adding ionic comonomers Polystep® and MAETAC.

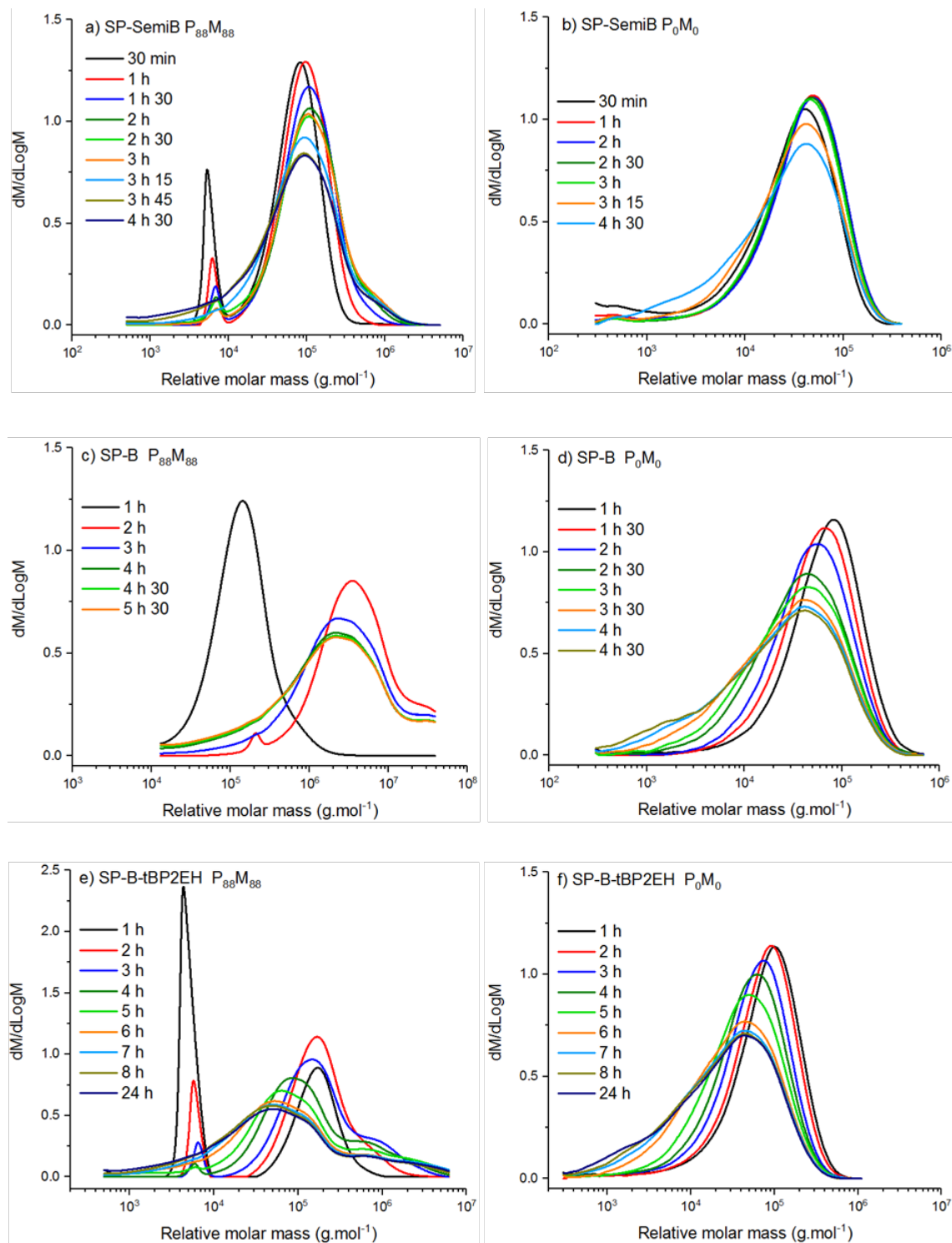


Figure 42. Relative molar mass distributions throughout reaction time of sample series 4

ii. Morphology of the polymer films

The AFM phase images of the three ionic copolymers ($P_{88}M_{88}$) films cross-sections are presented in Figure 43. As introduced in III.2.A., the polymerization in semi-batch results in a homogenous polymer film. But the images of the polymers prepared in batch (SP-B and SP-B t-BP2EH) witnessed the presence of two polymers. A polymer matrix of harder phase contrast was observed with darker areas (~ 200 nm of diameter) and suggest inclusions of a softer polymer. Images at $20\text{ }\mu\text{m}$ scale showed that this was not localized and spread over the whole polymer films.

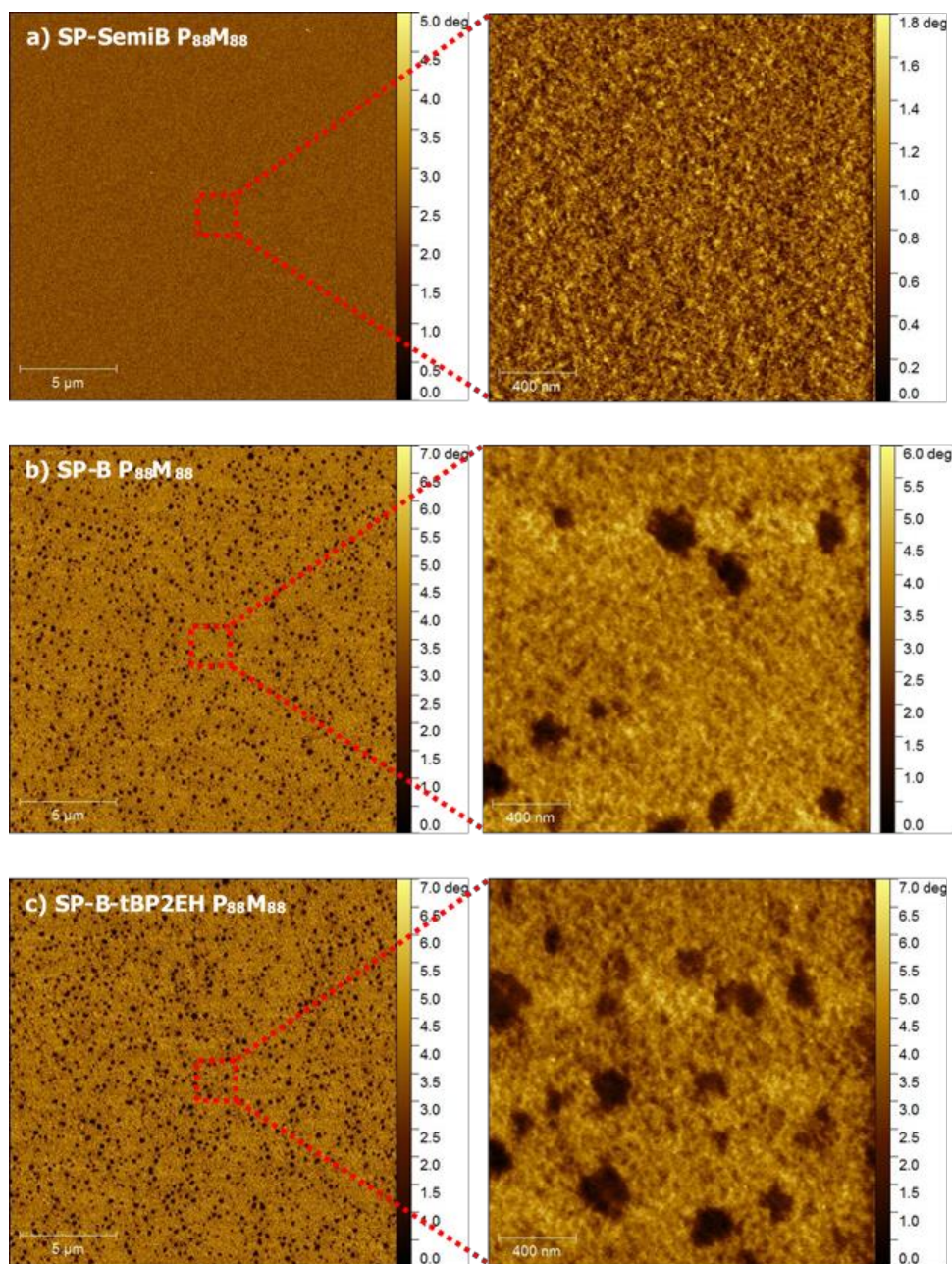


Figure 43. AFM phase images in tapping mode at 20 μm scale with enlargement at 2 μm of a) SP-SemiB, b) SP-B and c) SP-B-tBP2EH

iii. Mechanical characteristics of the polymer films

To compare the mechanical properties of the polymers prepared by the different processes, linear rheology was realized using TTS for the $P_{88}M_{88}$ polymer films, as described in the previous paragraphs. The master curves of G' and G'' calculated for $T=25^\circ\text{C}$ and $\tan \delta$ are available in Figure 44. Standard Frequency sweep measurements were realized in the same conditions on the pure n-BA/MMA copolymers, the curves are available in Appendix 44. The cross-over frequencies were reported in Appendix 45 and are displayed as function of the samples in Figure 45.

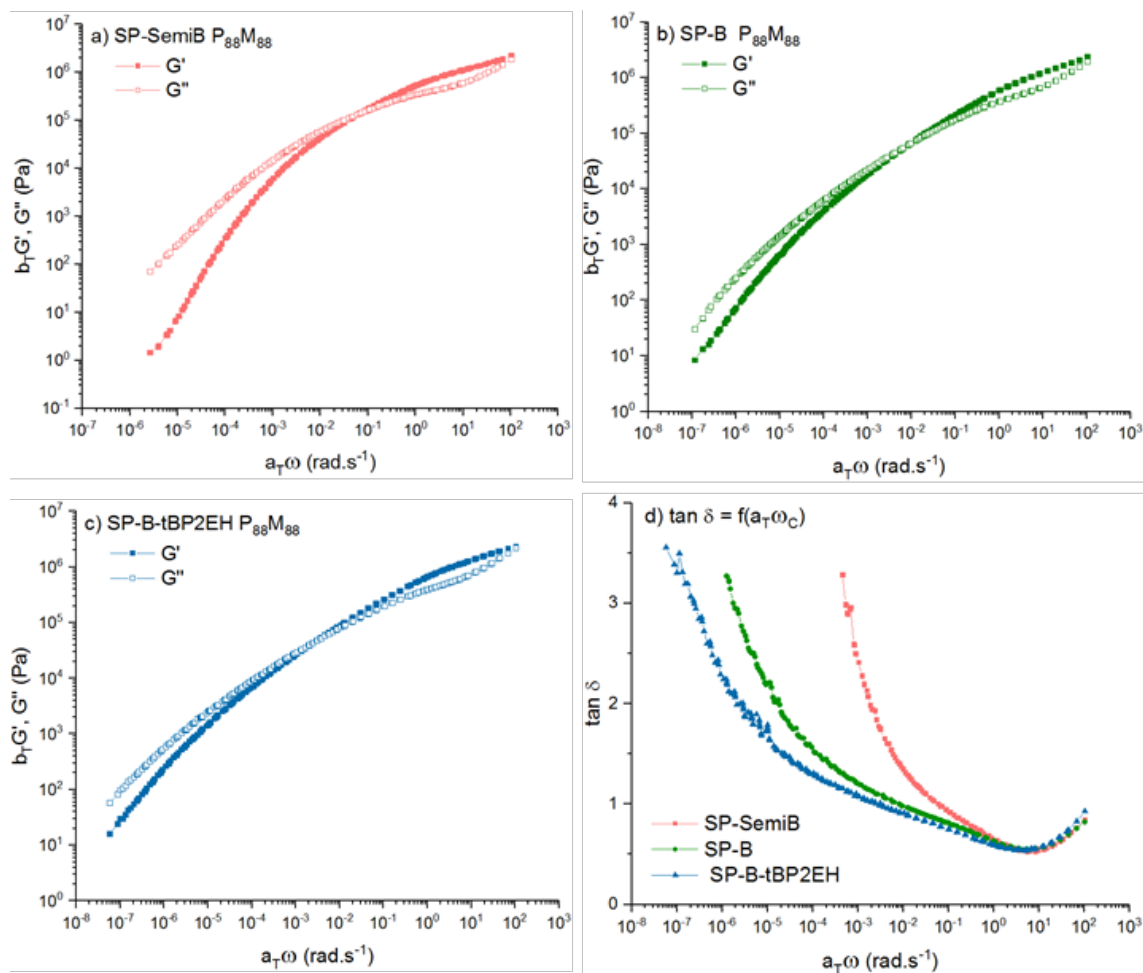


Figure 44. Master curves at 25°C of the elastic G' and Loss G'' moduli and $\tan \delta$ as function of the angular frequency obtained by Time-Temperature Superposition measurements

All three samples exhibited the same behaviour of low crosslinked materials with a rubbery region at high frequency and flowing behaviour at lower ω . However, the samples prepared in batch do not show full terminal relaxation as SP-SemiB with $G' \sim \omega^2$ and $G'' \sim \omega$. This indicated that more intermolecular interactions delayed the flowing of polymer chains, most likely due to high number of entanglements or polymer branches. It was also suggested by the decrease of cross-over frequencies with high M_w as seen in Figure 45; and the delayed increase of $\tan \delta$ at low frequencies. The measurements of the pure n-BA/MMA copolymers (available in Appendix 44) showed that they were all behaving as liquid-like already at high frequencies suggesting low M_w polymers.

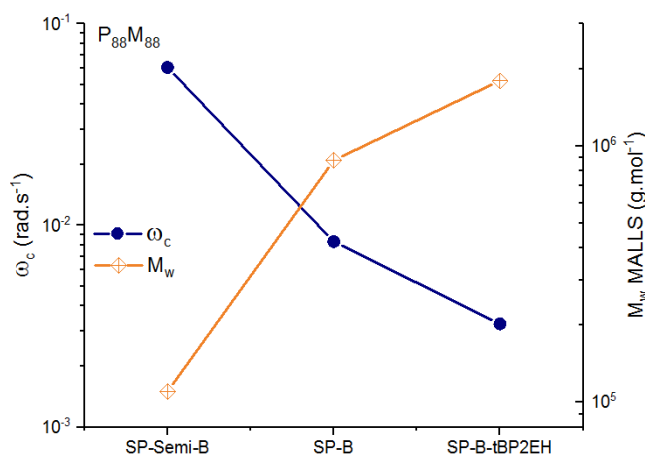


Figure 45. Cross-over frequency ω_c and weight average molecular weight M_w as function of the samples for $P_{88}M_{88}$ composition

The measurement of the mechanical properties for long deformation were carried out by tensile tests in the same conditions described in previous paragraphs. The stress-strain curves obtained for $P_{88}M_{88}$ samples are available in Figure 46; P_0M_0 series could not be measured. Data is available in Appendix 46.

SP-B and SP-B t-BP2EH showed brittle behaviour towards uniaxial deformation, this is caused by their high M_w a potentially high branching density. It was seen by a large strain hardening, a maximal stress reaching respectively 316 and 425 kPa and fracture at 1460 and 1250 %.

This further confirmed that high number of entanglements, branching or crosslinking were present making the materials more resistant to strain.

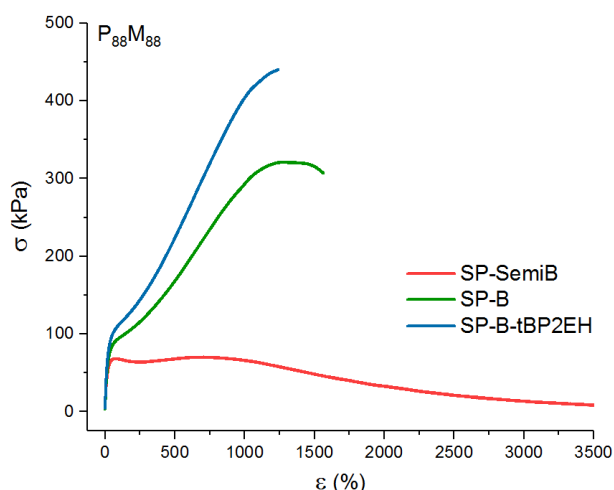


Figure 46. Comparison of the stress-strain curves for SP-SemiB, SP-B and SP-B-tBP2EH

iv. Adhesive properties of the polymer films

The adhesive performance of the sample series 4 were measured as reported in previous sections. The peel mean forces are displayed in Figure 47, static shear resistance in Figure 48 and the values are reported in Appendix 47.

Generally, for the $P_{88}M_{88}$ compositions, F_{mean} was measured to be close to zero and adhesive/filmic failure modes were observed using the batch process; this implicates that M_w was increased to the high detriment of adhesion either for short or long contact times. SP-SemiB showed therefore higher peel performance.

However, the contrary was found in the case of pure n-BA/MMA copolymers. F_{mean} , for SP-SemiB, was $\sim 0 \text{ N.25 mm}^{-1}$ for dwelling times of 2 min, 24 h and 48 h; but cohesive failures were seen, implying the adhesive was too tacky and viscous to resist to debonding so low peel forces were recorded.

In the case of SP-B and SP-B t-BP2EH P_0M_0 , F_{mean} was measured $\sim 5 \text{ N.25 mm}^{-1}$ for all contact times and led to cohesive failure. Therefore, in comparison to SP-Semi B P_0M_0 , they were more resistant to peeling thanks to the presence of more interactions between polymer chains.

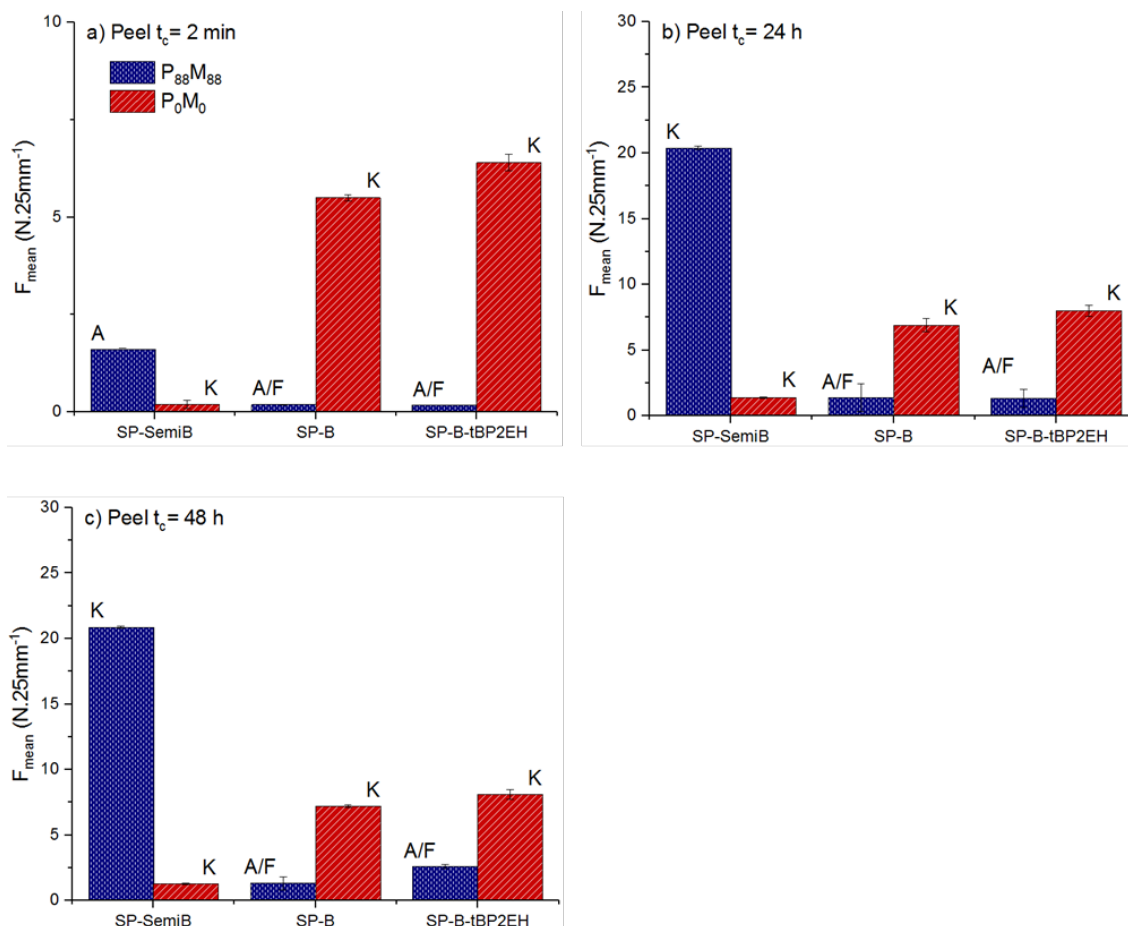


Figure 47. Peel mean force F_{mean} as function of the process for a) 2 min, b) 24 h and c) 48 h dwelling times; and comparison of F_{mean} for all dwelling times

Concerning shear resistance displayed in Figure 48, SP-SemiB $P_{88}M_{88}$ showed the highest holding power of 929 min even with a lower M_w than SP-B and SP-B t-BP2EH. But these two failed adhesively meaning they failed in creating enough contact with the surface to measure their real shear strengths. Zero shear resistance was measured for pure acrylate compositions due to a lack of internal cohesion via entanglements (low M_w), branching or crosslinking.

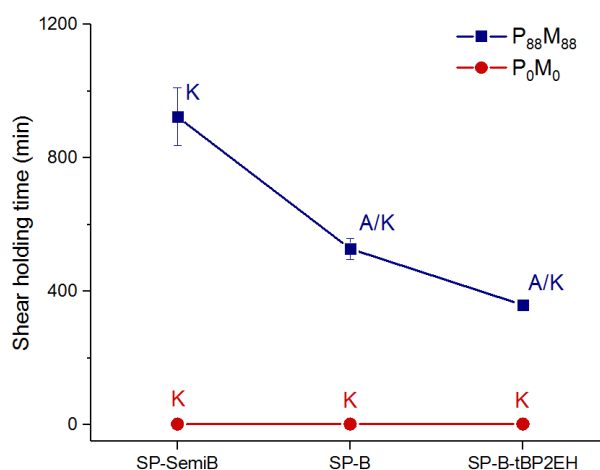


Figure 48. Dependence of shear strength over sample series 4 for $P_{88}M_{88}$ and P_0M_0 compositions

v. Discussion

The target of this section was to increase the molecular weight of SP- $P_{88}M_{88}$ to $\sim 400\,000$ to $500\,000\text{ g.mol}^{-1}$, in order to improve its shear resistance and further adhesion/cohesion balance. This was done by decreasing the ratio between monomer concentration and initiator radical, using a batch process and by using t-BP2EH as initiator which had a lower decomposition rate at 70°C than t-BPPVT.

It was seen that for all processes, the comonomers and especially n-BA did not have the same reactivities, therefore much residual monomer was left before the chemical deodorization. The increase of temperature and the second feed of initiator, accelerated the conversion rate and thus led to branching (rather than covalent crosslinking because no gel was measured) but also to the polymerization of shorter chains; respectively observed by the increase in M_w and the relative molar mass distribution in Figure 42.

Low reactivity or conversion rate of n-BA can be explained by chain transfer to isopropanol. Indeed, it was reported that the chain transfer constant of iPrOH for n-BA is $C_s=14.12$ at 80°C while $C_s=0.47$ in Methanol[55].

Moreover, the reactivity ratios of n-BA and MMA copolymerization at 60°C gave $r_{n-BA}=0.2$ for $r_{MMA}=1.74$ [56] which could further lower the consumption rate of n-BA.

Two phases were observed in the polymer films of the batch polymerization and are a direct consequence of the composition drifts created (most probably) at the end of the reactions. It is likely that, one high M_w polymer was synthesized during the feed and short chains of low M_w were synthesized at the end.

Due to high difference in M_w [57] and probably in chemical composition, the two polymers could not blend and led to phase-separation in the polymer film. The inhomogeneity of the polymer films and the very high M_w obtained in batch, was entirely detrimental to the adhesion as very low peel forces were measured. The shear strength could also not be determined as the PSA failed in adhesion to the substrate.

In summary, the optimization of the molecular weight using batch processes and initiator and higher half-life temperature was successful. However, for future work, the solvent should be chosen in accordance (methanol or ethanol) with monomers to insure similar reactivities.

III.3. GENERAL CONCLUSION

The present chapter provides a route to polyampholyte polymers for PSA prepared by free-radical solution polymerization and studies the parameters that influence the mechanical and adhesive properties of the final polymers.

Using free-radical solution polymerization to produce statistical acrylate-based copolymers bearing oppositely charged ionic functionalities, was successful. Although the presence of dimers in the anionic comonomer (Polystep®) introduced branching in polymer chains, the effect of the ionic crosslinking density on the mechanical and adhesive properties was seen.

Ionic networks made the polymers more resistant to small and large deformations which increased shear resistance under static load, but the balance between toughness and extensibility allowed the polymers to gain in adhesion (peel force) and cohesion (shear resistance). The mechanical response and adhesive performance could be tuned by changing the stoichiometry between ionic moieties and the nature of ionic interactions.

Indeed, a stoichiometric amount of ionic comonomers in the polymer (SP-P₁₀₀M₁₀₀) increased the number of ionic crosslinks and therefore the stiffness of the material in comparison to SP-P₅₀M₁₀₀ and SP-P₁₀₀M₅₀. However, after the addition of KOH, SP-P₁₀₀M₅₀ showed a higher resistance to shear and performed as well as SP-P₁₀₀M₁₀₀, but contained twice less possible crosslinks formed from the interactions between Polystep® and MAETAC. It was suggested that the physical network of SP-P₁₀₀M₅₀ was reinforced by crosslinks occurring between phosphate groups. This implies that ionic crosslinking may not be necessarily between oppositely charged groups but can be done with acid moieties alone; and the crosslinking density could be tuned by different neutralization degrees.

In III.2.D., it was seen that the PSA based on polyampholytes reached with no doubts the performances of commercialized products. But there is still room to increase their tackiness by lowering the T_g . This could be done by increasing the part of n-BA, yet it undergoes high chain transfer to solvent in isopropanol.

It would thus require using other solvents provided that they dissolve both acrylates and ionic comonomers. Another solution would be to replace n-BA by another 'soft' acrylate monomer but this risks to change the miscibility of the polymer chains and the viscoelastic properties of the films.

To improve further the shear resistance of the ionomers, optimization of molecular weight was carried out using batch processes, but as mentioned, n-butyl acrylate undergoes chain transfer with isopropanol. This led to high compositions shift, which didn't favour adhesion, and resulted in low shear resistance.

Although the acrylate-based ionomers prepared in solution showed high potential for PSA applications, the use of an organic solvent is problematic for a product development in industry; therefore, the preparation of secondary water-borne dispersions from these polymers was studied in the next Chapter.

III.4. REFERENCES

1. Lowe, A.B. and C.L. McCormick, *Synthesis and solution properties of zwitterionic polymers*. Chemical Reviews, 2002. **102**: p. 4177-4189.
2. Peiffer, D.G. and R.D. Lundberg, *Synthesis and viscometric properties of low charge density ampholytic ionomers*. Polymer, 1985. **26**: p. 1058-1068.
3. Salamone, J.C., et al., *Acrylic ampholytic ionomers*. Polymer, 1982. **23**: p. 843-848.
4. Bouix, M., et al., *Synthesis of amphiphilic polyelectrolyte block copolymers using "living" radical polymerization: Application as stabilizers in emulsion polymerization*. Macromolecules Rapid Communications, 1998. **19**: p. 209-213.
5. Chen, W.-Y., et al., *Effect of block size and sequence on the micellization of ABC triblock methacrylic polyampholytes*. Macromolecules, 1995. **28**: p. 8604-8611.
6. Patrickios, C.S., et al., *Diblock, ABC triblock, and random methacrylic polyampholytes: synthesis by group transfer polymerization and solution behavior*. Macromolecules, 1994. **27**: p. 930-937.
7. Webster, O.W., et al., *Group-transfer polymerization. 1. A new concept for addition polymerization with organosilicon initiators*. Journal of the American Chemical Society, 1983. **105**: p. 5706-5708.
8. Schellman, J.A., *The application of the Bjerrum ion association theory to the binding of anions by proteins*. Journal of Physical Chemistry, 1953. **57**(4): p. 472-475.
9. Levin, Y. and M.C. Barbosa, *Conformational phase transition of a polyampholyte in a low dielectric solvent*. Europhysics Letters, 1995. **31**(9): p. 513-518.
10. Zhao, Q., et al., *Underwater contact adhesion and microarchitecture in polyelectrolyte complexes actuated by solvent exchange*. Nat Mater, 2016. **15**(4): p. 407-12.
11. Stewart, R.J., et al., *The role of coacervation and phase transitions in the sandcastle worm adhesive system*. Adv Colloid Interface Sci, 2017. **239**: p. 88-96.
12. Stevens, M.J., et al., *Multiscale structure of the underwater adhesive of *Phragmatopoma californica*: a nanostructured latex with a steep microporosity gradient*. Langmuir, 2007. **23**: p. 5045-5049.
13. Stewart, R.J., et al., *The tube cement of *Phragmatopoma californica* - a solid foam*. The Journal of Experimental Biology, 2004. **216**: p. 4727-4734.
14. S.Wang, C. and R.J. Stewart, *Localization of the bioadhesive precursors of the sandcastle worm, *Phragmatopoma californica* (Fewkes)*. The Journal of Experimental Biology, 2012. **215**: p. 351-361.

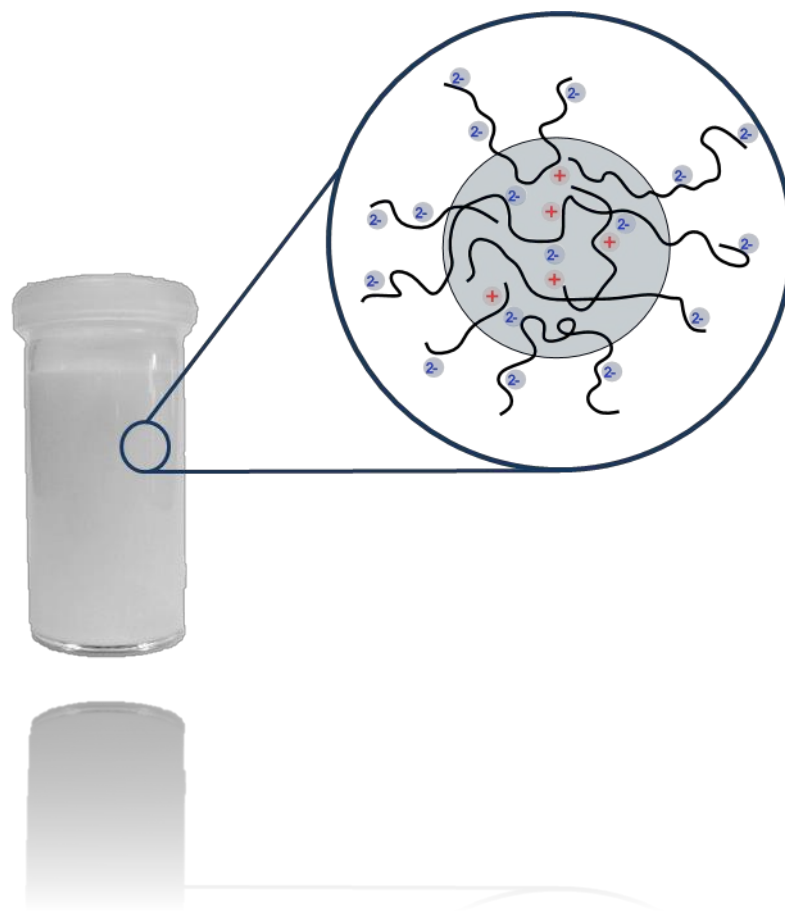
15. Zhao, H., et al., *Cement proteins of the tube-building polychaete phragmatopoma californica*. The Journal of Biological Chemistry, 2005. **280**: p. 42938–42944.
16. Mann, L.K., et al., *Fetal membrane patch and biomimetic adhesive coacervates as a sealant for fetoscopic defects*. Acta Biomaterialia, 2012. **8**: p. 2160-2165.
17. Jones, J.P., et al., *Water-borne endovascular embolics inspired by the undersea adhesive of marine sandcastle worms*. Advanced Healthcare Materials, 2016. **5**: p. 795-801.
18. Shao, H. and R.J. Stewart, *Biomimetic underwater adhesives with environmentally triggered setting mechanisms*. Adv Mater, 2010. **22**(6): p. 729-33.
19. Stewart, R.J., C.S. Wang, and H. Shao, *Complex coacervates as a foundation for synthetic underwater adhesives*. Advances in Colloid and Interface Science, 2011. **167**: p. 85-93.
20. Stewart, R.J., *Protein-based underwater adhesives and the prospects for their biotechnological production*. Applied Microbiology and Biotechnology, 2011. **89**: p. 27-33.
21. Locock, K.E., L. Meagher, and M. Haeussler, *Oligomeric cationic polymethacrylates: a comparison of methods for determining molecular weight*. Anal Chem, 2014. **86**(4): p. 2131-7.
22. Rollings, J.E., *Use of on-line scattering coupled to chromatographic separations for the determination of molecular weight, branching, size and shape distributions of polysaccharides*, in *Laser light scattering in Biochemistry*, S.E. Harding, D.B. Sattelle, and V.A. Bloomfield, Editors. 1992. p. 275-293.
23. Capek, I., *Nature and properties of ionomer assemblies. II*. Advances in Colloid Interface Science, 2005. **118**(1-3): p. 73-112.
24. Eisenberg, A., *Clustering of ions in organic polymers - a theoretical approach*. Macromolecules, 1970. **3**(2): p. 147-154.
25. Zosel, A., *The effect of bond formation on the tack of polymers*. Journal of Adhesion Science and Technology, 1997. **11**(11): p. 1447-1457.
26. Zosel, A., *Effect of crosslinking on tack and peel strength of polymers*. Journal of Adhesion, 1991. **34**(1-4): p. 201-209.
27. T. Yamaguchi, K.K., M. Doi, *In situ observation of stereoscopic shapes of cavities in soft adhesives*. Europhysics Letters, 2007. **77**(6): p. 64002-64006.
28. S. Poivet, F.N., C. Gay, P. Fabre, *Cavitation-induced force transition in confined viscous liquids under traction*. Europhysics Letters, 2003. **62**(2): p. 244-250.
29. Chang, E.P., *The Viscoelastic Window of PSAs*. The Journal of Adhesion, 1991. **34**(1-4): p. 189-200.

30. Eisenberg, A., B. Hird, and R.B. Moore, *A new multiplet-cluster model for the morphology of random ionomers*. Macromolecules, 1990. **23**: p. 4098-4107.
31. Deng, G. and K.A. Cavicchi, *Tuning the viscoelastic properties of poly(n-butyl acrylate) ionomer networks through the use of ion-pair comonomers*. Macromolecules, 2017. **50**(23): p. 9473-9481.
32. Weiss, R.A. and H.Y. Zhao, *Rheological behavior of oligomeric ionomers* Journal of Rheology, 2009. **53**: p. 191-213.
33. Kima, J.-S., et al., *Clustering in poly(methyl acrylate) ionomers*. Polymer, 2000. **41**: p. 3099–3102.
34. Kima, J.-S., Y.H. Naha, and S.-S. Jarng, *Comparison of clustering in various acrylate ionomers*. Polymer, 2001. **42**: p. 5567-5571.
35. Zosel, A. and G. Ley, *Influence of crosslinking on structure, mechanical properties, and strength of latex films*. Macromolecules, 1993. **26**: p. 2222-2227.
36. Lee, J.-H., et al., *Molecular weight and crosslinking on the adhesion performance and flexibility of acrylic PSAs*. Journal of Adhesion Science and Technology, 2016. **30**(21): p. 2316-2328.
37. Villey, R., et al., *In-situ measurement of the large strain response of the fibrillar debonding region during the steady peeling of pressure sensitive adhesives*. International Journal of Fracture, 2017. **204**: p. 175-190.
38. Costelloa, P.A., et al., *Branched methacrylate copolymers from multifunctional monomers: chemical composition and physical architecture distributions*. Polymer, 2002. **43**: p. 245-254.
39. Dealy, J.M. and R.G. Larson, *Structure and rheology of molten polymers: from structure to flow behavior and back again*. 2006: Carl Hanser Verlag GmbH & Co. KG.
40. Chen, Q., G.J. Tudryn, and R.H. Colby, *Ionomer dynamics and the sticky Rouse model*. Journal of Rheology, 2013. **57**(5): p. 1441-1462.
41. Tobing, S.D. and A. Klein, *Molecular parameters and their relation to the adhesive performance of emulsion acrylic pressure-sensitive adhesives*. Journal of Applied Polymer Science, 2001. **79**: p. 2230-2244.
42. Krencieski, M.A. and J.F. Johnson, *Shear, tack, and peel of polyisobutylene: effect of molecular weight and molecular weight distribution*. Polymer Engineering and Science, 2004. **29**: p. 36-43.
43. Bose, R.K., et al., *Connecting supramolecular bond lifetime and network mobility for scratch healing in poly(butyl acrylate) ionomers containing sodium, zinc and cobalt*. Phys Chem Chem Phys, 2015. **17**(3): p. 1697-704.

44. Bose, R.K., et al., *Relationship between the network dynamics, supramolecular relaxation time and healing kinetics of cobalt poly(butyl acrylate) ionomers*. Polymer, 2015. **69**: p. 228-232.
45. Das, A., et al., *Ionic modification turns commercial rubber into a self-healing material*. ACS Appl Mater Interfaces, 2015. **7**(37): p. 20623-30.
46. Levada, T.I. and M.M. Feldstein, *Relationship between intermolecular bonding, nanostructure, phase behavior, and macroscopic physical properties of pressure-sensitive adhesives based on polyelectrolyte complexes*. Journal of Applied Polymer Science, 2012. **125**: p. 448-470.
47. Feldstein, M.M. and A.P. Moscalets, *Electroconducting pressure-sensitive adhesives based on polyelectrolyte complexes*, in *Innovations in Pressure-Sensitive Adhesive products*. 2016, Smithers Rapra. p. 45-54.
48. Feldstein, M.M., E.E. Dormidontovad, and A.R. Khokhlov, *Pressure-sensitive adhesives based on interpolymer complexes*. Progress in Polymer Science, 2015. **42**: p. 79-153.
49. Feldstein, M.M., et al., *Mechanisms of molecular interactions in polybase-polyacid complex formed by copolymers of N,N-dimethylaminoethylmethacrylate with alkylmethacrylates and methacrylic acid with ethylacrylate*. Journal of Applied Polymer Science, 2009. **112**(3): p. 1142-1165.
50. B. Kronberg, K.H., B. Lindman, *Polymers in Solution*, in *Surface chemistry of surfactants & polymers*, W.W. Sons, Editor. 2014.
51. Kudaibergenov, S.E., *Recent advances in the study of synthetic polyampholytes in solutions*, in *Polymer Latexes - Epoxide resins - Polyampholytes*, Springer, Editor. 1999. p. 115-197.
52. Abdilla, A., et al., *Multistimuli responsive ternary polyampholytes: Formation and crosslinking of coacervates*. Journal of Polymer Science Part A: Polymer Chemistry, 2016. **54**(14): p. 2109-2118.
53. Barson, C.A., *Free-radical polymerization - Chain Transfer*, in *Comprehensive Polymer Science*, G. Allen and J.C. Bevington, Editors. 1996, Elsevier Ltd.
54. Braun, D. and W.K. Czerwinski, *Free-radical polymerization - Rates of copolymerization*, in *Comprehensive Polymer Science*, G. Allen and J.C. Bevington, Editors. 1996, Elsevier Ltd.
55. Nandi, U.S. and M. Singh, *Chain transfer of alcohols in the polymerization of acrylic esters*. Macromolecular Chemistry and Physics, 1982. **183**: p. 1467-1472.
56. Bevington, J.C. and D. Harris, *Reactivities of acrylates and methacrylates*. Polymer Letters, 1967. **5**: p. 799-802.
57. Gelles, R. and C.W. Frank, *Effect of molecular weight on polymer blend phase separation kinetics*. Macromolecules, 1983. **16**: p. 1448-1456.

IV.

**Secondary dispersions:
from dissolved to dispersed**



IV. Secondary dispersions: from dissolved to dispersed.....215

IV.1. Introduction	217
IV.2. Results.....	220
A. Synthesis of polyampholytes	220
B. Preparation and characterization of secondary dispersions	221
C. Physico-chemical properties of the polymers and their dried films.....	225
D. Mechanical properties of the polymer films.....	227
E. Adhesive properties of the polymer films.....	235
IV.3. Discussion	242
IV.4. Conclusion	246
IV.5. References	247

IV.1. INTRODUCTION

In the previous chapters, ionic functional groups were introduced in acrylate polymers to obtain physically crosslinked networks using two classical free radical polymerization techniques: solution and emulsion polymerization. It was seen that the ionic interactions act as true crosslinkers and give a good balance between cohesion and adhesion, plus the adhesive performance could be tuned by changing the stoichiometry or the nature of ionic moieties. However, the two polymerization techniques used to prepare the adhesive polymers are not industrially viable as the emulsions gave inconclusive results and inhomogeneous mixtures, and current regulations on the use of Volatile Organic content (VOC) push industries to avoid solvent-borne products (Directive 2004/42/CE[1]).

Apart from emulsion polymerization, self-assembly of block copolymers is an interesting strategy to prepare water-based dispersions from presynthesized polymers. Self-assembling di-block copolymers can be obtained by reversible addition-fragmentation chain transfer polymerization (RAFT)[2] among other controlled radical polymerization techniques like NMP, ATRP...[3]; the A and B blocks should have antagonist solvent miscibility to produce the self-induced assemblies[4, 5]. Various structures can be obtained using different degree of polymerization (DP) of each block and provide specific film morphologies and responsive features[6] (illustration given in Figure 1). However, RAFT polymerizations tend to be avoided on an industrial scale, as the rate of polymerization is usually slow, the process not very efficient and the use of thio compounds as RAFT agents should be avoided for price, odour and colour issues.

Polymerizable surfactants called surfmers[7, 8] can also be used to prepare water-borne dispersions through self-assembly. Surfmers are included in the final polymers, but their reactivity needs to be controlled to avoid homopolymerization which can result in poor emulsion stabilization.

Colloidal assembly of polyampholytes by formation of complex coacervates has also been proposed for the encapsulation of ingredients, drugs and proteins[9-13]. This technique could be used to encapsulate a soft acrylate polymer with oppositely charged polyelectrolytes that would provide both colloidal stabilization and ionic crosslinking. However, these dispersions may not form good PSA films as the coacervate shell are usually hard and might not be coatable.

Complex coacervate core-micelle dispersed in water have also been developed[14-18]. Micelles form at 'preferred micellar condition PMC' i.e. stoichiometry between oppositely charged ionic groups; and the co-assembly depends also on the right conditions of pH, ionic strength. But this preparation mean requires the whole system to be hydrophilic and cannot be applied to acrylate-based copolymers.

An industrially relevant example of surfactant-free polymer dispersions are polyurethanes dispersions (PUD). Usually, the polyaddition of isocyanate, polyols and reactive dispersing agent (hydrophilic or ionic monomer) is carried out in a solvent (e.g. acetone, methylethylketone, toluene...). As water is added to the mixture, a phase separation of the polyurethane occurs and results, after removal of the solvent, in a stable dispersion thanks to the hydrophilic and thus surface-active groups[19-23].

The ionic functional groups present in the polymers prepared in solution in Chapter III are hydrophilic; they are thus susceptible to stabilize an interface water/hydrophobic acrylate backbone (nBA/MMA) in the same way observed for PUDs. Therefore, the dispersibility in water of polymers prepared as described in the chapter III was studied in this chapter. The stoichiometry of the ionic moieties was varied to avoid complex coacervation and obtain dispersed polymer particles. In these cases, characterization of the polymers, measurement of their mechanical and adhesive properties was carried out and compared to those of the original solvent-borne polymers.

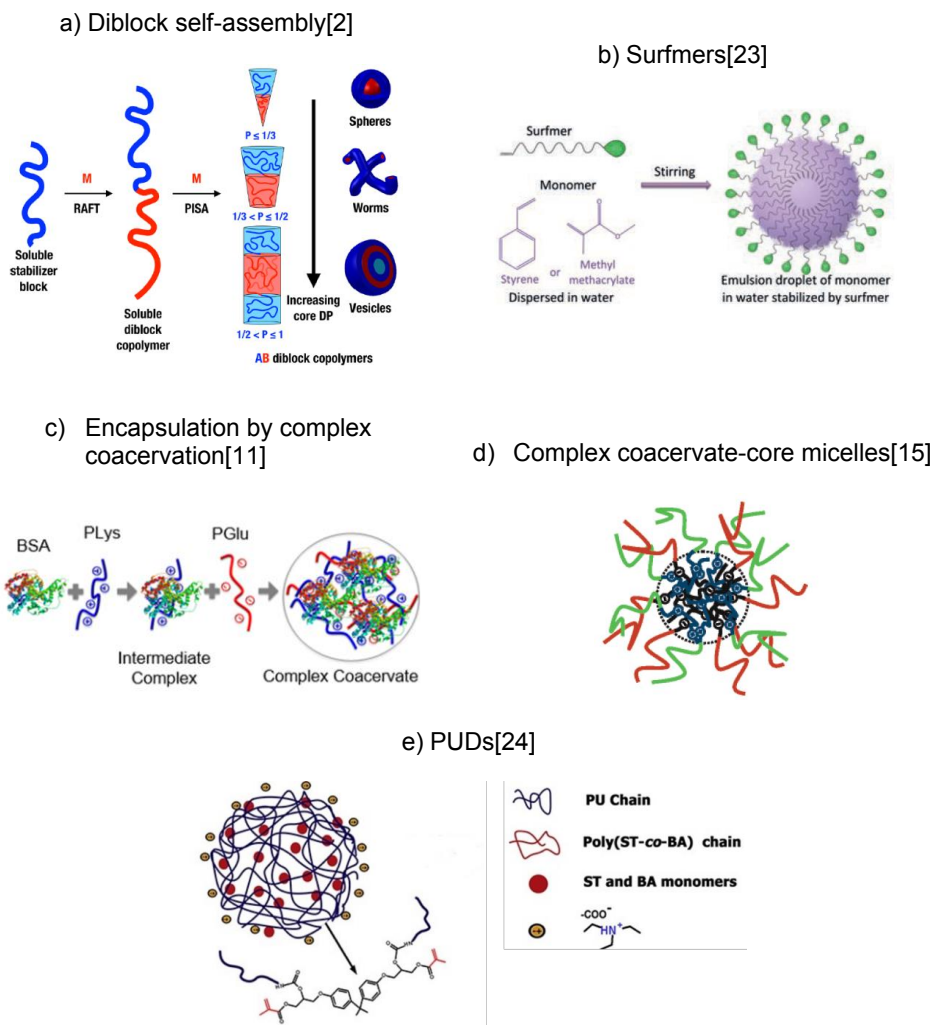


Figure 1. Techniques reported in the literature to prepare emulsifier-free water-based dispersions[2, 12, 16, 24, 25]

IV.2. RESULTS

A. Synthesis of polyampholytes

In primary dispersions, the polymer synthesis occurs in a pre-dispersed system (as in emulsion polymerization). In contrast, secondary dispersions are prepared by dispersing existing polymers in a solvent. This means that dispersing/stabilizing groups should be present in the polymer (ionic or hydrophilic groups if dispersion in water). A minimum amount of dispersing groups is needed to obtain stable secondary dispersions but it was shown that with PUDs this value varies with the monomers composition (content of hydrophobic and/or hydrophilic monomers)[22] and is therefore a property of each system.

In this chapter, secondary dispersions were prepared from copolymers of n-BA, MMA, Polystep® and MAETAC, previously synthesized by solution polymerization as described in Chapter III. In this system, both anionic and/or cationic monomers, (i.e. Polystep® and/or MAETAC) are potential stabilizing species. However, as the two monomers are susceptible to interact together during the dispersive process; there should thus be an excess of one ionic group to provide an overall charge to the polymer. Polystep® was selected as the dispersive species for its diacidity.

As the oppositely charged monomers might nonetheless interact (even with an excess of anions), the number of dispersive groups was calculated as $n_A = n_{\text{Polystep}} - n_{\text{MAETAC}}$ (n =moles of monomer) and was further referred to as available acid groups in mmol per kilo of dispersion. To study the required amount of free dispersing groups n_A (in IV.2.B) copolymers of n-BA, MMA, Polystep® and MAETAC were prepared with varying content of Polystep® and MAETAC, as described in Table 1.

Table 1. Polymers prepared by solution polymerization and their composition

Experiment	Polystep [®] (mmol)	MAETAC (mmol)	n _{AA} (mmol/kg)
SD-P₁₀₀M₁₀₀	100	100	0
SD-P₁₀₀M₅₀	100	50	53
SD-P₁₅₀M₅₀	150	50	96
SD-P₂₀₀M₅₀	200	50	138
SD-P₂₀₀M₁₀₀	200	100	89

B. Preparation and characterization of secondary dispersions

To prepare the secondary dispersions, the polymers listed in Table 1, were diluted to 30 wt% in isopropyl alcohol (iPrOH) and x equivalent of Potassium hydroxide (KOH) was added to deprotonate the phosphoric acid groups and produce charged anionic moieties. The boundaries of the dispersibility of the system in water were investigated. For this purpose, various degrees of acid neutralization were used (i.e. various x) and counter-examples containing few dispersive groups were used.

A large excess of demineralized water was then used to dilute the system before evaporating isopropyl alcohol and concentrating the polymers in water. iPrOH and H₂O are miscible and form a minimum-boiling azeotrope with a 87.4-87.7% weight fraction of iPrOH under atmospheric conditions which evaporates at 80.3-80.4°C[26]. For this reason, evaporating the organic solvent without overconcentrating the dispersion was challenging. Water was thus added after evaporating about 40% of the mixture iPrOH-H₂O, and then slow removal of residual iPrOH was carried out. An illustration of the procedure is given in Figure 2. Pictures of failed experiments are given in Appendix 48 and successful in Appendix 49.

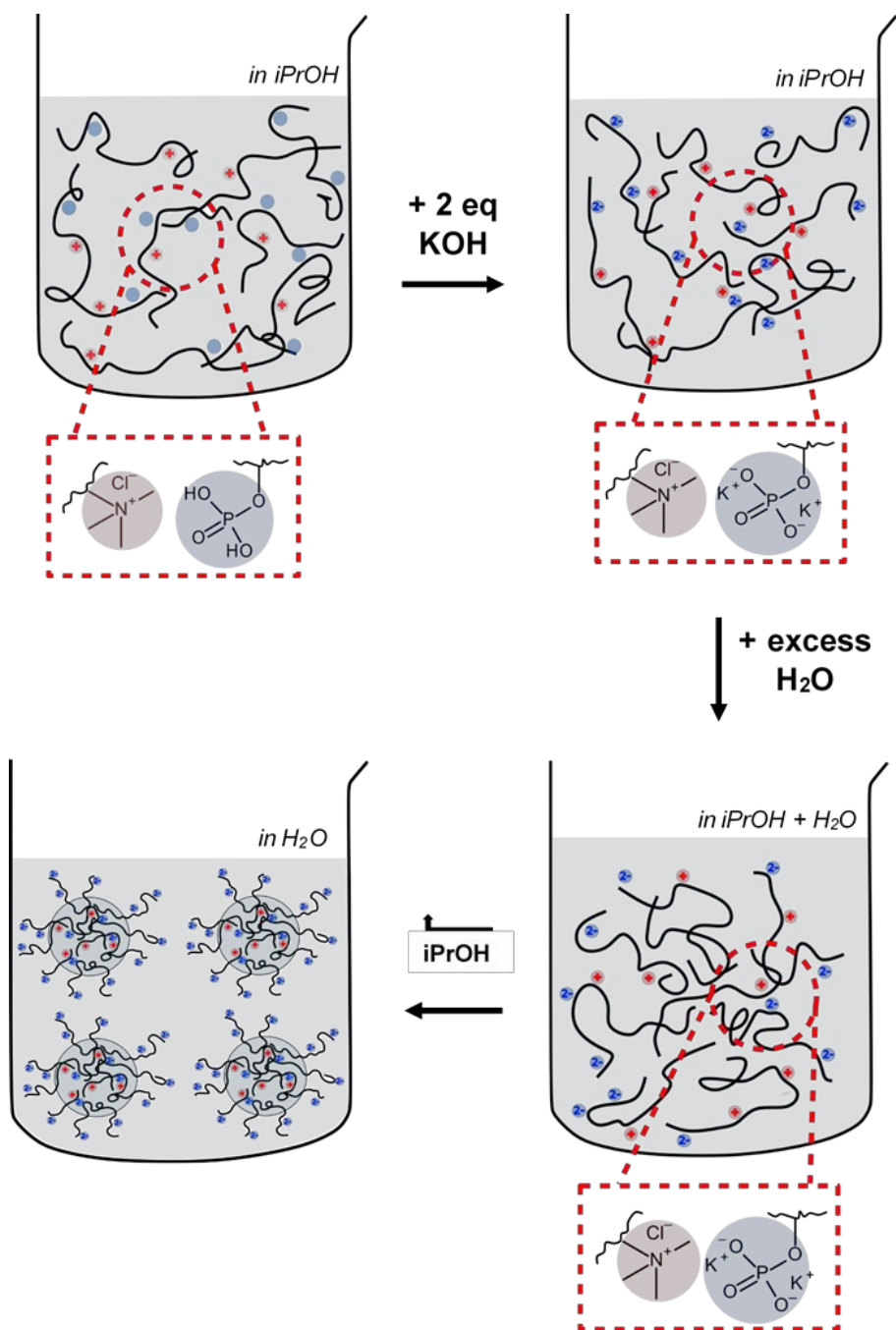


Figure 2. Illustration of the procedure for dispersing the solution polymers in water

Table 2 summarizes the results obtained for dispersibility. Water-based dispersions were only obtained from copolymers comprising a minimum amount of 90 mmol/kg stabilizing groups. Within the set of experiments studied, dispersions were obtained only for SD-P₁₅₀M₅₀, SD-P₂₀₀M₅₀ and SD-P₂₀₀M₁₀₀; the rest of the study was focused on these three samples. It was also necessary to add two equivalents of KOH, making phosphate groups anions with a 2⁻ net charge. The large excess of Polystep® and the full neutralization of the phosphate groups are likely to insure the polymers overall anionic charge and thus dispersibility in water without coacervation or precipitation.

Table 2. Description and dispersibility results of the sample series

Experiment	Equivalent of KOH	Dispersibility
SD-P₁₀₀M₁₀₀	0	X
	0.5	X
	1	X
	2	X
SD-P₁₀₀M₅₀	0	X
	0.5	X
	1	X
	2	X
SD-P₁₅₀M₅₀	0	X
	0.5	X
	1	X
	2	✓
SD-P₂₀₀M₅₀	0	X
	0.5	X
	1	X
	2	✓
SD-P₂₀₀M₁₀₀	0	X
	0.5	X
	1	X
	2	✓

In this chapter, 2 levels of data were used for comparative studies. The first level concerns the different contents of functional groups (i.e. SD-P₁₅₀M₅₀, SD-P₂₀₀M₅₀ and SD-P₂₀₀M₁₀₀). The second refers to the “state”, meaning as in solution (S), in solution with added KOH (S+KOH) or dispersed in water (D). For each sample the S+KOH and D series are obtained from the “mother” sample in solution (S).

The residual isopropanol contained in the dispersions was measured by Gas Chromatography (GC), the values are given in Table 3. Almost all isopropanol was removed, and the polymer dispersions could be considered water-based. The polymer particle sizes of the dispersions were determined by Analytical Ultracentrifugation (AUC), SD-P₂₀₀M₅₀ showed the smallest particle size with $D_{90\%} \approx 110$ nm. However, whilst SD-P₂₀₀M₁₀₀ was monomodal, SD-P₁₅₀M₅₀ was bimodal with $D_{90\%} \approx 190$ nm; this could have been induced when concentrating the dispersion by water evaporation. Too strong evaporation might have destabilized the dispersion and the particle size distribution was broadened. Detailed values are shown in Table 3 and the particle diameter weight distributions are given in Appendix 50.

Table 3. Residual isopropanol measured in dispersions by GC and particle size of the dispersions obtained by AUC

Experiment	GC	AUC		
	Residual iPrOH (mg.100g ⁻¹)	D _{10%} (nm)	D _{50%} (nm)	D _{90%} (nm)
SD-P₁₅₀M₅₀	4.0	51	103	203
SD-P₂₀₀M₅₀	30.0	30	59	113
SD-P₂₀₀M₁₀₀	2.5	50	111	191

AFM studies confirmed that defined particles were obtained using Single Particle Preparation as seen in Figure 3. The samples were prepared by strongly diluting the dispersion in demineralized water and coating a thin layer on mica or a silicon wafer, so that one or several particles are isolated over the surface.

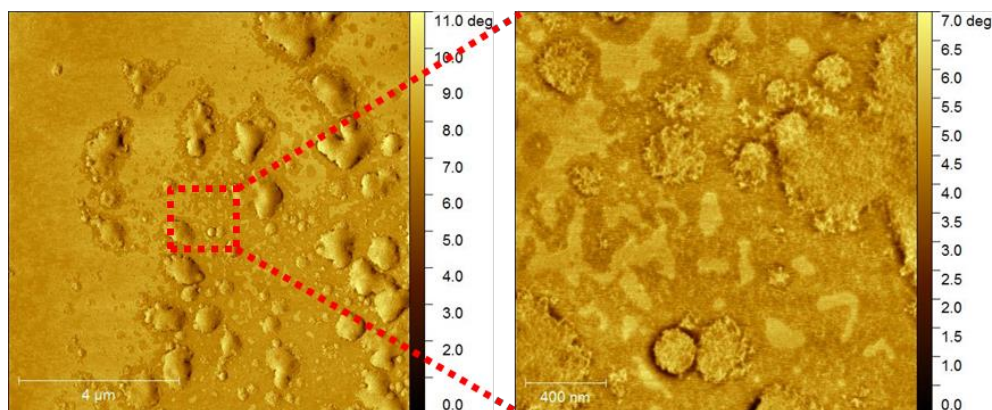


Figure 3. AFM pictures of the dispersion of SD-P₂₀₀M₁₀₀ using Single Particle Preparation

C. Physico-chemical properties of the polymers and their dried films

The molecular weight distributions of SD-P₁₅₀M₅₀, SD-P₂₀₀M₅₀ and SD-P₂₀₀M₁₀₀ were measured by Size exclusion chromatography (SEC) using both refractive index (RI) and multi-angle light scattering (MALLS) detectors, the values are given in Appendix 51. M_w values of 185 000 g.mol⁻¹ with RI detection and higher than 400 000 g.mol⁻¹ with MALLS were obtained. A significantly higher molecular weight was measured for SP-P₂₀₀M₅₀ (M_w =750 000 g.mol⁻¹) which might be caused by high degree of branching introduced by Polystep® as discussed in III.2.A. It was seen with the wide relative molar mass distribution available in Appendix 52.

The glass transition temperatures were obtained by DSC, values are available in Appendix 51. The T_g of all polymers was around -21°C, within the admissible range for PSA applications.

No gel content was found in the S samples, neither in Methyleneethylketone (MEK) nor in Ethanol (EtOH), suggesting that covalent crosslinking did not occur during the polymerization reaction. However, S+KOH and D samples showed a gel content ~10% in MEK and no gel content in EtOH. This is most likely due to the strong ionic interactions triggered by the addition of KOH which cannot be destabilized in the apolar solvent.

As seen in Chapter II and III, the morphology of the adhesive films is crucial for adhesion. In the system described hereby, a pre-organised structure might form during film drying as ionic groups would point towards the water phase. As the supernatant evaporates, the particles will stick to one another, the ionic moieties might interact and form ion clusters and hinder the interdiffusion of the acrylate backbone in the core of the particles. This might result in hard-shell soft-core like pattern[27]. AFM phase images of dried films cross sections (Figure 4 and Appendix 53) demonstrated that S+KOH and D films had homogenous morphologies and no ordered structure was found in the dispersions. It is worthwhile mentioning that on images of scale 5 μm in Appendix 53, white dots (higher phase contrast areas) were seen and resemble to salt (in this case KCl) aggregates. These aggregates were washed off from the cut with water and were not observed afterwards.

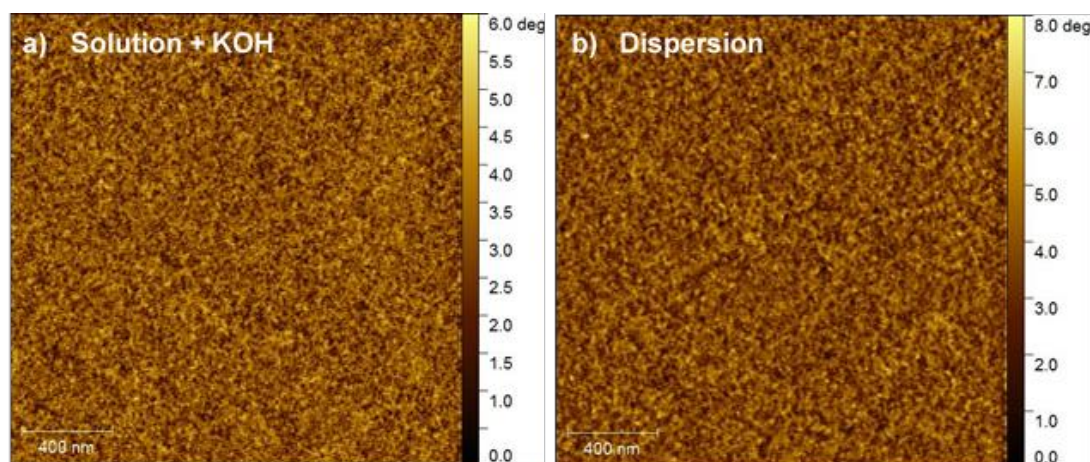


Figure 4. AFM phase images in tapping mode of SD-P₂₀₀M₁₀₀ cross-cuts as a) S+KOH and b) D

D. Mechanical properties of the polymer films

The mechanical properties of the polymer films at small-strains ($\epsilon < 100\%$) were measured using oscillatory rheology and Time-Temperature Superposition. Master curves were obtained for $T=25^\circ\text{C}$ and are available in Figure 5.

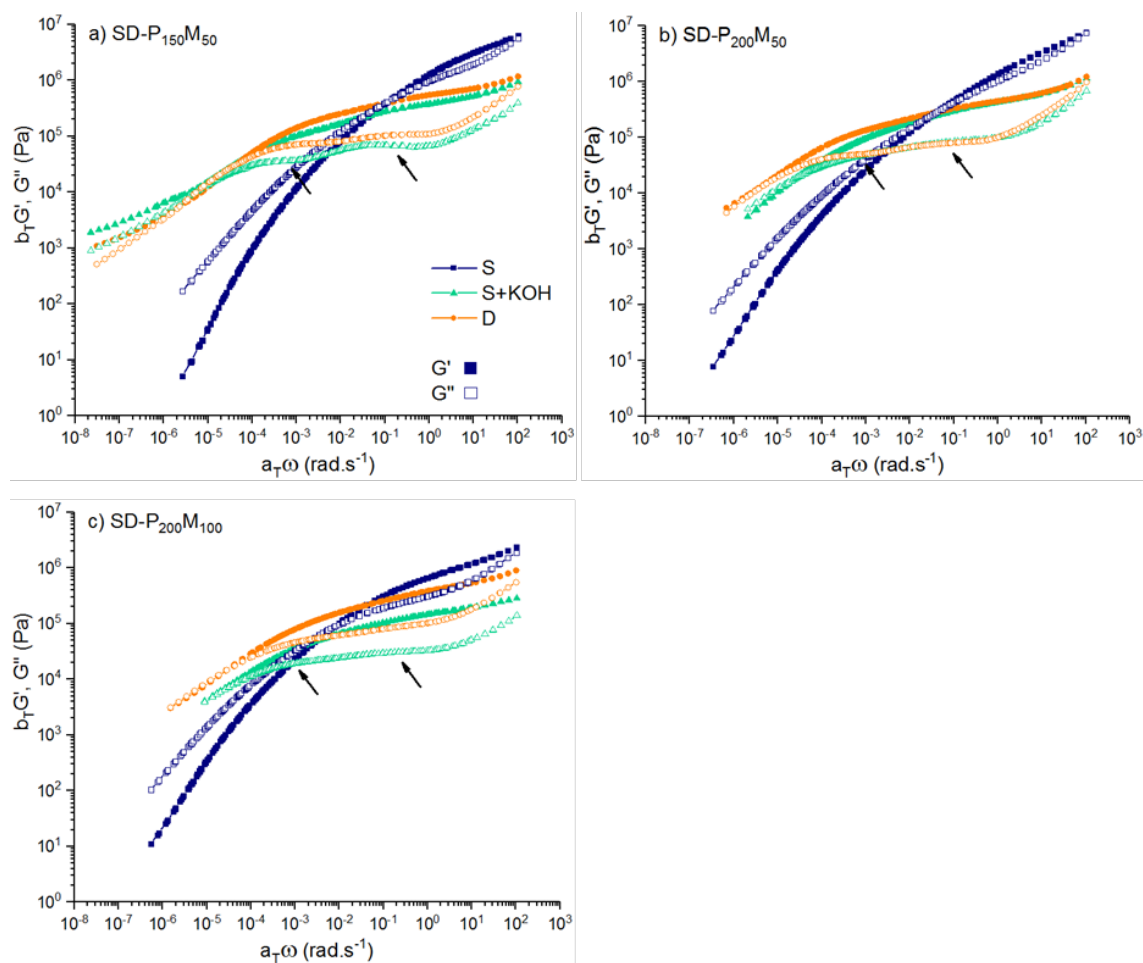


Figure 5. Master curves at 25°C for S, S+KOH and D states with elastic G' and Loss G'' moduli as function of the angular frequency obtained by Time-Temperature Superposition measurements

The three solution polymers behaved as low crosslinked material, exhibiting a cross-over point between elastic and loss modulus at $10^{-2} < \omega < 1 \text{ rad.s}^{-1}$, followed by a flowing region (Figure 5). The cross-over point moved to lower frequencies as ionicX in the samples increased, presumably due to the stiffening of the polymer with higher density of ionic crosslinks ($\omega_c = 1.3 \cdot 10^{-1} \text{ rad.s}^{-1}$ for SD-P₁₅₀M₅₀, $\omega_c = 4.0 \cdot 10^{-2} \text{ rad.s}^{-1}$ for SD-P₂₀₀M₅₀ and $\omega_c = 7.5 \cdot 10^{-3} \text{ rad.s}^{-1}$ for SD-P₂₀₀M₁₀₀). It is important to note that the solution samples exhibited a very high modulus at high frequency $G' > 10^6 \text{ Pa}$, most likely due to high content of ionic comonomers; they might already aggregate as clusters and reinforce the films.

S+KOH and D samples showed long rubbery plateaus with nearly constant values of G' and G'' , and $\tan \delta$ was decreased by more than 2 with $\omega < 10 \text{ rad.s}^{-1}$ as displayed in Figure 6. This indicates the polymers behaved as elastic solids and were highly crosslinked. The ionic interactions are expected to become stronger upon addition of KOH and stiffen the polymers. However, G' decreased by around one degree of magnitude in the rubbery region and implying that the materials became softer at high frequency. A possible explanation to this effect could be a charge shielding due to salts and/or to new polymer organisation in the films.

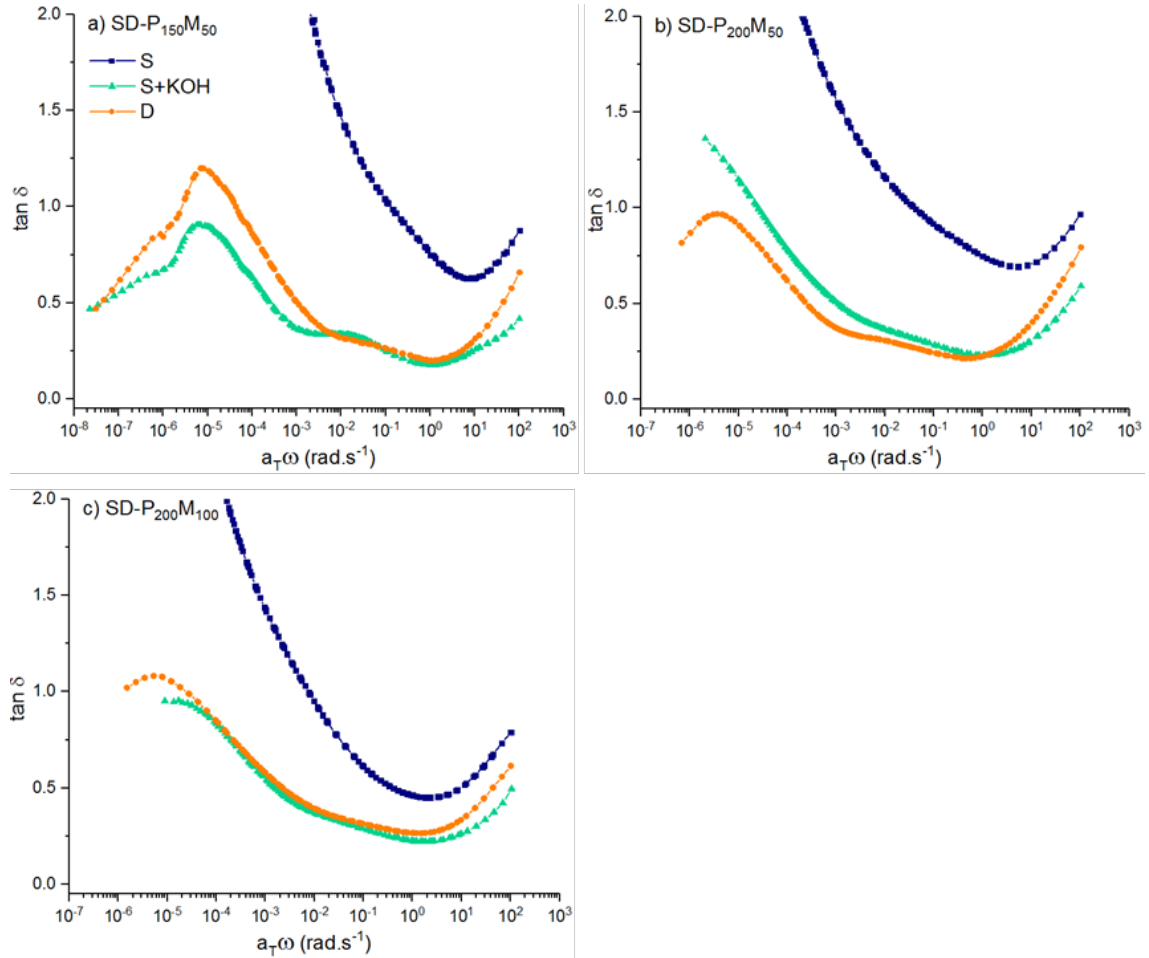


Figure 6. Comparison of $\tan \delta$ as function of the corrected angular frequency for the three samples in S, S + KOH and D states and separate comparison of dispersions

Furthermore, two 'steps' in the middle of the rubbery plateau (indicated by the black arrows) especially for SD-P₁₅₀M₅₀ and G'' at $10^{-3} < \omega < 10^{-1} \text{ rad.s}^{-1}$, were observed (Figure 5). A potential hypothesis is the formation of two different structures or morphologies inside the polymer (either ionic clusters in a polymer matrix or two distinct polymers), which render the material stiffer. A closer look at the rheology curves (Figure 7) showed that there was no cross-over of the G and G' curves between the rubbery plateau and the flowing region. Instead, a second elastic plateau could be seen for SD-P₁₅₀M₅₀. This suggests that for S+KOH and D, the effect ionic interactions are strong and remain effective at very low frequencies.

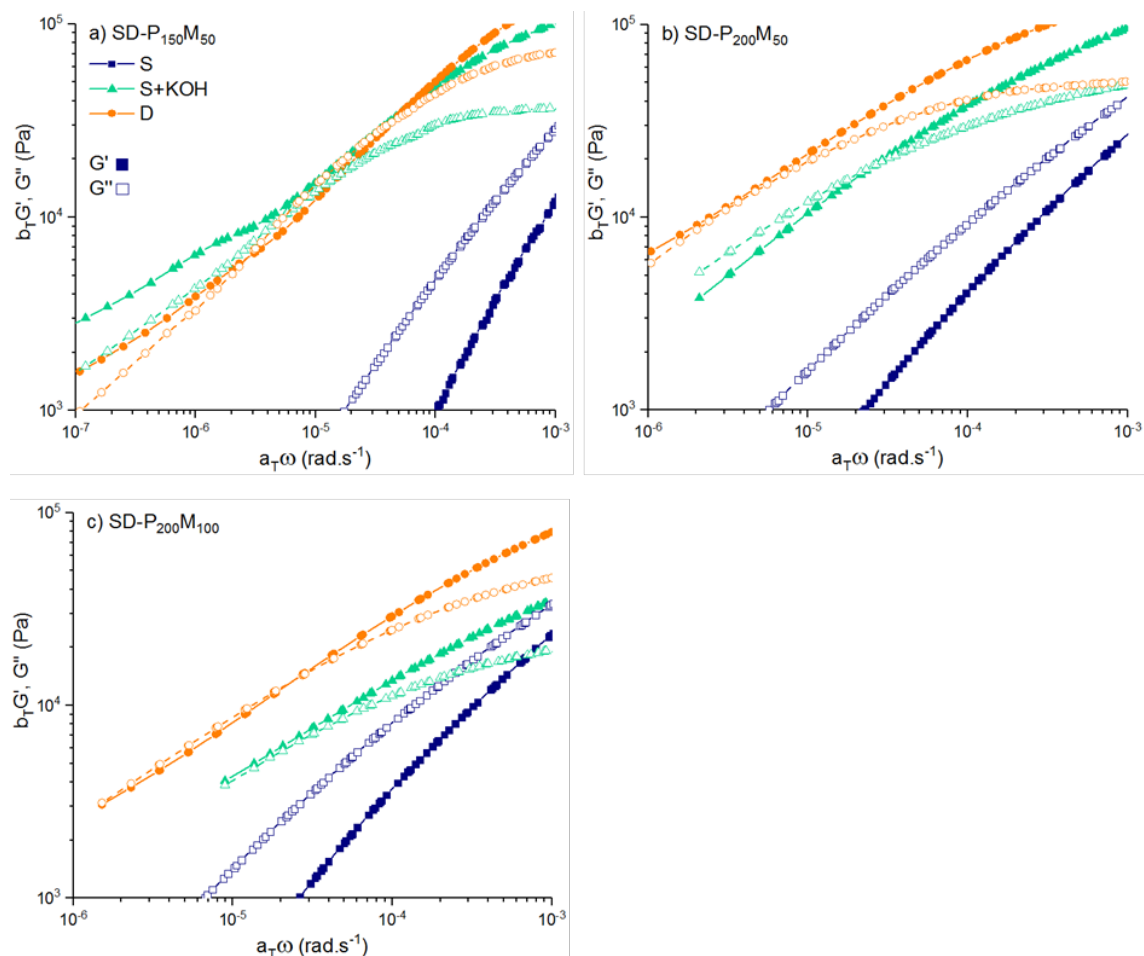


Figure 7. Enlargement of the curves of G' and G'' obtained by TTS over the transitions to flowing regions for S+KOH and D

Differences between S+KOH and D states were not observed, except for SD-P₂₀₀M₁₀₀ where the curve of S+KOH was slightly shifted to lower modulus; but it attributed to an error of the measurement or to low reproducibility of the film drying.

The master curves of the three dispersions SD-P₁₅₀M₅₀, SD-P₂₀₀M₅₀ and SD-P₂₀₀M₁₀₀ were compared to each other (displayed in Figure 8, image c). The rheological behaviour of the films was similar for the three tested compositions.

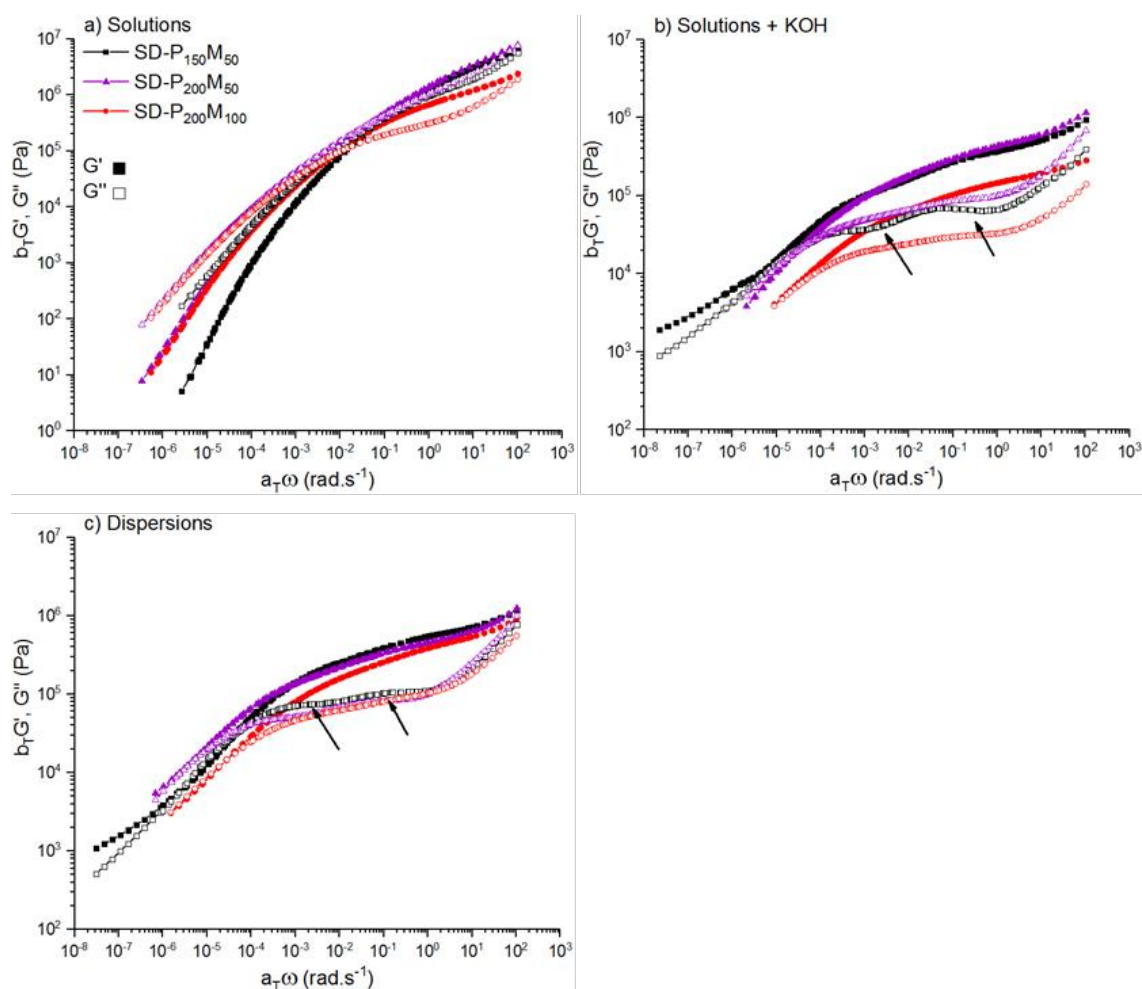


Figure 8. Master curves of a) solutions, b) solutions + KOH and d) dispersions at 25°C with the elastic G' and Loss G'' moduli as function of the angular frequency obtained by Time-Temperature Superposition measurements

Tensile measurements were carried out to study the effect of KOH on the materials properties at elongation $\epsilon > 100\%$, stress-strain curves can be seen in Figure 9. A comparison of stress-strain curves of the three samples at each state is given in Figure 10. The values of stress and elongation at break are available in Appendix 54 and presented in Figure 11. The Young's modulus E obtained from the stress-strain curves are reported in Appendix 56.

In the solution state S , the polymers films showed different behaviours. SD-P₁₅₀M₅₀ exhibited a viscoelastic behaviour with $\sigma_{\max} \sim 175$ kPa and $\epsilon_B \sim 3000$ % (Figure 11). The other two samples behaved as brittle materials with strong strain-hardening; it showed already that the polymers with 200 mmol of Polystep® were stiffer than with 150 mmol and this might be due to higher grafting density. Also, SD-P₂₀₀M₁₀₀ had a higher maximal stress and should be even tougher than SD-P₂₀₀M₅₀; as it contains more MAETAC, it could be explained by more ionic aggregation (clusters) or complexation (crosslinks).

For the three samples, the stiffening of the polymer by increasing the crosslinking density (addition of KOH) was seen with lower compliance to high strains as the elongations at break were lowered by more than half. This effect was even more noticeable for SD-P₁₅₀M₅₀: ϵ_B was reduced by a factor of 5 while σ_B was multiplied more than 10 times going from ~ 60 to 850 kPa. SD-P₂₀₀M₅₀ did contain a similar content of theoretical crosslinks (determined by limiting monomer MAETAC in moles) but the effect on ϵ_B and σ_B were less significant given the high stiffness in S states (due to high content of ionic comonomers); the same applied to SD-P₂₀₀M₁₀₀.

SD-P₁₅₀M₅₀ and SD-P₂₀₀M₁₀₀ exhibited similar trend while SD-P₂₀₀M₅₀ showed a lower $\epsilon_B \approx 200$ % and a σ_B of 400 kPa higher; such difference could be coming from a higher grafting density introduced by Polystep® (mentioned with the determination of the polymers molar masses).

E moduli measured for the three samples in the three states, were almost similar (Appendix 56), except for the dispersions. This was not expected given the large decrease of the elastic moduli for $S+KOH$ and D at a similar frequency of measurement seen in Figure 5; ~ 0.6 rad.s⁻¹ for a test done at 200 mm.min⁻¹ on a 35 mm sample length.

But this could be due to the film drying conditions given the different solvents but also the internal polymer distribution (considering the different grafting densities).

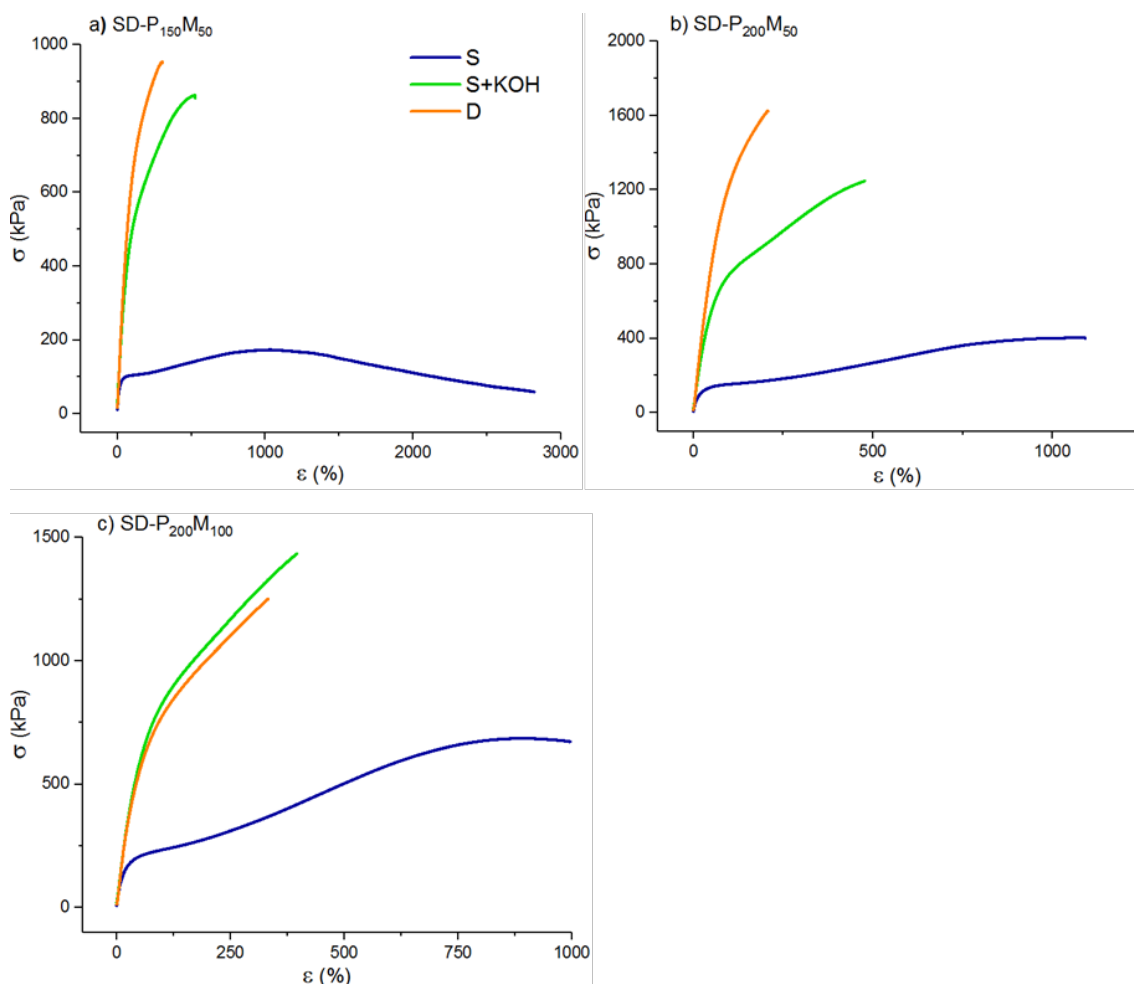


Figure 9. Stress-strain curves of all samples for a) SD-P₁₅₀M₅₀, b) SD-P₂₀₀M₅₀ and c) SD-P₂₀₀M₁₀₀ in all S, S+KOH and D states

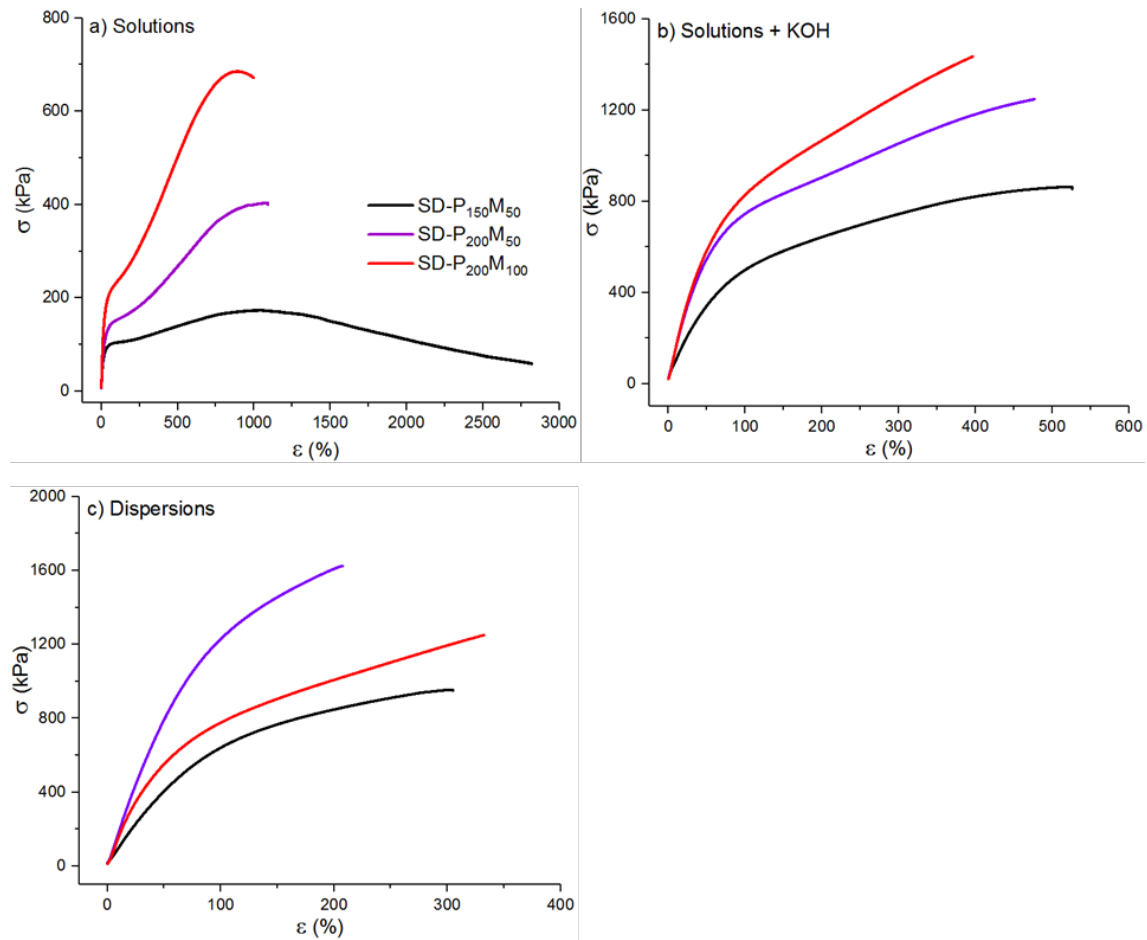


Figure 10. Comparison of the stress-strain curves of the three samples obtained by tensile test in the three different states a) S, b) S+KOH and c) D

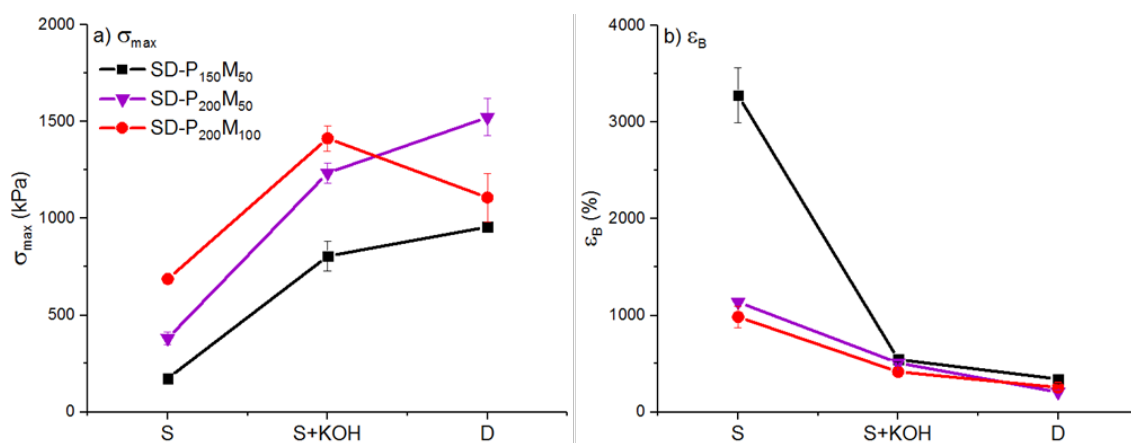


Figure 11. Evolution and comparison of a) maximal stress and b) elongation at break for the three samples at S, S+KOH and D states

E. Adhesive properties of the polymer films

Concerning the adhesive properties, peel tests at 180° with contact time $t_c = 2\text{ min}$, 24 h and 48 h were carried out. The peel mean forces F_{mean} for the different t_c are displayed in Figure 12 and Figure 13. Failure modes (Adhesive A, Cohesive K, Zippy Z) were reported on the graphs and the values are also given in Appendix 57.

All samples at all states showed an increase in F_{mean} by at least 2 after 24 h of contact and stabilized after 48h, due to better surface wetting. At $t_c = 2\text{ min}$ the peel force was slightly increased in S+KOH state but even more for the dispersions by at least 2 to 5 times. This was also true after 24 and 48 hours. The main trend observed was an increase of at least 40% in F_{mean} when comparing (and considering the errors) the original solutions of polymers series to S+KOH and D, plus cohesive failures were observed. This suggests that in S+KOH and D, even though the polymers are highly crosslinked they were able to form better contact with the steel substrate and to dissipate much more efficiently the energy during peeling. An exception was found in the case of SD-P₁₅₀M₅₀ for which peel forces after 24 h were equal to $\sim 11\text{ N}\cdot 25\text{ mm}^{-1}$ for S, S+KOH and D.

In terms of compositions, differences were seen for $t_c = 2\text{ min}$ for S+ KOH and D and for $t_c = 24\text{ h}$ with solution samples. Peel mean force after short contact time for S+KOH and D was decreased going from SD-P₁₅₀M₅₀ to SD-P₂₀₀M₁₀₀. Samples with high amounts of ionic moieties were most likely tougher and adhesion was lowered from poorer contact with the surface. Similar observation could be made after 24 h of dwelling and the solutions samples.

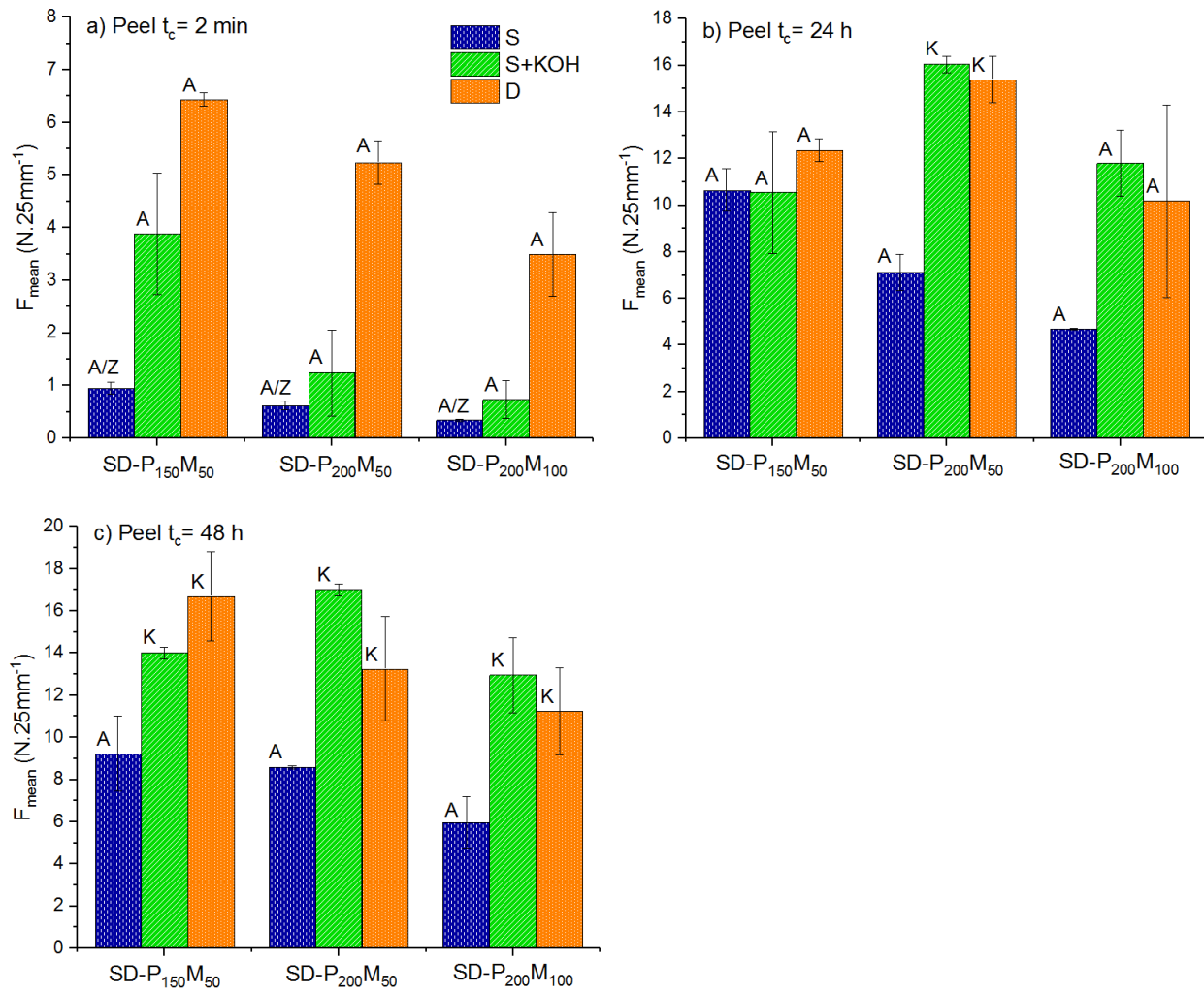


Figure 12. Comparison of the peel mean force F_{mean} between the three samples for S, S+KOH and D for
a) $t_c = 2$ min, b) $t_c = 24$ h and c) $t_c = 48$ h

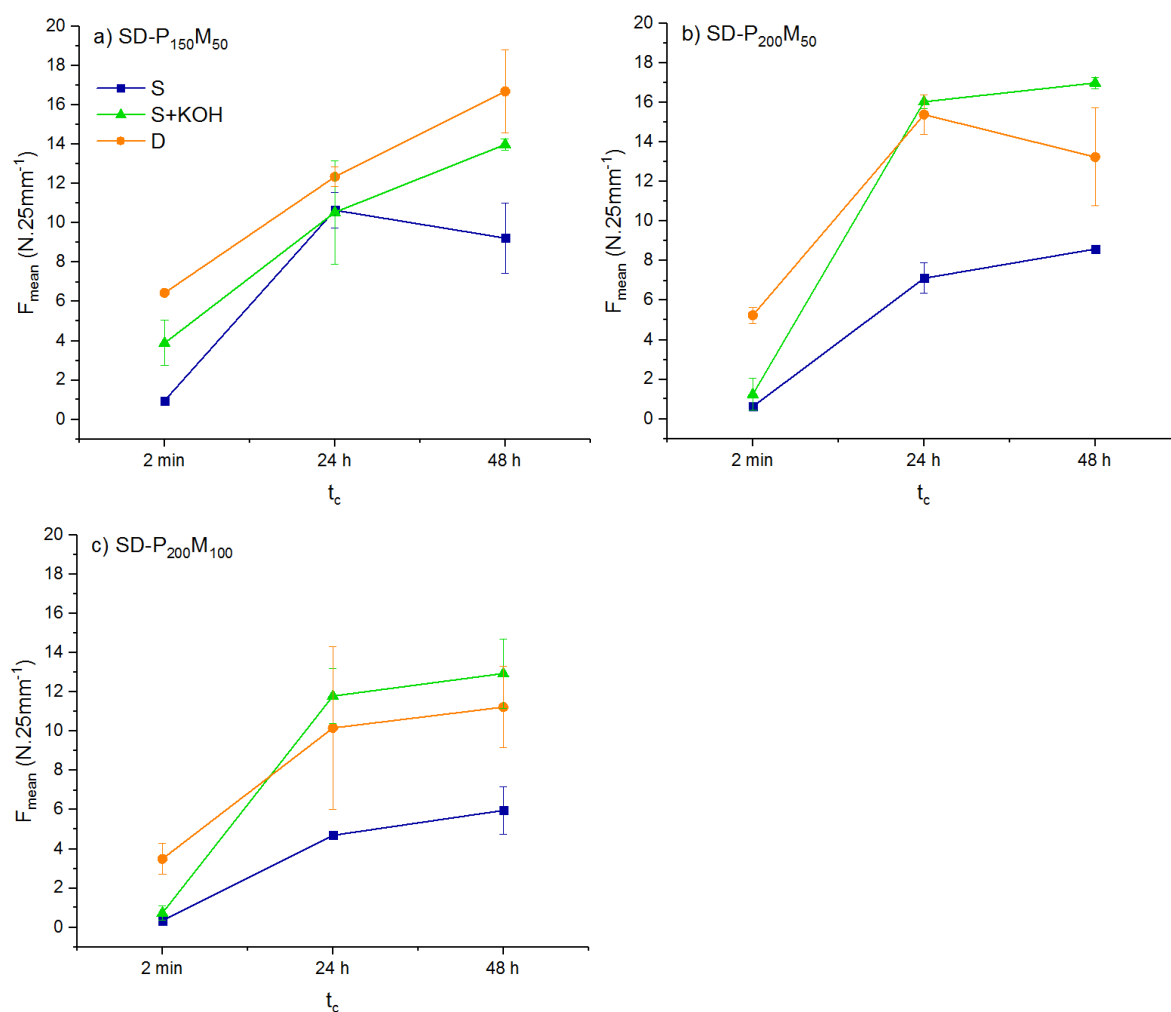


Figure 13. Comparison of the peel mean force F_{mean} for their different states as function of contact time for

a) SD-P₁₅₀M₅₀, b) SD-P₂₀₀M₅₀ and c) SD-P₂₀₀M₁₀₀

Finally, the adhesive performance of the three dispersions were compared in Figure 14. SD-P₂₀₀M₁₀₀ showed overall and for all t_c , lower adhesion but taking the errors into account, peel forces and failures were comparable for SD-P₁₅₀M₅₀ and SD-P₂₀₀M₅₀.

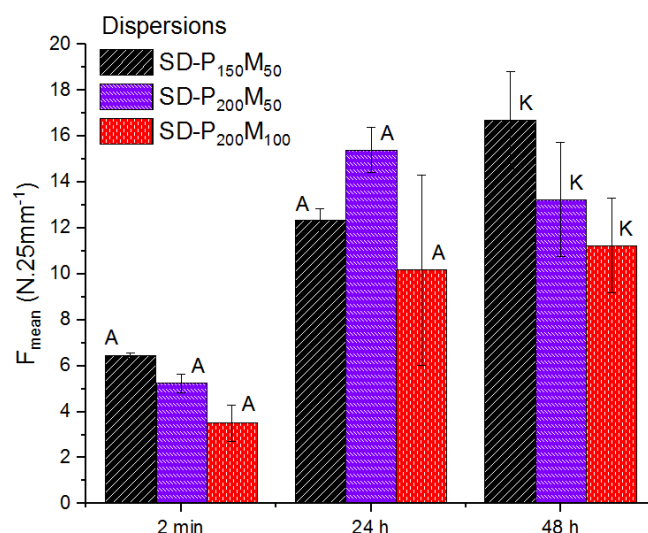


Figure 14. Comparison of the peel values between the three dispersions for the different contact times
2 min, 24 h and 48 h

The cohesion of the samples was also measured by static shear tests with 1.5 kg on steel, the results are displayed in Figure 15, values can be found in Appendix 57. When considering the series of solution samples, the shear holding power was multiplied by almost 3 from SD-P₁₅₀M₅₀ to SD-P₂₀₀M₅₀ and SD-P₂₀₀M₁₀₀. For the samples in S+KOH, SD-P₁₅₀M₅₀ and SD-P₂₀₀M₁₀₀ reached values ≥ 12000 min while the effect of KOH on SD-P₂₀₀M₅₀'s shear strength could not be seen. In general, shear properties were largely decreased for the dispersed samples in comparison to the S+KOH series. This could be induced by hydroplastification (residual water content plasticizing the polymer) and/or low interparticle connectivity.

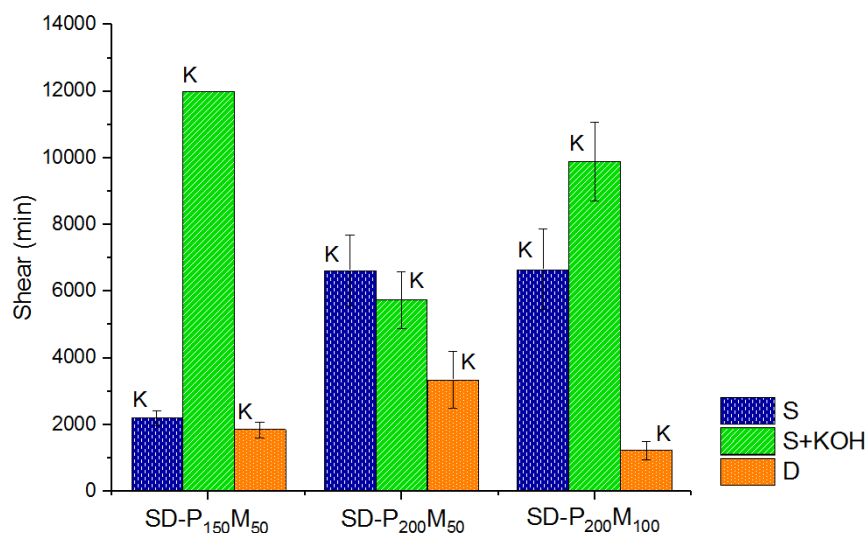


Figure 15. Shear resistance for SP-P₁₅₀M₅₀, SP-P₂₀₀M₅₀ and SP-P₂₀₀M₁₀₀ at S, S+KOH and D states

Karl-Fischer titrations were carried out to measure the residual water content in the dispersions using the 'oven' method, results are found in Table 4. Around 2 wt% of residual water was found for each sample. The shear tests were reproduced after drying the films 3 days in a desiccator (filled with silica gel) and were displayed, in comparison to the S+KOH and D films dried under normal conditions, in Figure 16. Values can be found in Appendix 58.

Table 4. Residual water in the dried polymer films of the dispersion samples measured by Karl-Fischer oven method

Dispersions dried films	Residual H ₂ O (wt%)
SD-P₁₅₀M₅₀	1.7
SD-P₂₀₀M₅₀	2.6
SD-P₂₀₀M₁₀₀	2.7

Controlled drying didn't show influence on the holding power with 1.5 kg for SD-P₁₅₀M₅₀ and SD-P₂₀₀M₅₀. However, the shear strength for SD-P₂₀₀M₁₀₀ increased over 12000 min and exhibited adhesive/cohesive failure. This might suggest the adhesive failed in contact rather than in bulk properties. Yet the results are scattered and suggest the polymers may not show good reproducibility.

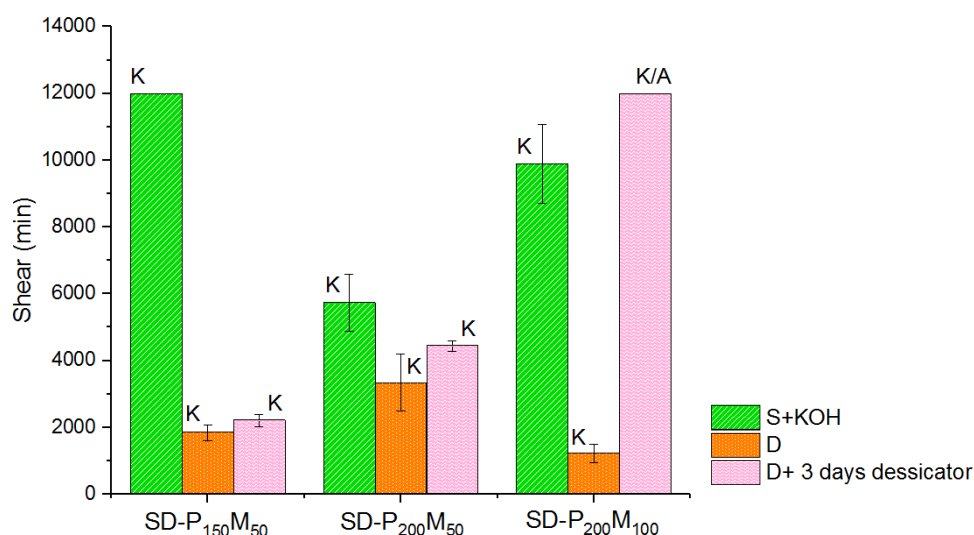


Figure 16. Comparison of the shear resistance of SD-P₁₅₀M₅₀, SD-P₂₀₀M₅₀ and SD-P₂₀₀M₁₀₀ at S+KOH, D and D after drying 3 days in a desiccator

However, all cohesion (holding power) values were sufficient for product applications. In that way, the adhesive properties of the three samples were compared to those of commercialized products Acronal® V 215 and Acronal® 3633 described in III.2.D. The peel forces are displayed in Figure 17 and shear strengths in Figure 18.

For short contact time, peel mean forces F_{mean} of the three secondary dispersions were lower than Acronal® 3633 but competed with Acronal® V 215 $F_{\text{mean}} \sim 6 \text{ N.25mm}^{-1}$. After 24 h of contact, F_{mean} measured for SD-P₂₀₀M₅₀ was around 15 N.25mm^{-1} , similar to Acronal® V 215 and close to Acronal® 3633. SD-P₁₅₀M₅₀ and SD-P₂₀₀M₁₀₀ were slightly less adhesive in peel.

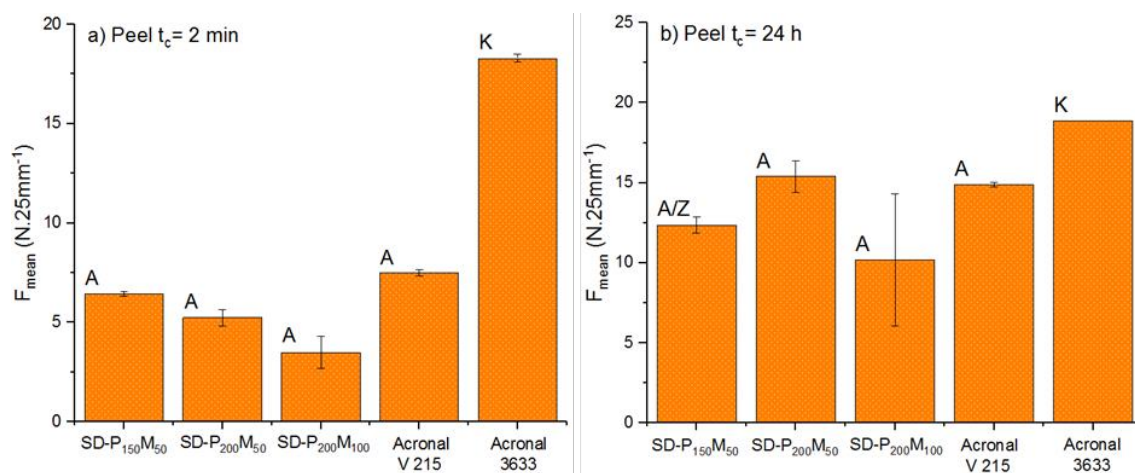


Figure 17. Comparison of Peel mean force F_{mean} of the three dispersions with Acronal® V 215 and Acronal® 3633 for a) $t_c=2$ min and b) $t_c=24$ h

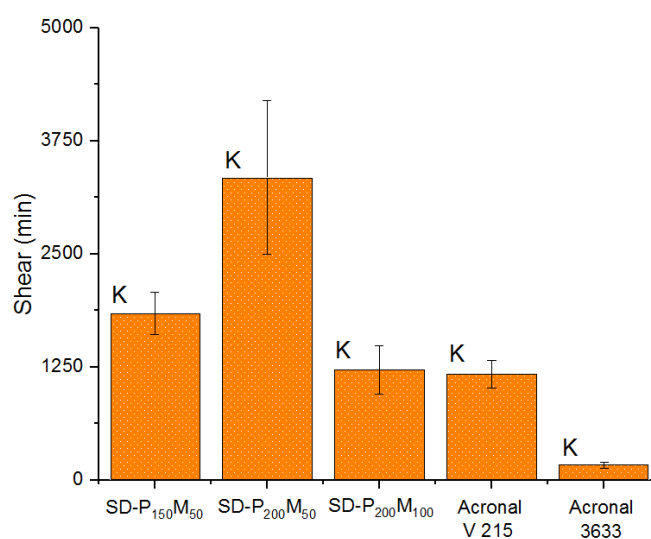


Figure 18. Comparison of the shear resistance with a 1.5 kg load on steel of the three dispersions with Acronal® V 215 and Acronal® 3633

The shear holding power for 1.5 kg on steel of the three dispersions were equal ~ 1200 min or higher than for the two Acronal®, especially for SD-P₂₀₀M₅₀ (3345 min). Considering the shear strength and the peel force for 24 h dwelling time, SD-P₂₀₀M₅₀ showed the highest balance between adhesion and cohesion in comparison to the commercialized adhesives.

IV.3. DISCUSSION

This chapter investigates the possible formation of water-borne dispersions based on co-acrylate polyampholytes prepared by free-radical polymerization in solution and the properties of the derived PSA formulations.

AFM phase pictures from SPP (Figure 3) and AUC measurements demonstrated that defined polymer particles were obtained from the successive addition of 2 eq of KOH and water, followed by the evaporation of iPrOH for polymers containing at least 90 mmol/kg of “available” phosphoric acid moieties. The polymers were composed of a hydrophobic acrylate backbone (min 86 wt% in polymer composition) and at least 8.9 wt% ionic functional groups from Polystep® and MAETAC.

These specific conditions should be fulfilled because the hydrophobicity of the backbone does not make the miscibility of the polymers in water energetically favourable, thus the polymer precipitates upon addition of water as seen in Appendix 48. The ionic groups, hydrophilic by nature, can stabilize the system by migrating to the interface between water and the hydrophilic backbone to give dispersed particles but sufficient ionic units must be present to stabilize the particles surface[22]. Moreover, as the polymer chains contain oppositely charged groups, stoichiometry between ionic moieties should be avoided to prevent complex coacervation[28-33]. With addition of a strong base, the phosphate groups are deprotonated but also the salt concentration increases which hinders coacervation[34]. The phase-behaviour of polyelectrolytes with ionic strength is inherent to the whole system. In this chapter, stability was reached only with 2 equivalents of KOH. However, to form the dispersed particles, the polymer chains are likely to collapse into dense coils independently of the ionic strength. This can happen locally by ionic inter and/or intramolecular interactions[35] but given the salt concentration in the medium it should be driven only by favourable thermodynamics of the hydrophobic chain parts. Local coils or collapse might already be observed after the addition of KOH in iPrOH only (seen on pictures in Appendix 49) as the solution turns turbid with addition of the salt.

The mechanical properties of SD-P₁₅₀M₅₀, SD-P₂₀₀M₅₀ and SD-P₂₀₀M₁₀₀ in their 3 defined states solution (S), solution with added KOH (S+KOH) and dispersion (D) were studied. It was observed from linear rheology and tensile measurements, that the addition of KOH to the three samples resulted in the same behaviours observed in Chapter III: the appearance of a rubbery-plateau for small deformation and at high strain, a strong decrease in elongation at break plus a strong increase of the stress at break. These results suggest, as proposed in Chapter III, that the addition of KOH increased the number of crosslink points within the dried polymer due to the deprotonation of the phosphate RPO₄H₂ groups.

In linear rheology, elastic moduli over 1 MPa were found for the solutions samples suggesting the polymers were already stiffened by the presence of high number of ionic comonomers through ionic aggregation (but not observed with AFM). After triggering the ionic interactions, in S+KOH and D, a rubbery plateau was measured over almost 6 decades of angular frequency delaying the terminal relaxation of the polymers. Such observation implies that reptation (i.e. viscous flow) was hindered by the molecular (ionic) interactions taking place between the polymer chains. This phenomenon is known as 'sticky reptation' in ionomers, where under shear, ionic crosslinks act as 'sticky points' that can break and recombine further one along the polymer chain until the entanglement length[36, 37]. Sticky reptation was further enhanced by the possibility of high branching[38-40] of the polymer chains with high amount of Polystep® (discussed in III.2.A.).

Finally, the decrease in modulus over the rubbery plateau for S+KOH and D, and the non-relevance of Young's modulus to G' at 0.6 rad.s⁻¹ could be due to different associative behaviour during polymer formation[41].

Differences in the mechanical properties induced by various aggregation behaviours were also seen in Tensile test. In Figure 10, the stress-strain curves obtained are in accordance with the polymers compositions. SD-P₂₀₀M₁₀₀ showed the highest stiffness due to high number of ionic moieties and SD-P₁₅₀M₅₀ the lowest.

However, for S+KOH and D, the results are no longer linear regarding the composition. SD-P₂₀₀M₅₀ becomes tougher than SD-P₂₀₀M₁₀₀, which might be explained by the ionic clusters distributions, which in this case would be invisible in AFM. The following hypothesis is proposed and is supported by the AUC results: SD-P₂₀₀M₅₀ contains freer Polystep® groups (considering 50 mmol will interact with 50 mmol of MAETAC) i.e. 150 mmol of free pendant diacid groups are available in comparison to 100 mmol in SD-P₁₅₀M₅₀ and SD-P₂₀₀M₁₀₀. The more acid groups are available, the bigger the total stabilized surface area of the particles and therefore smaller particles are formed. As the particles are smaller and contain these "punctual aggregates" formed from the ionic interactions of oppositely charged Polystep® and MAETAC; they may be better distributed over the entire sample during film formation and form less large ionic gatherings. This may provide in the end a more homogeneous repartition of the ionic interactions in the polymer film and provide a higher resistance to stresses.

Concerning the adhesive performance, for all three samples, S+KOH and D series exhibited up to 6 times better adhesion in peel at short contact time in comparison to the solutions as seen in Figure 12 and Figure 13. Considering the high elastic moduli measured in linear rheology at high frequency (over 10^5 Pa), high instant peel forces can only be improved thanks to available RPO_4^{2-} groups which favour adhesion to steel substrates[42]. F_{mean} was further increased for the dispersions as the phosphate groups should be more present at the adhesive interface with the substrate; but maybe also thanks to the wetting agent added to help the film formation. Moreover, when the time of contact is ≥ 24 h, the failure mode of SD-P₂₀₀M₅₀ becomes cohesive and the same is observed after 48h for SD-P₂₀₀M₁₀₀. This implies that the interactions between the phosphate groups and the steel predominate for cohesive failure, because the S series does not exhibit cohesive failures while it was seen (from linear rheology) that the transition of the polymers to viscous regime took place at higher frequencies in comparison to S+KOH and D.

The shear strengths were improved by the addition of KOH and triggering of ionic complexation; as predicted by the delay of material flow in linear rheology by sticky flow and reptation. However, shear strength dropped for dispersions.

Although not so strong differences were seen in linear rheology and tensile tests between the mechanical resistance of S+KOH and D, the resistance under shear might be different. The connectivity/interpenetration of polymers inside the particles may be hindered by ionic aggregates that form at the particles interface. This might result in a hard-shell soft-core like film morphology[27, 43] non-observable in AFM.

Nonetheless, holding power of the dispersions was mostly higher (Figure 18) than those of commercialized PSA dispersions Acronal® V 215 and Acronal® 3633.

SD-P₂₀₀M₅₀ showed especially good balance between adhesion and cohesion and outperformed the Acronal®.

IV.4. CONCLUSION

The dispersibility of acrylate polyelectrolytes prepared by solution polymerization in isopropanol was studied in this chapter. Several n-BA/MMA/Polystep[®]/MAETAC copolymers were prepared with varying Polystep[®] and MAETAC concentrations; but an excess of at least 90 mmol of anionic monomer per kilo of solution (in comparison to MAETAC) and 2 equivalents of KOH were necessary to obtain dispersibility in water. The obtained dispersions showed defined particles of around 200 nm in diameter. Linear rheological measurements have showed the dispersions films are rubbery-like materials due to sticky flowing and reptation and sustain higher normal stress than solution polymers. Although the samples contained a high number of ionic moieties i.e. crosslinkers, the adhesive values even at low contact time, were satisfactory thanks to available phosphate groups which highly favoured the adhesion to steel substrates.

As conclusion, the secondary dispersions maintained the high adhesive performances of the original solution polymers, plus they are waterborne and easy to process; they have therefore high potential to be produced and used in industry.

IV.5. REFERENCES

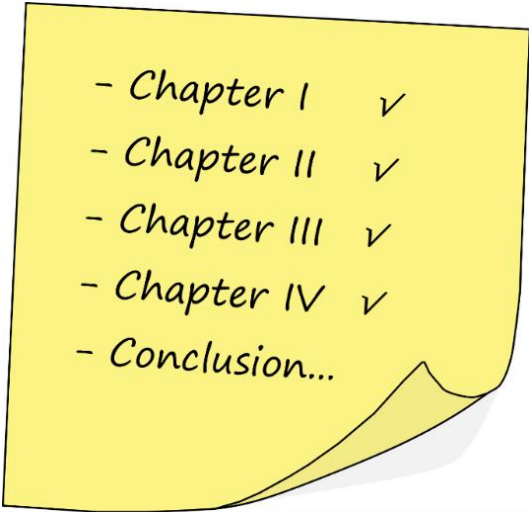
1. Directive 2004/42/CE of the European Parliament and of the Council of 21 April 2004 on the limitation of emissions of volatile organic compounds due to the use of organic solvents in certain paints and varnishes and vehicle refinishing products and amending Directive 1999/13/EC, in *Official Journal of the European Union*. 2004.
2. Canning, S.L., G.N. Smith, and S.P. Armes, *A critical appraisal of RAFT-mediated polymerization-induced self-assembly*. *Macromolecules*, 2016. **49**: p. 1985–2001.
3. Destarac, M., *Controlled radical polymerization: industrial stakes, obstacles and achievements*. *Macromolecular Reaction Engineering*, 2010. **4**: p. 165–179.
4. Newman, S., *Note on colloidal dispersion from block copolymers*. *Journal of Applied Polymer Science*, 1962. **6**(21).
5. Chen, Y., et al., *Synthesis and self-assembly of amphiphilic gradient copolymer via RAFT emulsifier-free emulsion polymerization*. *Journal of Colloid and Interface Science*, 2012. **369**: p. 46–51.
6. Lowe, A.B., *RAFT alcoholic dispersion polymerization with polymerization-induced self-assembly*. *Polymer*, 2016. **106**: p. 161–181.
7. Kaczorowski, M. and G. Rokicki, *Reactive surfactants – Chemistry and applications: part I polymerizable surfactants*. *Polimery*, 2016. **61**(11/12): p. 747–757.
8. Guyot, A., et al., *Reactive surfactants in heterophase polymerization*. *Acta Polymerica*, 1999. **50**: p. 57–66.
9. Arshady, R., *Microspheres and microcapsules, a survey of manufacturing techniques Part II: Coacervation*. *Polymer Engineering and Science*, 1990. **30**: p. 905–914.
10. Dong, W. and R. Bodmeier, *Encapsulation of lipophilic drugs within enteric microparticles by a novel coacervation method*. *International Journal of Pharmaceutics*, 2006. **326**: p. 128–138.
11. Burke, N.A.D., et al., *Polyelectrolyte complexation between poly(methacrylic acid, sodium salt) and poly(diallyldimethylammonium chloride) or poly[2-(methacryloyloxyethyl) trimethylammonium chloride]*. *Journal of Polymer Science Part A: Polymer Chemistry*, 2007. **45**: p. 4129–4143.
12. Black, K.A., et al., *Protein encapsulation via polypeptide complex coacervation*. *ACS Macro Letters*, 2014. **3**(10): p. 1088–1091.
13. Ach, D., et al., *Formation of microcapsules by complex coacervation*. *The Canadian Journal of Chemical Engineering*, 2015. **93**(2): p. 183–191.

14. Voets, I.K., et al., *Electrostatically driven coassembly of a diblock copolymer and an oppositely charged homopolymer in aqueous solutions*. *Macromolecules*, 2007. **40**: p. 8476-8482.
15. Voets, I.K., A.d. Keizer, and M.A.C. Stuart, *Complex coacervate core micelles*. *Advances in Colloid and Interface Science*, 2009. **147-148**: p. 300-318.
16. Voets, I.K., A.d. Keizer, and M.A.C. Stuart, *Core and corona structure of mixed polymeric micelles*. *Macromolecules*, 2006. **39**: p. 5952-5955.
17. Burgh, S.v.d., A.d. Keizer, and M.A.C. Stuart, *Complex coacervation core micelles. Colloidal stability and aggregation mechanism*. *Langmuir*, 2004. **20**: p. 1073-1084.
18. van der Kooij, H.M., et al., *On the stability and morphology of complex coacervate core micelles: from spherical to wormlike micelles*. *Langmuir*, 2012. **28**(40): p. 14180-91.
19. Dieterich, D., *Aqueous emulsions, dispersions and solutions of polyurethanes: synthesis and properties*. *Progress in Organic Coatings*, 1981. **9**: p. 281-340.
20. Kim, B.K., *Aqueous polyurethane dispersions*. *Colloid and Polymer Science*, 1996. **274**: p. 599-611.
21. Lee, S.Y., J.S. Lee, and B.K. Kim, *Preparation and properties of water-borne polyurethanes*. *Polymer International*, 1997. **42**: p. 67-76.
22. Sardon, H., et al., *Waterborne polyurethane dispersions obtained by the acetone process: a study of colloidal features*. *Journal of Applied Polymer Science*, 2011. **120**(4): p. 2054-2062.
23. Mohaghegh, S.M.S., M. Barikani, and A.A. Entezami, *Preparation and properties of aqueous polyurethane dispersions*. *Iranian Polymer Journal*, 2005. **14**: p. 163-167.
24. *Annual Report*. 2015, University of Stuttgart, Institute of Interfacial Process Engineering and Plasma Technology.
25. Alvarez, G.A., et al., *Hybrid waterborne polyurethane/acrylate dispersion synthesized with bisphenol A-glycidylmethacrylate (Bis-GMA) grafting agent*. *Progress in Organic Coatings*, 2018. **118**: p. 30-39.
26. Baelen, G.v., et al., *Isopropyl alcohol recovery by heteroazeotropic batch distillation in European Meeting on Chemical industry & Environment EMChIE*. 2010: Mechelen, Belgium.
27. Tiggelman, I. and P.C. Hartmann, *Ionic autocrosslinking of water-based polymer latices: a new concept of acid–base interaction occurring upon film formation*. *Progress in Organic Coatings*, 2010. **67**: p. 76-83.
28. Spruijt, E., et al., *Structure and dynamics of polyelectrolyte complex coacervates studied by scattering of neutrons, X-rays, and light*. *Macromolecules*, 2013. **46**: p. 4596-4605.

29. Spruijt, E., et al., *Binodal compositions of polyelectrolyte complexes*. *Macromolecules*, 2010. **43**: p. 6476-6484.
30. van der Gucht, J., et al., *Polyelectrolyte complexes: bulk phases and colloidal systems*. *J Colloid Interface Sci*, 2011. **361**(2): p. 407-22.
31. Sing, C.E., *Development of the modern theory of polymeric complex coacervation*. *Adv Colloid Interface Sci*, 2017. **239**: p. 2-16.
32. Li, L., et al., *Phase behavior and salt partitioning in polyelectrolyte complex coacervates*. *Macromolecules*, 2018. **51**(8): p. 2988-2995.
33. Jha, P., et al., *pH and salt effects on the associative phase separation of oppositely charged polyelectrolytes*. *Polymers*, 2014. **6**(5): p. 1414-1436.
34. K.-I.Tainaka, *Effect of counterions on complex coacervation*. *Biopolymers*, 1980. **19**: p. 1289-1298.
35. Dobrynin, A.V. and M. Rubinstein, *Cascade of transitions of polyelectrolytes in poor solvents*. *Macromolecules*, 1996. **29**: p. 2974-2979.
36. Chen, Q., G.J. Tudryn, and R.H. Colby, *Ionomer dynamics and the sticky Rouse model*. *Journal of Rheology*, 2013. **57**(5): p. 1441-1462.
37. Colby, L.L.J.M.R.R.H., *Dynamics of reversible networks*. 1991. **24**: p. 4701-4707.
38. Ahmadi, M., et al., *Time Marching Algorithm for Predicting the Linear Rheology of Monodisperse Comb Polymer Melts*. *Macromolecules*, 2011. **44**(3): p. 647-659.
39. van Ruymbeke, E., R. Keunings, and C. Bailly, *Prediction of linear viscoelastic properties for polydisperse mixtures of entangled star and linear polymers: Modified tube-based model and comparison with experimental results*. *Journal of Non-Newtonian Fluid Mechanics*, 2005. **128**(1): p. 7-22.
40. Ruymbeke, E.v., et al., *A General Methodology to Predict the Linear Rheology of Branched Polymers*. *Macromolecules*, 2006. **39**: p. 6248-6259.
41. Ahmadi, M., et al., *Dynamics of Entangled Linear Supramolecular Chains with Sticky Side Groups: Influence of Hindered Fluctuations*. *Macromolecules*, 2015. **48**(19): p. 7300-7310.
42. Vietti, D.E., J.J. Zupancic, and J. Barrus, *Phosphate adhesion promoter*. 2017.
43. Gurney, R.S., et al., *Mechanical properties of a waterborne pressure-sensitive adhesive with a percolating poly(acrylic acid)-based diblock copolymer network: Effect of pH*. *Journal of Colloid and Interface Science*, 2015. **448**: p. 8-16.

V.

General conclusions

- 
- Chapter I ✓
 - Chapter II ✓
 - Chapter III ✓
 - Chapter IV ✓
 - Conclusion...

The design of PSAs is challenging as they should combine antagonist properties: the polymer chains should be mobile (low T_g and moderate M_w) for a high tack and energy dissipation during deformation, but interpolymer interactions (chemical and/or physical crosslinking) should also be strong enough for strain and shear resistance. However, enhancing cohesive strength decreases polymer mobility and thus tackiness and dissipation mechanisms. The use of non-permanent (i.e. reversible and reconfigurable) molecular interactions as crosslinks in PSAs is an interesting strategy to overcome this challenge by providing cohesion and energy dissipation pathways without compromising polymer mobility.

In this thesis, ionic crosslinks have been used to prepare high-performance PSAs. The objective of this thesis was to find a suitable synthetic way of preparing ionically crosslinked polyacrylate formulations for application as PSAs in the industry, that exhibit a convenient adhesion and cohesion balance. The aim was also to understand how their mechanical behaviour is related to the ionic composition and how it influences the adhesive performance. The following conclusions can be extracted from the performed work:

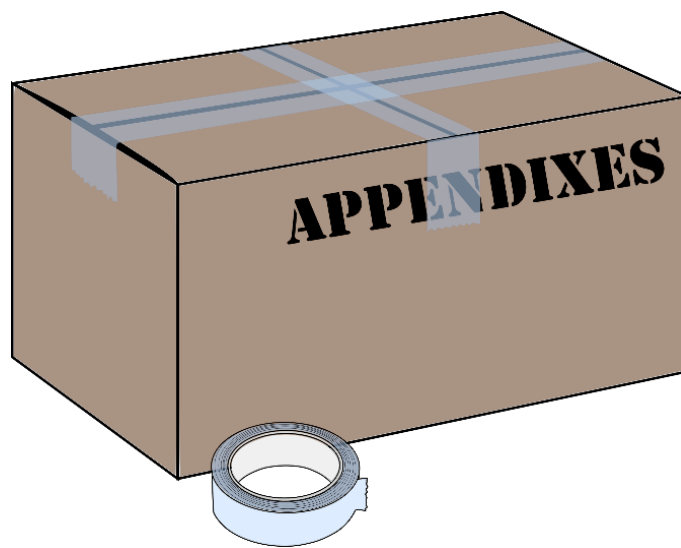
1. The emulsion copolymerization of n-butyl acrylate (n-BA) and styrene with the ionic monomers methacrylic acid (MAA, anionic monomer) and [2-(methacryloyloxy)ethyl trimethylammonium chloride (MAETAC, cationic monomer) required the use of cationic or non-ionic surfactants in combination with neutral or cationic radical initiators in order to get stable emulsions. The ionic monomers polymerized preferentially in the serum (water) phase, outside the polymer particles. Consequently, the resulting polymers were poorly controlled, the derived adhesive films showed two different phases and there was no clear correlation between the mechanical/adhesive properties and the ionic content of the products.

2. Ionic interactions between MAETAC and MAA were pH dependent. This allowed external triggering of the formation of ionic crosslinks by addition of KOH to the emulsion. Increasing ionic crosslinking resulted in a stiffening of the film, and transformed a tacky and non-cohesive adhesive to a more elastic polymer (EP-MAA₉₅M₁₀₀).
3. Random polyampholytes containing strong cationic (MAETAC) and anionic (Polystep®) moieties and hydrophobic n-BA and MMA comonomers in controllable ratios could be successfully obtained by solution polymerization in isopropanol. The stiffness of the resulting adhesive films correlated with the ionic comonomers content. Ionic clustering and polymer branching enabled stiffening of the film while maintaining viscosity for a good adhesion.
4. PSA formulations with high concentration of ionic comonomers outperformed existing commercial products at 24 hours contact while retaining high resistance to shear.
5. The stoichiometry and nature of ionic moieties influenced the performance of the formulations. Higher toughness was found when using a stoichiometric content of ionic groups and the peel forces were generally lowered. However, holding powers were mostly increased by the excess of deprotonated phosphate groups regardless of stoichiometry.
6. The adhesion after short contact times was particularly influenced by the presence of Polystep®. Peel forces after 2 min of dwelling, decreased for stiffer materials obtained with Polystep®; whereas the shear strength was found higher than 1200 min after deprotonation of the acid groups.

7. The polymerization method affected the properties of the final material. The molecular weight was increased using batch processes, yet composition drifts were induced as the instant monomer consumption was low and as isopropanol acted as a chain-transfer agent for n-BA; it thus lowered its incorporation with comonomers. The inhomogeneity of polymer films coupled with their high M_w and grafting density, resulted in low adhesion and shear strength.
8. Secondary dispersions in water could be obtained from the solution copolymers using the ionic moieties as stabilizing species. An overall anionic charge, by an excess of 90 mmol of anionic groups vs. cationic monomer per kilo of dispersion and by fully deprotonating the phosphate groups, was required.
9. Ionic clustering in polymeric films from secondary dispersions led to stiff films with high elastic moduli. Additional interpolymer ionic complexation further stiffened the materials and made them highly resistant to uniaxial and shear deformations due to sticky reptation.
10. Interfacial interactions between steel substrates and the phosphate groups highly favoured adhesion at short contact times. High resistance to shear and favourable adhesion on steel gave a good adhesion/cohesion balance to the PSAs prepared from the secondary dispersions. They also competed very well with commercialized PSAs dispersions and could thus be used as a final product.

VI.

Appendixes



VI. Appendixes.....	257
VI.1. Experimental part	264
A. Materials	264
B. Chapter II - Synthesis by emulsion polymerization	265
C. Chapter III - Synthesis by free radical solution polymerization	268
D. Chapter IV – Preparation of secondary dispersions	271
E. Characterization of the polymers and their films	273
VI.2. Additional graphs and data tables	280
A. Chapter II. Adhesive polyampholyte particles prepared by emulsion polymerization.....	280
Appendix 1. Table of characteristics for the set of samples.....	280
Appendix 2. AFM pictures of EP-MAA ₉₅ M ₁₀₀ at pH 2 before and after cleaning with water.....	281
Appendix 3. ATR-IR spectra of the sediment of EP-MAA ₉₅ M ₁₀₀ at a) pH 2 and b) pH 8.....	282
Appendix 4. ATR-IR spectra of the sediment of EP-MAA ₁₁₅ M ₁₂₀ at a) pH 2 and b) pH 8.....	283
Appendix 5. ATR-IR spectra of the serum of EP-MAA ₁₁₅ M ₁₂₀ at a) pH 2 and b) pH 8..	284
Appendix 6. ATR-IR spectra of the cationic monomer MAETAC	285

Appendix 7. Elastic G' and loss G'' modulus as function of angular frequency ω	286
Appendix 8. Transition zone observed on the master curve of EP-MAA ₄₅ M ₅₀	287
Appendix 9. Cross-over frequencies of first and second transitions for the set of samples as function of ionicX.....	288
Appendix 10. Individual stress-strain curves obtained in tensile tests.....	289
Appendix 11. Repeatability of tensile measurement for EP-MAA ₉₅ M ₁₀₀ at pH 2	290
Appendix 12. Tensile measurements data for the set of samples with increasing ionicX.....	291
Appendix 13. Individual stress-strain curves obtained in probe-tack	292
Appendix 14. Summary of the images obtain during probe-tack tests at pH 2 and 8.....	293
Appendix 15. Repeatability of probe-tack measurement for EP-MAA ₄₅ M ₅₀ at pH 8.....	294
Appendix 16. Probe-tack measurements data for the set of samples with increasing ionicX.....	295
Appendix 17. Peel and shear tests measurements data for the set of samples with increasing ionicX	296
B. Chapter III. Adhesive polyampholyte polymers prepared by solution polymerization.....	297
Appendix 18. Table of characteristics for the set of samples 1 with increasing ionicX.....	297
Appendix 19. Relative molar mass distributions obtained with RI signal in SEC.....	298

Appendix 20. Logarithmic representation of the radius of gyration as function of molar mass measured by SEC-MALLS for samples series 1 and linear fit to obtain the conformation factor ν	299
Appendix 21. AFM phase pictures for samples a) SP-P ₈₈ M ₈₈ and b) SP-P ₁₀₀ M ₁₀₀ with addition of 1 equivalent of KOH.....	300
Appendix 22. Tan δ as function of the corrected angular frequency with enlargement between $10^{-3} < \omega < 10^2$	301
Appendix 23. Summary of the cross-over frequencies measured by oscillatory rheology for the sample series 1	302
Appendix 24. Elastic and loss moduli at bonding and debonding frequency obtained by oscillatory rheology	303
Appendix 25. Summary of the parameters extracted from the stress-strain curves obtained by tensile tests for sample series 1	304
Appendix 26. Individual stress-strain curves obtained by tensile tests for the sample series 1.....	305
Appendix 27. Summary of the peel mean force data and shear holding power for the sample series 1.....	306
Appendix 28. ³¹ P NMR of Polystep® with enlargement to propose peak distribution of mono- and dimer	307
Appendix 29. Table of characteristics for the set of samples 2 with different ionic comonomers stoichiometry	308

Appendix 30. Logarithmic representation of the radius of gyration as function of molar mass measured by SEC-MALLS for samples series 2 and linear fit to obtain the conformation factor ν	309
Appendix 31. Summary of the cross-over frequencies measured by oscillatory rheology for the sample series 2.....	310
Appendix 32. Individual stress-strain curves obtained by tensile tests for the sample series 2.....	311
Appendix 33. Summary of the parameters extracted from the stress-strain curves obtained by tensile tests for sample series 2.....	312
Appendix 34. Summary of the peel mean force data and shear holding power for the sample series 2.....	313
Appendix 35. Table of characteristics for the set of samples 3 with different ionic comonomers.....	314
Appendix 36. Logarithmic representation of the radius of gyration as function of molar mass measured by SEC-MALLS for samples series 3 and linear fit to obtain the conformation factor ν	315
Appendix 37. Summary of the cross-over frequencies measured by oscillatory rheology for the sample series 3.....	316
Appendix 38. Individual stress-strain curves obtained by tensile tests for the sample series 3.....	317
Appendix 39. Summary of the parameters extracted from the stress-strain curves obtained by tensile tests for sample series 3.....	318

Appendix 40. Summary of the peel mean force data and shear holding power for the sample series 3...	319
Appendix 41. Summary of the peel mean force data and shear holding power for the adhesive performance comparison of SP-P ₈₈ M ₈₈ , SP-P ₅₀ M ₁₀₀ and SP-P ₈₈ D ₈₈ to Acronal® V 215 and Acronal® 3633.....	320
Appendix 42. Logarithmic representation of the radius of gyration as function of molar mass measured by SEC-MALLS for samples series 4 and linear fit to obtain the conformation factor ν	321
Appendix 43. Table of final characteristics for the set of samples 4 using different processes and ionic comonomers compositions	322
Appendix 44. Elastic G' and Loss G'' moduli curves as function of the angular frequency obtained by oscillatory rheology at room temperature for the samples series 4 and P ₀ M ₀ composition.....	323
Appendix 45. Summary of the cross-over frequencies measured by oscillatory rheology for the sample series 4	324
Appendix 46. Summary of the parameters extracted from the stress-strain curves obtained by tensile tests for sample series 4	325
Appendix 47. Summary of the peel mean force data and shear holding power for the sample series 4.	326
C. Chapter IV. Secondary dispersions: from dissolved to dispersed	327
Appendix 48. Images of the phase-separation observed with addition of water to SP-P ₂₀₀ M ₁₀₀ without or with prior addition of KOH using 0.5 and 1 equivalent.....	327

Appendix 49. Images of SD-P ₂₀₀ M ₁₀₀ during the different steps of the dispersive procedure.....	328
Appendix 50. Particle diameter weight distribution of the dispersion obtained by AUC.....	329
Appendix 51. Table of characteristics of SD-P ₁₅₀ M ₅₀ , SD-P ₂₀₀ M ₅₀ and SD-P ₂₀₀ M ₁₀₀ for S, S+KOH and D states	330
Appendix 52. Relative molar mass distributions of SD-P ₁₅₀ M ₅₀ , SD-P ₂₀₀ M ₅₀ and SD-P ₂₀₀ M ₁₀₀ obtained by SEC-RI	331
Appendix 53. AFM phase images (5 and 2 μm) measured in tapping mode of films cross-sections of a) SD-P ₁₅₀ M ₅₀ , b) SD-P ₂₀₀ M ₅₀ and c) SD-P ₂₀₀ M ₁₀₀	332
Appendix 54. Summary of the parameters extracted from the stress-strain curves obtained by tensile tests for the set of samples.....	333
Appendix 55. Repeatability of tensile test for the dispersion of SD-P ₁₅₀ M ₅₀	334
Appendix 56. Young's modulus E obtained from tensile test and elastic modulus G' obtained with oscillatory rheology at $\omega=0.6 \text{ rad.s}^{-1}$	335
Appendix 57. Summary of the peel mean force and shear holding power for the set of samples.....	336
Appendix 58. Summary of shear holding power for comparison after 3 days in desiccator.....	337

VI.1. EXPERIMENTAL PART

A. Materials

n-Butylacrylate (n-BA), Styrene (St) and Methacrylic Acid (MAA), Methyl methacrylate (MMA), tert-Butyl hydroperoxide (10%), tert-Butyl peroxy-pivalate (t-BPPVT, 75 wt%), tert-Butyl peroxy-2-ethylhexanoate (t-BP2EH, 80wt%), sodium formaldehyde sulfoxylate (Rongalit® C), sodium Persulfate (NaPS), sodium acetone Bisulfite, tert-Dodecyl mercaptan (t-DMK), Iron II trisulfate heptahydrate ($\text{Fe}_2(\text{SO}_4)_3$), Ethanol (EtOH), Isopropyl alcohol (iPrOH), Disponil® FES 77, Lutensol® AT 18 were purchased internally from BASF.

(2-(Methacryloyloxy)ethyl)trimethylammonium chloride solution (MAETAC, 80%) and Potassium Hydroxide (KOH, ≥ 85 wt%) were purchased from Sigma-Aldrich.

Dodecyl trimethylammonium chloride (DTMACl) was purchased from TIC.

Dowfax® 2A1 was purchased from Dow. Wako V 50 was purchased from Wako Chemicals.

Stepanquat® BC 40, Petrostep® Q 5018 and Phosphoric acid 2-hydroxyethyl methacrylate ester (Polystep® HPE) were kindly provided by Stepan.

Ammonia (NH_3 , 10%) and Hydrogen Peroxide (H_2O_2 , 30%) were purchased from Bernd Kraft GmbH.

Tegopren® 5847 was purchased from Evonik.

All chemicals were used as received.

B. Chapter II - Synthesis by emulsion polymerization

i. Preparation of the cationic seed

The cationic seed was prepared by radical emulsion polymerization in a 2 litres semi-automated glass reactor under nitrogen atmosphere. The typical seed recipe is found in Table 1.

The initial charge was loaded in the reactor and heated up to 70°C. The monomer and initiator feed were then continuously added over 3 hours. The seed was then used after checking the particle size by Hydrodynamic Chromatography (HDC) and the mean value found to be 35 nm.

Table 1. Recipe for the cationic seed

Feed	Ingredient	mol	pphm
Initial charge	Demineralized H ₂ O	-	210.0
	St	0.350	20.0
	DTMACI	0.140	20.0
	Fe ₂ (SO ₄) ₃ .H ₂ O	0.001	0.2
Monomer Feed	St	1.380	80.0
Initiator Feed	Demineralized H ₂ O	-	150.0
	H ₂ O ₂	0.180	3.3

The ingredients amounts are expressed in mmol and as parties per hundred monomer (pphm).

ii. Polymerization in emulsion

All polymerizations were carried out in a semi-automated glass reactor of 2 liters under nitrogen atmosphere. The syntheses were prepared by seeded radical emulsion polymerization. The typical dispersion recipe is found in Table 2. The Monomer feed 1 was prepared by pre-emulsification of the monomers.

The surfactant was dissolved in water, the CTA was then added as well as the mixture of monomers while stirring with a magnetic stirrer with an agitation speed ~ 700 rpm. The initial charge was directly loaded in the reactor and heated up to 70°C , 10% of the initiators feeds was then added to the reactor for 2 minutes and after waiting 3 minutes, the monomers and initiator feeds were added continuously over 4 hours. Afterwards, the residual monomers were minimized thanks to a second redox feed added over 30 minutes. Once the dispersion was cooled down, it was filtered on a 125 nm mesh to remove destabilized particles (coagulum). The pH of the dispersions was then increased to 8 with NH_3 10wt%.

Table 2. Recipe of the emulsion polymerization

Feed	Ingredient	mmol	pphm
Initial charge	Demineralized H ₂ O	-	5.00
	Cationic seed	n.a.	2.00
Initiator shot 1	Demineralized H ₂ O	-	1.50
	t-BHP	2.5	0.06
Initiator shot 2	Demineralized H ₂ O	-	1.50
	Rongalit® C	1.0	0.03
Monomer Feed 1	Demineralized H ₂ O	-	8.30
	DTMACI	15.0	1.00
	n-BA	2692.0-2945.0	69.00-77.80
	St	893.0-975.0	18.60-21.20
	MAA	0-195.0	0-3.4
	t-DMK	0-2.0	0-0.1
	Demineralized H ₂ O	-	10.00
Monomer Feed 2	Demineralized H ₂ O	-	2.20
	MAETAC	0-200	0-9.00
Initiator Feed 1	Demineralized H ₂ O	-	13.30
	t-BHP	22.0	0.50
Initiator Feed 2	Demineralized H ₂ O	-	13.30

C. Chapter III - Synthesis by free radical solution polymerization

All polymers were synthesized by free radical polymerization in isopropyl alcohol (iPrOH). The reactions were carried out in a semi-automated glass reactor of 2 liters under flowing nitrogen atmosphere.

i. Procedure for Semi-Batch process:

The initial charge was directly loaded in the reactor and heated up to 70°C, 5 wt% of the monomer feed was then added to the reactor in 2 minutes, followed by 5 wt% of the initiator feed. After a waiting time of 3 minutes, the monomers and initiator feeds were added continuously over 3 hours.

After this time, the temperature of the reactor was increased to 90°C and the last initiator feed was added for 30 minutes to remove all residual monomers.

The viscosity of the solution was carefully followed throughout the polymerization, to avoid gel-effect and reaction runaway.

An additional waiting period of 30 minutes was given and finally the reactor was cooled down to room temperature, the solution was taken out of the reactor and the solid content was measured. The general recipe is found in the following Table 3.

Table 3. General recipe of the free radical solution polymerization in Semi Batch

Process	Feed	Ingredient	mol	pphm
Semi Batch	Initial charge	iPrOH	2.5 – 3.3	25.0-40.0
	Monomer Feed	iPrOH	1.7	20.0
		n-BA	2.8 – 3.7	71.9 – 78.8
		MMA	1 – 1.3	19.4 – 21.2
		Polystep® HPE	0– 0.1	0 – 4.6
		MAETAC	0 – 0.1	0 – 4.2
	Initiator Feed 1	iPrOH	2.0	23.8
		t-BPPVT	0.008	0.3
	Initiator Feed 2	iPrOH	1.0	12.5
		t-BPPVT	0.008	0.2

ii. Procedure for Batch process with t-BPPVT as initiator:

The initial charge containing solvent and monomers was directly loaded in the reactor and heated up to 70°C. Once reaction temperature reaction was reached, the initiator feed was added continuously over 3 hours. For removal of residual monomers, the temperature of the reactor was increased gradually in 1 h to 90°C. The second initiator feed was then added for 30 min. The viscosity of the solution was carefully followed throughout the polymerization, to avoid gel-effect and reactions runaway. Post-polymerization was extended to 30 minutes and finally the reactor was cooled down to room temperature, the solution was taken out of the reactor and the solid content was measured. A general recipe for the Batch process is available in Table 4.

iii. Procedure for Batch process with t-BP2EH:

The initial charge containing solvent and monomers was directly loaded in the reactor and heated up to 70°C. Once reaction temperature reaction was reached, the initiator feed was added continuously over 3 hours. Polymerization was let to react for 1 h at 70°C before increasing the temperature gradually to 75°C over 1 h. The second initiator feed was then added for 2 hours.

The viscosity of the solution was carefully followed throughout the polymerization, to avoid gel-effect and reactions runaway. Post-polymerization was carried out at 75°C for 16 h and finally the reactor was cooled down to room temperature, the solution was taken out of the reactor and the solid content was measured.

Table 4. General recipe of the free radical solution polymerization in Batch

Process	Feed	Ingredient	mol	pphm
Batch	Initial charge	iPrOH	9.300	160.0
		n-BA	2.800 – 3.700	71.9 – 78.8
		MMA	1.000 – 1.300	19.4 – 21.2
		Polystep® HPE	0 – 0.088	0 – 4.0
		MAETAC	0 – 0.088	0 – 3.7
	Initiator Feed 1	iPrOH	1.500	25.0
		t-BPPVT or t-BP2EH	0.008	0.3
	Initiator Feed 2	iPrOH	1.000	12.5
		t-BPPVT or t-BP2EH	0.008	0.2

The original recipes were calculated in party per hundred monomers (pphm), the number of functional moieties were varied but the ratio between n-BA and MMA was kept constant.

D. Chapter IV – Preparation of secondary dispersions

i. Synthesis of polymers by solution polymerization

All polymers were synthesized by free radical polymerization in isopropyl alcohol (iPrOH) in semi-batch. The reactions were carried out in a semi-automated glass reactor of 2 liters under flowing nitrogen atmosphere. The general recipe is found in the following Table 5.

The initial charge was directly loaded in the reactor and heated up to 70°C, 5 wt% of the monomer feed was then added to the reactor in 2 minutes, followed by 5 wt% of the initiator feed. After a waiting time of 3 minutes, the monomers and initiator feeds were added continuously over 3 hours.

After this time, the temperature of the reactor was increased to 90°C and the last initiator feed was added for 30 minutes to remove all residual monomers.

The viscosity of the solution was carefully followed throughout the polymerization, to avoid gel-effect and reactions runaway.

An additional waiting period of 30 minutes was given and finally the reactor was cooled down to room temperature, the solution was taken out of the reactor and the solid content was measured.

The original recipes were calculated in party per hundred monomers (pphm), the number of functional moieties were varied but the ratio between n-BA and MMA was kept constant.

Table 5. General recipe of the free radical solution polymerization

Feed	Ingredient	mol	pphm
Initial charge	iPrOH	4.200 - 5.400	50.0 – 65.0
Monomer Feed	iPrOH	1.700	20.0
	n-BA	2.600 - 2.800	68.0 – 76.0
	MMA	0.900 – 1.000	18.0 – 21.0
	Polystep® HPE	0.150 – 0.200	4.7 – 9.1
	MAETAC	0.050 – 0.100	2.5 – 4.2
Initiator Feed 1	iPrOH	2.000	23.8
	t-BPPVT	0.008	0.3
Initiator Feed 2	iPrOH	1.000	12.5
	t-BPPVT	0.008	0.2

ii. Dispersion in water of the solution polymers

Firstly, all samples were diluted to 30 wt% in iPrOH.

A solution of 0.75 M of KOH in isopropanol was prepared.

None, 1 or 2 equivalents of a KOH solution (0.75 M); equivalent in mol to the fraction of Polystep® in the polymer; were added to the polymer solutions under fast mechanical agitation ≈ 700 rpm. The samples were then further diluted to 10 wt% with Demineralized water still under fast mechanical agitation.

About 40% of the total diluent (iPrOH and water) was evaporated under vacuum ($P \approx 110$ mbar) using a Rotavapor with a 50°C oil bath and a rotation speed of 90 rpm. 20 wt% of the previously added water was again added to the solution.

Finally, the diluents were evaporated under vacuum ($P \approx 80$ mbar) using a Rotavapor with a 60°C oil bath and rotation speed of 90 rpm, until a dispersion of about 25% solid content was obtained.

E. Characterization of the polymers and their films

i. Calculation of the gel content

Polymer films were obtained from drying the solutions/dispersions in silicon-paper moulds for 1 week at room temperature followed by another week at 50°C.

Known amounts of polymer films m_i were diluted in Methylenechloride (MEK) or Ethanol (EtOH) to obtain 1 wt% mixtures.

The films were let to dissolve without shaking for 48 hours. The insoluble parts were then recovered with filters (of weight m_F and pore size 125 μm), which were dried overnight in the fume hood and finally for 2 hours in the oven at 50°C. The dried filters were weighted m_P and allowed the calculation of the gel content:

$$\text{Gel content (\%)} = \frac{m_P - m_F}{m_i} \times 100$$

ii. Size-Exclusion Chromatography (SEC)

All molecular weights were measured using Size Exclusion Chromatography (SEC) in a mixture of Hexafluoroisopropanol and 0,05% Trifluoro acetic acid calcium salt.

The samples had a concentration of 1.5 mg/mL, were filtered on Millipore Millex FG (0.2 μm) before being injected with a volume of 50 μL .

The calibration was carried out with closely distributed polymethylmethacrylate (PMMA) standards with a range molecular weight from $M = 800$ to $M = 2.200.000$ g/mol. The values outside the elution range were then extrapolated. Refractive Index (RI) and Multi-Angle Laser Light Scattering (MALLS) were used as detection techniques.

iii. High Performance Liquid Chromatography (HPLC)

For samples studied in III.2.E., the concentration of the monomers in the medium were carried out using Agilent 1290 Infinity II-System Liquid Chromatograph, equipped 1290 High Speed Pump G7120A, 1290 Multisampler G7167B, 1290 MultiColumn Thermostat G7116B and 1290 Diode Array Detector G4212A. The samples were diluted to 0.001 mg.mL^{-1} in a 50:50 Acetonitrile:Water (ACN:H₂O) solution. The different methods used for the monomers are summarized in Table 6.

NB: H₃PO₄ stands for phosphoric acid

Table 6. Summary of methods used in HPLC for the different group of monomers

		n-BA/MMA	Polystep® HPE/MAETAC
Reference concentrations (mg.L ⁻¹)		0.1 - 33	0.5 - 290
Mobile phase	1	H ₂ O + 1% H ₃ PO ₄	H ₂ O + 0.1 % H ₃ PO ₄
	2	98% ACN + 1.99% H ₂ O + 0.01 % H ₃ PO ₄	ACN + 0.1 % H ₃ PO ₄
Column	Name	TriArt EXRS	Fluofix 120 E
	Dimensions	150*3 mm, 3µm	250*4.6 mm, 5 µm
	Temperature (°C)	25	25
	Injection volume (µL)	10	10
	Pressure (bar)	380	-
	Elution rate (mL.min ⁻¹)	0.7	1
	Measurement time (min)	20	55

iv. Gas chromatography (GC)

Residual amounts of isopropanol in the dispersions were measured with a Headspace-GC Perkin Elmer Clarus 680 equipped with an autosampler Turbomatrix 110 and an FID detector at 300°C. Samples were diluted to 0.1 g.mL^{-1} in water. The measurements were carried out using the method detailed in Table 7.

Table 7. Detailed method used for the measurement of residual isopropanol by GC

Mobile phase		N ₂
Column	Name	DB1 USB 477 727 H
	Dimensions	30 m*0.25mm, 1.0 µm
	Injection temperature (°C)	150
	Pressure (bar)	0.65
	Elution rate (mL.min ⁻¹)	5.0
	Measurement time (min)	40
Oven	Preheating	50°C, 5 min
	1 st cycle	130°C, 5°C.min ⁻¹
	2 nd cycle	260°C, 15°C.min ⁻¹
	Post-heating	260°C, 10 min

v. Hydrodynamic Chromatography (HDC)

The dispersions were diluted with demineralized water to ~20 g.L⁻¹, filtered through PTFE filters of 1.20 µm pore size before being injected in the instrument 1260 Infinity II from Agilent technologies equipped with a PL-PSDA Cartridge type 2 column of 10 µm size polystyrene beads and a Cary 60 UV-vis detector of $\lambda=254$ nm. The eluent was composed of a solution of demineralized water with 0.24 g.L⁻¹ of monosodium phosphate, 0.5 g.L⁻¹ of sodium dodecyl sulphate, 2 g.L⁻¹ of Brij35 detergent and 0.2 g.L⁻¹ of sodium azide; the elution speed was set to 1 mL.min⁻¹.

vi. Karl-Fischer titration

The residual amounts of water present in the dried films of dispersions were measured by the Karl-Fischer Oven method. 0.5 g of the polymer dried films were put in an oven Metrohm Modell 874 at 140°C for 1 h. Residual evaporated water was transported by nitrogen in the measuring cell of the Karl-Fischer titrator Metrohm Titrando Modell 852.

vii. Analytic Ultra Centrifuge (AUC)

The dispersions were diluted to $\sim 2 \text{ g.L}^{-1}$ in demineralized H_2O and D_2O , all samples were put to separation over 16h at 30000 U.min^{-1} with a Beckman Coulter XLI Ultracentrifuge 80k, equipped with a laser of $\lambda=456 \text{ nm}$.

viii. Attenuated total reflectance infrared Spectroscopy (ATR-IR)

The samples were dried over at 50°C then recovered and IR spectra were measured thanks to a Diamond-ATR from HEGOGA.

ix. Microscopy imaging

For cross-cuts images, one drop of polymer solution was poured on a droplet sample holder, which was then turned upside down to allow the formation of a homogeneous droplet.

The sample was dried overnight at room temperature and 24 hours in the oven at 50°C .

The cross sections were realized with a Leica UCT 7 equipped with a cryochamber ($T=-80^\circ\text{C}$) and an "ultra 35°"-knife from Diatome.

Atomic Force Microscopy (AFM) pictures were taken thanks to a Bruker AFM Dimension Icon with Stargate Scanner and Olympus OMCL-AC160TS-R3 Cantilever ($k=26 \text{ N.m}^{-1}$) in tapping mode.

Transmission Electron Microscopy (TEM) pictures were taken thanks to a Zeiss Libra with 120 kV and equipped with LaB6 Cathode. Agents such as Uranylacetate, PWS and Ruthenium oxide were also used to emphasize the contrasts.

Energy Dispersive X-ray spectroscopy (EDX) mapping was realized thanks to a FEI Osiris with 200 kV and equipped with a Field Emitter Gun (FEG).

x. Differential Scanning Calorimetry (DSC)

The glass transition temperatures of the samples were measured by Differential Scanning Calorimetry (DSC) using a TA Instruments Q2000.

The samples were heated from -70°C to 150°C with a heating rate of $20^{\circ}\text{C}.\text{min}^{-1}$ during a first heating cycle, they were cooled down to -70°C and finally heated to 150°C during a second heating cycle.

xi. Oscillatory Rheology

The solutions/dispersions were poured in silicon-paper moulds, they were dried one week at room temperature and a second week at 50°C in a ventilated oven.

The films obtained were around 1.2 mm in thickness. Samples were cut at the size of the plate geometry with a round shape die-cutter.

The measurements were realized with an Anton-Paar Rheometer MCR 302 equipped with a Julabo HE thermostat and a Polycold PGC 152AC cooler. Plus, a parallel plate 25 mm in diameter was used as measuring geometry.

To determine the limits of the linear viscoelastic regime of each sample, amplitude sweeps were realized with a deformation range of $0.01 < \gamma < 100\%$ at a frequency of $10 \text{ rad}.\text{s}^{-1}$.

Frequency sweeps ($0.1 < \omega < 100 \text{ rad}.\text{s}^{-1}$) were then realized with an amplitude of 1%; which was in accordance to each sample's linear regime limits. Each measurement was repeated at least 3 times, the repeatability was considered good for all samples; only the most representative samples are shown in paragraphs.

Time-Temperature Superposition measurements were realized with temperatures starting from 25 then 30 to 180°C , in 10°C steps, with an amplitude γ of 1% and a frequency range from 1 to $100 \text{ rad}.\text{s}^{-1}$.

xii. Tensile measurements

The dispersions were poured in silicon-paper moulds, then dried one week at room temperature and a second week at 50°C in a ventilated oven.

Before the measurements the films were laid overnight in the measuring room under control temperature and humidity, respectively 23°C and 50%.

The thicknesses of the films obtained was around 1.2 mm. Dog bone specimen were cut with a die-cutter at the DIN 53504 S3A size. Measurements were carried out on a Zwick Z050/zmart.pro machine at a cross-head velocity of 200 mm.min⁻¹ with a force motor of 20 N. For each sample, the tests were carried out at least 3 times, the repeatability was considered good and only the most representative samples are shown in graphs. Examples of repeatability are given in Appendix 11 and Appendix 55. The data shown in the tables (in the various appendixes) are the average values.

xiii. Probe-tack

All tests were carried out at ESPCI Paris. They were performed with a stainless-steel probe of 9.7 mm diameter with an approach velocity of $v_{app}=30\text{ }\mu\text{m/s}$, a contact force of $F=70\text{ N}$ and a contact time of $t_c=1\text{ s}$. The debonding velocity v_{deb} was varied between 1 and 1000 $\mu\text{m/s}$. The force was measured by a 250 N load cell and the displacement was recorded by a mechanical extensometer. The real contact area was calculated, and the measurements were followed and recorded thanks to a video camera.

The dispersions or solutions were coated on glass plates thanks to a doctor blade, they were disposed under a bell jar overnight to dry slowly at room temperature then dried for 2 hours at 50°C. The thickness was measured by optical profilometer. Dispersions polymers had thickness around 150 μm and solutions polymers around 100 μm .

After their preparation, the samples were used within 2 days. 3 to 5 measurements were done for each sample at each debonding velocity, the repeatability was considered good (an example is given in Appendix 15) and the most representative samples are given in the paragraphs.

xiv. Adhesion testing

The films were prepared in the same way for peel, loop tack and shear tests.

The samples were coated on PET foils with a doctor blade to obtain films with a grammage of 20 g.m⁻². They were then cured at room temperature for 10 min and at 90°C for 15 min. They were finally protected by silicon paper, cut into strips of 25 mm width, stored in a room with controlled temperature and humidity, respectively 23°C and 50%; and used within 1 week after preparation.

To improve the wetting of the dispersions on PET and thus obtain regular films, 0.5 wt% dry of Tegopren® 5847 (wetting agent) were added prior coating.

Peel tests were realized using a Zwick Roell RetroLine Test control II equipped with a load cell of 200 N and pneumatic clamps in a climate room (53% humidity and 25°C).

Measurements were done on steel plates with an angle of 180° over a length of 15 mm with a strain rate of 300 mm.min⁻¹.

And finally shear strength were realized on steel plates over an area of $\approx 625 \text{ mm}^2$ ($\approx 1 \text{ inch}^2$) using shear bench and a weight of 1.5 kg.

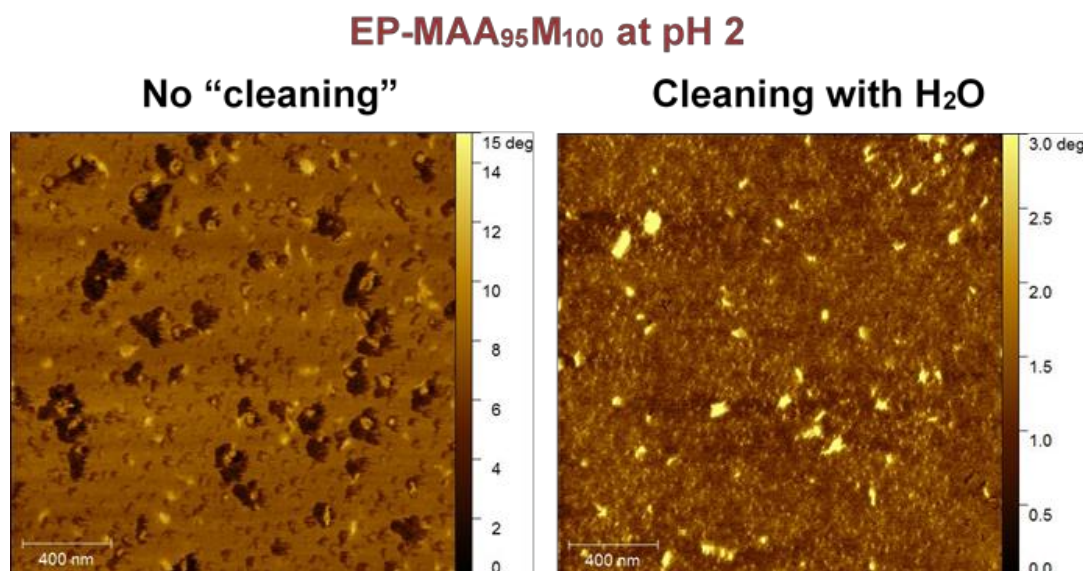
VI.2. ADDITIONAL GRAPHS AND DATA TABLES

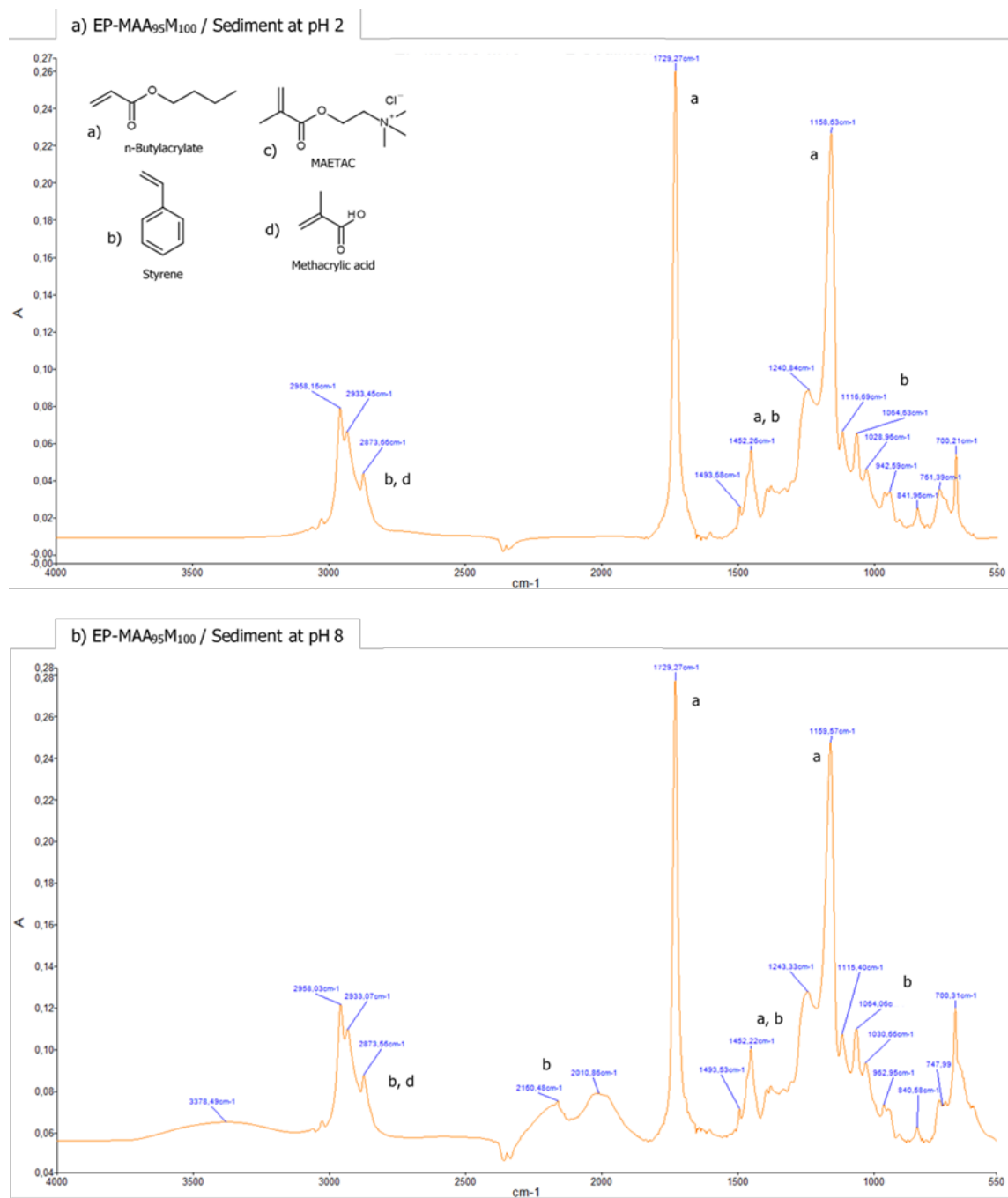
A. Chapter II. Adhesive polyampholyte particles prepared by emulsion polymerization

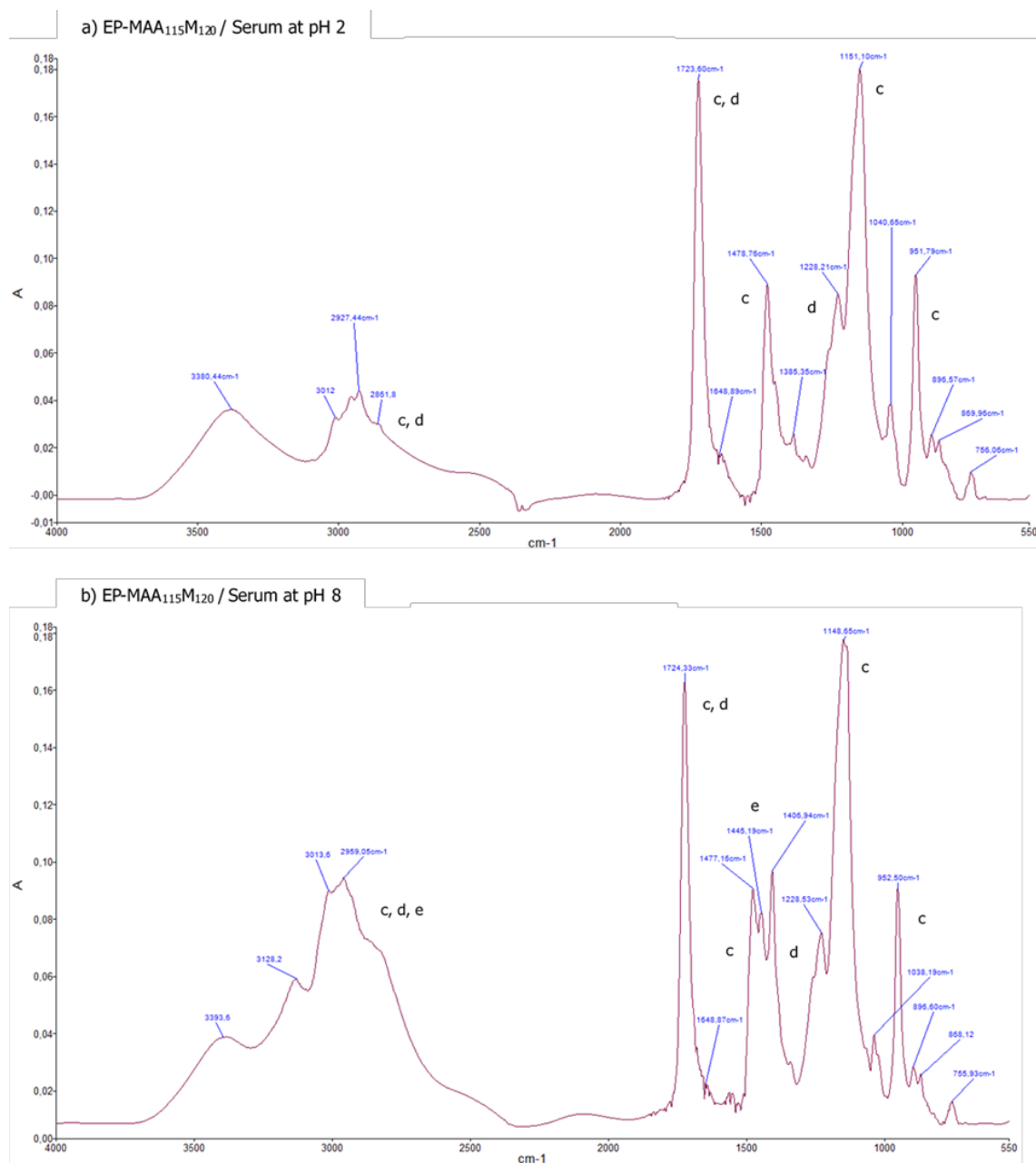
Appendix 1. Table of characteristics for the set of samples

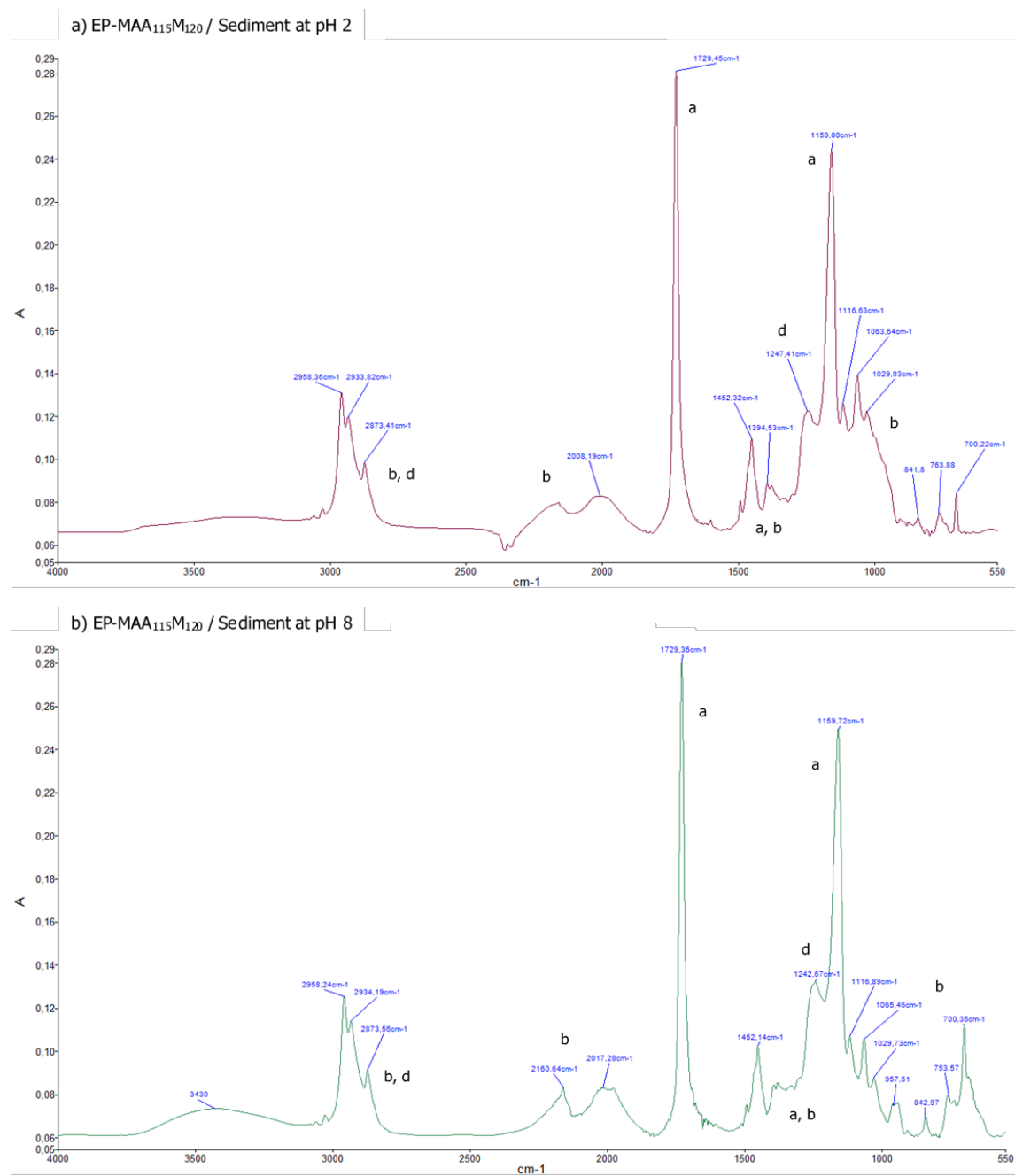
Experiment	MAA (mmol)	MAETAC (mmol)	pH	T _g (°C)	Particle size (nm)	Gel%		SEC	
						in MEK	in EtOH	M _w (g.mol ⁻¹)	M _n (g.mol ⁻¹)
EP-M ₁₀₀	0	100	2	-22.0	155	52	83	206 000	44 200
			8	-21.9	147 + t*	51	87		
EP-MAA ₄₅ M ₅₀	45	50	2	-21.3	117, 198	46	81	220 000	41 700
			8	-19.8	175, 284 + t	47	84		
EP-MAA ₉₅ M ₁₀₀	95	100	2	-19.4	152, 228 + t	36	59	222 000	35 800
			8	-19.3	258 + t	38	73		
EP-MAA ₁₁₅ M ₁₂₀	115	120	2	-19.0	200 + t	32	0.7	259 000	35 500
			8	-19.4	n.a.	35	1.7		
EP-MAA ₁₉₅ M ₂₀₀	195	200	2	-18.7	189 + t	28	1.6	237 000	38 100
			8	-18.9	n.a.	26	0.7		

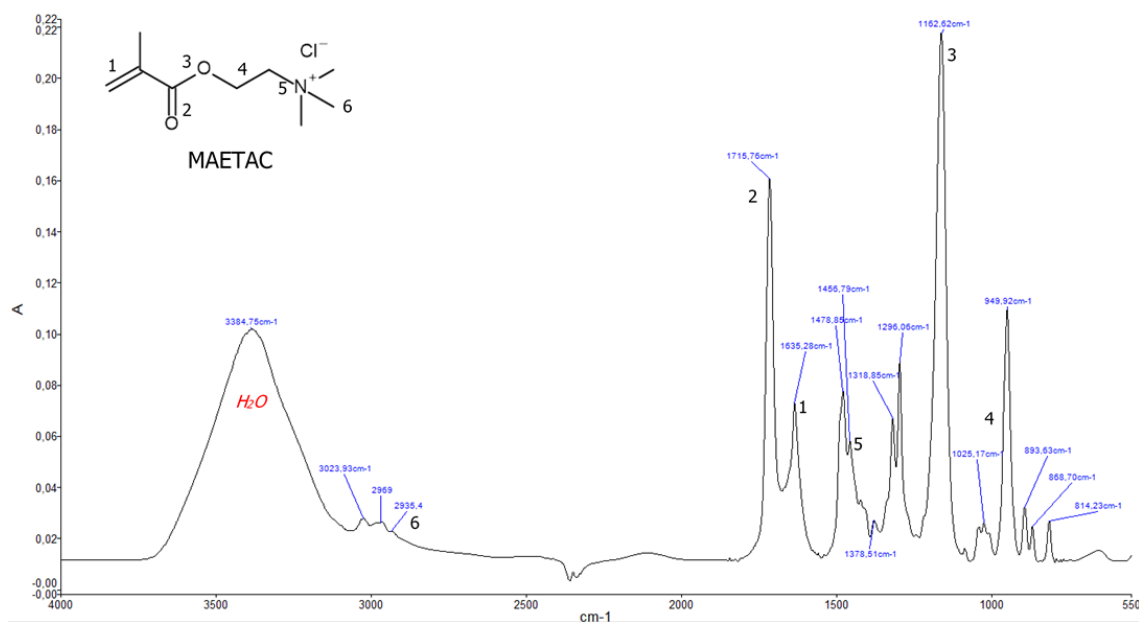
*t=tailing

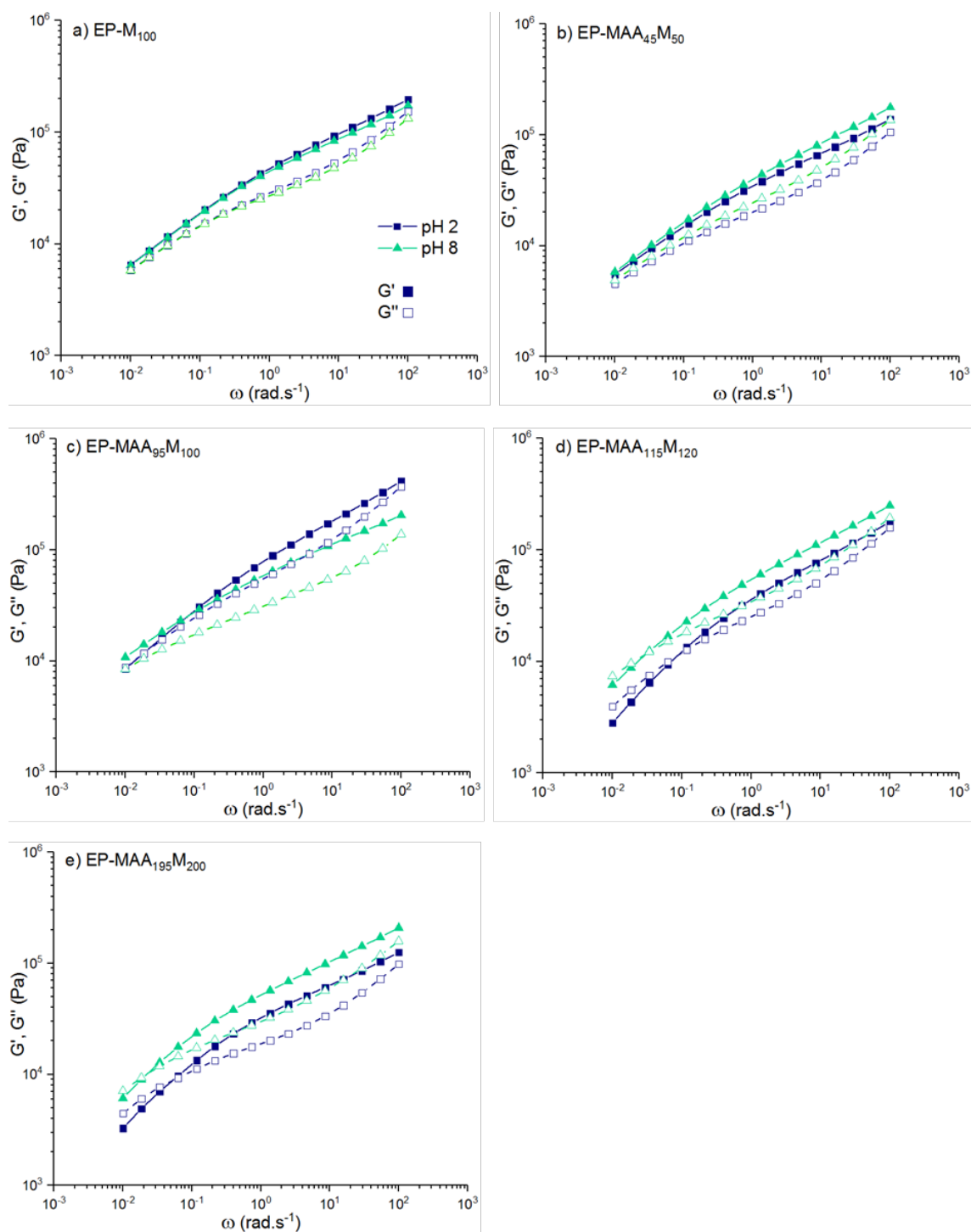
Appendix 2. AFM pictures of EP-MAA₉₅M₁₀₀ at pH 2 before and after cleaning with water

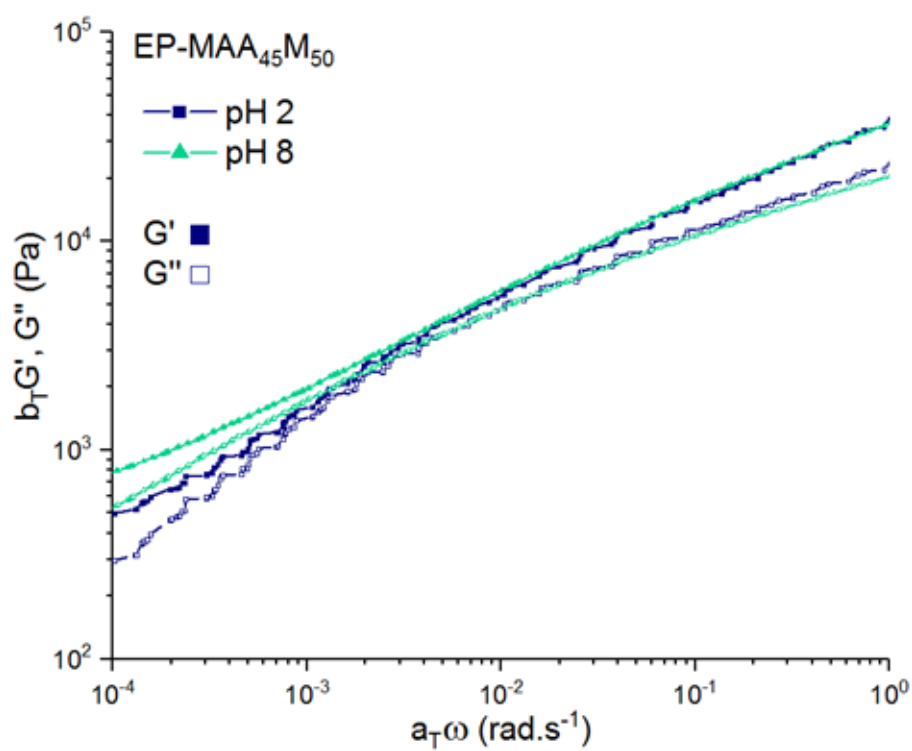
Appendix 3. ATR-IR spectra of the sediment of EP-MAA₉₅M₁₀₀ at a) pH 2 and b) pH 8

Appendix 4. ATR-IR spectra of the sediment of EP-MAA₁₁₅M₁₂₀ at a) pH 2 and b) pH 8

Appendix 5. ATR-IR spectra of the serum of EP-MAA₁₁₅M₁₂₀ at a) pH 2 and b) pH 8

Appendix 6. ATR-IR spectra of the cationic monomer MAETAC

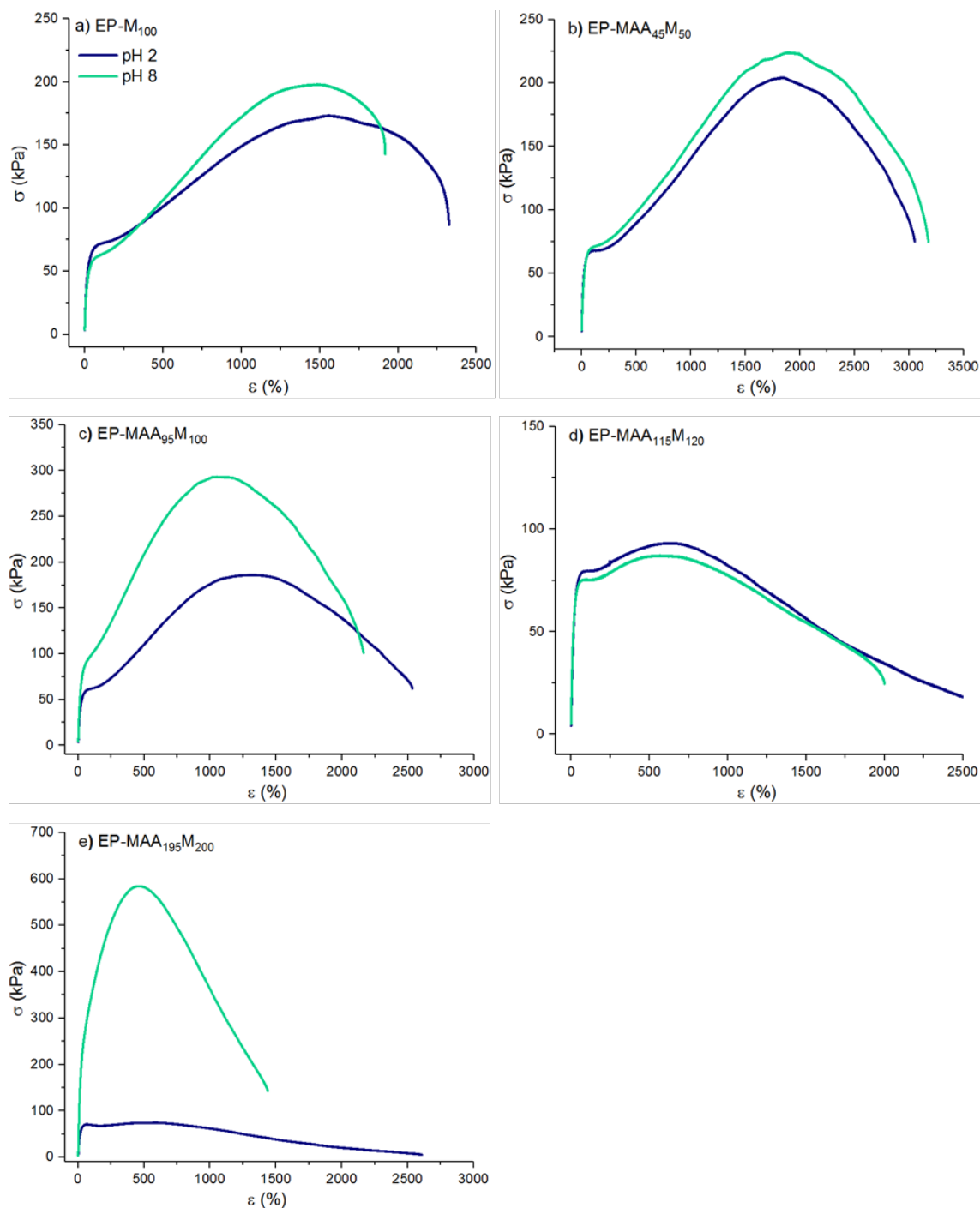
Appendix 7. Elastic G' and loss G'' modulus as function of angular frequency ω 

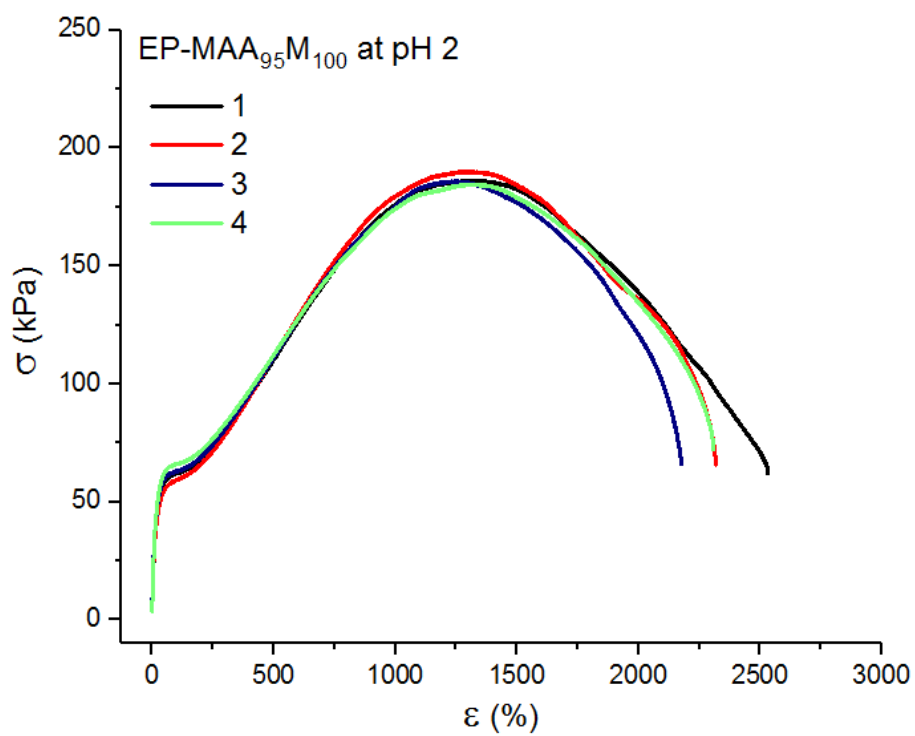
Appendix 8. Transition zone observed on the master curve of EP-MAA₄₅M₅₀

Appendix 9. Cross-over frequencies of first and second transitions for the set of samples as function of ionicX

Experiment	pH	First transition ($\omega > 10^{-3} \text{ rad.s}^{-1}$)	Second transition ($\omega < 10^{-3} \text{ rad.s}^{-1}$)
		$\omega_{c1} \text{ (rad.s}^{-1}\text{)}$	$\omega_{c2} \text{ (rad.s}^{-1}\text{)}$
EP-M₁₀₀	2	3.3×10^{-3}	2.6×10^{-4}
	8	4.7×10^{-3}	2.6×10^{-4}
EP-MAA₄₅M₅₀	2	-	-
	8	-	-
EP-MAA₉₅M₁₀₀	2	1.9×10^{-2}	4.7×10^{-4}
	8	1.7×10^{-3}	5.3×10^{-4}
EP-MAA₁₁₅M₁₂₀	2	1.0×10^{-1}	5.6×10^{-5}
	8	3.0×10^{-2}	3.4×10^{-6}
EP-MAA₁₉₅M₂₀₀	2	5.0×10^{-2}	4.0×10^{-5}
	8	3.0×10^{-2}	3.9×10^{-5}

Appendix 10. Individual stress-strain curves obtained in tensile tests

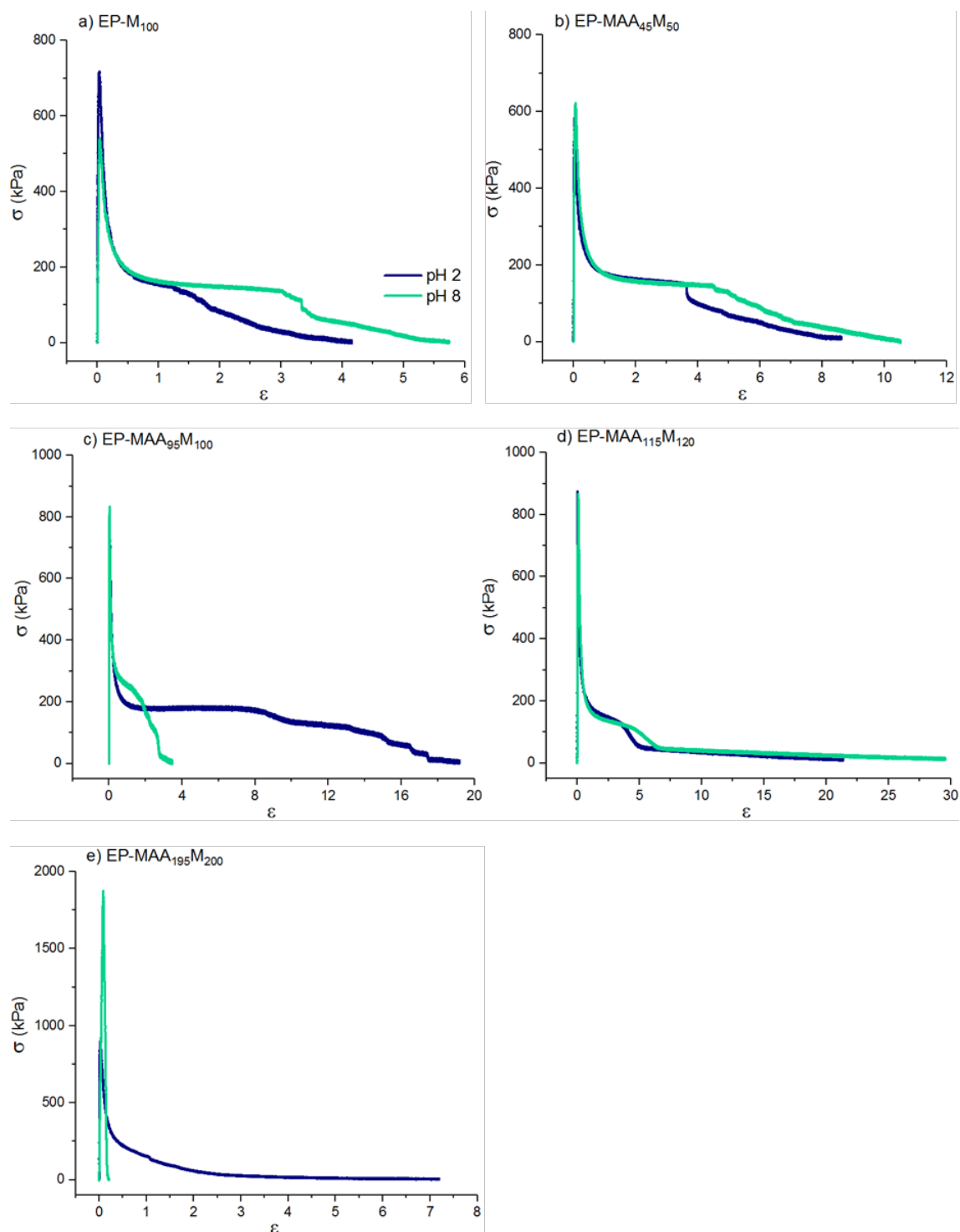


Appendix 11. Repeatability of tensile measurement for EP-MAA₉₅M₁₀₀ at pH 2

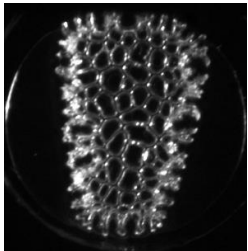
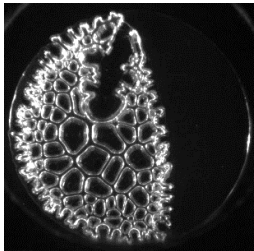
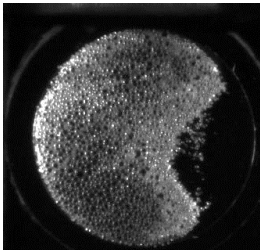
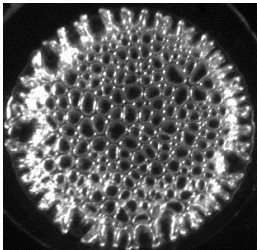
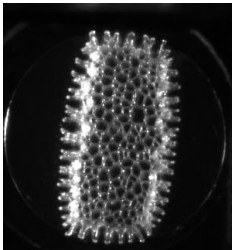
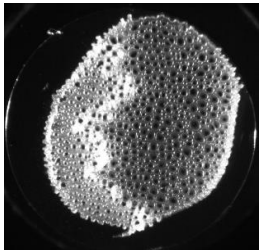
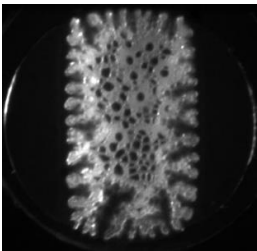
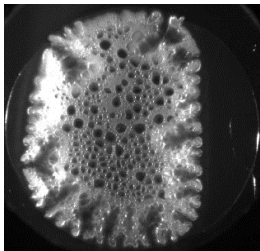
Appendix 12. Tensile measurements data for the set of samples with increasing ionicX

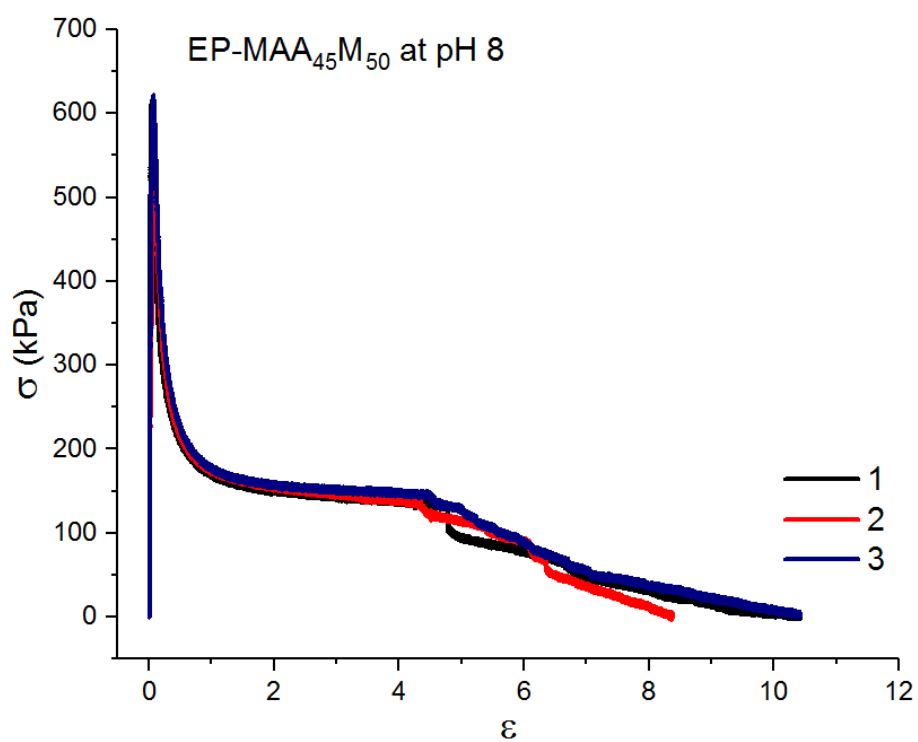
Experiment	pH	σ_y (kPa)	σ_{max} (kPa)	ϵ_{max} (%)	σ_B (kPa)	ϵ_B (%)
EP-M ₁₀₀	2	-	173 ± 7	1515 ± 45	93 ± 10	2311 ± 31
	8	62 ± 6	195 ± 3	1545 ± 80	134 ± 18	2072 ± 136
EP-MAA ₄₅ M ₅₀	2	65 ± 3	200 ± 5	1796 ± 81	89 ± 14	2814 ± 305
	8	65 ± 4	227 ± 9	1840 ± 67	93 ± 20	3047 ± 192
EP-MAA ₉₅ M ₁₀₀	2	62 ± 5	187 ± 2	1300 ± 33	66 ± 4	2334 ± 148
	8	-	275 ± 20	1106 ± 80	108 ± 41	2170 ± 280
EP-MAA ₁₁₅ M ₁₂₀	2	72 ± 4	94 ± 5	650 ± 38	13 ± 2	2542 ± 127
	8	76 ± 8	94 ± 8	572 ± 53	15 ± 9	2190 ± 316
EP-MAA ₁₉₅ M ₂₀₀	2	67 ± 5	75 ± 2	549 ± 18	4 ± 2	2869 ± 390
	8	-	578 ± 15	439 ± 21	177 ± 43	1290 ± 107

Appendix 13. Individual stress-strain curves obtained in probe-tack



Appendix 14. Summary of the images obtain during probe-tack tests at pH 2 and 8

	pH 2	pH 8
EP-M ₁₀₀		
EP-MAA ₄₅ M ₅₀		
EP-MAA ₉₅ M ₁₀₀		
EP-MAA ₁₁₅ M ₁₂₀		

Appendix 15. Repeatability of probe-tack measurement for EP-MAA₄₅M₅₀ at pH 8

Appendix 16. Probe-tack measurements data for the set of samples with increasing ionicX

Experiment	pH	σ_{peak} (kPa)	$\sigma_{plateau}$ (kPa)	ϵ_{max} (-)	W_{deb} (J.m ⁻²)	Failure mode*
EP-M ₁₀₀	2	633 ± 80	155 ± 8	4.5 ± 1.1	217 ± 8	A
	8	530 ± 69	144 ± 50	5.3 ± 0.8	318 ± 3	A
EP-MAA ₅ M ₅₀	2	572 ± 72	168 ± 20	6.8 ± 1.2	102 ± 1	A
	8	568 ± 58	147 ± 5	8.8 ± 1.8	193 ± 37	A
EP-MAA ₉₅ M ₁₀₀	2	745 ± 55	174 ± 14	16.1 ± 4.1	428 ± 60	A
	8	985 ± 204	326 ± 52	5.0 ± 2.0	232 ± 90	A
EP-MAA ₁₁₅ M ₁₂₀	2	1078 ± 334	152 ± 8	16.4 ± 3.9	299 ± 6	K
	8	1068 ± 241	149 ± 29	13.9 ± 3.4	317 ± 29	K
EP-MAA ₁₉₅ M ₂₀₀	2	832 ± 64	-	6.6 ± 0.8	275 ± 14	K
	8	1494 ± 296	-	0.2 ± 0.1	49 ± 17	A

*A=Adhesive
K=Cohesive

Appendix 17. Peel and shear tests measurements data for the set of samples with increasing ionicX

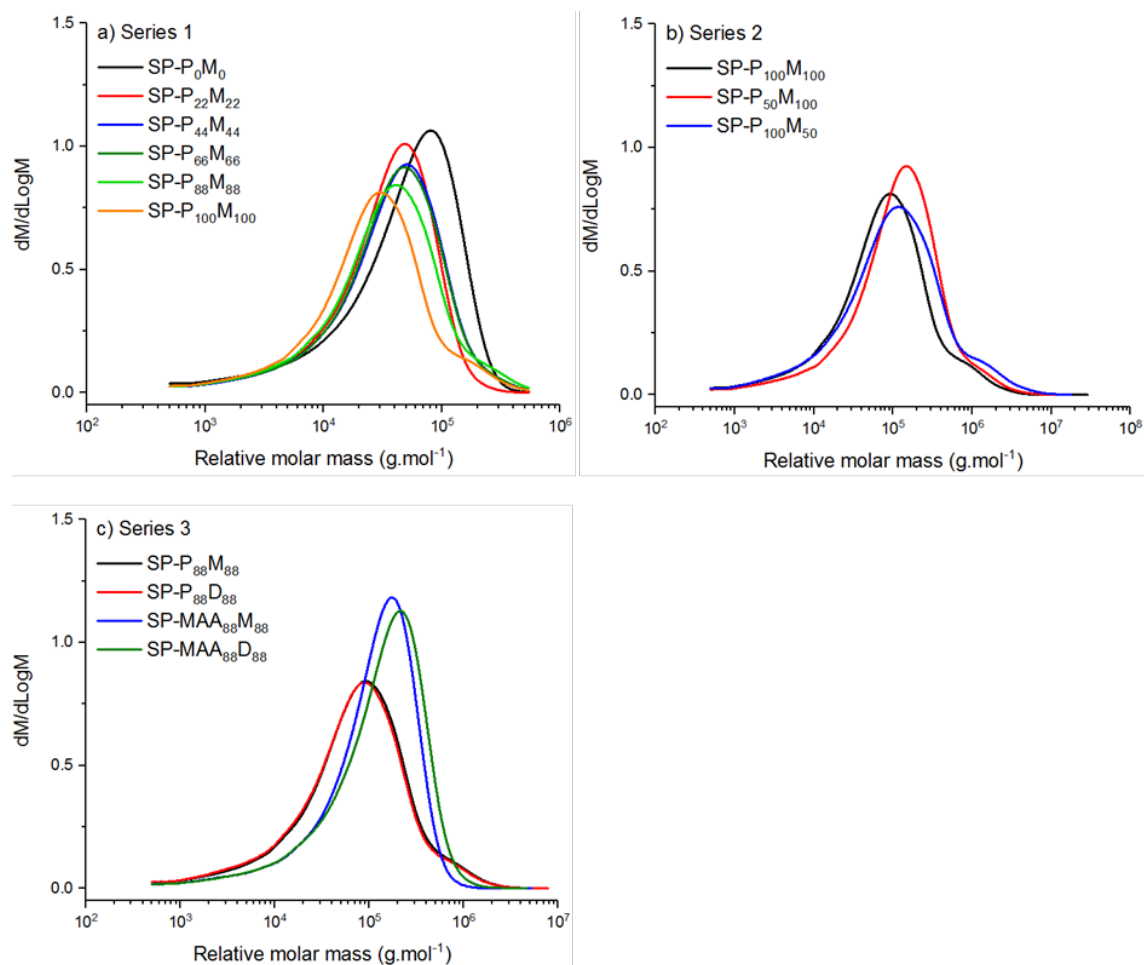
Experiment	Peel steel F_{mean} (N.25mm ⁻¹)					Shear strength steel	
	pH	$t_c = 2 \text{ min}$	Failure*	$t_c = 24 \text{ h}$	Failure*	min	Failure*
EP-M₁₀₀	2	8.2 ± 1.3	A	13.4 ± 0.5	A/F	665 ± 15	K
	8	8.1 ± 0.7	A	19.3 ± 5.6	A/F	706 ± 12	K
EP-MAA₄₅M₅₀	2	7.7 ± 0.8	A	10.3 ± 0.6	A/F	1066 ± 42	K
	8	5.7 ± 0.2	A	8.7 ± 3.1	A/F	825 ± 78	K
EP-MAA₉₅M₁₀₀	2	6.6 ± 2.8	A	9.3 ± 2.0	A/F	915 ± 62	K
	8	4.2 ± 0.3	A	12.9 ± 0.2	A/F	1050 ± 17	K
EP-MAA₁₁₅M₁₂₀	2	9.3 ± 1.8	A	13.1 ± 1.1	A/F	347 ± 8	K
	8	8.8 ± 0.4	A	12.4 ± 0.8	A/F	182 ± 54	K
EP-MAA₁₉₅M₂₀₀	2	6.2 ± 0.6	A	11.3 ± 0.6	A/F	476 ± 15	K
	8	8.8 ± 0.9	A	16.4 ± 3.1	A/F	601 ± 27	K

*A=Adhesive
K=Cohesive
F=Filmic

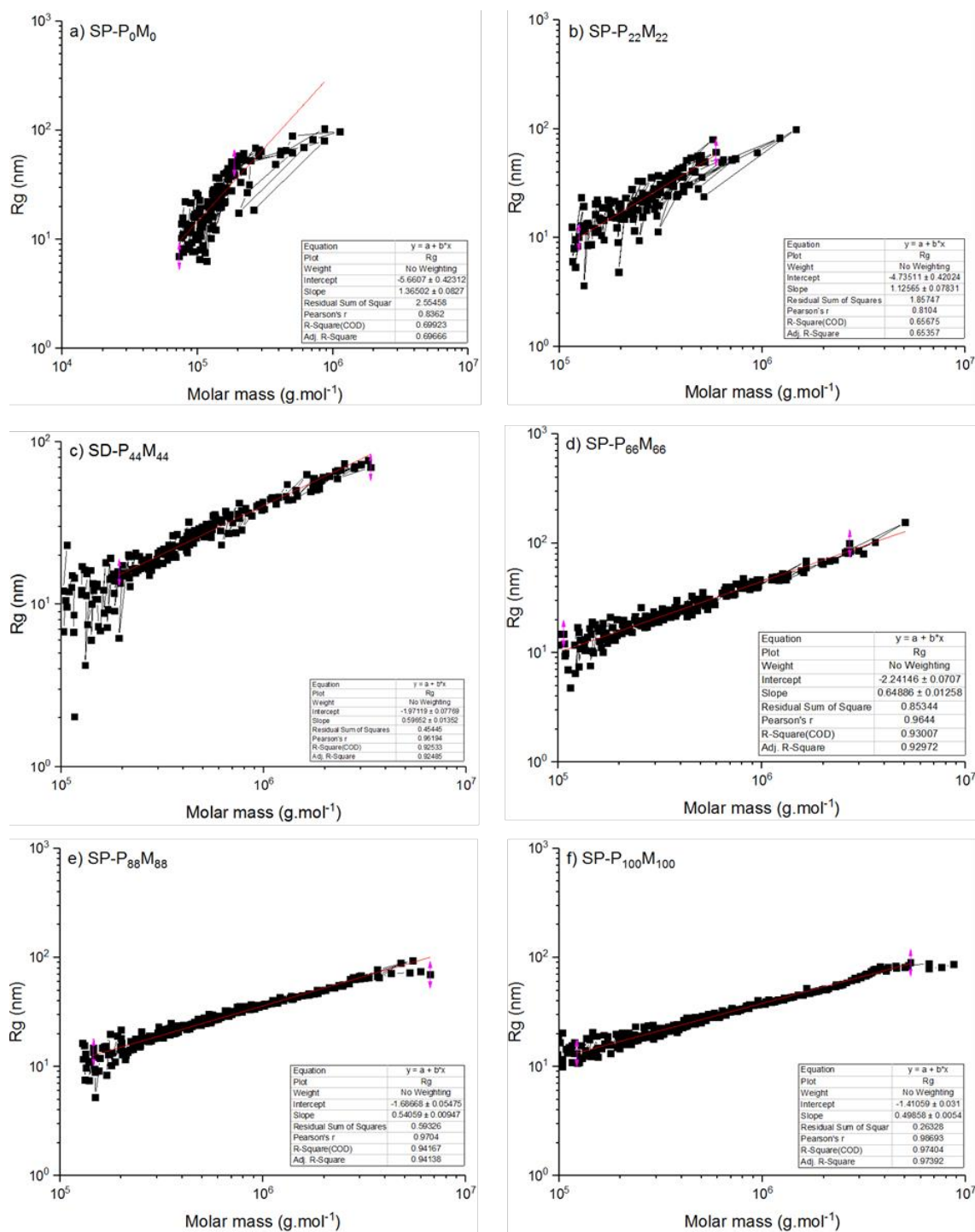
B. Chapter III. Adhesive polyampholyte polymers prepared by solution polymerization

Appendix 18. Table of characteristics for the set of samples 1 with increasing ionicX

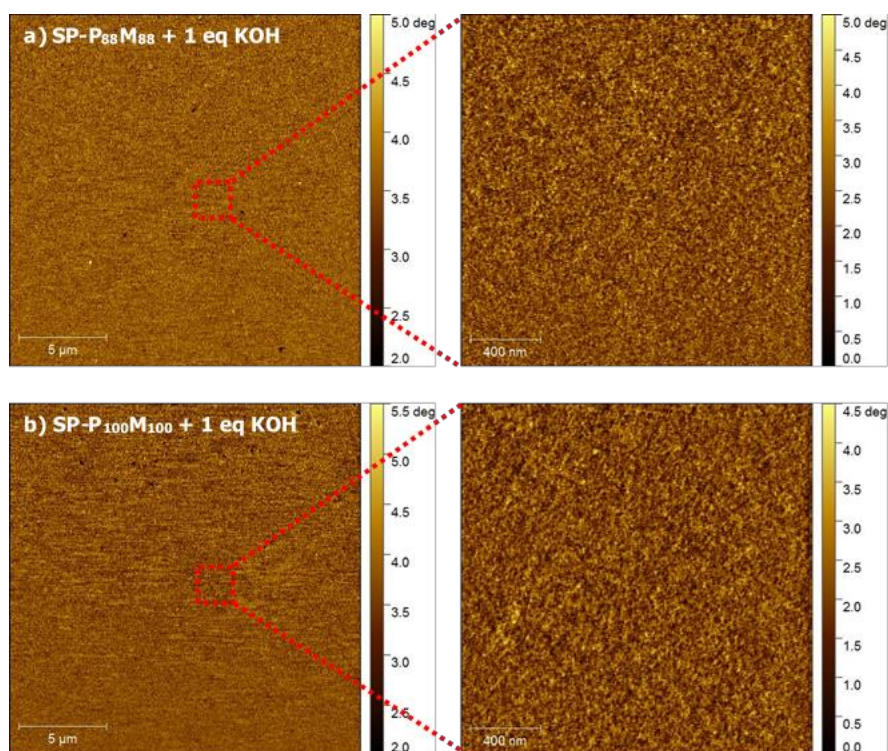
Series #	Experiment	Anionic monomer (mmol)	Cationic monomer (mmol)	KOH eq	T _g (°C)	Gel content (%)			SEC		
						in MEK	in EtOH	M _w (g·mol ⁻¹)	M _n (g·mol ⁻¹)	PDI	M _w with MALLS (g·mol ⁻¹)
1	SP-P ₀ M ₀	0	0	0	-29.2	0.6	0.6	69 100	14 900	4.6	35 000
	SP-P ₂₂ M ₂₂	P-22	M-22	0	-25.5	1.4	1.5	83 700	17 400	4.8	50 000
				1	-25.5	1.1	1.8	84 100	17 800	4.7	49 000
	SP-P ₄₄ M ₄₄	P-44	M-44	0	-25.4	0.9	1.7	113 000	19 300	5.9	69 000
				1	-24.5	1.4	2.5				
1	SP-P ₆₆ M ₆₆	P-66	M-66	0	-22.4	1.0	1.5	111 000	18 600	6.0	66 000
				1	-23.3	1.4	1.1				
	SP-P ₈₈ M ₈₈	P-88	M-88	0	-22.8	1.4	1.5	147 000	19 100	7.7	100 000
				1	-22.2	1.4	2.6				
	SP-P ₁₀₀ M ₁₀₀	P-100	M-100	0	-18.2	0.8	1.7	157 000	17 600	8.9	150 000
				1	-21.5	1.5	1.9	166 000	17 500	9.5	160 000

Appendix 19. Relative molar mass distributions obtained with RI signal in SEC

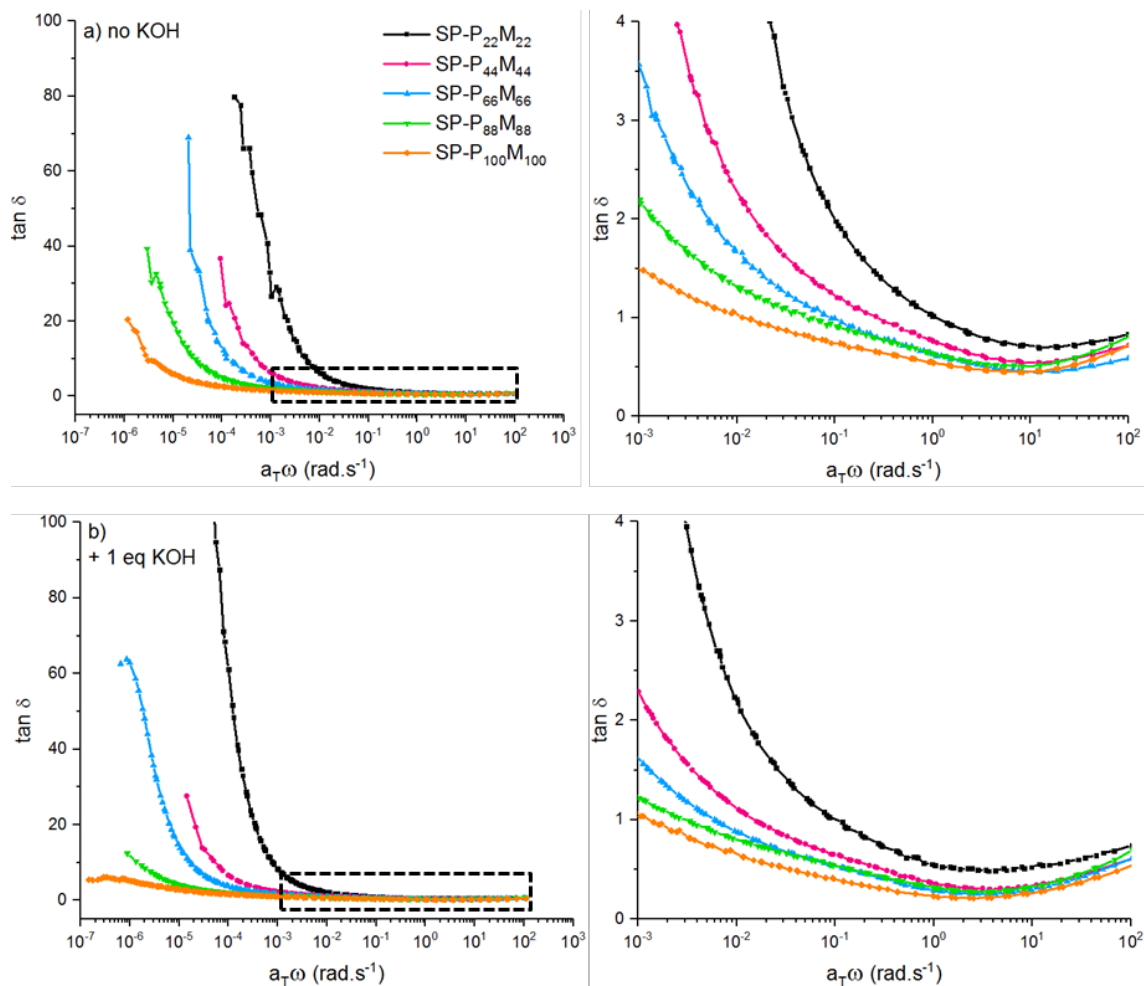
Appendix 20. Logarithmic representation of the radius of gyration as function of molar mass measured by SEC-MALLS for samples series 1 and linear fit to obtain the conformation factor ν



Appendix 21. AFM phase pictures for samples a) SP-P₈₈M₈₈ and b) SP-P₁₀₀M₁₀₀ with addition of 1 equivalent of KOH



Appendix 22. $\tan \delta$ as function of the corrected angular frequency with enlargement
between $10^{-3} < a_T \omega < 10^2$



Appendix 23. Summary of the cross-over frequencies measured by oscillatory rheology
for the sample series 1

Cross-over to flowing region				
Series #	Experiment	KOH eq	ω_c (rad.s ⁻¹)	$G_c = G' = G''$ (Pa)
1	SP-P ₀ M ₀	0	$>10^2$	$>10^5$
	SP-P ₂₂ M ₂₂	0	1.1×10^0	2.9×10^4
		1	1.0×10^{-1}	9.1×10^3
	SP-P ₄₄ M ₄₄	0	2.7×10^{-1}	2.6×10^4
		1	1.5×10^{-2}	1.1×10^4
	SP-P ₆₆ M ₆₆	0	8.9×10^{-2}	1.4×10^4
		1	6.0×10^{-3}	1.2×10^4
	SP-P ₈₈ M ₈₈	0	5.2×10^{-2}	2.6×10^4
		1	3.0×10^{-3}	1.5×10^4
	SP-P ₁₀₀ M ₁₀₀	0	1.2×10^{-2}	9.5×10^3
		1	1.0×10^{-3}	1.0×10^4

Appendix 24. Elastic and loss moduli at bonding and debonding frequency obtained by oscillatory rheology

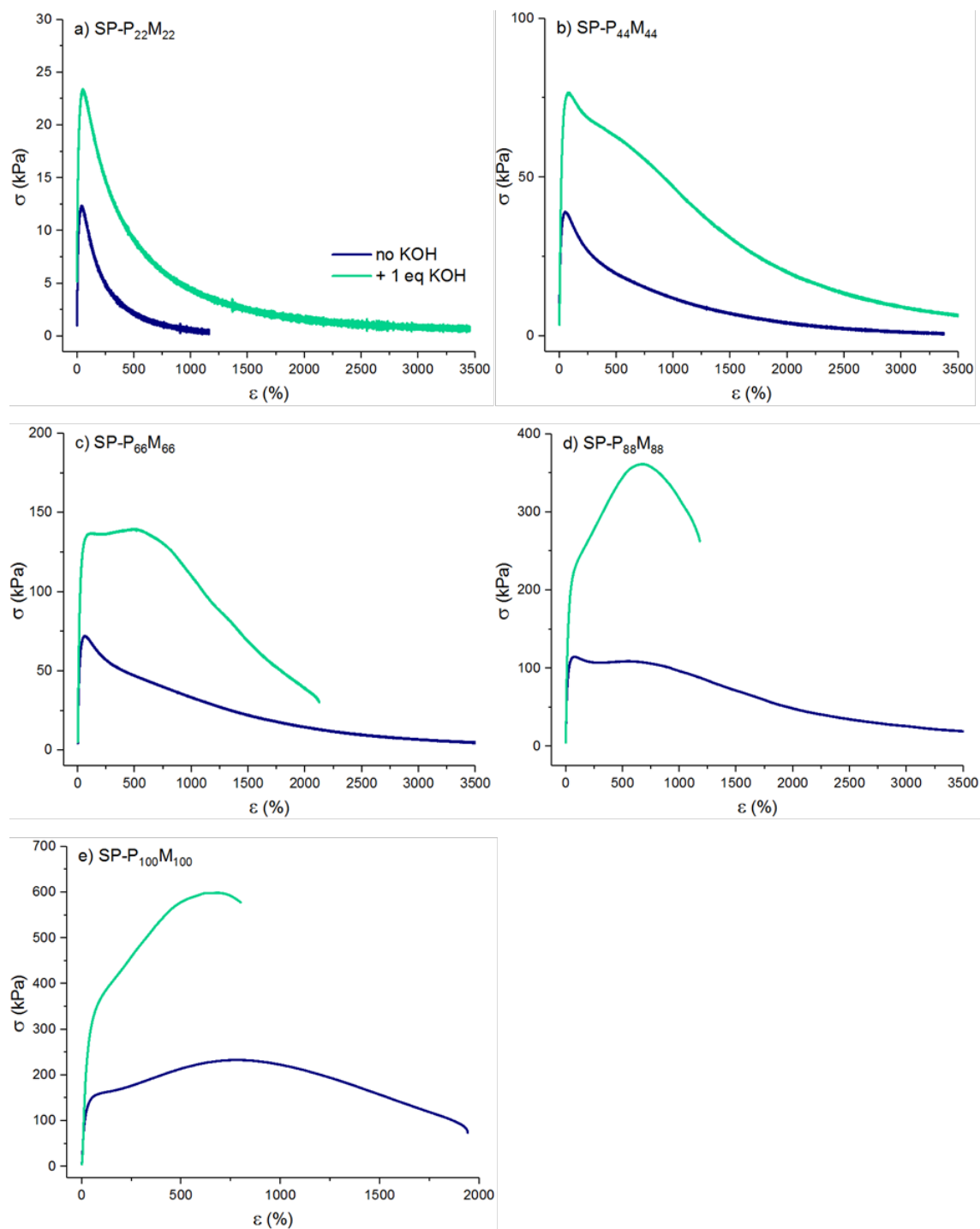
		$\omega_{\text{Bonding}} = 0.01 \text{ rad.s}^{-1}$				$\omega_{\text{Debonding}} = 100 \text{ rad.s}^{-1}$			
Series #	Experiment	KOH eq	G' (Pa)	G'' (Pa)	tan δ	G' (Pa)	G'' (Pa)	tan δ	
1	SP-P ₀ M ₀	0	0.9x10 ⁰	1.0x10 ²	112.1	1.0x10 ⁵	1.2x10 ⁵	1.2	
		0	2.5x10 ²	1.5x10 ³	6.1	1.9x10 ⁵	1.6x10 ⁵	0.8	
	SP-P ₂₂ M ₂₂	1	1.3x10 ³	2.0x10 ³	1.5	1.0x10 ⁵	7.7x10 ⁴	0.7	
		0	2.2x10 ³	4.9x10 ³	2.2	2.4x10 ⁵	1.7x10 ⁵	0.7	
	SP-P ₄₄ M ₄₄	1	9.0x10 ³	9.9x10 ³	1.1	1.6x10 ⁵	9.8x10 ⁴	0.6	
		0	3.2x10 ³	5.4x10 ³	1.7	1.6x10 ⁵	5.7x10 ³	0.6	
	SP-P ₆₆ M ₆₆	1	1.6x10 ⁴	1.4x10 ⁴	0.9	1.9x10 ⁵	1.2x10 ⁵	0.6	
		0	9.5x10 ³	1.2x10 ⁴	1.3	4.3x10 ⁵	3.5x10 ⁵	0.8	
	SP-P ₈₈ M ₈₈	1	3.1x10 ⁴	2.4x10 ⁴	0.8	3.4x10 ⁵	2.3x10 ⁵	0.7	
		0	9.4x10 ³	9.4x10 ³	1.0	2.3x10 ⁵	1.7x10 ⁵	0.7	
	SP-P ₁₀₀ M ₁₀₀	1	3.0x10 ⁴	1.9x10 ⁴	0.6	1.9x10 ⁵	1.1x10 ⁵	0.6	
		0	9.4x10 ³	9.4x10 ³	1.0	2.3x10 ⁵	1.7x10 ⁵	0.7	

Appendix 25. Summary of the parameters extracted from the stress-strain curves obtained by tensile tests for sample series 1

Series #	Experiment	KOH eq	σ_Y (kPa)	σ_{max} (kPa)	ϵ_{max} (%)	σ_B (kPa)	ϵ_B (%)
1	SP-P ₀ M ₀	0	n.a.*				
	SP-P ₂₂ M ₂₂	0	10 ± 1	12 ± 1	34 ± 3	0.7 ± 0.2	1166 ± 89
		1	22 ± 6	24 ± 5	49 ± 7	0.9 ± 0.2	2427 ± 760
	SP-P ₄₄ M ₄₄	0	40 ± 3	41 ± 3	54 ± 3	1.3 ± 0.6	3397 ± 163
		1	78 ± 9	78 ± 9	73 ± 1	6 ± 1	3512 ± 3
	SP-P ₆₆ M ₆₆	0	70 ± 6	70 ± 6	63 ± 4	4 ± 2	3502 ± 3
		1	140 ± 6	140 ± 7	471 ± 61	28 ± 6	2200 ± 143
	SP-P ₈₈ M ₈₈	0	112 ± 6	113 ± 5	76 ± 9	14 ± 5	3471 ± 61
		1	-	365 ± 3	677 ± 14	272 ± 10	1148 ± 71
	SP-P ₁₀₀ M ₁₀₀	0	-	232 ± 11	791 ± 14	71 ± 19	1934 ± 272
		1	-	601 ± 32	636 ± 40	583 ± 28	753 ± 62

*n.a. not available

Appendix 26. Individual stress-strain curves obtained by tensile tests for the sample series 1



Appendix 27. Summary of the peel mean force data and shear holding power for the sample series 1

Series #	Experiment	KOH eq	Peel steel F_{mean} ($\text{N} \cdot 25 \text{ mm}^{-1}$)					Shear strength steel	
			$t_c = 2 \text{ min}$	Failure*	$t_c = 24 \text{ h}$	Failure	$t_c = 48 \text{ h}$	Failure	min
1	SP-P ₀ M ₀	0	3.2 ± 0.1	K	4.5 ± 0.1	K	4.6 ± 0.1	K	2 ± 0
	SP-P ₂₂ M ₂₂	0	12.3 ± 0.4	K	14.4 ± 0.0	K	14.5 ± 0.1	K	55 ± 1
		1	13.2 ± 0.0	K	14.3 ± 0.3	K	14.4 ± 0.1	K	61 ± 11
	SP-P ₄₄ M ₄₄	0	8.3 ± 1.7	A	19.6 ± 0.4	K	19.8 ± 0.1	K	244 ± 9
		1	10.2 ± 0.3	A	19.6 ± 0.3	K	19.8 ± 0.2	K	456 ± 15
	SP-P ₆₆ M ₆₆	0	6.3 ± 1.1	A	18.9 ± 0.6	K	19.6 ± 0.3	K	425 ± 37
		1	3.5 ± 0.8	A	18.1 ± 0.1	K	18.8 ± 0.0	K	962 ± 42
	SP-P ₈₈ M ₈₈	0	1.8 ± 0.5	A	18.9 ± 1.5	K	20.7 ± 0.0	K	699 ± 72
		1	2.2 ± 0.2	A	17.3 ± 1.6	K	13.9 ± 0.5	A	1297 ± 19
	SP-P ₁₀₀ M ₁₀₀	0	1.2 ± 0.1	A	10.0 ± 3.1	A	18.9 ± 0.9	K	1469 ± 119
		1	1.0 ± 0.1	A	13.4 ± 1.2	A	8.7 ± 1.2	A	3336 ± 269

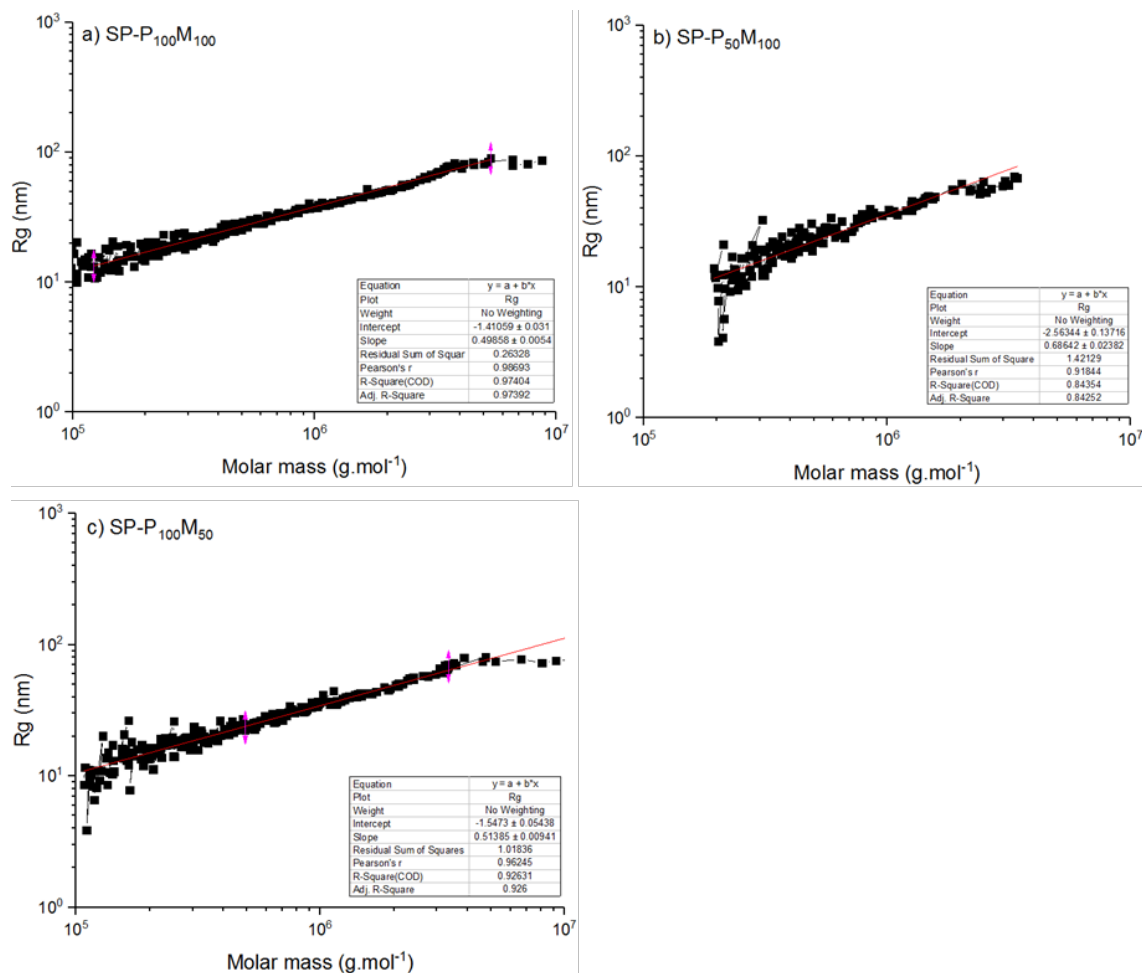
*A=Adhesive
K=Cohesive



Appendix 29. Table of characteristics for the set of samples 2 with different ionic comonomers stoichiometry

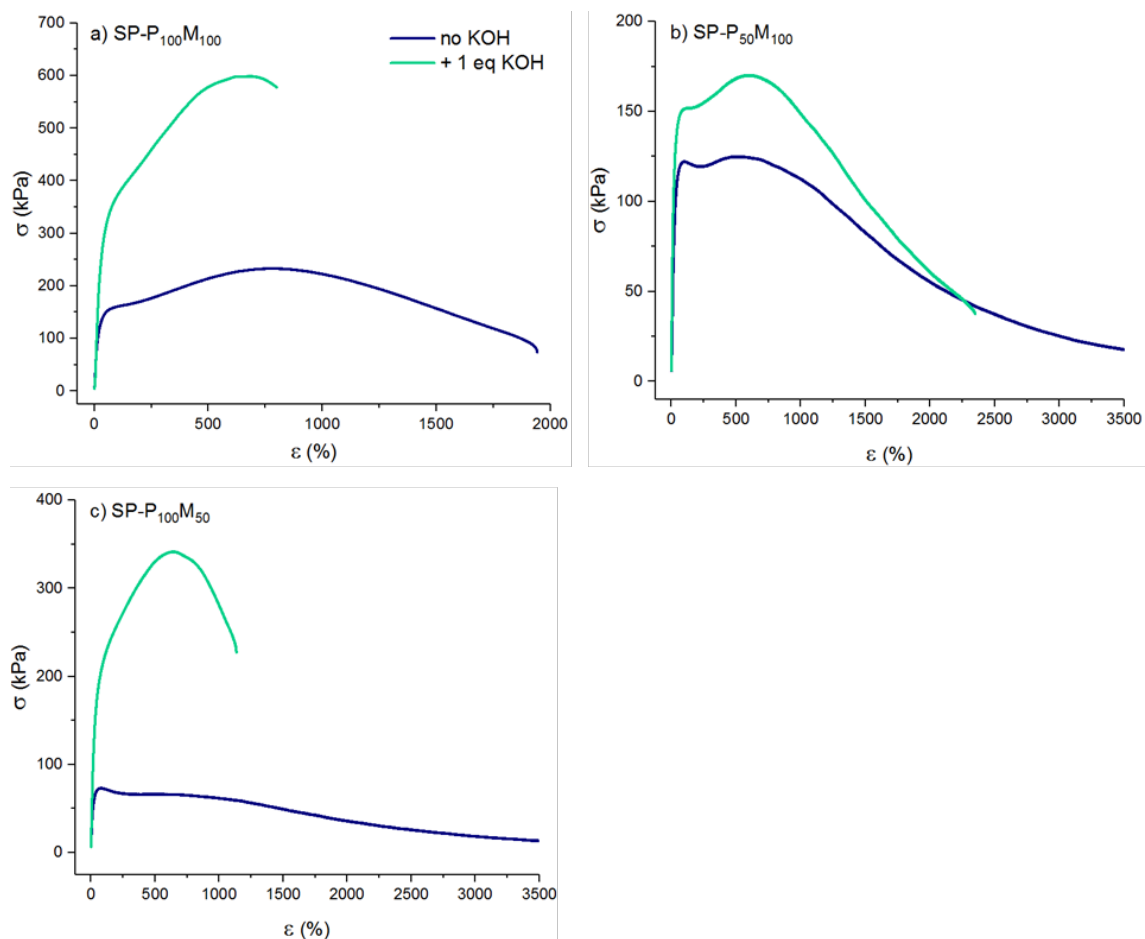
Series #	Experiment	Anionic monomer (mmol)	Cationic monomer (mmol)	KOH eq	T _g (°C)	Gel content (%)			SEC		
						in MEK	in EtOH	M _w (g.mol ⁻¹)	M _n (g.mol ⁻¹)	PDI	M _w with MALLS (g.mol ⁻¹)
2	SP-P ₁₀₀ M ₁₀₀	P-100	M-100	0	-18.2	0.8	1.7	157 000	17 600	8.9	150 000
				1	-21.5	1.5	1.9	166 000	17 500	9.5	160 000
	SP-P ₅₀ M ₁₀₀	P-50	M-100	0	-22.1	3.5	2.3	138 000	21 600	6.4	90 000
				1	-24.6	0.2	0.7				
	SP-P ₁₀₀ M ₅₀	P-100	M-50	0	-22.3	2.4	2.4	142 000	15 900	9.0	150 000
				1	-23.8	0.4	0.3				

Appendix 30. Logarithmic representation of the radius of gyration as function of molar mass measured by SEC-MALLS for samples series 2 and linear fit to obtain the conformation factor ν



Appendix 31. Summary of the cross-over frequencies measured by oscillatory rheology
for the sample series 2

Cross-over to flowing region				
Series #	Experiment	KOH eq	ω_c (rad.s ⁻¹)	$G_c=G'=G''$ (Pa)
2	SP-P ₁₀₀ M ₁₀₀	0	1.2×10^{-2}	9.5×10^3
		1	1.0×10^{-3}	1.0×10^4
	SP-P ₅₀ M ₁₀₀	0	4.3×10^{-2}	3.0×10^4
		1	4.6×10^{-3}	9.3×10^3
	SP-P ₁₀₀ M ₅₀	0	4.2×10^{-2}	1.3×10^4
		1	1.4×10^{-2}	2.0×10^4

Appendix 32. Individual stress-strain curves obtained by tensile tests for the sample series 2

Appendix 33. Summary of the parameters extracted from the stress-strain curves obtained by tensile tests for sample series 2

Series #	Experiment	KOH eq	σ_Y (kPa)	σ_{max} (kPa)	ϵ_{max} (%)	σ_B (kPa)	ϵ_B (%)
2	SP-P ₁₀₀ M ₁₀₀	0	-	232 ± 11	791 ± 14	71 ± 19	1934 ± 272
		1	-	601 ± 32	636 ± 40	583 ± 28	753 ± 62
	SP-P ₅₀ M ₁₀₀	0	123 ± 3	125 ± 3	422 ± 211	15 ± 3	3500 ± 4
		1	-	167 ± 7	598 ± 51	39 ± 12	2276 ± 501
	SP-P ₁₀₀ M ₅₀	0	74 ± 4	74 ± 4	81 ± 4	13 ± 1	3494 ± 3
		1	-	342 ± 8	665 ± 34	244 ± 11	1115 ± 65

Appendix 34. Summary of the peel mean force data and shear holding power for the sample series 2

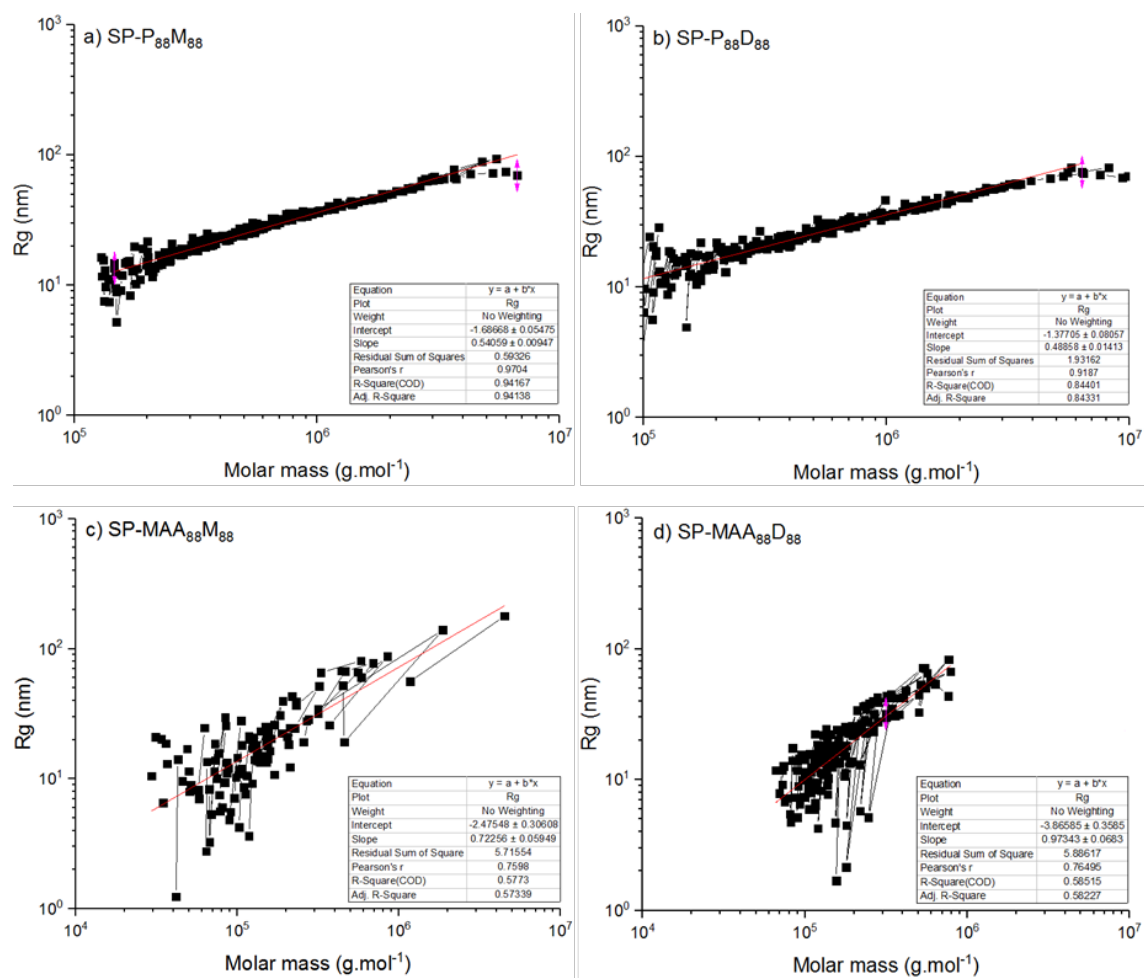
Series #	Experiment	KOH eq	Peel steel F_{mean} (N.25 mm ⁻¹)						Shear strength steel	
			$t_c=2$ min	Failure*	$t_c=24$ h	Failure*	$t_c=48$ h	Failure*	min	Failure*
2	SP-P ₁₀₀ M ₁₀₀	0	1.2 ± 0.1	A	10.0 ± 3.1	A	18.9 ± 0.9	K	1469 ± 119	K
		1	1.0 ± 0.1	A	13.4 ± 1.2	A	8.7 ± 1.2	A	3336 ± 269	K
	SP-P ₅₀ M ₁₀₀	0	2.1 ± 0.3	A	14.7 ± 2.3	K	16.1 ± 0.2	K	803 ± 59	K
		1	2.7 ± 0.7	A	20.1 ± 0.3	K	20.8 ± 0.0	K	1231 ± 53	K
	SP-P ₁₀₀ M ₅₀	0	3.2 ± 0.2	A	17.3 ± 4.5	K	19.1 ± 2.2	K	777 ± 138	K
		1	1.4 ± 0.4	A	13.2 ± 4.0	K	15.8 ± 0.1	K	2623 ± 784	K

*A=Adhesive
K=Cohesive

Appendix 35. Table of characteristics for the set of samples 3 with different ionic comonomers

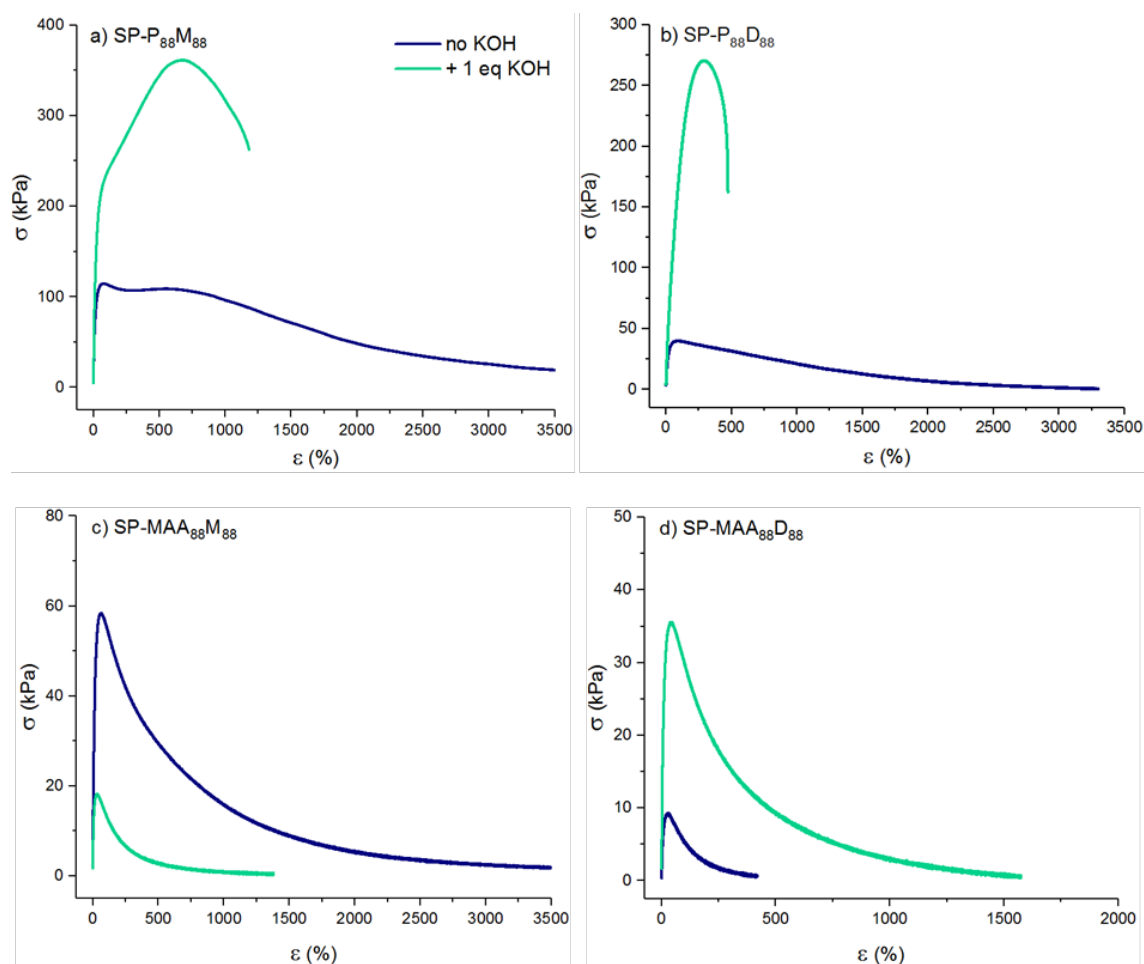
Series #	Experiment	Anionic monomer (mmol)	Cationic monomer (mmol)	KOH eq	T _g (°C)	Gel content (%)			SEC		
						in MEK	in EtOH	M _w (g.mol ⁻¹)	M _n (g.mol ⁻¹)	PDI	M _w with MALLS (g.mol ⁻¹)
3	SP-P ₈₈ M ₈₈	P-88	M-88	0	-22.8	1.4	1.5	147 000	19 100	7.7	100 000
				1	-22.2	1.4	2.6				
	SP-P ₈₈ D ₈₈	P-88	D-88	0	-25.2	1.8	3.3	135 000	17 200	7.8	115 000
				1	-24.4	0.0	0.1				
	SP-MAA ₈₈ M ₈₈	MAA-88	M-88	0	-24.5	3.4	1.9	91 600	21 800	4.2	39 500
				1	-26.0	0.5	1.3				
	SP-MAA ₈₈ D ₈₈	MAA-88	D-88	0	-22.7	2.0	2.6	98 800	21 600	4.6	45 500
				1	-22.8	0.3	0.3				

Appendix 36. Logarithmic representation of the radius of gyration as function of molar mass measured by SEC-MALLS for samples series 3 and linear fit to obtain the conformation factor ν



Appendix 37. Summary of the cross-over frequencies measured by oscillatory rheology
for the sample series 3

Cross-over to flowing region				
Series #	Experiment	KOH eq	ω_c (rad.s ⁻¹)	$G_c=G'=G''$ (Pa)
3	SP-P ₈₈ M ₈₈	0	5.2×10^{-2}	2.6×10^4
		1	3.0×10^{-3}	1.5×10^4
	SP-P ₈₈ D ₈₈	0	4.3×10^{-2}	7.4×10^3
		1	2.7×10^{-2}	9.7×10^3
	SP-MAA ₈₈ M ₈₈	0	7.2×10^{-2}	1.8×10^4
		1	1.5×10^0	4.6×10^4
	SP-MAA ₈₈ D ₈₈	0	<i>No cross-over $G'' > G'$</i>	
		1	2.4×10^{-2}	9.9×10^3

Appendix 38. Individual stress-strain curves obtained by tensile tests for the sample series 3

Appendix 39. Summary of the parameters extracted from the stress-strain curves obtained by tensile tests for sample series 3

Series #	Experiment	KOH eq	σ_Y (kPa)	σ_{max} (kPa)	ϵ_{max} (%)	σ_B (kPa)	ϵ_B (%)
3	SP-P88M88	0	112 ± 6	113 ± 5	76 ± 9	14 ± 5	3471 ± 61
		1	-	365 ± 3	677 ± 14	272 ± 10	1148 ± 71
	SP-P88D88	0	38 ± 1	39 ± 1	92 ± 5	0.7 ± 0.1	3224 ± 369
		1	-	269 ± 11	296 ± 14	194 ± 18	468 ± 27
	SP-MAA88M88	0	61 ± 3	61 ± 3	65 ± 2	2 ± 1	3229 ± 532
		1	16 ± 3	17 ± 3	34 ± 3	0.6 ± 0.1	1321 ± 130
	SP-MAA88D88	0	7 ± 1	9 ± 1	25 ± 4	0.6 ± 0.4	474 ± 93
		1	33 ± 3	35 ± 3	42 ± 2	0.7 ± 0.1	1659 ± 293

Appendix 40. Summary of the peel mean force data and shear holding power for the sample series 3

Peel steel F_{mean} (N.25 mm ⁻¹)										Shear strength steel	
Series #	Experiment	KOH eq	t _c = 2 min	Failure *	t _c = 24 h	Failure*	t _c = 48 h	Failure*	min	Failure*	
3	SP-P ₈₈ M ₈₈	0	1.8 ± 0.5	A	18.9 ± 1.5	K	20.7 ± 0.0	K	699 ± 72	K	
		1	2.2 ± 0.2	A	17.3 ± 1.6	K	13.9 ± 0.5	A	1297 ± 19	K	
	SP-P ₈₈ D ₈₈	0	11.6 ± 0.1	A	18.6 ± 0.1	K	19.3 ± 0.1	K	139 ± 8	K	
		1	6.8 ± 0.8	A	16.0 ± 0.2	K	16.5 ± 0.1	K	1403 ± 49	K	
	SP-MAA ₈₈ M ₈₈	0	10.4 ± 0.1	A	20.5 ± 0.2	K	21.2 ± 0.1	K	215 ± 34	K	
		1	15.4 ± 0.3	K	16.1 ± 0.4	K	17.5 ± 0.6	K	49 ± 1	K	
	SP-MAA ₈₈ D ₈₈	0	19.6 ± 3.4	K	25.5 ± 0.2	K	25.2 ± 0.1	K	31 ± 1	K	
		1	11.2 ± 0.6	A	22.3 ± 0.3	K	22.1 ± 0.3	K	86 ± 3	K	

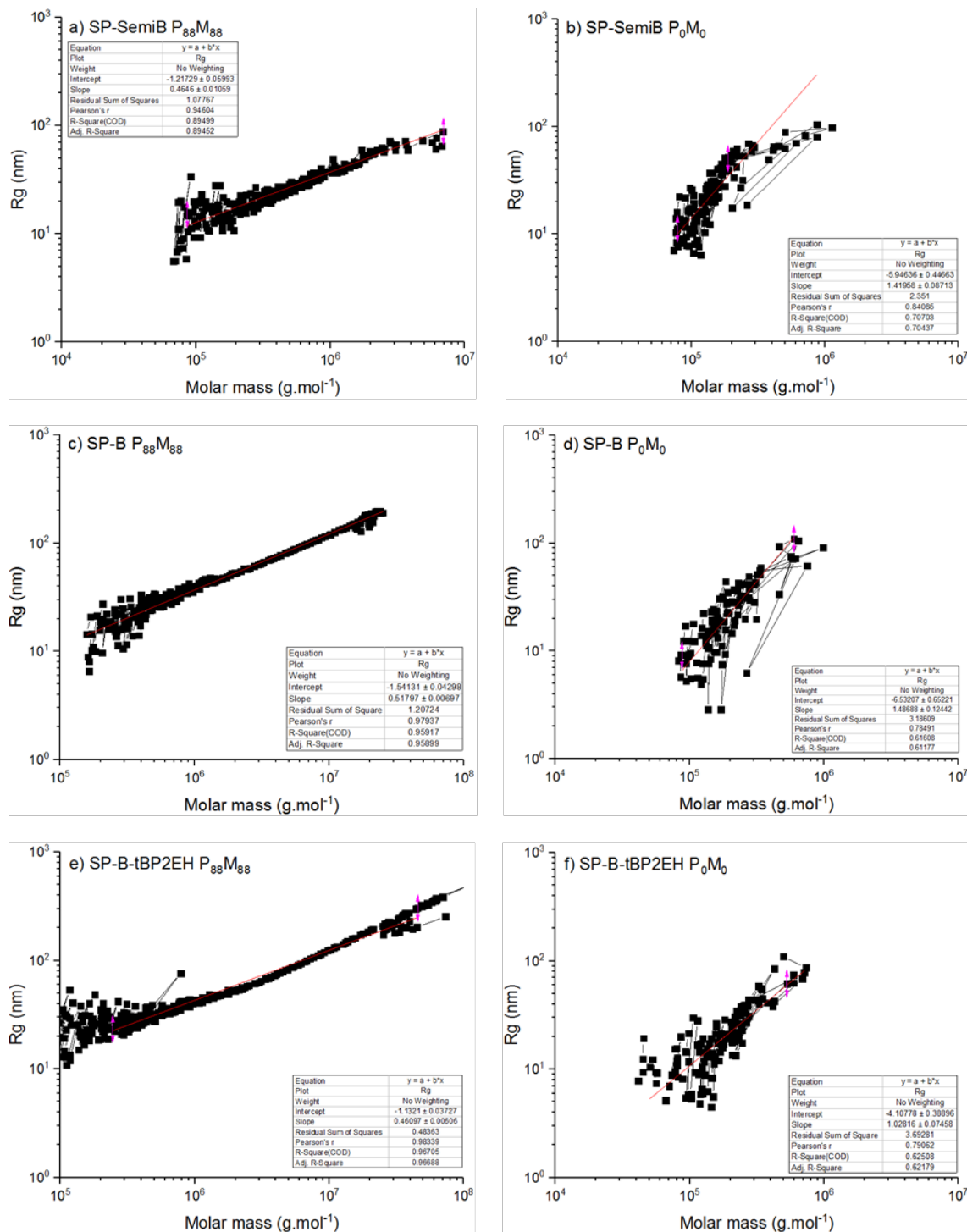
*A=Adhesive
K=Cohesive

Appendix 41. Summary of the peel mean force data and shear holding power for the adhesive performance comparison of SP-P₈₈M₈₈, SP-P₅₀M₁₀₀ and SP-P₈₈D₈₈ to Acronal® V 215 and Acronal® 3633

Product	KOH eq	Peel steel F _{mean} (N.25 mm ⁻¹)				Shear strength steel	
		t _c = 2 min	Failure*	t _c = 24 h	Failure	min	Failure
SP-P ₈₈ M ₈₈	0	1.8 ± 0.5	A	18.9 ± 1.5	K	699 ± 72	K
	1	2.2 ± 0.2	A	17.3 ± 1.6	K	1297 ± 19	K
SP-P ₅₀ M ₁₀₀	0	2.1 ± 0.3	A	14.7 ± 2.3	K	803 ± 59	K
	1	2.7 ± 0.7	A	20.1 ± 0.3	K	1231 ± 53	K
SP-P ₈₈ D ₈₈	0	11.6 ± 0.1	A	18.6 ± 0.1	K	139 ± 8	K
	1	6.8 ± 0.8	A	16.0 ± 0.2	K	1403 ± 49	K
Acronal V 215	7.5 ± 0.1	A	14.9 ± 0.1	A	1170 ± 149	A	
Acronal 3633	18.3 ± 0.2	K	18.9 ± 0.1	K	164 ± 37	K	

*A=Adhesive
K=Cohesive
**n.a.=not applicable

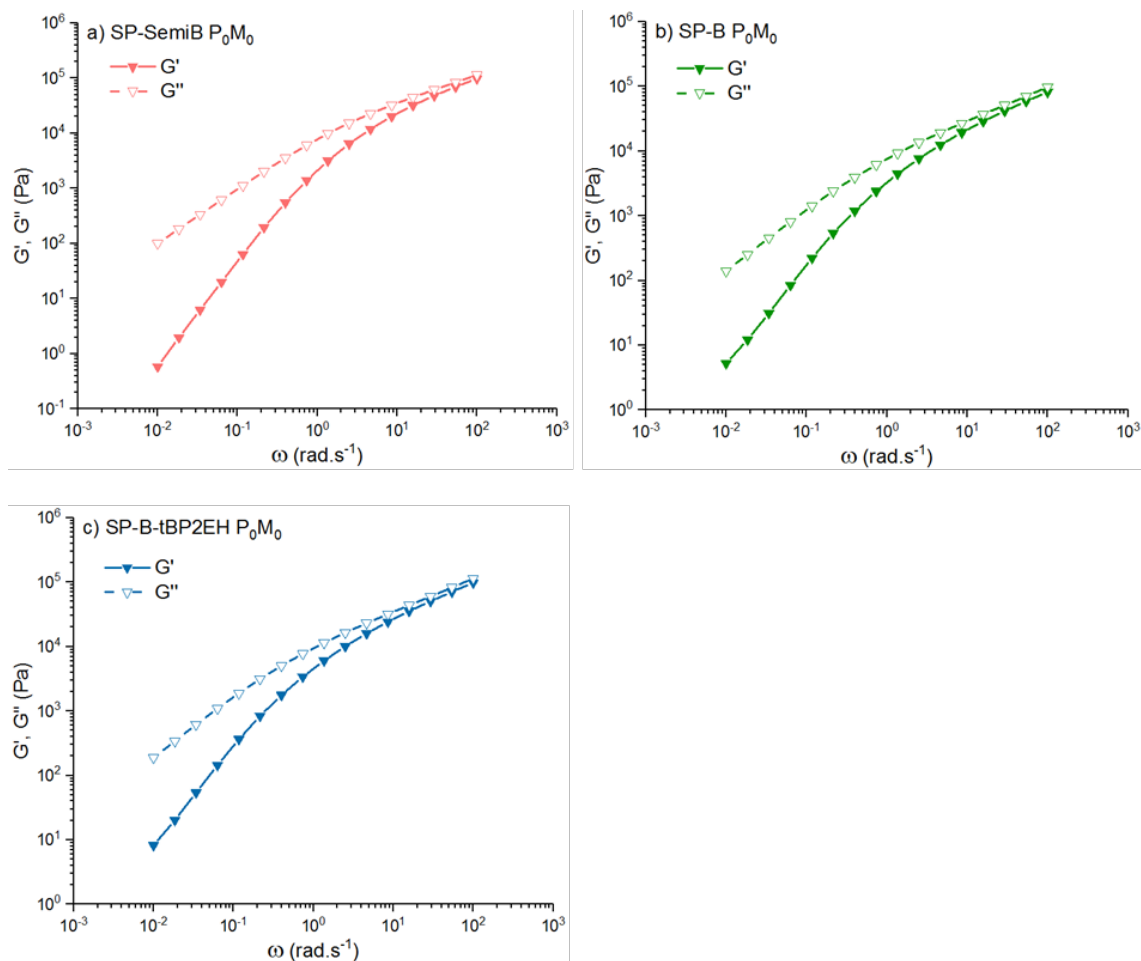
Appendix 42. Logarithmic representation of the radius of gyration as function of molar mass measured by SEC-MALLS for samples series 4 and linear fit to obtain the conformation factor ν



Appendix 43. Table of final characteristics for the set of samples 4 using different processes and ionic comonomers compositions

Series #	Experiment	Process	Initiator	Composition	T _g (°C)	Gel (%)			SEC		
						in MEK	in EtOH	M _w (g.mol ⁻¹)	M _n (g.mol ⁻¹)	PDI	M _w with MALLS (g.mol ⁻¹)
4	SP-SemiB	Semi Batch	t-BHPV	P ₈₈ M ₈₈	-21.5	1.8	3.5	148 000	23 000	6.5	110 000
				P ₀ M ₀	-29.2	0.6	0.6	69 100	14 900	4.6	34 700
	SP-B	Batch		P ₈₈ M ₈₈	-24.0	2.1	2.6	448 000	12 700	35.3	880 000
				P ₀ M ₀	-30.4	0.2	1.4	73 100	14 200	5.1	37 100
	SP-B-tBP2EH	Batch		P ₈₈ M ₈₈	-26.6	2.5	2.9	611 000	14 000	43.4	1 800 000
				P ₀ M ₀	-30.3	0.6	0.5	74 800	13 500	5.5	40 800

Appendix 44. Elastic G' and Loss G'' moduli curves as function of the angular frequency obtained by oscillatory rheology at room temperature for the samples series 4 and P_0M_0 composition



Appendix 45. Summary of the cross-over frequencies measured by oscillatory rheology
for the sample series 4

Cross-over to flowing region				
Series #	Experiment		$\omega_c \text{ (rad.s}^{-1}\text{)}$	$G_c = G' = G'' \text{ (Pa)}$
4	SP-SemiB	$P_{88}M_{88}$	6.1×10^{-2}	1.4×10^5
		P_0M_0		$G'' > G'$
	SP-B	$P_{88}M_{88}$	8.3×10^{-3}	6.2×10^4
		P_0M_0		$G'' > G'$
	SP-B-tBP2EH	$P_{88}M_{88}$	3.3×10^{-3}	5.0×10^4
		P_0M_0		$G'' > G'$

Appendix 46. Summary of the parameters extracted from the stress-strain curves obtained by tensile tests for sample series 4

Series #	Experiment	Composition	σ_y (kPa)	σ_{max} (kPa)	ϵ_{max} (%)	σ_B (kPa)	ϵ_B (%)
4	SP-SemIB	P ₈₈ M ₈₈ P ₀ M ₀	69 ± 4	69 ± 4	61 ± 7 n.a.*	9 ± 1	3503 ± 1
	SP-B	P ₈₈ M ₈₈ P ₀ M ₀	-	316 ± 13	1302 ± 34 n.a.	297 ± 31	1460 ± 176
	SP-B-tBP2EH	P ₈₈ M ₈₈ P ₀ M ₀	-	425 ± 28	1249 ± 52 n.a.	425 ± 28	1250 ± 52

*n.a.=not available

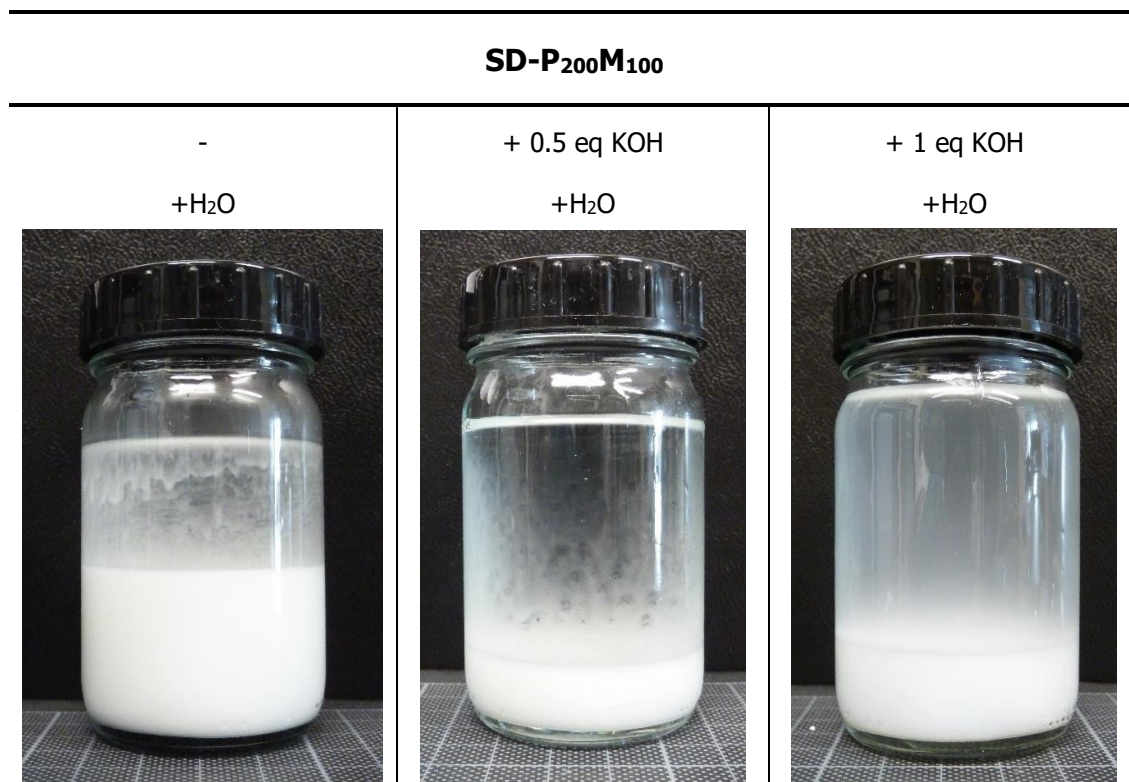
Appendix 47. Summary of the peel mean force data and shear holding power for the sample series 4

Series #	Experiment	Composition	Peel steel F_{mean} (N.25 mm ⁻¹)						Shear strength steel	
			$t_c = 2$ min	Failure*	$t_c = 24$ h	Failure*	$t_c = 48$ h	Failure*	min	Failure*
4	SP-SemiB	P ₈₈ M ₈₈	1.6 ± 0.0	A	20.4 ± 0.1	K	20.9 ± 0.1	K	929 ± 87	K
		P ₀ M ₀	3.2 ± 0.1	K	4.5 ± 0.1	K	4.6 ± 0.1	K	2 ± 0	K
	SP-B	P ₈₈ M ₈₈	0.2 ± 0.0	A/F	1.4 ± 1.1	A/F	1.3 ± 0.5	A/F	528 ± 32	A/K
		P ₀ M ₀	5.5 ± 0.1	K	6.9 ± 0.5	K	7.2 ± 0.1	K	2 ± 0	K
	SP-B-tBP2EH	P ₈₈ M ₈₈	0.2 ± 0.0	A/K	1.3 ± 0.7	A/F	2.6 ± 0.2	A/F	359 ± 5	A/K
		P ₀ M ₀	6.4 ± 0.2	K	8.0 ± 0.4	K	8.1 ± 0.4	K	2 ± 0	K





*A=Adhesive
K=Cohesive
F=Fillic

C. Chapter IV. Secondary dispersions: from dissolved to dispersed

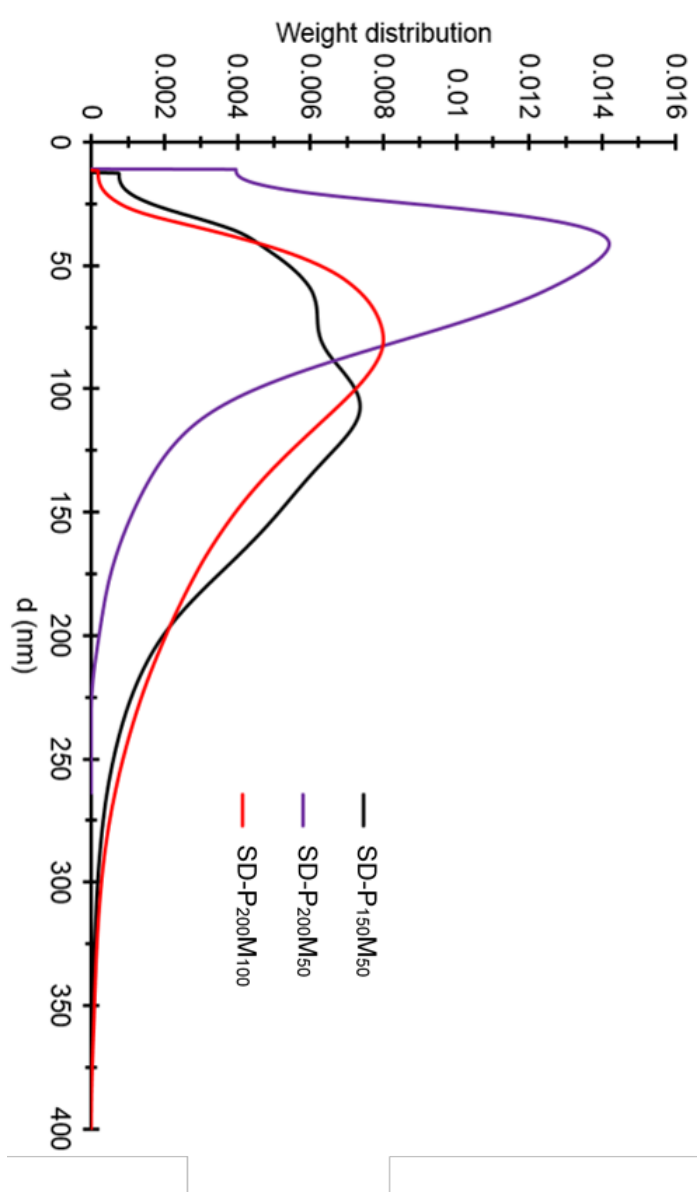
Appendix 48. Images of the phase-separation observed with addition of water to SP-P₂₀₀M₁₀₀ without or with prior addition of KOH using 0.5 and 1 equivalent



Appendix 49. Images of SD-P₂₀₀M₁₀₀ during the different steps of the dispersive procedure

SD-P ₂₀₀ M ₁₀₀			
Solution	Solution + 2 eq KOH		Dispersion
iPrOH	iPrOH	iPrOH + H ₂ O	H ₂ O
			

Appendix 50. Particle diameter weight distribution of the dispersion obtained by AUC

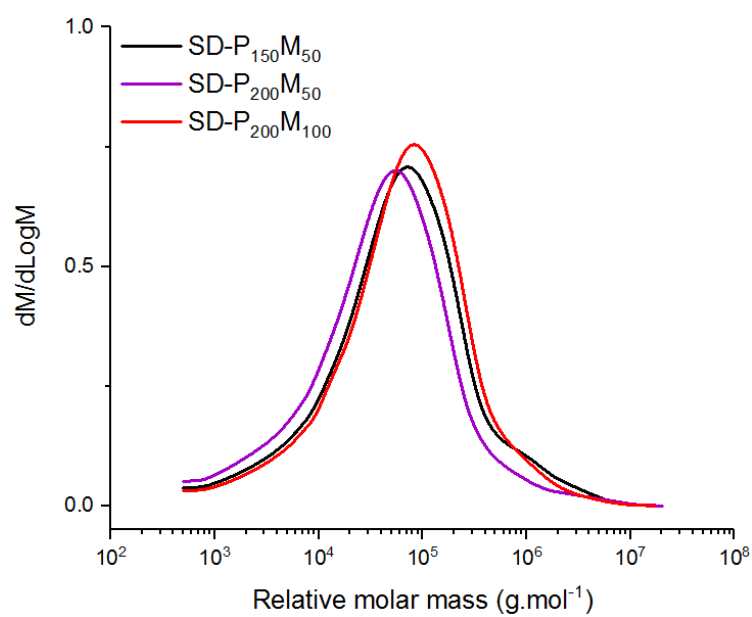


Appendix 51. Table of characteristics of SD-P₁₅₀M₅₀, SD-P₂₀₀M₅₀ and SD-P₂₀₀M₁₀₀ for S, S+KOH and D states

Experiment	State	KOH eq	pH	T _g (°C)	Gel content (%)			SEC		
					in MEK	in EtOH	M _w (g.mol ⁻¹)	M _n (g.mol ⁻¹)	PDI	M _w with MALLS (g.mol ⁻¹)
SD-P₁₅₀M₅₀	S	0	n.a.*	-17.5	1.0	0.8				
	S+KOH	2	n.a.*	-23.0	15.7	0.1	205 000	14 700	13.9	400 000
	D	2	9.6	-23.7	12.4	1.0				
SD-P₂₀₀M₅₀	S	0	n.a.	-18.2	0.9	1.8				
	S+KOH	2	n.a.	-21.3	14.2	0.2	187 000	11 700	15.9	750 000
	D	2	9.8	-21.8	15.2	1.2				
SD-P₂₀₀M₁₀₀	S	0	n.a.	-16.2	1.1	1.1				
	S+KOH	2	n.a.	-22.5	6.6	2.2	162 000	16 000	10.1	460 000
	D	2	9.3	-21.8	6.8	1.3				

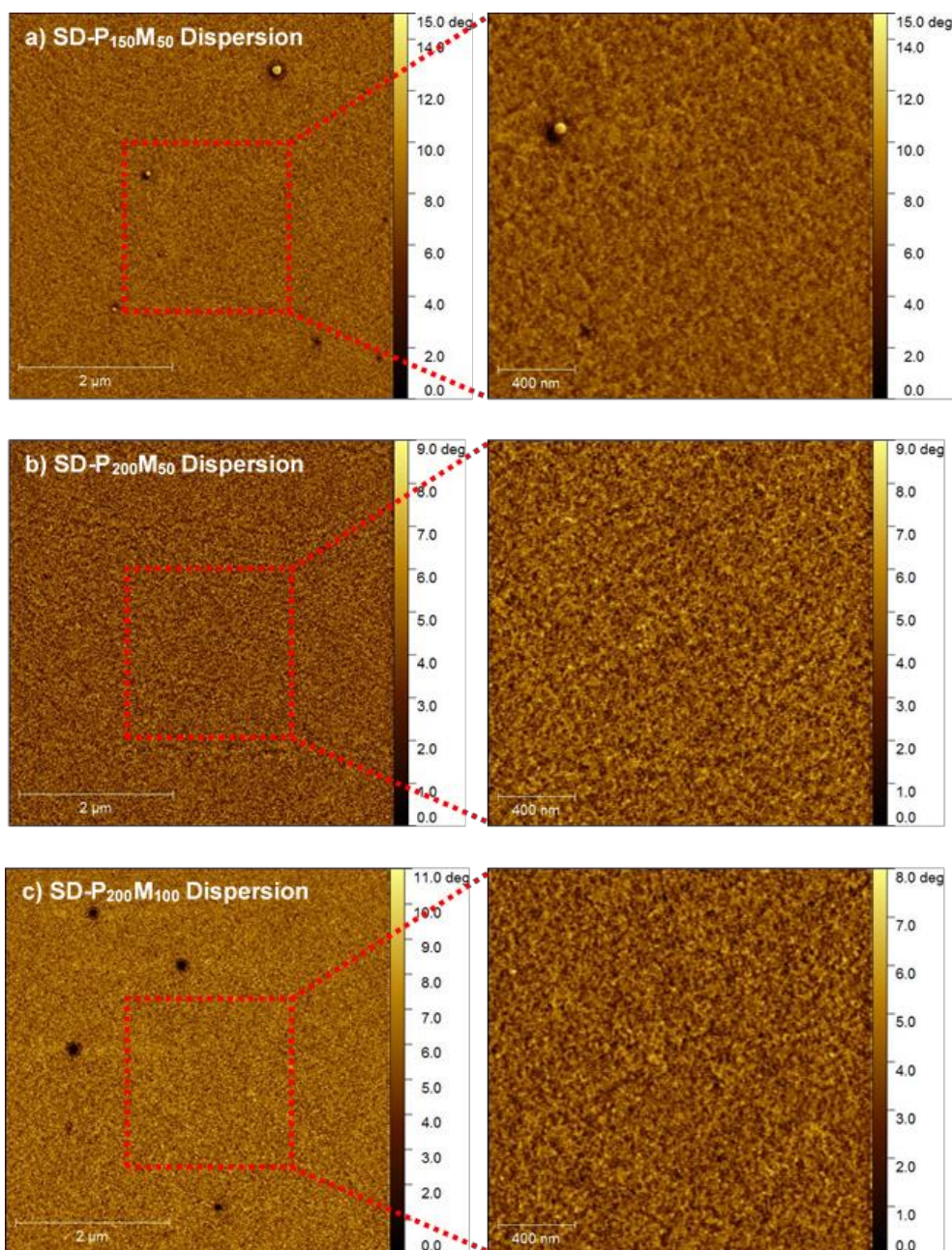
*n.a.=not available

Appendix 52. Relative molar mass distributions of SD-P₁₅₀M₅₀, SD-P₂₀₀M₅₀ and SD-P₂₀₀M₁₀₀
obtained by SEC-RI



Appendix 53. AFM phase images (5 and 2 μm) measured in tapping mode of films cross-sections of

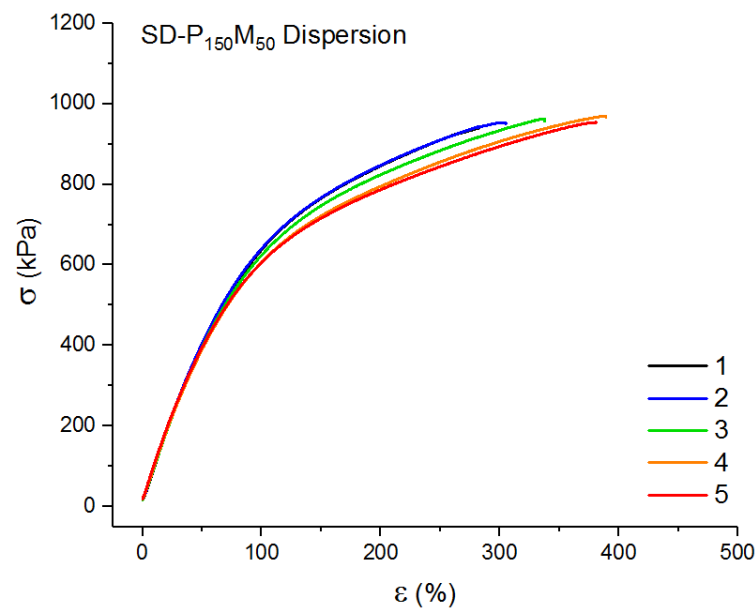
a) SD-P₁₅₀M₅₀, b) SD-P₂₀₀M₅₀ and c) SD-P₂₀₀M₁₀₀



Appendix 54. Summary of the parameters extracted from the stress-strain curves obtained by tensile tests for the set of samples

Experiment	State	σ_y (kPa)	σ_{max} (kPa)	ϵ_{max} (%)	σ_b (kPa)	ϵ_b (%)
SD-P₁₅₀M₅₀	S	-	174 ± 5	1014 ± 35	37 ± 11	3277 ± 286
	S+KOH	-	805 ± 76	536 ± 21	783 ± 115	544 ± 26
	D	-	956 ± 11	341 ± 47	953 ± 10	342 ± 46
SD-P₂₀₀M₅₀	S	-	381 ± 33	1079 ± 11	376 ± 33	1137 ± 43
	S+KOH	-	1235 ± 52	509 ± 35	1228 ± 44	509 ± 35
	D	-	1522 ± 96	205 ± 23	1519 ± 96	206 ± 22
SD-P₂₀₀M₁₀₀	S	-	687 ± 11	892 ± 16	661 ± 27	985 ± 110
	S+KOH	-	1413 ± 66	417 ± 49	1412 ± 65	417 ± 49
	D	-	1108 ± 125	255 ± 54	1102 ± 128	255 ± 53

Appendix 55. Repeatability of tensile test for the dispersion of SD-P₁₅₀M₅₀



Appendix 56. Young's modulus E obtained from tensile test and elastic modulus G' obtained with oscillatory rheology at $\omega=0.6 \text{ rad.s}^{-1}$

Experiment	State	E (kPa)	G' at $\omega=0.6 \text{ rad.s}^{-1}$ (kPa)
SD-P₁₅₀M₅₀	S	1073 ± 80	971
	S+KOH	968 ± 50	508
	D	695 ± 90	350
SD-P₂₀₀M₅₀	S	1143 ± 133	1117
	S+KOH	1289 ± 311	429
	D	941 ± 85	422
SD-P₂₀₀M₁₀₀	S	1317 ± 210	583
	S+KOH	1154 ± 87	359
	D	880 ± 81	137

Appendix 57. Summary of the peel mean force and shear holding power for the set of samples

Peel steel F_{mean} (N.25 mm ⁻¹)										Shear strength steel	
Experiment	State	$t_c = 2$ min	Failure*	$t_c = 24$ h	Failure*	$t_c = 48$ h	Failure*	min	Failure*		
SD-P ₁₅₀ M ₅₀	S	1.0 ± 0.1	A/Z	10.7 ± 0.9	A	9.2 ± 1.8	A	2184 ± 222	K		
	S+KOH	3.9 ± 1.2	A	10.5 ± 2.6	A	14.0 ± 0.3	K	> 12000	K		
	D	6.4 ± 0.1	A	12.4 ± 0.5	A	5.2 ± 0.4	K	1844 ± 238	K		
SD-P ₂₀₀ M ₅₀	S	0.6 ± 0.1	A/Z	7.1 ± 0.8	K	8.6 ± 0.1	A	6630 ± 1068	K		
	S+KOH	1.2 ± 0.8	A	16.1 ± 0.4	K	17.0 ± 0.3	K	5738 ± 852	K		
	D	5.2 ± 0.4	A	15.4 ± 1.0	A	13.3 ± 2.5	K	3345 ± 847	K		
SD-P ₂₀₀ M ₁₀₀	S	0.3 ± 0.0	A/Z	4.7 ± 0.1	A	6.0 ± 1.2	A	6658 ± 1205	K		
	S+KOH	0.7 ± 0.4	A	11.8 ± 1.4	A	13.0 ± 1.8	K	9895 ± 1178	K		
	D	3.5 ± 0.8	A	10.2 ± 4.1	A	11.2 ± 2.1	K	1216 ± 269	K		

*A =Adhesive
K=Cohesive
Z=Zippy

*A=Adhesive
K=Cohesive
Z=Zippy

Appendix 58. Summary of shear holding power for comparison after 3 days in desiccator

Experiment	State	Shear strength steel	
		min	Failure*
SD-P₁₅₀M₅₀	S+KOH	> 12000	K*
	D	1844 ± 238	K
	D+dessicator	2204 ± 183	K
SD-P₂₀₀M₅₀	S+KOH	5738 ± 852	K
	D	3345 ± 847	K
	D+dessicator	4434 ± 161	K
SD-P₂₀₀M₁₀₀	S+KOH	9895 ± 1178	K
	D	1216 ± 269	K
	D+dessicator	>12000	K/A

*A=Adhesive
K=Cohesive

A ma famille,

"Be not astonished at new ideas; for it is well known to you that a thing does not therefore
cease to be true because it is not accepted by many."

« Ne soyez pas étonnés des idées nouvelles ; vous savez bien qu'une chose ne cesse pas d'être
vraie car elle n'est pas acceptée par beaucoup. »

Baruch Spinoza